

Supporting Information for

Two-photon, visible light water splitting at a molecular ruthenium complex

Jacob Schneidewind*, Miguel A. Argüello Cordero, Henrik Junge, Stefan Lochbrunner, Matthias Beller

*Corresponding author, e-mail: Jacob.Schneidewind@catalysis.de

Other supplementary materials for this manuscript:

Original data and analysis code are publicly available at:

<https://github.com/jschneidewind/Water-Splitting>

1 Table of Contents	
1.1 Table of Figures	4
1.2 Table of Tables	6
2 Methods and Materials.....	7
3 Synthesis Procedures and Characterization	8
3.1 Synthesis of Complex 1.....	8
3.1.1 Synthesis using N ₂ O	8
3.1.2 Photographs Showing Synthesis and Product	10
3.1.3 Synthesis using Ag ₂ O	11
3.1.4 Synthesis via Reflux of 2-trans	11
3.2 Synthesis of Complex 2-trans.....	12
3.2.1 Synthesis in H ₂ O.....	12
3.2.2 Crystallization of 2-trans	12
3.3 Synthesis of (p-cymene)RuCl ₂ (CO)	12
3.4 Synthesis of (PNN)RuCl ₂ (CO)	12
4 Procedures for Irradiation and Subsequent Data Analysis.....	13
4.1 NMR Scale Irradiation	13
4.1.1 Irradiation Procedure	13
4.1.2 Interpretation of NMR Results	13
4.1.3 Data Analysis for Concentration-Time Profile.....	14
4.1.4 Data Analysis for Dual Irradiation	15
4.2 Liquid Phase O ₂ Measurement.....	16
4.2.1 Irradiation Procedure	16
4.2.2 General Remarks on Data Analysis	17
4.2.3 Data Analysis for Intensity Experiments	18
4.2.4 Data Analysis for Kinetic Isotope Effect and Temperature Dependence.....	18
4.2.5 Data Analysis for Dual Irradiation Experiments	19
4.2.6 Note on Reaction Order/Concentration Dependence	20
4.3 Gas Phase O ₂ Measurement.....	21
4.3.1 Irradiation Procedure	21
4.3.2 Data Analysis and O ₂ Consumption Reaction	21
4.4 Comparison of 2-cis and O ₂ Formation Rates.....	22
4.5 Photographs of Irradiation Set-Ups	24
5 H₂O₂ Disproportionation	26
5.1 Experimental Procedure	26
5.2 Data Analysis.....	26
6 Chemical Actinometry	28
6.1 Light Source Spectra	28
6.2 Experimental Procedure	29
6.3 Chemical Actinometry Data and Analysis	29
7 NMR Data	31
7.1 Characterization of 1.....	31
7.2 Characterization of 2-trans.....	40
7.3 Characterization of (p-cymene)RuCl ₂ (CO)	42
7.4 Characterization of (PNN)RuCl ₂ (CO)	43
7.5 Data for Irradiated Samples	45
7.6 Isomerization Reactions in the Dark	56
7.7 Data for $\delta(^{31}P) = 86$ ppm Product	59
8 Other Analytical Data	61
8.1 IR Spectrum of Complex 1	61
8.2 EPR Spectrum of Complex 1 Synthesis Raw Product.....	62
9 Ultrafast Pump-Probe Spectroscopy.....	63

9.1 Experimental Procedure and Analysis.....	63
9.2 Results and Interpretation.....	63
10 Photochemical Kinetic Model	66
10.1 Description of Kinetic Model.....	66
10.2 Relationship between Initial Rate and Photon Flux	66
10.3 Interpretation of Results.....	67
10.4 Comparison of Experimental Dual Irradiation Rates with Kinetic Model	68
11 Computational Section	69
11.1 Computational Methods	69
11.1.1 DFT Methods	69
11.1.2 CASSCF Methods	70
11.2 DFT Results	71
11.2.1 Relative Energies of [A] and [B] Isomers, Oxo Dimer, $[F]S_0 \rightarrow [A\text{-Mono}]S_0$	71
11.2.2 TD-DFT Computed UV-Vis Spectra	73
11.2.3 Natural Transition Orbitals for $[A]S_0$	74
11.2.4 Natural Transition Orbitals for $[B]T_0$	80
11.2.5 Natural Transition Orbitals for $[B\text{-Mono}]D_0$ (Me Model)	82
11.2.6 Spin Density Plots	83
11.2.7 Scan-[DE] T_0	86
11.2.8 O-O Bond Formation Scans	87
11.2.9 Theoretical NMR Data for $[F]S_0$ Isomers	88
11.3 CASSCF Results	89
11.3.1 Comparison of DFT and CASSCF Energies and Absorption Wavelengths	89
11.3.2 Energy Profile including PCM Solvation	90
11.3.3 Active Space Orbitals	91
11.3.4 Surfaces for $[B\text{-Mono}]D_n$	93
11.3.5 Difference Orbitals for Conical Intersections	94
11.3.6 Surfaces for $[C\text{-Mono}]D_0$	95
11.4 Integration of Computational and Experimental Results	96
11.4.1 Dual Irradiation Experiments	96
11.4.2 Decay Associated Spectra	98
11.5 Structures and Coordinates for Computed Species.....	99
12 References	130

1.1 Table of Figures

Figure 3.1-1 Photographs of synthesis stages during preparation of complex 1	10
Figure 3.1-2 Reaction set-up for reaction of 2-trans with N ₂ O	10
Figure 3.1-3 Complex 1 as a solid (left) and in aqueous solution (right)	11
Figure 4.1-1 Concentration-time profile for irradiation of complex 1 with QTH light source	15
Figure 4.2-1 Exemplary liquid phase O ₂ raw data (320 – 500 nm, 1 W intensity setting)	17
Figure 4.2-2 Exemplary liquid phase O ₂ data analyzed as described in 4.2.2 (320 – 500 nm, 1 W intensity setting)	18
Figure 4.3-1 Gas phase O ₂ detection data for irradiation of complex 1 with Hg light source (320 – 500 nm)	21
Figure 4.5-1 Set-up for irradiation on NMR scale	24
Figure 4.5-2 Set-up for irradiation with liquid phase O ₂ detection	24
Figure 4.5-3 Irradiation set-up (liquid phase O ₂ detection) in use (left) and close-up of assembled reactor	25
Figure 5.2-1 Liquid phase O ₂ measurement for H ₂ O ₂ disproportionation catalyzed by complex 1	27
Figure 6.1-1 Spectral power distribution of Hg light source with used filter settings	28
Figure 6.1-2 Measured power of QTH light source with different longpass filters	28
Figure 6.3-1 Chemical actinometry data for different power setting of Hg light source (320 – 500 nm)	29
Figure 7.1-1 ¹ H NMR spectrum of 1 in H ₂ O (298 K)	31
Figure 7.1-2 ³¹ P{ ¹ H} NMR spectrum of 1 in H ₂ O (298 K)	32
Figure 7.1-3 ¹ H NMR spectrum of 1 in DMSO-d ₆ (298 K)	33
Figure 7.1-4 ¹³ C{ ¹ H} NMR spectrum of 1 in DMSO-d ₆ (298 K)	34
Figure 7.1-5 ³¹ P{ ¹ H} NMR spectrum of 1 in DMSO-d ₆ (298 K)	35
Figure 7.1-6 ¹ H NMR spectrum of 1 in H ₂ O (298 K) synthesized using Ag ₂ O	36
Figure 7.1-7 ³¹ P{ ¹ H} NMR spectrum of 1 in H ₂ O (298 K) synthesized using Ag ₂ O	37
Figure 7.1-8 ¹ H NMR of 2-trans in H ₂ O (298 K) after three days of reflux, displaying formation of 1	38
Figure 7.1-9 ³¹ P{ ¹ H} NMR of 2-trans in H ₂ O (298 K) after three days of reflux, displaying formation of 1	39
Figure 7.2-1 ¹ H NMR spectrum of 2-trans in H ₂ O (298 K)	40
Figure 7.2-2 ³¹ P{ ¹ H} NMR spectrum of 2-trans in H ₂ O (298 K)	41
Figure 7.3-1 ¹ H NMR spectrum of (p-cymene)RuCl ₂ (CO) in CD ₂ Cl ₂ (298 K)	42
Figure 7.4-1 ¹ H NMR spectrum of (PNN)RuCl ₂ (CO) in CD ₂ Cl ₂ (298 K)	43
Figure 7.4-2 ³¹ P{ ¹ H} NMR spectrum of (PNN)RuCl ₂ (CO) in CD ₂ Cl ₂ (298 K)	44
Figure 7.5-1 ¹ H NMR spectrum of 1 (in H ₂ O, 298 K) after irradiation with QTH light source for 46h	45
Figure 7.5-2 ³¹ P{ ¹ H} NMR spectrum of 1 (in H ₂ O, 298 K) after irradiation with QTH light source for 46h	46
Figure 7.5-3 ¹ H- ³¹ P HMBC (hydride region) NMR spectrum of 1 (in H ₂ O, 298 K) after irradiation	48
Figure 7.5-4 ¹ H- ³¹ P HMBC (aliphatic region) NMR spectrum of 1 (in H ₂ O, 298 K) after irradiation	49
Figure 7.5-5 ¹ H NMR spectrum of 2-trans (in H ₂ O, 298 K) after irradiation (320 – 500 nm, 4h) in presence of O ₂	50
Figure 7.5-6 ³¹ P{ ¹ H} NMR spectrum of 2-trans (in H ₂ O, 298 K) after irradiation (320 – 500 nm, 4h) in presence of O ₂	51
Figure 7.5-7 ¹ H NMR spectrum of 1 (in 52 mM KOH aq., 298 K, Ag ₂ O synthesis route) in air before irradiation.	52
Figure 7.5-8 ³¹ P{ ¹ H} NMR spectrum of 1 (in 52 mM KOH aq., 298 K, Ag ₂ O synthesis route) in air before irradiation.	53
Figure 7.5-9 ¹ H NMR spectrum of 1 (in 52 mM KOH aq., 298 K, Ag ₂ O synthesis route) in air after irradiation (QTH, 16h)	54
Figure 7.5-10 ³¹ P{ ¹ H} NMR spectrum of 1 (in 52 mM KOH aq., 298 K, Ag ₂ O synthesis route) in air after irradiation (QTH, 16h)	55
Figure 7.6-1 Stacked ¹ H NMR spectra of 1 (in H ₂ O, 298 K) immediately after irradiation (top, green) and same sample after two more days in the dark (bottom, red)	56
Figure 7.6-2 Superimposed ³¹ P{ ¹ H} NMR spectra of 1 (in H ₂ O, 298 K) immediately after irradiation (green) and same sample after two more days in the dark (red)	57
Figure 7.6-3 ³¹ P{ ¹ H} NMR spectrum of 1 (in 52 mM KOH aq., 298 K, Ag ₂ O synthesis route) immediately after irradiation (top) and the same sample after twelve more days in the dark	58
Figure 7.7-1 ¹ H NMR spectrum of raw product (in D ₂ O, 298 K) after reaction of 2-trans with N ₂ O for 20h in presence of 83 equivalents of H ₂ O	59
Figure 7.7-2 ³¹ P{ ¹ H} NMR spectrum of raw product (in D ₂ O, 298 K) after reaction of 2-trans with N ₂ O for 20h in presence of 83 equivalents of H ₂ O	60
Figure 8.1-1 IR Spectrum (ATR) of complex 1 along with theoretical spectrum for [A]S ₀	61
Figure 8.2-1 EPR spectrum of green raw product obtained via reaction of 2-trans with N ₂ O	62
Figure 9.2-1 Decay associated spectra (magic angle polarization) and predicted DAS for [B-Trans]T ₀	64
Figure 9.2-2 Decay associated spectra (magic angle polarization) and predicted DAS for [A]T ₀	64
Figure 9.2-3 Decay associated spectra (magic angle polarization) and predicted DAS for [B]T ₀	65

Figure 10.3-1 Photochemical kinetic model used to describe the two-photon water splitting reaction	67
Figure 11.2-1 UV-Vis spectra computed for [A]S ₀ and [B]T ₀ along with isomers/monomers	73
Figure 11.2-2 Transition 1 (405 nm, f = 0.033) for [A]S ₀ , particle (top) and hole (bottom), isovalue = 0.02	74
Figure 11.2-3 Transition 2 (391 nm, f = 0.0141) for [A]S ₀ , particle (top) and hole (bottom), isovalue = 0.02	75
Figure 11.2-4 Transition 3 (383 nm, f = 0.014) for [A]S ₀ , particle (top) and hole (bottom), isovalue = 0.02	76
Figure 11.2-5 Transition 4 (371 nm, f = 0.0065) for [A]S ₀ , particle (top) and hole (bottom), isovalue = 0.02	77
Figure 11.2-6 Transition 5 (353 nm, f = 0.0596) for [A]S ₀ , particle (top) and hole (bottom), isovalue = 0.02	78
Figure 11.2-7 Transition 6 (352 nm, f = 0.0287) for [A]S ₀ , particle (top) and hole (bottom), isovalue = 0.02	79
Figure 11.2-8 Transition 2 (933 nm, f = 0.0029) for [B]T ₀ , particle (top) and hole (bottom), isovalue = 0.1	80
Figure 11.2-9 Transition 8 (539 nm, f = 0.0066) for [B]T ₀ , particle (top) and hole (bottom), isovalue = 0.1	81
Figure 11.2-10 Transition 2 (804 nm, f = 0.0004) for [B-Mono]D ₀ (Me model), hole (left) and particle (right), isovalue = 0.1	82
Figure 11.2-11 Transition 4 (495 nm, f = 0.0027) for [B-Mono]D ₀ (Me model), hole (left) and particle (right), isovalue = 0.1	82
Figure 11.2-12 Spin density (isovalue = 0.004) for [B]T ₀	83
Figure 11.2-13 Spin density (isovalue = 0.004) for [C]T ₀	84
Figure 11.2-14 Spin density (isovalue = 0.004) for [D]T ₀ [F]S ₀ (Dimer Model)	85
Figure 11.2-15 Energy profile for relaxed PES Scan-[DE]T ₀ (gas phase and SMD energies)	86
Figure 11.2-16 Energy profiles for relaxed PES scans of O-O bond formation	87
Figure 11.3-1 CASSCF energy profile including PCM solvation	90
Figure 11.3-2 Active space orbitals of [B-Mono]D ₀ used for CASSCF(13,11) calculations (isovalue = 0.05)	92
Figure 11.3-3 Singly occupied MO (left, isovalue = 0.05) and spin density (right, isovalue = 0.006) for [B-Mono]D ₀	93
Figure 11.3-4 Unrelaxed transition difference density for [B-Mono]D ₀ → [B-Mono]D ₂	93
Figure 11.3-5 Difference orbitals for [BC] D ₂ /D ₁ MECI with largest population changes (isovalue = 0.05)	94
Figure 11.3-6 Difference orbitals for [BC] D ₁ /D ₀ MECI with largest population changes (isovalue = 0.05)	94
Figure 11.3-7 Singly occupied MO (left, isovalue = 0.05) and spin density (right, isovalue = 0.006) for [C-Mono]D ₀	95
Figure 11.4-1 Dual irradiation data and predicted behavior of [A]S ₀ (scaled)	96
Figure 11.4-2 Dual irradiation data and predicted behavior of [A]T ₀ (scaled)	97
Figure 11.4-3 Dual irradiation data and predicted behavior of [B-Mono]D ₀ (scaled)	98
Figure 11.5-1 [A]S ₀ Structure and Coordinates	99
Figure 11.5-2 [A-RR]S ₀ Structure and Coordinates	100
Figure 11.5-3 [A-RS-1]S ₀ Structure and Coordinates	101
Figure 11.5-4 [A-RS-2]S ₀ Structure and Coordinates	102
Figure 11.5-5 [A]T ₀ Structure and Coordinates	103
Figure 11.5-6 [A-Mono]S ₀ Structure and Coordinates	104
Figure 11.5-7 [B]T ₀ Structure and Coordinates	105
Figure 11.5-8 [B-Mono]D ₀ (Me Model) Structure and Coordinates	106
Figure 11.5-9 [B-Mono]D ₀ Structure and Coordinates	107
Figure 11.5-10 [B-Mono-Up]D ₀ Structure and Coordinates	108
Figure 11.5-11 [B-Trans]T ₀ Structure and Coordinates	109
Figure 11.5-12 [B-Mono-Trans]D ₀ Structure and Coordinates	110
Figure 11.5-13 [B-Mono-Trans-Up]D ₀ Structure and Coordinates	111
Figure 11.5-14 [B-Alt]T ₀ Structure and Coordinates	112
Figure 11.5-15 [BC] D ₁ /D ₀ MECI Structure and Coordinates	113
Figure 11.5-16 [BC] D ₂ /D ₁ MECI Structure and Coordinates	114
Figure 11.5-17 [C]T ₀ Structure and Coordinates	115
Figure 11.5-18 [C-Mono]D ₀ Structure and Coordinates	116
Figure 11.5-19 [C-Mono]D ₀ (Me Model) Structure and Coordinates	117
Figure 11.5-20 TS-[CD]T ₀ Structure and Coordinates	118
Figure 11.5-21 [D]T ₀ [F]S ₀ (Dimer Model) Structure and Coordinates	119
Figure 11.5-22 [D]T ₀ Structure and Coordinates	120
Figure 11.5-23 Scan-[DE]T ₀ Geometry 5 Structure and Coordinates	121
Figure 11.5-24 [E]S ₀ Structure and Coordinates	122
Figure 11.5-25 ³ O ₂ Coordinates	122
Figure 11.5-26 [F]S ₀ Structure and Coordinates	123
Figure 11.5-27 [F-Up]S ₀	124
Figure 11.5-28 [F-Trans]S ₀ Structure and Coordinates	125
Figure 11.5-29 [F-Trans-Up]S ₀ Structure and Coordinates	126
Figure 11.5-30 [F-Cis]S ₀ Structure and Coordinates	127
Figure 11.5-31 [F-Cis-Up]S ₀	128
Figure 11.5-32 [Oxo Dimer]S ₀ Structure and Coordinates	129

1.2 Table of Tables

Table 4.1-1 Optimized parameters for kinetic model	15
Table 4.2-1 H/D kinetic isotope effect and temperature dependence of O ₂ formation	19
Table 4.4-1 Comparison of 2-cis and O ₂ initial rates of formation	23
Table 10.3-1 Optimized parameters for photochemical kinetic model ^[a]	67
Table 10.4-1 Comparison of experimental and predicted reaction probabilities	68
Table 11.2-1 Relative energies of [A]S ₀ and [A-Mono]S ₀	71
Table 11.2-2 Relative energies of [A] isomers	71
Table 11.2-3 Relative energies of [B]T ₀ isomers	71
Table 11.2-4 Relative energies of [B-Mono]D ₀ isomers	72
Table 11.2-5 Relative energy of [B-Alt]T ₀	72
Table 11.2-6 Relative energy of Oxo Dimer	72
Table 11.2-7 Reaction Energy for [F]S ₀ + H ₂ O → [A-Mono]S ₀ + H ₂	72
Table 11.2-8 Relative energies and theoretical NMR data for [F]S ₀ isomers	88
Table 11.3-1 Comparison of DFT and CASSCF reaction energies for [B] → [C] and absorption wavelengths for [B-Mono]D ₀	89

2 Methods and Materials

All experiments involving ruthenium complexes (unless stated otherwise) were carried out under argon using either standard Schlenk technique or in an argon filled glovebox (MBRAUN). Organic solvents were purified using a solvent purification system (Innovative Technology) and stored under argon. Water was purified using a Merck Milli-Q system, followed by degassing using argon sparging and storage under argon. Organic deuterated solvents were degassed using three freeze-pump-thaw cycles and stored over 3 Å molecular sieves. D₂O was distilled under argon.

Carbonylchlorohydridotris(triphenylphosphine)ruthenium(II) ((PPh₃)₃RuCl(CO)H) was purchased from Strem Chemicals, 2-((Di-tert-butylphosphinomethyl)-6-diethylaminomethyl)pyridine (in the following abbreviated as PNN) was purchased from Sigma Aldrich. Potassium *tert*-butoxide was purchased from TCI, nitrous oxide was purchased from Linde and all other chemicals were purchased from Sigma Aldrich. Chemicals were used as received.

(PNN)RuCl(CO)H was prepared as previously described.(1)

Nuclear magnetic resonance (NMR) spectra were recorded on a Bruker AV-300 (300 MHz), AV-400 (400 MHz) or f300 (300 MHz) spectrometer and analyzed using MestreNova. ¹H and ¹³C chemical shifts are reported relative to the respective solvent peak as parts per million. ³¹P chemical shifts are reported relative to 0.3M H₃PO₄ in D₂O (set to δ (³¹P) = -0.425 ppm) as parts per million. Multiplicities are indicated using the following abbreviations: s (singlet), d (doublet), t (triplet), q (quartet), m (multiplet), b (broad).

Infrared spectroscopy was performed using a Bruker-ALPHA FT-IR spectrometer in attenuated total reflectance measurement mode. The following abbreviations are used: br (broad), s (singlet), vs (very strong singlet), m (multiplet).

Electron paramagnetic resonance (EPR) spectroscopy was performed using a X-band Bruker EMX CW-micro EPR spectrometer equipped with an ER4119HS high-sensitivity resonator using a microwave power of ca. 6.9 mW, modulation frequency of 100 kHz and modulation amplitude up to 5 G.

UV/Vis spectroscopy was performed using an Analytik Jena SPECORD S 600 diode array UV/Vis spectrometer (40 ms integration time, 100 accumulations). Fluorescence spectroscopy was performed using a Cary Eclipse fluorescence spectrometer (Agilent), with 20 nm slit widths for excitation and emission (excitation wavelength: 370 nm).

Elemental analysis was performed using a Leco TruSpec Micro CHNS analyzer.

Oxygen measurements were performed using a FireStingO2 optical oxygen meter (PyroScience GmbH) along with trace range robust probes (PyroScience GmbH, for liquid phase measurements) or trace range oxygen sensor spots (PyroScience GmbH, for gas phase measurements). Temperature compensation was done using a Pt100 temperature sensor (Therma ThermoFühler GmbH).

Irradiation was performed using two different light sources:

(a) A Lumatec SUPERLITE S 04 with a liquid light guide (Lumatec, light guide diameter: 1 cm). This is a mercury vapor light source with an integrated filter wheel to select different wavelength regions (for the spectral power distribution of the selected filter configurations, see Figure 6.1-1). This light source is referred to as the "Hg light source" in the following.

(b) A 250 W quartz tungsten halogen (abbreviated as QTH) Research Light Source with a F/1, 1.5 inch, two element, plano convex condenser (Newport). The light source was equipped with a 6 cm quartz distilled water filter (Quantum Design), which filters out all wavelengths below 280 nm and above 1000 nm, and a manual light source shutter (Newport). Furthermore, the light source was combined with different colored class alternative longpass filters (Newport) to further control the irradiation wavelengths. This light source is referred to as the "QTH light source" in the following.

3 Synthesis Procedures and Characterization

3.1 Synthesis of Complex 1

3.1.1 Synthesis using N₂O

Complex 1 was synthesized following a modified version of the previously reported procedure.(2)

(PNN)RuCl(CO)H (302.5 mg, 0.62 mmol) and KOtBu (69.5 mg, 0.62 mmol) were placed in a Schlenk flask, followed by addition of 30 ml Et₂O, yielding a dark red suspension. The suspension was stirred at room temperature for one hour, yielding a dark red solution with a small amount of solid (KCl). The solution was filtered into a separate Schlenk flask to remove the formed KCl and then the solvent was removed under vacuum, yielding a black-red solid of (PNN*)Ru(CO)H (PNN* indicates dearomatization of the PNN ligand). (PNN*)Ru(CO)H was directly used for the next reaction step without further purification and assuming quantitative conversion.

To the Schlenk flask containing (PNN*)Ru(CO)H, 16 ml THF were added, yielding a dark red solution (see Figure 3.1-1). To this solution, 9 equivalents of H₂O (100 µl, 5.6 mmol) were added, resulting in an immediate color change from dark red to dark yellow/orange (see Figure 3.1-1) due to formation of complex **2-trans**. It is important at this stage to add no more than 9 equivalents of H₂O, as the presence of more water leads to a different reaction product (see Figure 7.7-1) when **2-trans** is exposed to N₂O.

The THF solution of **2-trans** containing 9 equivalents of H₂O was transferred to a separate reaction assembly (see Figure 3.1-2), where it was sparged with N₂O for 10 – 20 min. Afterwards, the Schlenk flask containing the solution of **2-trans** was closed under a N₂O atmosphere and was stirred at room temperature in the dark for 22 h. After the reaction time, a dark green solution was formed (see Figure 3.1-1). If more than 9 equivalents of water were present in the reaction solution, a dark red solution was formed instead, containing the different reaction product shown in Figure 7.7-1.

The dark green solution was concentrated in volume by roughly half, followed by addition of 100 ml Et₂O, leading to precipitation of a solid. The solid was filtered off, washed three times with 1 ml Et₂O each and dried under vacuum, yielding **1** as a yellow solid (70 mg, 23% yield with respect to (PNN)Ru(CO)ClH, see Figure 3.1-3). The final product typically contains up to 3% of unreacted **2-trans**, which could not be removed. Unfortunately, repeated attempts to crystallize **1** were unsuccessful.

We would like to note at this point that complex **1** is in fact a yellow solid, yielding a yellow solution in H₂O (see Figure 3.1-3), and not a green solid yielding a green aqueous solution as described before.(2) The green color of the solution after reaction with N₂O can be attributed to Ru(III) species, which are formed as side products during the reaction (see Figure 8.2-1 for an EPR spectrum of the green raw product after reaction with N₂O). Complex **1**, however is an EPR inactive Ru(II) species. The green color of the final product, which was previously described, might therefore be attributed to some residual Ru(III) species. These residual Ru(III) species might also explain the additional absorption features in the originally reported UV/Vis spectrum(2) compared to our UV/Vis spectrum. Furthermore, we found that in chlorinated solvents (such as dichloromethane, DCM), **1** can be converted to chloride complexes (possibly due to reaction with trace amounts of HCl present in the solvent). We therefore avoided the use of chlorinated solvents with **1**.

Spectroscopic data for **1**:

¹H NMR (400 MHz, H₂O, r.t.) δ 7.37 (t, J = 7.9 Hz, 1H, py-H⁴), 7.10 (d, J = 7.9 Hz, 1H, py-H³), 7.00 (d, J = 7.8 Hz, 1H, py-H⁵), 3.87 (dd, J = 15.3, 3.2 Hz, 1H, py-NCH₂), 3.75 (d, J = 15.2 Hz, 1H, py-NCH₂), 3.48 (dd, J = 17.5, 10.9 Hz, 1H, py-PCH₂), 3.04 (dd, J = 17.4, 7.4 Hz, 1H, py-PCH₂), 2.79 (dq, J = 13.9, 6.9 Hz, 1H, CH₂CH₃), 2.50 (dq, J = 14.4, 7.2 Hz, 1H, CH₂CH₃), 2.45 – 2.29 (m, 2H,

CH_2CH_3), 1.02 (d, $J = 14.5$ Hz, 9H, $P(C(CH_3)_3)_2$), 0.76 (t, $J = 7.0$ Hz, 3H, CH_2CH_3), 0.71 (t, $J = 7.1$ Hz, 3H, CH_2CH_3), 0.68 (d, $J = 13.0$ Hz, 9H, $P(C(CH_3)_3)_2$) ppm. (see Figure 7.1-1)

1H NMR data is provided in H_2O since it avoids disappearance of methylene protons (which occurs for D_2O). In the 1H NMR spectrum of **1** in DMSO- d_6 , a broadened singlet can be observed at $\delta(^1H) = 4.22$ ppm, integrating to 2H (see Figure 7.1-3). This signal might be attributed to the two hydroxo protons,(3) being shifted significantly downfield compared to the previously described value of $\delta(^1H) = -7.4$ due to interaction with DMSO- d_6 .

^{13}C NMR (101 MHz, DMSO- d_6 , r.t.) δ 207.92 (d, $J = 15.1$ Hz, CO), 164.41 (s, py- C^3), 160.55 (s, py- C^5), 138.51 (s, py- C^4), 122.22 (d, $J = 8.1$ Hz, py- C^6), 120.97 (s, py- C^2), 62.10 (s, py- NCH_2), 51.00 (s, CH_2CH_3), 44.17 (s, CH_2CH_3), 37.78 (d, $J = 12.9$ Hz, $P(C(CH_3)_3)_2$), 37.60 (d, $J = 24.8$ Hz, py- PCH_2), 36.51 (d, $J = 15.0$ Hz, $P(C(CH_3)_3)_2$), 30.48 (d, $J = 3.6$ Hz, $P(C(CH_3)_3)_2$), 28.97 (d, $J = 2.6$ Hz, $P(C(CH_3)_3)_2$), 9.28 (s, CH_2CH_3), 8.87 (s, CH_2CH_3) ppm. (see Figure 7.1-4)

$^{31}P\{^1H\}$ NMR (162 MHz, DMSO- d_6 , r.t.) δ 92.56 (s, P^tBu_2) ppm. (see Figure 7.1-5)

$^{31}P\{^1H\}$ NMR (162 MHz, H_2O , r.t.) δ 88.24 (s, P^tBu_2) ppm. (see Figure 7.1-2)

IR (ATR): $\tilde{\nu} = 3393$ br (OH), 2948m, 1917vs (CO), 1568s cm^{-1} . (see Figure 8.1-1)

UV/Vis (H_2O): λ_{abs} ($\epsilon / cm^{-1} M^{-1}$) = 370 (1630), 305 (3510).

Elemental analysis: anal. calc. for $C_{20}H_{37}N_2O_3PRu \bullet 3 H_2O$: C, 44.52; H, 8.03; N, 5.19. Found: C, 44.25; H, 8.078; N, 5.002.

3.1.2 Photographs Showing Synthesis and Product



Figure 3.1-1 Photographs of synthesis stages during preparation of complex 1

Left: Solution of $[\text{Ru}(\text{PNN}^*)(\text{CO})\text{H}]$ in THF (dark red solution).

Middle: Solution on the left after addition of 9 equivalents of H_2O , forming complex **2-trans** (dark yellow/orange solution).

Right: Solution in the middle after reaction with N_2O for 22h (dark green solution).

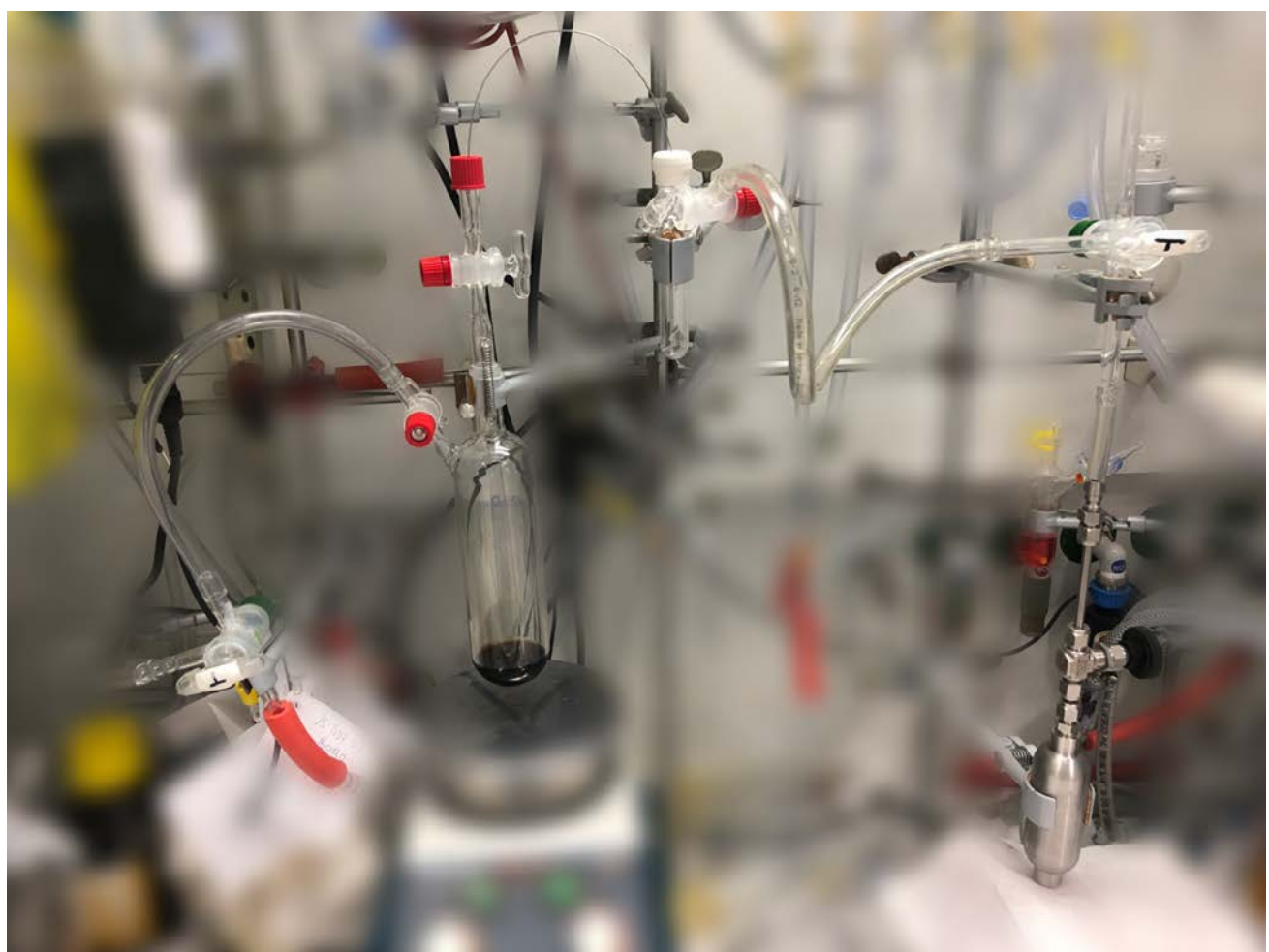


Figure 3.1-2 Reaction set-up for reaction of 2-trans with N_2O

From right to left: N_2O gas tank (right bottom) is connected to a T-piece (right), which leads to the Schlenk line (top connection) and to a Schlenk flask (top middle). This Schlenk flask is topped with a rubber septum containing a cannula (top), which leads into the main reaction flask (containing **2-trans**) through a septum (red cap) and a valve. The main reaction flask is connected to a second T-piece valve (left), which leads to the Schlenk line (bottom) and to a separate bubble counter (left). Background is blurred to highlight the reaction assembly.



Figure 3.1-3 Complex 1 as a solid (left) and in aqueous solution (right)

3.1.3 Synthesis using Ag₂O

(PNN)RuCl₂(CO) (66 mg, 0.126 mmol, mixture of cis and trans isomers) and Ag₂O (179 mg, 0.772 mmol) were placed in a Schlenk flask along with 4.5 ml of acetone and 0.6 ml of H₂O, yielding a dark yellow suspension. The suspension was stirred for 2 h in the dark, after which it was filtered into a separate Schlenk flask, yielding a dark yellow solution. Subsequently, all volatiles were removed under vacuum and the dark yellow residue was redissolved in 2.1 ml THF, yielding a dark yellow solution with some insoluble material. The insoluble materials were removed via filtration, and 18 ml Et₂O were added to the dark yellow THF solution to precipitate the product. The solid was filtered off, washed three times with 1 ml Et₂O each and dried under vacuum, yielding a yellow solid.

While this synthesis procedure does yield complex **1** (see Figure 7.1-6 and Figure 7.1-7 for NMR spectra of the product), the obtained product is less pure than the one obtained via the N₂O synthesis route. The main impurity can be observed at $\delta(^{31}\text{P}) = 55.12$ ppm, which might be attributed to an alkyl phosphinic acid resulting from ligand oxidation by Ag₂O. Due to the less pure nature of the product, the N₂O synthesis route was the preferred one. However, further improvements to this silver based synthesis route might offer a more simple and general access to ruthenium dihydroxo complexes.

3.1.4 Synthesis via Reflux of 2-trans

This is a modified version of the previously described procedure for the synthesis of **1** via reflux of **2-trans**.(2)

(PNN*)Ru(CO)H was synthesized as described in 3.1.1, using 53 mg (0.109 mmol) of (PNN)RuCl(CO)H. To the Schlenk flask containing solid (PNN*)Ru(CO)H, 2.5 ml of H₂O were added, yielding a clear, light yellow solution of **2-trans**.

The solution was then refluxed for three days, during which time the color of the solution changed to dark red/orange and a small amount of black, insoluble material formed.

At the end of the reaction time, the solution was cooled to room temperature and analyzed using NMR spectroscopy (see Figure 7.1-8 and Figure 7.1-9), showing formation of **1** along with unreacted **2-trans** and other, unidentified reaction products. The obtained product was not isolated.

3.2 Synthesis of Complex **2-trans**

3.2.1 Synthesis in H₂O

Complex **2-trans** was synthesized in H₂O as described in 3.1.4, yielding a clear, light yellow solution. The obtained product was analyzed using NMR spectroscopy (see Figure 7.2-1 and Figure 7.2-2) and was not isolated. Obtained NMR data was consistent with the previously described.(2)

3.2.2 Crystallization of **2-trans**

(PNN*)Ru(CO)H (31 mg, 0.069 mmol, synthesized as described in 3.1.1) was dissolved in 1.1 ml toluene, yielding a dark red solution. To this solution, 9 equivalents of H₂O (11 µl, 0.61 mmol) were added, leading to a rapid color change to form a clear orange solution with a small aqueous phase at the bottom. The organic phase was transferred to a separate Schlenk flask and stored at -32 °C overnight, yielding colorless/light yellow crystals. In an ice bath, the liquid phase was removed using a syringe and the crystals were washed twice with 0.4 ml ice-cold heptane.

The thus obtained crystals were used in both the N₂O and reflux synthesis route for complex **1**, yielding the same results as in situ prepared **2-trans** (as described above).

When the aqueous phase of this synthesis (still containing some of the toluene phase as well) was stored at room temperature for one day, colorless, plate-shaped crystals of **2-trans** suitable for X-ray crystallography were formed.

3.3 Synthesis of (p-cymene)RuCl₂(CO)

(p-cymene)RuCl₂(CO) was prepared using a previously described procedure.(4)

In a 50 ml Schlenk flask (internal volume ca. 65 ml), a orange/red solution of [(p-cymene)RuCl₂]₂ (200 mg, 0.33 mmol) in 4 ml DCM was placed under vacuum using freeze-pump-thaw and warmed back to room temperature. Subsequently, 16 ml of CO gas (ca. 0.66 mmol, 2 equivalents) were injected into the Schlenk flask through a septum using a gas-tight syringe. The solution was then stirred at room temperature for 45 min, during which the color changed to deep red. Subsequently, the solvent was removed, yielding a salmon pink solid (187 mg, 85% yield). Characterization by NMR spectroscopy (see Figure 7.3-1) was consistent with the previously reported data.(4)

3.4 Synthesis of (PNN)RuCl₂(CO)

(p-cymene)RuCl₂(CO) (375 mg, 1.12 mmol) was suspended in THF (10 ml) and a solution of PNN (376 mg, 1.17 mmol in 15 ml THF) was added, yielding a red suspension. It was then refluxed for 15 h, yielding an orange solution with a yellow solid. The reaction solution was cooled to room temperature and stored at -32 °C overnight, leading to precipitation of more yellow solid. After warming back to room temperature, the volume of the reaction solution was reduced by ca. 70% under vacuum, followed by addition of 80 ml of heptane. The solid was filtered off from the yellow suspension and washed three times with 4 ml of heptane, followed by drying under vacuum. This yielded a yellow solid (457 mg, 78% yield with respect to (p-cymene)RuCl₂(CO)). Characterization by NMR spectroscopy showed the presence of a mixture of the cis and trans isomers (see Figure 7.4-1 and Figure 7.4-2, ca. 3% of impurity are visible at $\delta(^{31}P) = 74.57$ ppm) and the obtained data was consistent with the previously reported.(5)

4 Procedures for Irradiation and Subsequent Data Analysis

4.1 NMR Scale Irradiation

4.1.1 Irradiation Procedure

550 μl of a 0.01M solution of **1** (prepared via the N_2O synthesis route) in H_2O was placed inside a J. Young NMR tube along with a flame sealed capillary containing a 0.3M H_3PO_4 solution in D_2O . ^1H and quantitative $^{31}\text{P}\{^1\text{H}\}$ NMR spectra were then recorded before irradiation. Subsequently, the NMR tube was irradiated with either the QTH or Hg light source (or both) while being cooled with a 20 W fan (for the irradiation set-up see Figure 4.5-1).

For the concentration-time profile experiments, only the QTH light source was used for irradiation, being equipped with the distilled water filter. The total irradiation time was 46.5 h. For dual irradiation experiments, either or both light sources were used, the Hg light source being filtered to 320 – 400 nm (see Figure 6.1-1, fixed intensity setting) and the QTH light source being equipped with a > 495 nm longpass filter in addition to the distilled water filter. For each dual irradiation experiment, the irradiation time was 17 h. In all cases care was taken not to alter the positioning of either the NMR tube or light sources between experiments, so as not to change the photon flux received by the NMR tube. QTH and Hg light sources were arranged at a 90° angle.

After irradiation with the QTH light source (no longpass filter) or Hg light source, the color of the solution changed to yellow/orange. In case of irradiation with the QTH light source equipped with a > 495 nm longpass filter, no color change occurred. Immediately after irradiation, ^1H and quantitative $^{31}\text{P}\{^1\text{H}\}$ NMR spectra were recorded.

Irradiation experiments could also be performed in the same way using complex **1** prepared via the Ag_2O synthesis route. In this case, however, **1** had to be dissolved in a 52 mM aqueous KOH solution instead of pure H_2O . This was likely necessary to compensate for the weakly acidic nature of **1** obtained via the Ag_2O route (likely due to the phosphinic acid impurity). When irradiation of **1** (Ag_2O route) was performed in 52 mM KOH aq., the results were effectively identical to those obtained using the above described procedure. For simplicity, however, all reported experiments (except noted otherwise) were performed using **1** obtained via the N_2O synthesis route in pure H_2O .

4.1.2 Interpretation of NMR Results

Irradiation with either the QTH light source (no longpass filter) or Hg light source resulted in the same qualitative changes as observed by NMR spectroscopy. Figure 7.5-1 and Figure 7.5-2 show representative examples of ^1H and $^{31}\text{P}\{^1\text{H}\}$ spectra recorded after irradiation, respectively. In the ^1H spectrum, appearance of a new hydride signal at $\delta(^1\text{H}) = -5.24$ ppm can be observed. In the $^{31}\text{P}\{^1\text{H}\}$ spectrum, the major changes are a significant reduction in signal intensity for $\delta(^{31}\text{P}) = 88.22$ ppm (complex **1**), and the appearance of two new signals at $\delta(^{31}\text{P}) = 104.36$ ppm and $\delta(^{31}\text{P}) = 95.12$ ppm (along with some smaller signals).

Through $^1\text{H}-^{31}\text{P}$ HMBC (see Figure 7.5-3) it could be established that the hydride at $\delta(^1\text{H}) = -5.24$ ppm and the $\delta(^{31}\text{P}) = 104.36$ ppm signal are coupled, showing that this is a species distinct from **2-trans** ($\delta(^1\text{H}) = -18.9$ ppm, $\delta(^{31}\text{P}) = 104.2$ ppm, see Figure 7.5-3). However, it can be observed that in the dark (over the course of hours and days), the $\delta(^{31}\text{P}) = 104.36$ ppm species converts to **2-trans** (see Figure 7.6-1 and Figure 7.6-2). Furthermore, when **2-trans** is irradiated (Hg light source, 320 – 500 nm) in the presence of O_2 , it converts to the $\delta(^{31}\text{P}) = 104.36$ ppm species (see Figure 7.5-5 and Figure 7.5-6). The interconversion of these two species indicates that they are isomers. When comparing their NMR characteristics, the biggest difference is the significantly downfield shifted hydride signal at $\delta(^1\text{H}) = -5.24$ ppm for the $\delta(^{31}\text{P}) = 104.36$ ppm species. Such a chemical shift is consistent with the hydride being trans to a CO ligand.^(6, 7) This is corroborated by DFT calculations for different isomers of **2**, which predict a change of ca. 10 ppm for the hydride signal when the hydride ligand is trans to the CO ligand (see Table 11.2-8), as compared to being trans to

the OH ligand (as is the case for **2-trans**). Furthermore, DFT calculations predict **2-cis** (where the hydride ligand is trans to CO and the OH ligand is in the equatorial position) to be less stable than **2-trans** by more than 10 kcal/mol. This difference in stability would explain the spontaneous conversion of the $\delta(^{31}\text{P}) = 104.36$ ppm species to **2-trans**. Based on the characteristic hydride shift and these DFT results, we therefore assign the $\delta(^{31}\text{P}) = 104.36$ ppm species to **2-cis**.

The second major product of irradiation can be observed at $\delta(^{31}\text{P}) = 95.12$ ppm. For this species, the phosphorous signal couples to two different tert-butyl groups (see ^1H - ^{31}P HMBC of aliphatic region in Figure 7.5-4). This indicates that, just like complex **1**, this complex has no symmetry, resulting in two chemically distinct tert-butyl groups. This observation rules out that this species is the trans isomer of **1**. In the dark, the species slowly converts back to **1** (see Figure 7.6-3, in this case the experiment was performed using **1** prepared via the Ag_2O route in 52 mM KOH aq., but the same is observed using the standard reaction conditions). We tentatively assign this species to **Oxo Dimer**, an oxo-bridged dimer formed via formal dehydration of **1** (see Figure 11.5-32 for the computed structure). DFT calculations predict **Oxo Dimer** to be slightly less stable than **1**, explaining why slow hydrolysis back to **1** might occur in the dark. Furthermore, a reasonable pathway for photochemical **Oxo Dimer** formation can be proposed based on Ru-O bond formation in intermediate $[\text{B-Trans}]\text{T}_0$ (see 9.2).

Due to these isomerization reactions, NMR spectra for quantitative analysis were recorded immediately after irradiation.

4.1.3 Data Analysis for Concentration-Time Profile

For the concentration-time profile, quantitative $^{31}\text{P}\{^1\text{H}\}$ NMR spectra were recorded before ($t = 0$ h) and after 0.75, 2.97, 21.07, 24.44, 42.54 and 46.45 h of irradiation (irradiation of the sample was stopped after the indicated time, NMR spectra were recorded and irradiation was then resumed). For each time point, the relative concentrations of **1**, **2-cis** and **Oxo Dimer** were determined via integration of the corresponding $^{31}\text{P}\{^1\text{H}\}$ NMR signals. For $t = 0$ h, a small amount of **2-trans** could be observed, which was treated as **2-cis** in the following (since **2-trans** can photochemically convert to **2-cis**, see above). Therefore, the amount of **2-cis** at $t = 0$ h is not equal to zero. For all subsequent time points, no **2-trans** was observed.

For data analysis, the concentrations of **1**, **2-cis** and **Oxo Dimer** were normalized, so that for each time point the sum of the concentrations for these three compounds would be equal to one. This normalization ignores the formation of other products. However, since the amount of side products observable by $^{31}\text{P}\{^1\text{H}\}$ spectroscopy amounts to only around 7% after 46.45 h of irradiation this was deemed acceptable.

The resulting, normalized concentrations of **1**, **2-cis** and **Oxo Dimer** are shown in Figure 4.1-1 as dots. These datapoints were then fitted with a kinetic model based on the reaction network shown in Table 4.1-1, with k_1 , k_2 and k_3 being the optimization parameters. Fitting was performed via the following steps:

1. Converting the reaction network to the corresponding rate laws describing the time-dependent concentration changes of **1**, **2-cis** and **Oxo Dimer**;
2. At each optimization step, numerically solving the resulting system of differential equations with an updated guess for k_1 , k_2 and k_3 (generated using the L-BFGS-B algorithm), until convergence was reached. The optimized parameters for k_1 , k_2 and k_3 are shown in Table 4.1-1.

From the data shown in Figure 4.1-1 it can be seen that **Oxo Dimer** is not an intermediate formed en route to **2-cis**, as the rate of **2-cis** formation does not increase with increasing **Oxo Dimer** concentration.

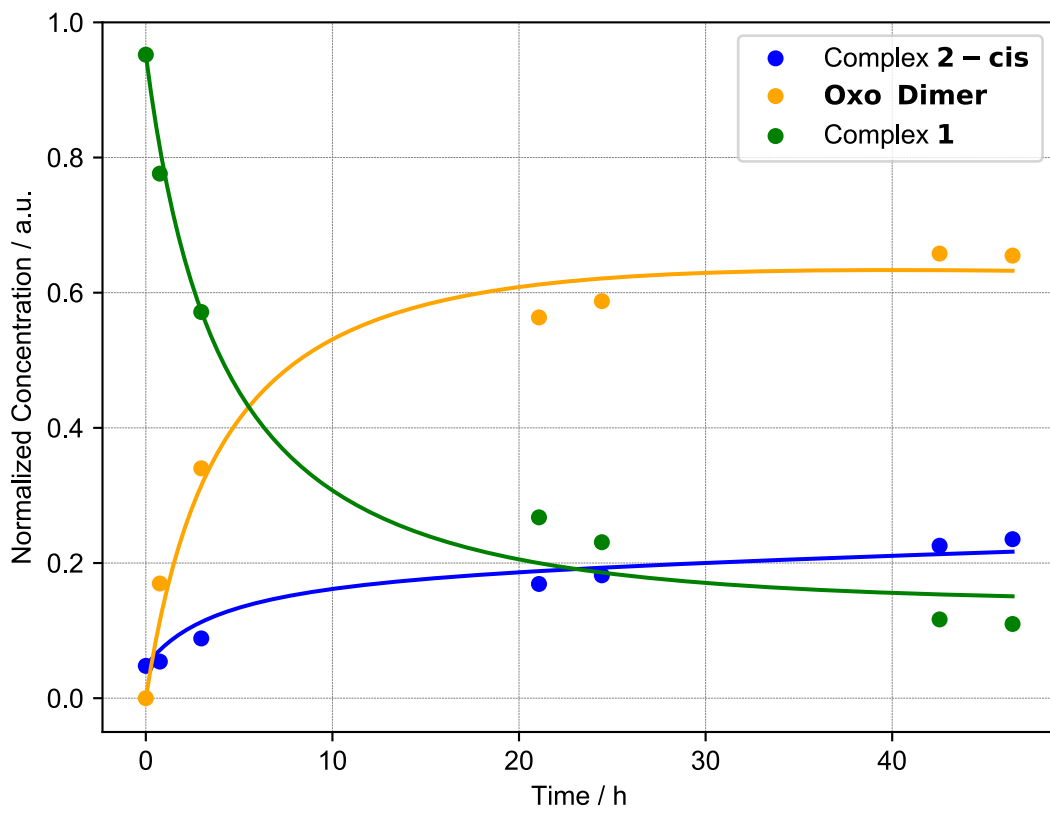


Figure 4.1-1 Concentration-time profile for irradiation of complex 1 with QTH light source

Dots show normalized concentrations obtained via integration of NMR spectra measured after indicated irradiation times. Straight lines are kinetic fit obtained using the kinetic model: $\text{1} + \text{1} \rightarrow \text{Oxo Dimer}$ (k_1), $\text{1} + \text{1} \rightarrow 2 \text{ 2-cis}$ (k_2), and $\text{Oxo Dimer} \rightarrow \text{1} + \text{1}$ (k_3).

Table 4.1-1 Optimized parameters for kinetic model

$\text{Oxo Dimer} \xrightleftharpoons[k_3]{k_1} 2 \text{ 1} \xrightarrow{k_2} 2 \text{ 2-cis (+ O}_2\text{)}$		
k_1 / h^{-1}	k_2 / h^{-1}	k_3 / h^{-1}
0.197	0.04	0.0076

4.1.4 Data Analysis for Dual Irradiation

For the dual irradiation data set, two irradiation experiments using only the Hg light source (320 – 400 nm), two experiments using both the Hg light source (320 – 400 nm) and the QTH light source (> 495 nm) as well as one experiment using only the QTH light source (> 495 nm) were performed.

For each experiment, quantitative $^{31}\text{P}\{\text{H}\}$ NMR spectra were recorded before and after irradiation. Relative concentrations of **1**, **2-trans** (before irradiation), **2-cis** (after irradiation), **Oxo Dimer** and an unidentified byproduct at $\delta(^{31}\text{P}) = \sim 97$ ppm were determined via integration. For each experiment, concentrations were normalized so that the sum of the concentrations of all components would be the same before and after irradiation. When comparing the different experiments, the sum of all normalized concentrations differed at most 4% between them.

For each experiment, the yield of **2-cis** was determined by subtracting the normalized concentration of **2-trans** before irradiation from the normalized concentration of **2-cis** after irradiation. This was done to correct for any **2-cis** that was formed via photochemical isomerization of **2-trans**. The thus

obtained corrected concentration of **2-cis** was divided by the sum of all concentrations for the experiment to give the yield of **2-cis**. Reported yields for irradiation with either the Hg light source (320 – 400 nm) or both light sources are the averages of two separate irradiation experiments.

4.2 Liquid Phase O₂ Measurement

4.2.1 Irradiation Procedure

A 5 ml Schlenk flask with a GL14-threaded neck was equipped with a 5 mm PTFE stirring bar and a trace range robust O₂ probe, positioned so that it would later be immersed in the liquid phase (see Figure 4.5-3). The O₂ probe was connected to the Schlenk flask in a gas tight manner via the GL14-threaded neck with a 3 mm BOLA laboratory screw joint.

The Schlenk flask was then connected to the Schlenk line using a T-piece adapter, with one connection to the Schlenk line, one to the Schlenk flask and one connection being closed with a septum. Subsequently, ca. 500 - 550 µl of an aqueous solution of **1** (prepared via the N₂O synthesis route, 0.01 or 0.005 M concentration, it was confirmed that both concentrations gave the same results, see 4.2.6) was transferred into the Schlenk flask. The transfer was done via cannula transfer through the septum inlet of the T-piece adapter and through the valve of the Schlenk flask, taking care not to introduce any external O₂ into the flask.

Once the transfer was complete, the Schlenk flask was closed and placed into a double-walled beaker filled with water (see Figure 4.5-2 and Figure 4.5-3), which was thermostatted to 16.5 °C (unless stated otherwise). A PT100 temperature sensor (for temperature compensation of the O₂ measurement) was placed next to the Schlenk flask into the same water bath and the whole assembly was allowed to equilibrate for 15 – 20 min while being stirred at 1400 rpm.

After equilibration, the baseline O₂ concentration was typically measured for 15 – 30 min. Afterwards the flask was irradiated for 240 – 400 s. In case of the intensity dataset, irradiation was performed using the Hg light source (320 – 500 nm) with variable intensity settings. The same light source was used to measure the kinetic isotope effect and temperature dependence of the reaction. For the dual irradiation dataset, irradiation was performed using the Hg light source (320 – 400 nm), the QTH light source (different longpass filters), or both. When both light sources were used, the shutters of both were opened simultaneously. See Figure 4.5-2 and Figure 4.5-3 for the irradiation set-ups. In all cases, care was taken not to alter the position of the light sources or the reactor between experiments, so as not to change the photon flux received by the reactor. Hg and QTH light source were arranged at a 90° angle.

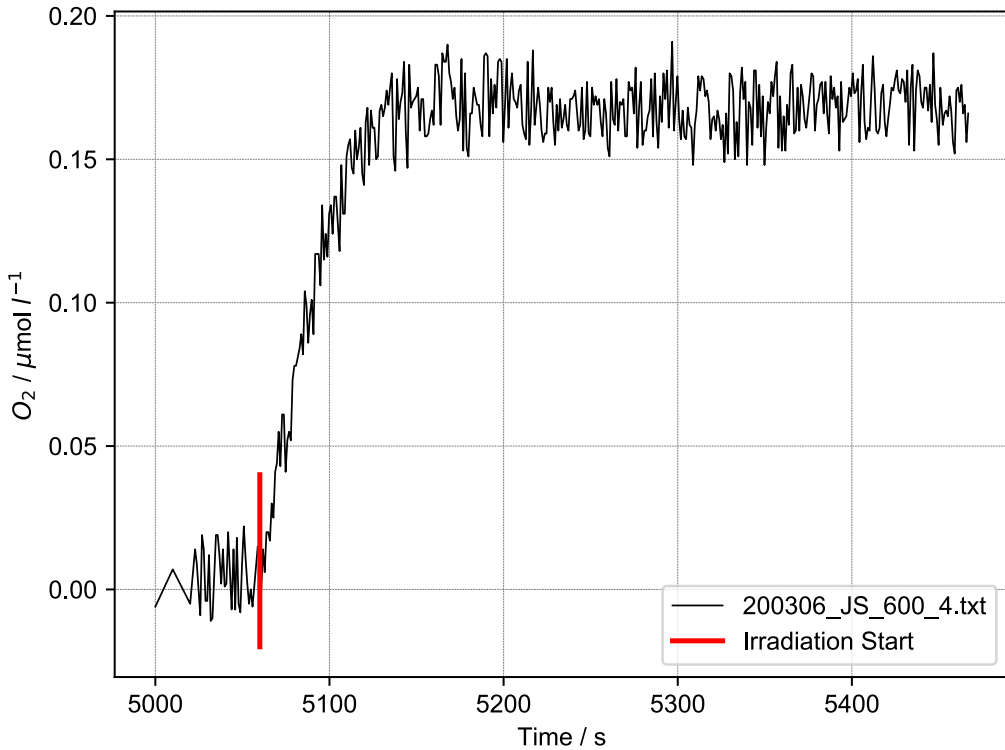


Figure 4.2-1 Exemplary liquid phase O₂ raw data (320 – 500 nm, 1 W intensity setting)

4.2.2 General Remarks on Data Analysis

For data analysis, the irradiation start point was set to $t = 0$ s. Furthermore, the baseline O₂ concentration was calculated using the average of all datapoints recorded before irradiation start and subtracted from the datapoints, so that $[O_2](t = 0 \text{ s}) = 0 \mu\text{mol/l}$.

To determine reaction rates, the following rate law was used:

$$\frac{d[O_2]}{dt} = k_0 - k_1[O_2] \quad \text{Equation (1)}$$

For this rate law, O₂ is assumed to be formed in a zero-order reaction with rate constant k_0 and to be consumed in a first-order reaction with rate constant k_1 . The assumption that O₂ is formed in a zero-order reaction stems from the fact that O₂ concentrations are only measured in the initial reaction phase, where the concentration change of 1 is negligible. The first order reaction consuming O₂ can be seen as an overall description of O₂ loss in the liquid phase due to diffusion into the gas phase and due to consumption by side reactions (see 4.3.2), both of which can be assumed to be first order in O₂ in the initial reaction phase.

When integrated, Equation (1) gives the following function:

$$[O_2](t) = [O_2]_0 e^{-k_1 t} - k_0 e^{-k_1 t} \frac{1}{k_1} + \frac{k_0}{k_1} \quad \text{Equation (2)}$$

With $[O_2]_0$ being the O₂ concentration at $t = 0$ s (which is equal to zero given our preprocessing). Equation (2) was fitted to all datapoints from $t = 0$ s until the end of irradiation, optimizing the parameters k_0 and k_1 . k_0 is not only the zero-order rate constant for O₂ formation but also the initial rate of O₂ formation (since $[O_2]_0 = 0 \mu\text{mol/l}$, unit of initial rate is $\mu\text{mol l}^{-1} \text{s}^{-1}$). k_1 is the overall observed rate constant for the disappearance of O₂ (due to diffusion and side reactions).

To obtain k_0 with higher precision (for kinetic isotope effect, temperature dependence and dual irradiation data sets), a second analysis procedure was also used (“average k_1 procedure”): for this

procedure, Equation (2) was first fitted to the data optimizing both k_0 and k_1 . Within one group of experiments (e.g. all experiments with the same intensity and temperature), the average k_1 value was determined. Afterwards, Equation (2) was fitted to the data of each experiment in the group again, this time fixing k_1 to be the group's average value. Therefore, only k_0 has to be optimized and it is obtained with higher precision.

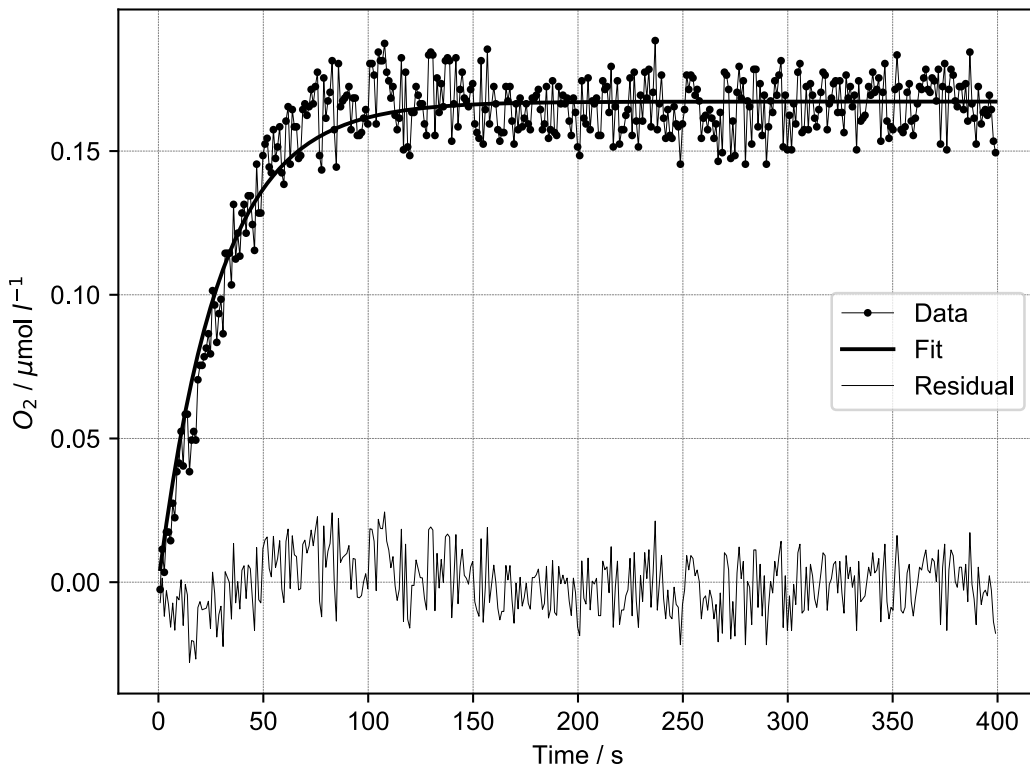


Figure 4.2-2 Exemplary liquid phase O_2 data analyzed as described in 4.2.2 (320 – 500 nm, 1 W intensity setting)

4.2.3 Data Analysis for Intensity Experiments

For the intensity dataset, irradiation was performed with five different intensity settings for the Hg light source (320 – 500 nm): 0.25, 0.375, 0.5, 0.75 and 1 W (the power values are not identical to the power received by the reactor, but they are proportional, see Chemical Actinometry section). For each intensity setting, at least two experiments were performed. Initial rates were calculated as described in 4.2.2 and for each intensity setting, the average of the corresponding experiments is reported (maximum deviation between experiments: $0.0005 \mu\text{mol l}^{-1} \text{s}^{-1}$). In case of the intensity dataset, no difference was observed whether the average k_1 procedure was used or not. Temperature changes during irradiation were negligible (typically below 0.6°C on the highest intensity setting).

The obtained initial rates were then fitted with a square function ($f(x) = ax^2$), optimizing only a . This showed that the dependence of initial O_2 formation rate on intensity can be described well using a square relationship.

4.2.4 Data Analysis for Kinetic Isotope Effect and Temperature Dependence

To determine a possible H/D kinetic isotope effect (KIE), the standard irradiation procedure was used, but instead of H_2O , **1** was dissolved in D_2O (due to rapid exchange of hydroxo protons, the deuterated derivative of **1** is quickly formed). Irradiation was performed using the Hg light source

(320 – 500 nm) with the 1 W intensity setting. Two separate experiments in D₂O were performed and initial rates were calculated as described in 4.2.2, using the average k_1 procedure, and then averaged. As a reference, 1 W experiments from the intensity dataset were used, which were also analyzed using the average k_1 procedure and averaged. The obtained H/D KIE is 1.18.

To determine a possible temperature dependence of the reaction, the standard irradiation procedure was used, but instead of setting the thermostat temperature to 16.5 °C, it was set to 26.5 °C. Irradiation was performed using the Hg light source (320 – 500 nm) with the 1 W intensity setting. Two separate experiment at 26.5 °C were performed and initial rates were calculated as described in 4.2.2, using the average k_1 procedure, and then averaged. As a reference, 1 W experiments from the intensity dataset were used, which were also analyzed using the average k_1 procedure and averaged. The obtained ratio of initial rates at 16.5 °C and 26.5 °C is 0.78. The fact that the observed initial rate is in fact slightly slower at higher temperature might be attributed to accelerated, thermal side reactions consuming O₂.

Table 4.2-1 H/D kinetic isotope effect and temperature dependence of O₂ formation

$\frac{k_0(H)}{k_0(D)}$	$\frac{k_0(26.5 \text{ } ^\circ\text{C})}{k_0(16.5 \text{ } ^\circ\text{C})}$
1.18	0.78

4.2.5 Data Analysis for Dual Irradiation Experiments

For the dual irradiation dataset, there are three distinct groups of experiments:

1. Irradiation using the Hg light source (320 – 400 nm, 0.3 W intensity setting)
2. Irradiation using the QTH light source (different longpass filters)
3. Irradiation using both the Hg (320 – 400 nm, 0.3 W intensity setting) and QTH (different longpass filters) light source (dual irradiation)

The QTH light source was used with five different longpass filters: 455 nm, 495 nm, 550 nm, 590 nm and 630 nm cut-on wavelength. For irradiation using the QTH light source or dual irradiation, there are thus five subgroups each, corresponding to each longpass filter.

For the dual irradiation dataset it was found that data analysis could be improved (lower spread of initial rates for reproduction experiments) by correcting the analysis start point: instead of fitting Equation (2) from the start of irradiation, the start point was shifted forward to the point minimizing the residual for the fit of Equation (2) (a correction of typically 0 – 30 s). This correction allows excluding early datapoints, which tend to underreport O₂ concentration due to a time delay caused by diffusion into the sensor matrix.

Furthermore, it should be noted that dual irradiation experiments proved to be very sensitive to the alignment of the two light sources, since the beams had to overlap properly to observe a synergistic effect. Thus, some experiments could not be used for data analysis due to improper light source alignment.

For experiments using only the Hg light source, initial rates were calculated as described in 4.2.2, using the average k_1 procedure. Thus obtained k_0 values were averaged to give the average 320 – 400 nm initial rate.

For both QTH and dual irradiation, the following procedure was used to calculate initial rates: Equation (2) was fitted to all experiments, optimizing both k_0 and k_1 . Subsequently, a linear regression model was fitted to the k_1 values of all QTH or dual irradiation experiments, respectively. For each group, this linear model provides a description of the dependence of k_1 on longpass filter cut-on wavelength. Subsequently, Equation (2) was again fitted to all experiments, this time fixing k_1 to be the linear regression value of the respective linear model (QTH or dual irradiation) and wavelength. For the dual irradiation group, thus obtained k_0 values were averaged for each wavelength. For the QTH irradiation group, another linear regression model was fitted to the k_0

values, this time yielding a linear model to describe the dependence of k_0 on longpass filter cut-on wavelength.

To give the reported excess initial rate of O₂ formation, the following method was used: for each wavelength, the average 320 – 400 nm initial rate as well as the QTH linear regression k_0 value for the respective wavelength were subtracted from the average dual irradiation initial rate.

At this point we would like to note that the small apparent O₂ signals observed when only the longpass filtered QTH light source was used are likely not due to actual O₂ evolution. This is based on the observation that no **2-cis** was formed when only the QTH light source (> 495 nm) was used for irradiation. Rather, the small signals might be caused by the temperature change of ca. 2 °C caused by the QTH light source despite the reactor being submersed in a water bath. Regardless, through the above described analysis method, any contribution of the QTH light source to the observed O₂ signal during dual irradiation is accounted for by subtracting the obtained QTH linear regression k_0 values. Furthermore, subtraction of the average 320 – 400 nm initial rate accounts for the contribution of the Hg light source during dual irradiation. Reported excess initial rates are therefore the result of a synergistic effect of both light sources.

4.2.6 Note on Reaction Order/Concentration Dependence

As noted in 4.2.1, the observed reaction rates are identical for 0.01 and 0.005 M solutions of **1**. This is because in this concentration range, complete photon absorption by the sample solution occurs, leading to an apparent zero order reaction in **1**.⁽⁸⁾ Attempts to perform measurements using solutions of significantly lower concentration, below the complete absorption regime, were unsuccessful. Hence, the actual reaction order in **1** could not be determined.

4.3 Gas Phase O₂ Measurement

4.3.1 Irradiation Procedure

A 5 ml Schlenk flask (internal volume ca. 10 ml) with a NS14 ground glass joint was topped with a hollow, flat top glass stopper, on the inside of which a contactless trace range oxygen sensor spot was glued. This allows measurement of gas phase O₂ concentration inside the reactor via contactless read out through the glass stopper. The Schlenk flask was then connected to the Schlenk line using a T-piece adapter, with one connection to the Schlenk line, one to the Schlenk flask and one connection being closed with a septum. Subsequently, 2 ml of an aqueous solution of **1** (prepared via the N₂O synthesis route, 0.01 M) was transferred into the Schlenk flask. The transfer was done via cannula transfer through the septum inlet of the T-piece adapter and through the valve of the Schlenk flask, taking care not to introduce any external O₂ into the flask.

Once the transfer was complete, the Schlenk flask was closed and stirred overnight in the dark at room temperature to equilibrate. A PT100 temperature sensor (for temperature compensation of the O₂ measurement) was placed next to the Schlenk flask.

After equilibration, an optical fiber was mounted to the outside of the flat top glass stopper to read out the oxygen sensor spot. Then, the baseline O₂ concentration was measured for ca. 4 h. Afterwards the flask was irradiated for 16 h using the Hg light source (320 – 500 nm, 0.15 W intensity setting), resulting in a color change to a yellow/orange solution. During irradiation the flask was cooled using a 20 W fan.

4.3.2 Data Analysis and O₂ Consumption Reaction

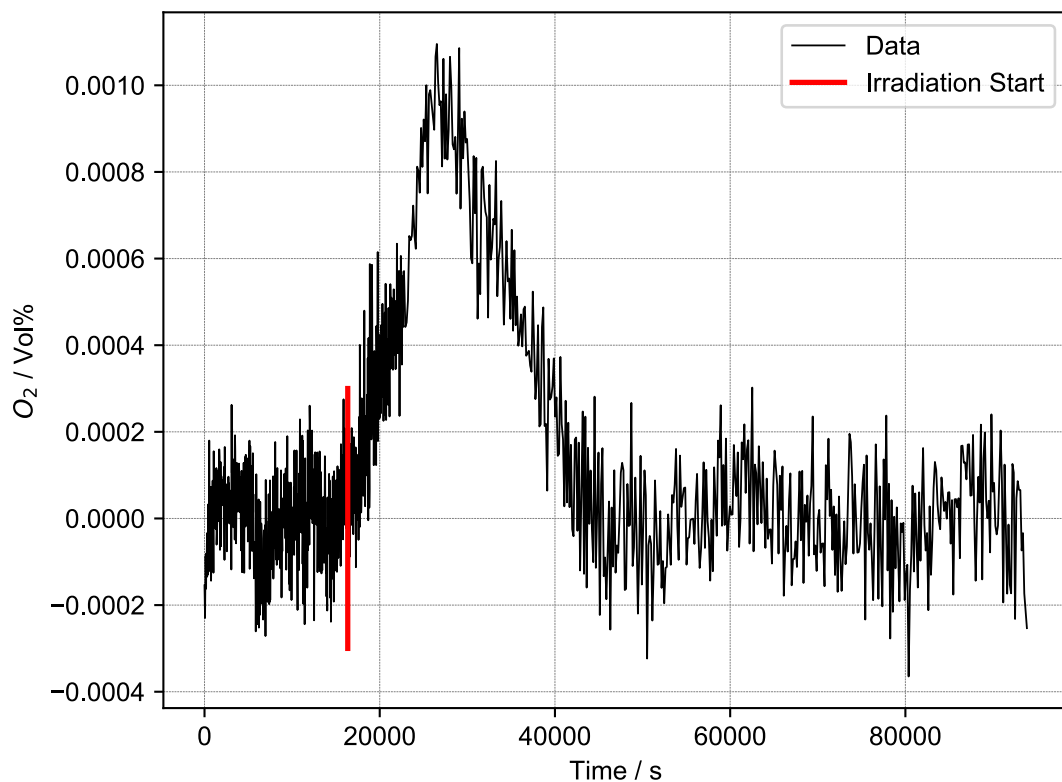


Figure 4.3-1 Gas phase O₂ detection data for irradiation of complex **1** with Hg light source (320 – 500 nm)

Data has been baseline corrected with a sixth-degree polynomial fitted to baseline intervals [0 s, 16350 s] and [46300 s, 94000 s]. Irradiation was turned on at t = 16350 and turned off at t = 76000 s.

The obtained gas phase O₂ concentration data shows a small peak shaped feature resulting from O₂ evolution superimposed on a continuously decreasing background. Therefore, a sixth-degree polynomial was fitted to baseline intervals [0 s, 16350 s] (t = 16350 s is the start time for irradiation) and [46300 s, 94000 s] and subtracted from the entire measurement to obtain a baseline corrected signal, shown in Figure 4.3-1.

As can be seen in Figure 4.3-1, once irradiated is started, an increase in the gas phase O₂ concentration can be detected due to O₂ evolution for ca. 3 h. Afterwards, the O₂ concentration drops back to baseline value again over the course of ca. 6 h. This kind of behavior is consistent with a two-reaction sequence, wherein O₂ is formed in the first reaction (O₂ evolution from **1**, decreasing reaction rate over time due to consumption of **1**) and consumed in the second reaction.

In a separate experiment, complex **1** (synthesized via Ag₂O synthesis route, in 52 mM KOH aq.) was irradiated using the QTH light source (only water filter) in air, resulting in conversion of **1** into mostly NMR inactive species (see Figure 7.5-7 - Figure 7.5-10). We hypothesized that **1**, when irradiated in the presence of O₂, oxidizes to form mostly Ru(III) species as well as phosphorous oxides. This can explain the consumption of O₂ during water splitting and the formation of NMR inactive species when **1** is irradiated in air.

4.4 Comparison of **2-cis** and O₂ Formation Rates

To confirm that **2-cis** and O₂ are indeed both formed in the same reaction, their initial rates of formation were compared. If both are formed in the same reaction, their normalized rates are expected to be identical. With the available experimental data and techniques, however, only an approximate comparison can be made since **2-cis** and O₂ formation had to be studied in different experimental set-ups (NMR scale irradiation and liquid phase O₂ measurement, respectively). Therefore, multiple normalizations had to be applied to enable comparison, which will be explained in the following.

For **2-cis**, the initial rate of formation was calculated from the kinetic model shown in Figure 4.1-1. The thus obtained initial rate is 1E-05 s⁻¹ in normalized units or 0.1 μmol l⁻¹ s⁻¹ (given a concentration of 0.01 M).

For O₂, the initial rate of formation was taken from the intensity data set for the 1 W intensity setting, being 0.0059 μmol l⁻¹ s⁻¹.

The first normalization is based on the stoichiometry of the reaction (see Table 4.4-1), which shows that **2-cis** would be formed at twice the rate of O₂. Hence, stoichiometry adjusted rates are 0.05 μmol l⁻¹ s⁻¹ for **2-cis** and 0.0059 μmol l⁻¹ s⁻¹ for O₂.

The second normalization that has to be applied has to correct for the different areas, which were irradiated in each set-up. For NMR scale irradiation, the irradiated area was 0.424 × 4 cm (1.696 cm²), while the irradiated area was 0.8 × 1 cm (0.8 cm²) for liquid phase O₂ measurements. Since the reaction rate is proportional to irradiated area for a photochemical reaction (the light cone was bigger than the reactor in both cases), initial rates normalized to 1 cm² are 0.0295 μmol l⁻¹ s⁻¹ for **2-cis** and 0.0074 μmol l⁻¹ s⁻¹ for O₂.

The last normalization is based on the different flux densities used in the experiments. The initial rate of O₂ formation is based on irradiation with the Hg light source with the 1 W intensity setting, which corresponds to a photon flux of 1.32E+18 s⁻¹ received by the reactor (see Chemical Actinometry). For NMR scale irradiation, the QTH light source (equipped with only the water filter) was used instead. The photon flux of the QTH light source cannot be easily determined using the applied chemical actinometry method, so it is estimated based on power meter measurements. It

should be noted that these power values are not identical to the power received by the reactor. Instead, they are only proportional.

Based on power meter measurements, ca. 27% of the QTH output power is in the useful wavelength range of 320 – 630 nm. Total power measured in the position of the NMR tube was 645 mW, giving ca. 173 mW of power in the 320 – 630 nm wavelength range, with a mean photon wavelength of 475 nm.

Using the same power meter, a power of 127 mW was measured in the position of the liquid phase O₂ reactor for the Hg light source (320 – 500 nm, 1.32E+18 s⁻¹ flux, mean photon wavelength of 410 nm). Based on the mean photon wavelengths (475 nm for QTH, 410 nm for Hg) and measured power values (173 mW for QTH, 127 mW for Hg), one can estimate a photon flux of ca. 2.09E+18 being received by the NMR tube using the following equation:

$$Flux_{QTH} = \frac{E_{Hg} P_{QTH}}{E_{QTH} P_{Hg}} Flux_{Hg} \quad \text{Equation (3)}$$

With E_{Hg} and E_{QTH} being the mean photon energies in eV for the QTH and Hg light sources, respectively, and P_{QTH} and P_{Hg} being the measured power values. Based on the intensity dataset, it was found that rate of O₂ formation shows a square dependence on photon flux. If we assume that the same holds true for **2-cis** (since **2-cis** has shown the same synergistic effect in dual irradiation experiments as O₂ formation), the square of the ratio between the Hg and QTH light source flux values gives a flux correction factor of 2.5. Applying this factor to the **2-cis** initial rate of formation gives a flux-normalized rate of 0.0118 μmol l⁻¹ s⁻¹. Comparing this to the normalized initial rate of O₂ formation, 0.0074 μmol l⁻¹ s⁻¹, shows that they differ by less than 40%. Considering that these two rates were measured using different methods (NMR and O₂ detection) and in different set-ups, we consider this to be an acceptable agreement.

Table 4.4-1 Comparison of 2-cis and O₂ initial rates of formation



Estimated, normalized initial rate of 2-cis formation / μmol l ⁻¹ s ⁻¹	Estimated, normalized, initial rate of O ₂ formation / μmol l ⁻¹ s ⁻¹
0.0074	0.0118

4.5 Photographs of Irradiation Set-Ups

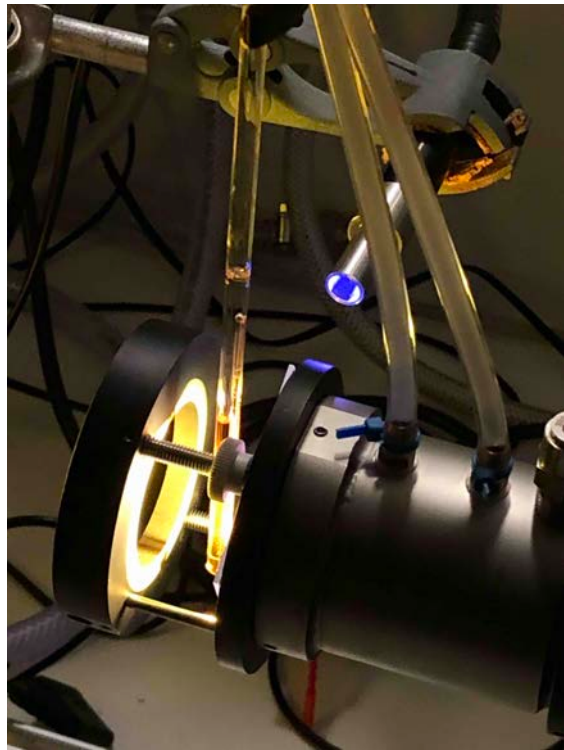


Figure 4.5-1 Set-up for irradiation on NMR scale

Hg light source provides irradiation through the light guide in the back (320 – 400 nm filtered in this picture) and the QTH light source is visible on the right (water cooled IR filter and filter holder are visible, > 495 nm filtered in this picture).

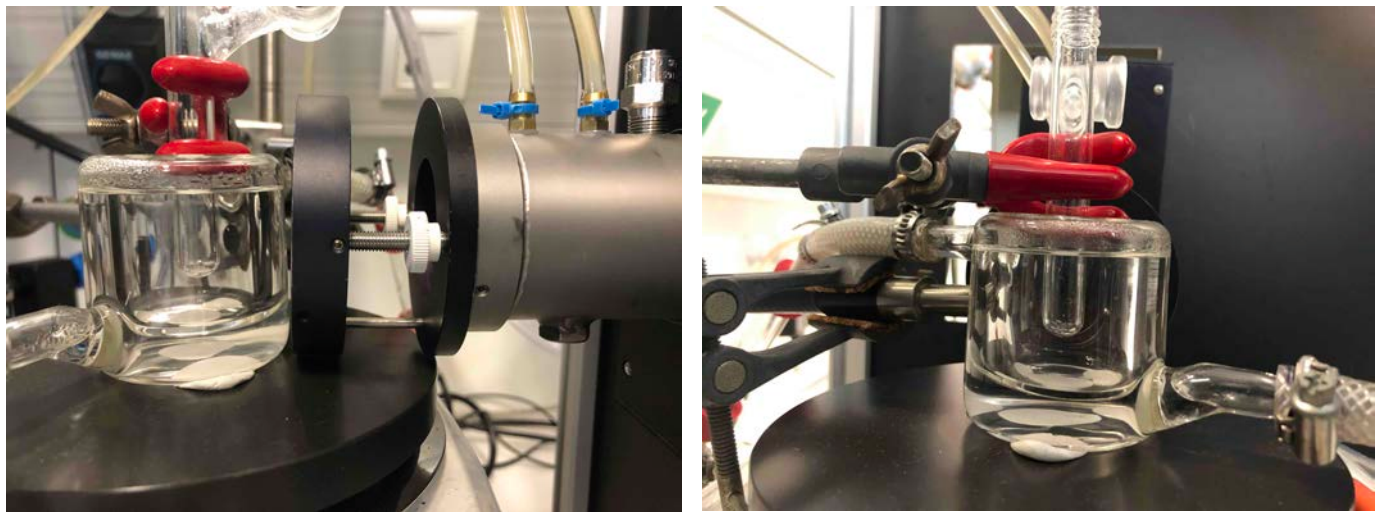


Figure 4.5-2 Set-up for irradiation with liquid phase O₂ detection

Left: Front view of set-up showing QTH light source (right) and water filled, thermostatted beaker with Schlenk flask reactor.

Right: Side view of set-up showing light guide of Hg light source (left) and side view of thermostatted reaction assembly.

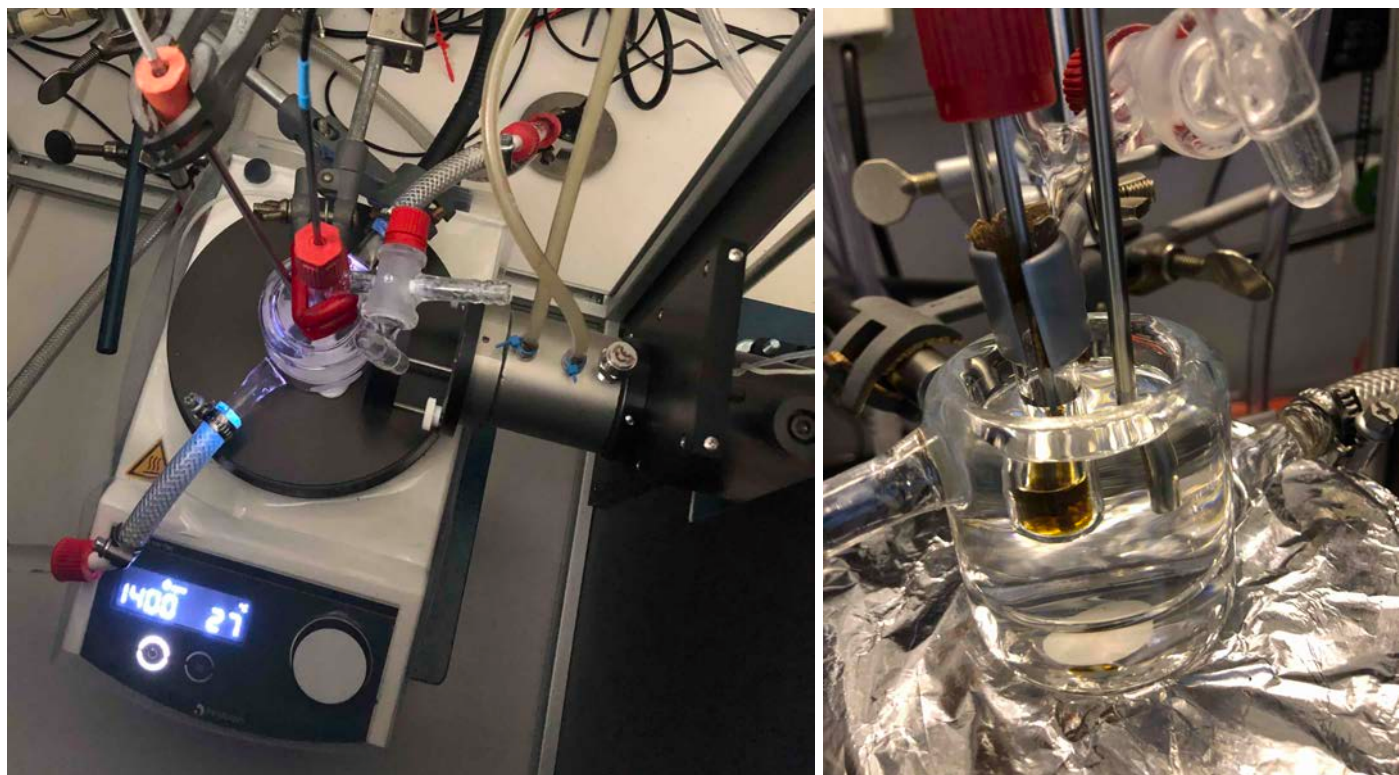


Figure 4.5-3 Irradiation set-up (liquid phase O₂ detection) in use (left) and close-up of assembled reactor

Left: Irradiation set-up in use (only Hg light source, 320 – 400 nm filtered, is turned on). QTH light source (with shutter, water cooled IR filter and filter holder) is visible on the right. Center shows the Schlenk reactor submerged in the thermostatted beaker with an O₂ sensor connected via a BOLA laboratory screw joint (red cap). Next to the reactor, a PT100 temperature sensor is submerged in the thermostatted beaker. Note that the temperature shown on the stir plate is not indicative of the actual reaction temperature.

Right: Close-up of assembled reactor with submerged PT100 temperature sensor on the right. Inside of the reactor, an aqueous solution of complex 1 can be seen, inside of which the O₂ sensor is submerged.

5 H₂O₂ Disproportionation

5.1 Experimental Procedure

Following the procedure described in 4.2.1, ca. 400 µl of degassed 5×10⁻⁵ M aqueous H₂O₂ were transferred into a Schlenk flask equipped for liquid phase O₂ measurement. Throughout the experiment, the flask was connected to the Schlenk line (under argon), allowing for the injection of other reagents. A PT100 temperature sensor was placed next to the flask for temperature compensation of the O₂ measurement. While being stirred and at room temperature, the baseline O₂ concentration was measured, followed by injection of 500 µl of an aqueous solution of **1** (synthesized using N₂O synthesis route, 0.005 M) through the septum of the T-piece adapter. After 50 min, 100 µl of a degassed 3 M potassium iodide (KI) solution were injected, followed by another 40 min of O₂ measurement.

5.2 Data Analysis

This H₂O₂ disproportionation experiment was performed to investigate the feasibility of a stepwise water splitting mechanism, wherein irradiation of **1** first produces H₂O₂, followed by H₂O₂ disproportionation to O₂ and H₂O catalyzed by **1**. In our view, complex **1** would be the only viable candidate for a H₂O₂ disproportionation catalyst in this scenario, since O₂ formation occurs directly at the start of irradiation (see for example Figure 4.2-1). At the start of the reaction, only **1** is present in significant quantities and it would therefore be the only compound that could catalyze H₂O₂ disproportionation at this point.

The used quantity of H₂O₂ (20 nmol) corresponds to roughly 200 times the amount of O₂ formed within the first 90 s of a liquid phase O₂ measurement experiment (Hg light source, 320 – 500 nm, 1 W setting, ~ 0.11 nmol). Furthermore, it is roughly 1% of the amount of **1** used (2.5 µmol). Therefore, this amount it is likely an overestimation of the highest H₂O₂ concentration that might occur for a H₂O₂ mechanism. Thus, the observed rate of H₂O₂ disproportionation catalyzed by **1** will be an upper bound for the H₂O₂ disproportionation rate possible under water splitting reaction conditions. If this rate is slower than the observed initial rate of O₂ formation during liquid phase O₂ measurement, a mechanism involving H₂O₂ disproportionation can be seen as unlikely.

The results of the experiment are shown in Figure 5.2-1. It can be seen that the baseline O₂ concentration of the H₂O₂ solution is elevated (1.9 µmol l⁻¹), since it proved challenging to remove all dissolved O₂ from it. Addition of the solution of **1** (having a lower O₂ concentration) at t = 150 s therefore leads to a drop in O₂ concentration. After equilibration, a linear increase in O₂ concentration with a rate of 1.2×10⁻⁵ µmol l⁻¹ s⁻¹ can be observed (see Figure 5.2-1B). We attribute this to H₂O₂ disproportionation catalyzed by **1**. At t = 3100 s, a 3 M KI solution was added to the reactor. Since KI is a known and fast-acting H₂O₂ disproportionation catalyst, this was done to confirm that H₂O₂ disproportionation can be observed under these reaction conditions. Indeed, addition of KI leads to a rapid increase in O₂ concentration, followed by return to baseline value (likely due to diffusion of O₂ into the gas phase). Importantly, after addition of KI and equilibration, no increase in O₂ concentration can be observed anymore (see Figure 5.2-1B). This suggests that all H₂O₂ has been consumed by KI catalyzed disproportionation. In turn, this supports the hypothesis that the increase in O₂ concentration before KI addition was due to catalytic H₂O₂ disproportionation and not some other process (such as leakage).

Within this interpretation, the rate of H₂O₂ disproportionation catalyzed by **1** (1.2×10⁻⁵ µmol l⁻¹ s⁻¹) is more than an order of magnitude slower than the initial O₂ formation rate during water splitting (5.9×10⁻³ µmol l⁻¹ s⁻¹ for Hg light source, 320 – 500 nm, 1 W setting). Therefore, it is unlikely that a mechanism involving H₂O₂ disproportionation is responsible for O₂ evolution in this system. However, a variable not included in this experiment is irradiation. It is possible that irradiation could accelerate H₂O₂ disproportionation. This possibility could not be investigated in this experiment since irradiation would lead to a combined increase of O₂ concentration due to H₂O₂

disproportionation and O₂ evolution from **1**, which could not be distinguished. Theoretical evidence, however, also suggests that light-induced H₂O₂ formation from **1** is unlikely (see 11.2.8).

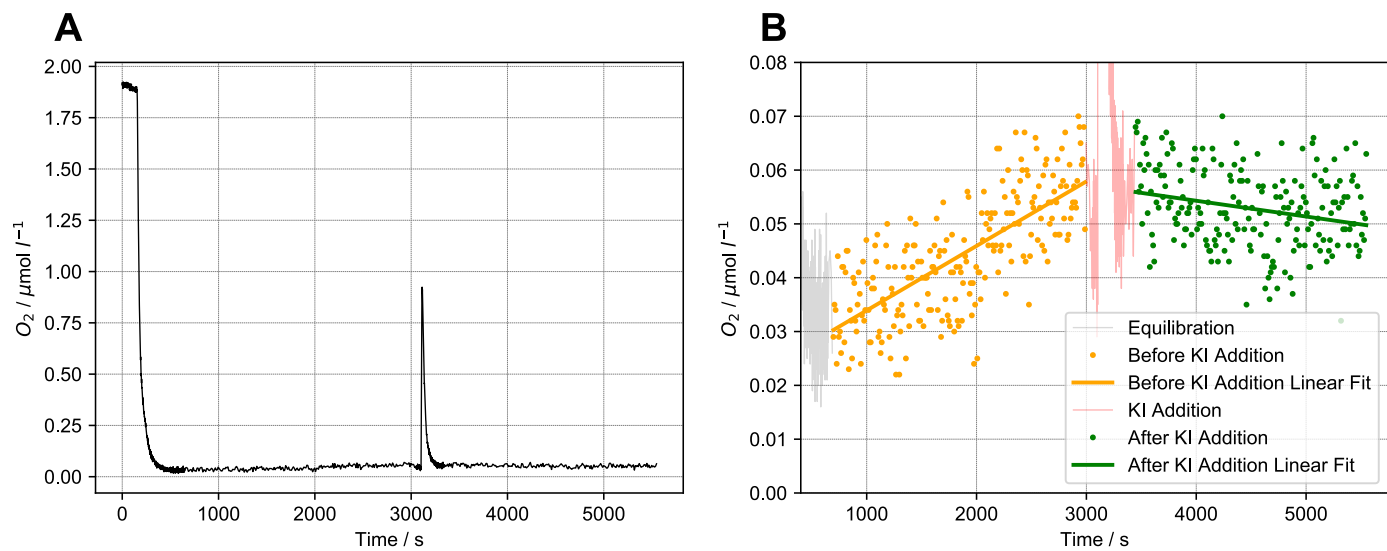


Figure 5.2-1 Liquid phase O₂ measurement for H₂O₂ disproportionation catalyzed by complex 1

A Overview of entire liquid phase O₂ measurement. At t = 0 s, only the aqueous 4×10^{-5} M H₂O₂ solution is present in the reactor. At t = 150 s, the ca. 5×10^{-3} M aqueous solution of complex **1** is injected, leading to a drop in the liquid phase O₂ concentration (since the solution of complex **1** had a lower O₂ concentration compared to the H₂O₂ solution). At t = 3100 s, 3 M aqueous KI solution was added, leading to a spike in the O₂ concentration (O₂ concentration drops again due to diffusion into the gas phase).

B Zoom-in of region before (yellow) and after (green) KI addition, with linear fits. The slope before KI addition is 1.2×10^{-5} $\mu\text{mol l}^{-1} \text{s}^{-1}$, after KI addition it is -2.9×10^{-6} $\mu\text{mol l}^{-1} \text{s}^{-1}$.

6 Chemical Actinometry

6.1 Light Source Spectra

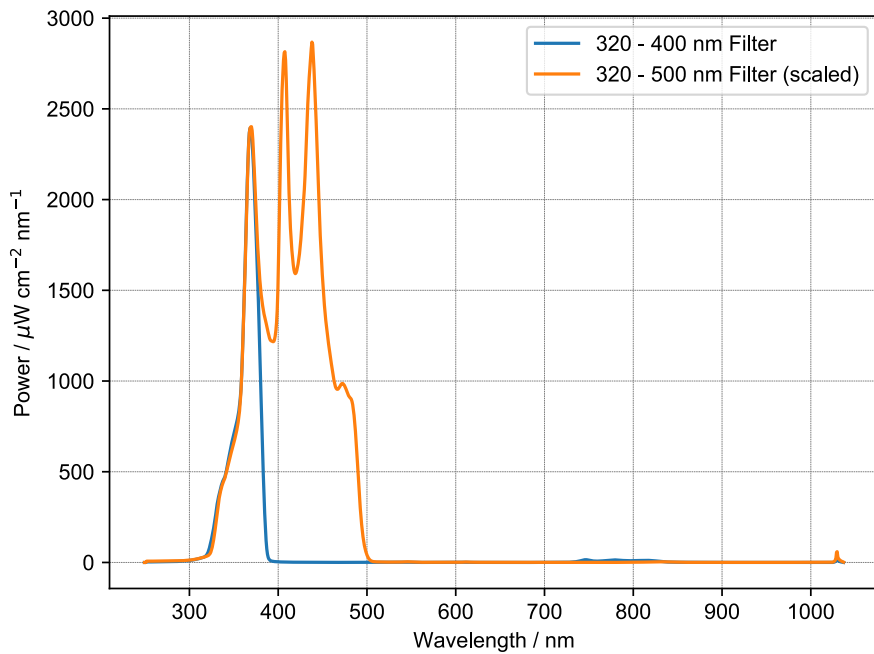


Figure 6.1-1 Spectral power distribution of Hg light source with used filter settings

Note: the actual amount of power reaching the reaction solution depends strongly on the reaction configuration, which is why chemical actinometry was performed (see below).

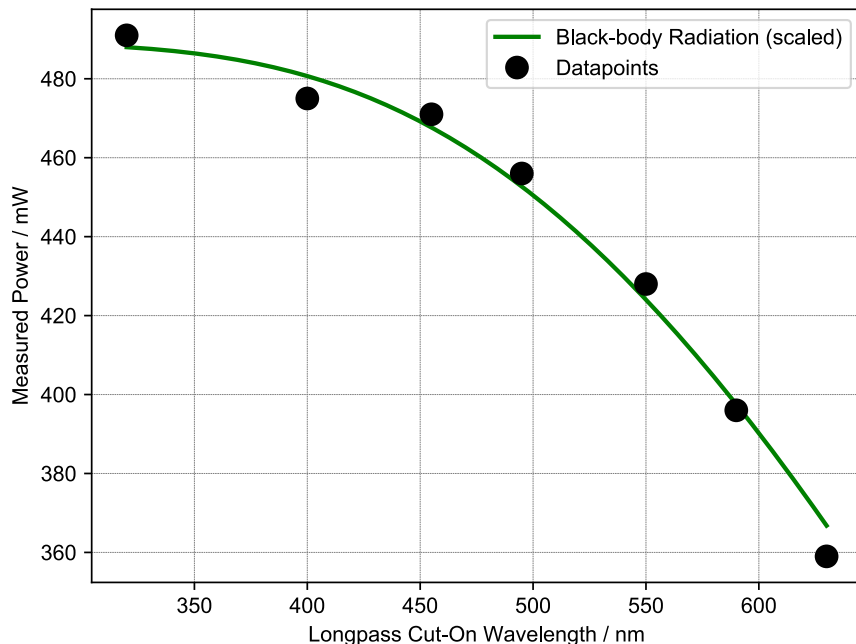


Figure 6.1-2 Measured power of QTH light source with different longpass filters

Graph shows power measured in liquid phase O_2 reactor position with different longpass filters (black dots). The scaled, predicted behavior for an ideal blackbody radiation source (3400 K) is shown in green.

6.2 Experimental Procedure

Potassium ferrioxalate actinometry was performed as described in ref. (9). All experiments were carried out in air and in the dark. The $K_3[Fe(C_2O_4)_3]$ solution was prepared by combining an aqueous 0.2 M solution of $Fe_2(SO_4)_3$ with an aqueous 1.2 M solution of $K_2C_2O_4$. Blank experiments were performed to confirm that the absorbance of the solution was below 0.06 at 510 nm.

For each actinometry experiment, 550 μ l of $K_3[Fe(C_2O_4)_3]$ solution were transferred into the liquid phase O_2 measurement reactor, which was positioned in the same way as during liquid phase O_2 measurements. It was then irradiated using the Hg light source (320 – 400 nm or 320 – 500 nm filter) for a precise amount of time (between 3 – 10 s, depending on the intensity setting). Afterwards, an aliquot of 100 μ l was removed from the reactor, combined with 2 ml of a 0.2 wt% phenanthroline solution, 50 μ l of buffer solution and diluted up to 10 ml in a volumetric flask. Afterwards, the absorbance of the solution at 510 nm was measured using UV/Vis spectroscopy in a 1 cm cuvette.

6.3 Chemical Actinometry Data and Analysis

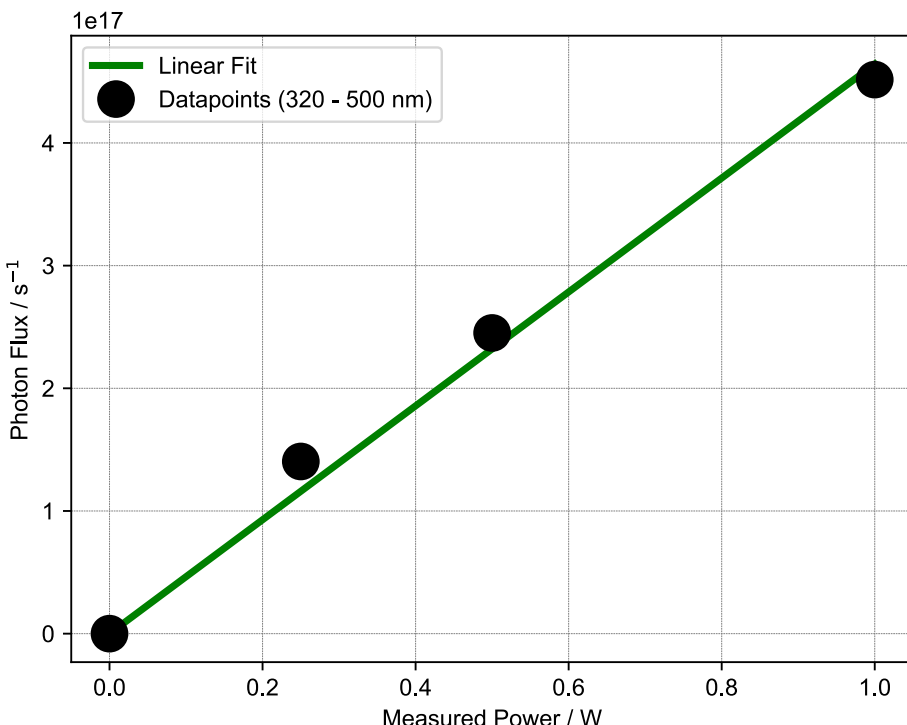


Figure 6.3-1 Chemical actinometry data for different power setting of Hg light source (320 – 500 nm)

Slope of linear fit: 4,64E+17. Note that the used ferrioxalate method does not detect all photons with wavelengths > 400 nm, which is why in the following a correction is applied to the raw photon flux values shown in this figure.

Using the obtained absorbance values, photon flux received by the reactor was calculated using the formula in ref. (9), using a quantum yield of 1.16 and the previously reported extinction coefficient of $1.11E+04 \text{ M}^{-1} \text{ cm}^{-1}$ for the iron(II) phenanthroline complex.

Figure 6.3-1 shows the obtained photon flux values for 0.25, 0.5 and 1 W intensity settings of the Hg light source (320 – 500 nm), establishing a linear correlation between intensity settings and photon flux received by the reactor.

For the 320 – 400 nm filtered Hg light source, a photon flux of 4.15E+17 s⁻¹ was determined (0.3 W intensity setting).

Due to the short path length of the liquid phase O₂ measurement reactor (8 mm) and the low extinction coefficient of K₃[Fe(C₂O₄)₃] for wavelengths longer than 400 nm,(9) photon flux values for the 320 – 500 nm filtered Hg light source are underestimated. In contrast, for the 320 – 400 nm filtered Hg light source, it can be assumed that quantitative photon absorption occurred. Hence, the determined photon flux value (for 320 – 400 nm) combined with the spectral power distribution of the light source (see Figure 6.1-1) can be used to calculate the correct 320 – 500 nm photon flux values:

1. The 320 – 520 nm spectral power distribution is converted to a spectral photon distribution through division of the power distribution by respective photon energies.
2. The spectral photon distribution is integrated from 320 – 500 nm and 320 – 390 nm (390 nm is the actual cut-off of the 320 – 400 nm filter, see Figure 6.1-1).
3. The 320 – 390 nm integral is used to scale the spectral photon distribution, so that the 320 – 390 nm integral is equal to the experimental photon flux of 4.15E+17 s⁻¹.
4. Integration of the scaled spectral photon distribution from 320 – 500 nm gives the corresponding photon flux for this filter setting, which is 1.56E+18 s⁻¹. It has to be considered, however, that this is the 320 – 500 nm photon flux when the light source is in the 0.3 W 320 – 400 nm intensity setting.
5. Experimentally, it was determined that the 0.3 W intensity setting (320 – 400 nm) corresponds to 1.18 W for 320 – 500 nm. Based on the linear relationship between intensity setting and photon flux (see Figure 6.3-1), it can therefore be determined that for the 1 W intensity setting (320 – 500 nm), the photon flux is 1.32E+18 s⁻¹.
6. Therefore, intensity settings for 320 – 500 nm can be converted to photon flux by multiplication by 1.32E+18 s⁻¹.

7 NMR Data

7.1 Characterization of 1

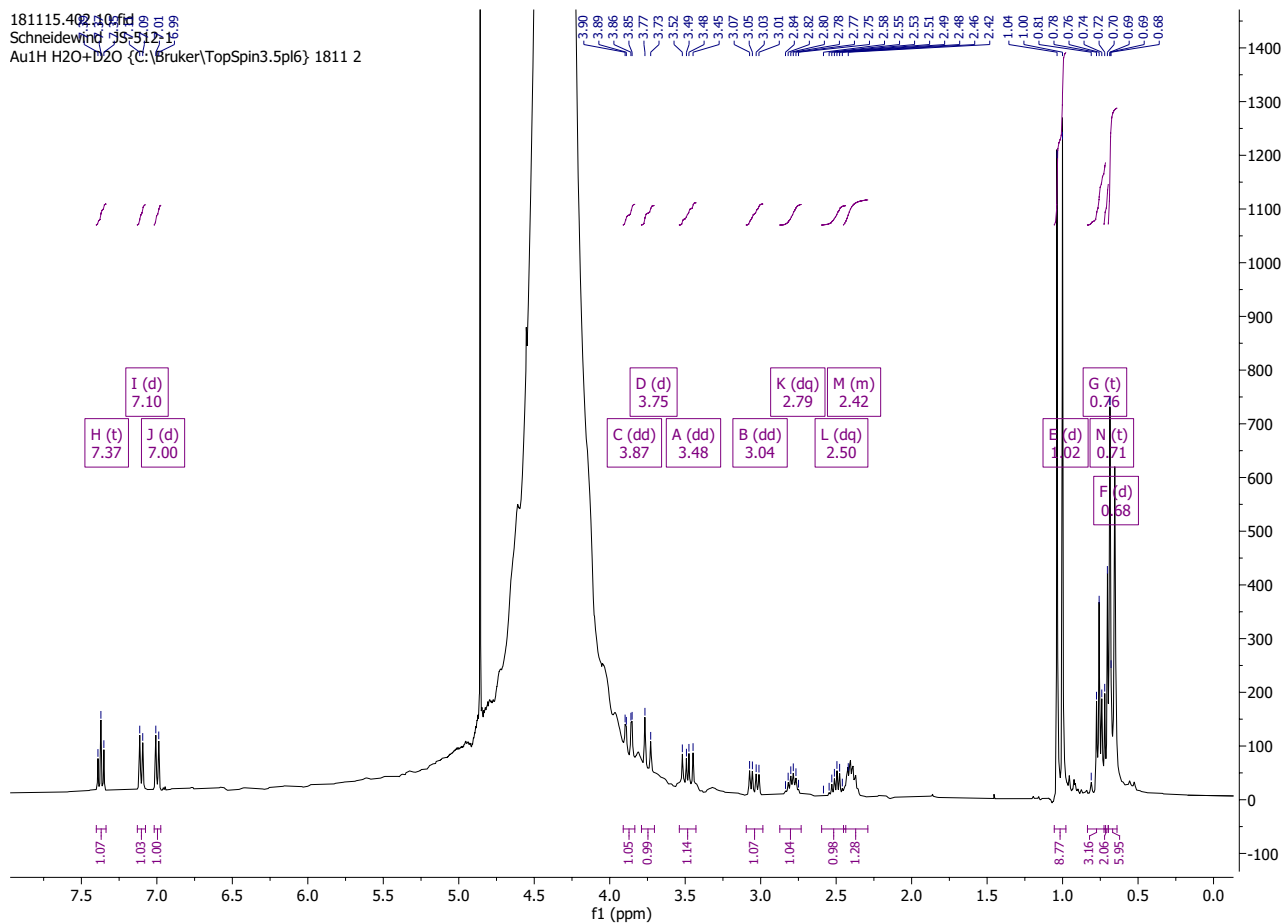


Figure 7.1-1 ^1H NMR spectrum of 1 in H_2O (298 K).

181115.402.11.fid
Schneidewind JS-512-1
Au31P-quant H2O+D2O {C:\Bruker\TopSpin3.5pl6} 1811 2

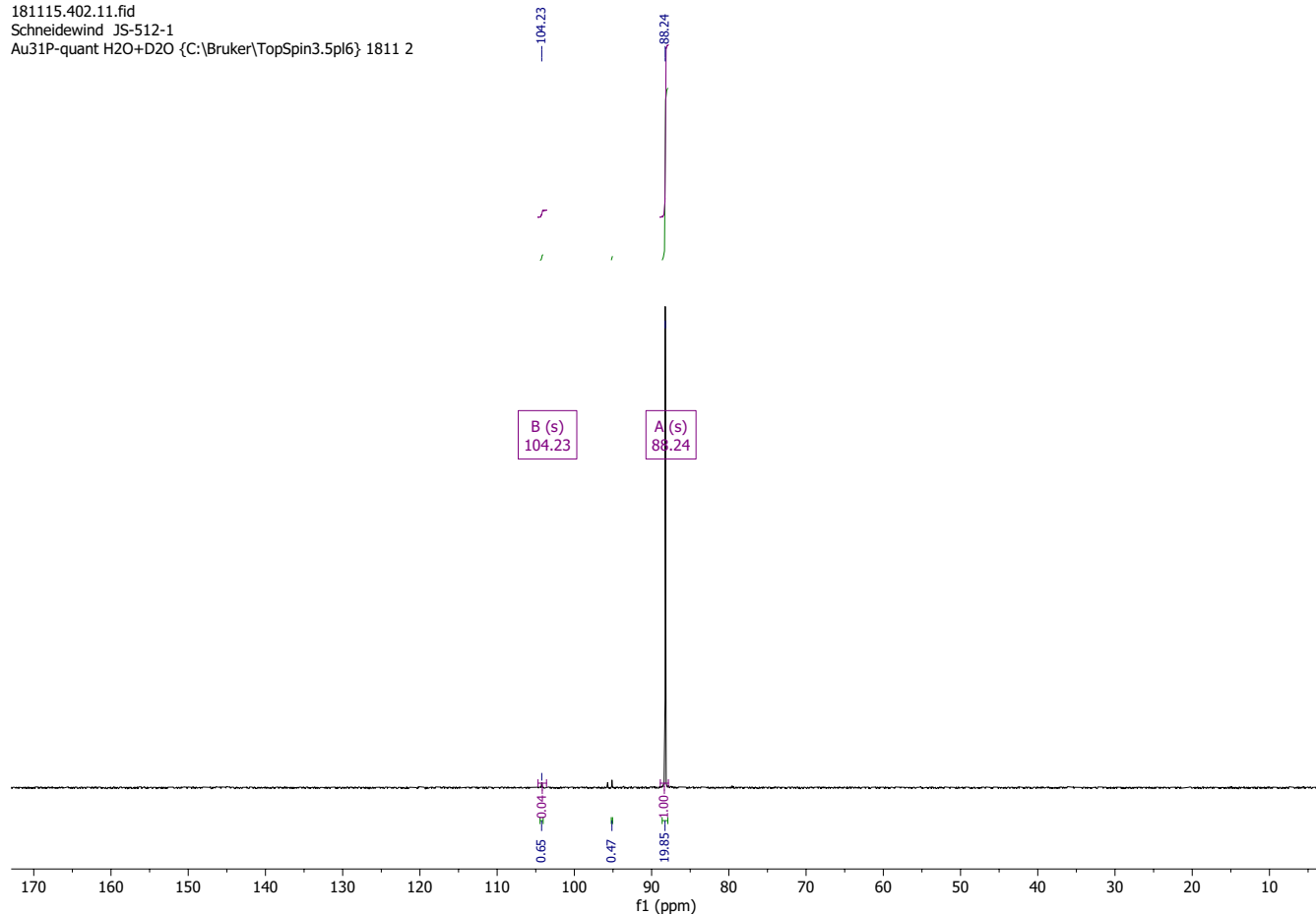


Figure 7.1-2 ${}^{31}\text{P}\{\text{H}\}$ NMR spectrum of **1** in H_2O (298 K)
(small amount of residual **2-trans** is visible at $\delta({}^{31}\text{P}) = 104.23$ ppm)

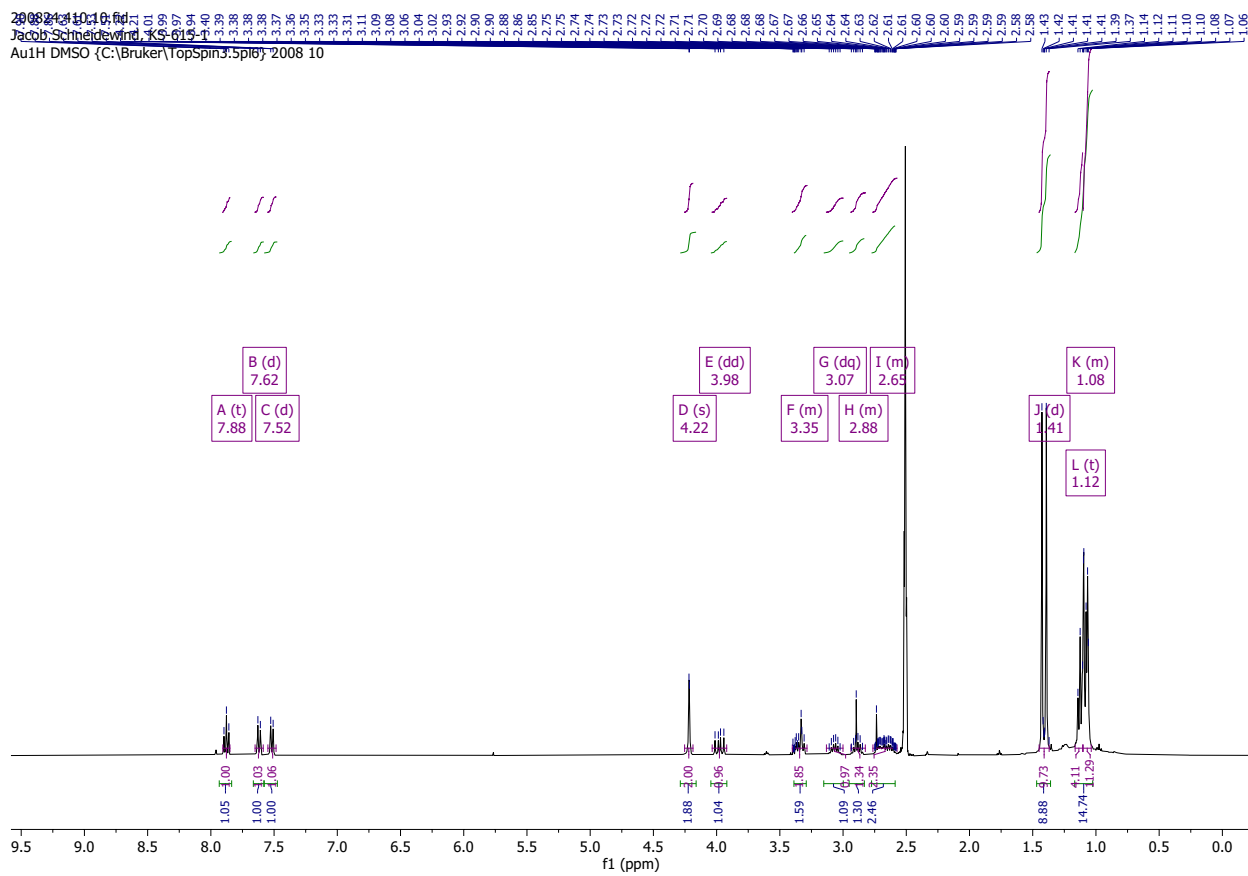


Figure 7.1-3 ^1H NMR spectrum of **1** in DMSO-d_6 (298 K)

200824.410.12.fid
Jacob Schneidewind, KS-615-1
Au¹³C DMSO {C:\Bruker\TopSpin3.5pl6} 2008.10

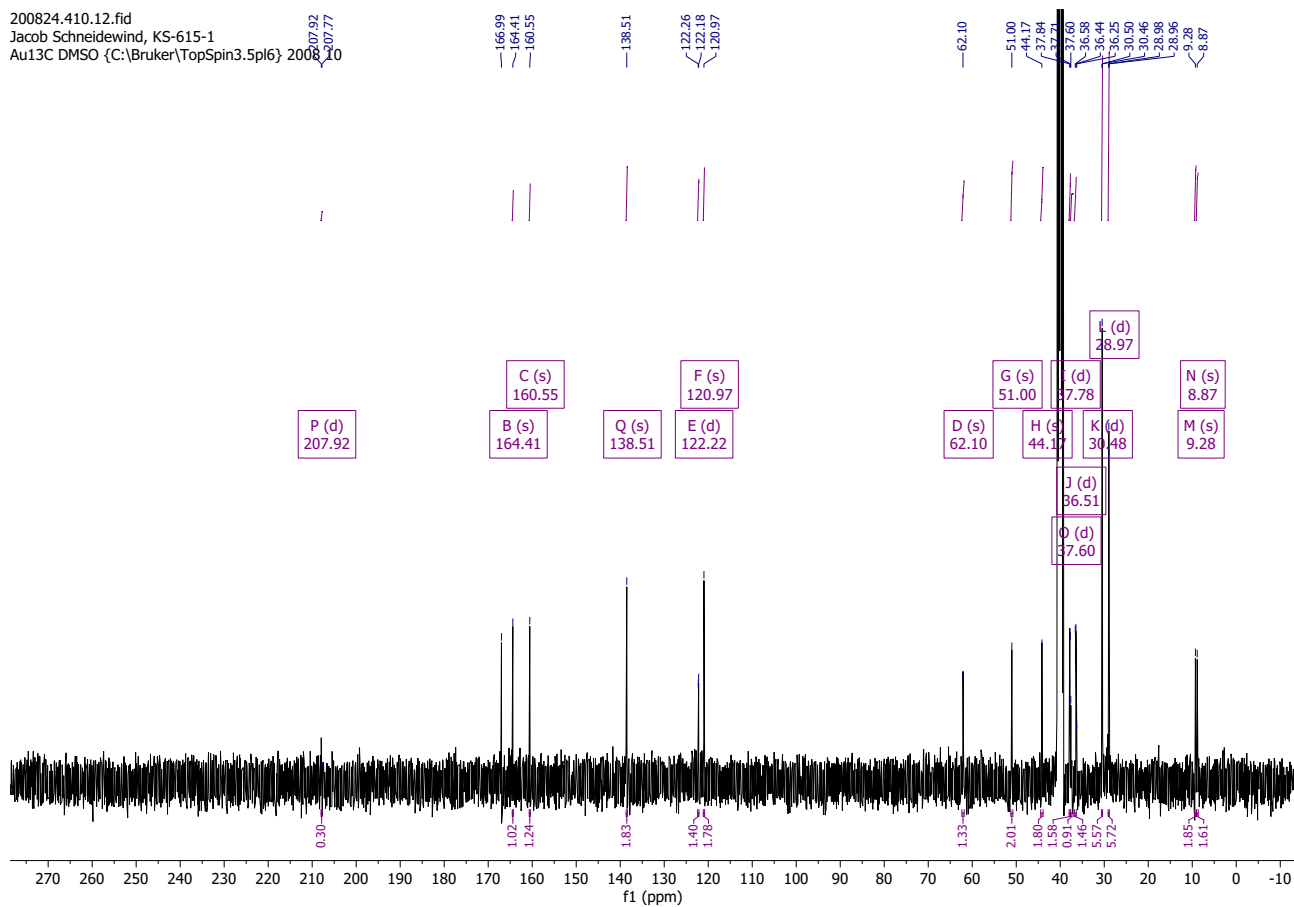


Figure 7.1-4 ¹³C{¹H} NMR spectrum of 1 in DMSO-d₆ (298 K)

200824.410.11.fid
Jacob Schneidewind, KS-615-1
Au31P-quant DMSO {C:\Bruker\TopSpin3.5pl6} 2008 10

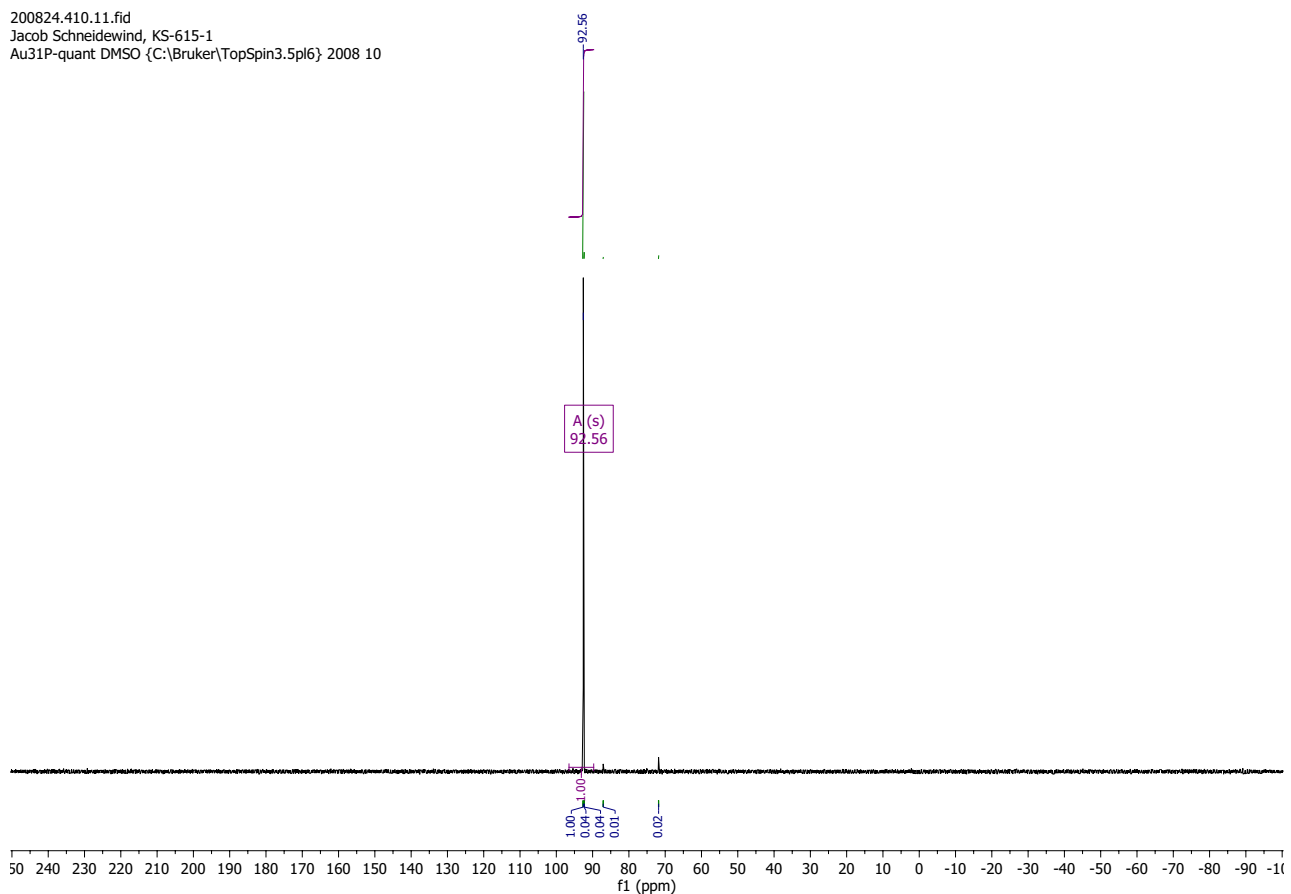


Figure 7.1-5 ${}^{31}\text{P}\{{}^1\text{H}\}$ NMR spectrum of **1** in DMSO-d_6 (298 K)

191024.402.10.fid
Schneidewind JS-575-1
Au1H H2O+D2O {C:\Bruker\TopSpin3.5pl6} 1910 2

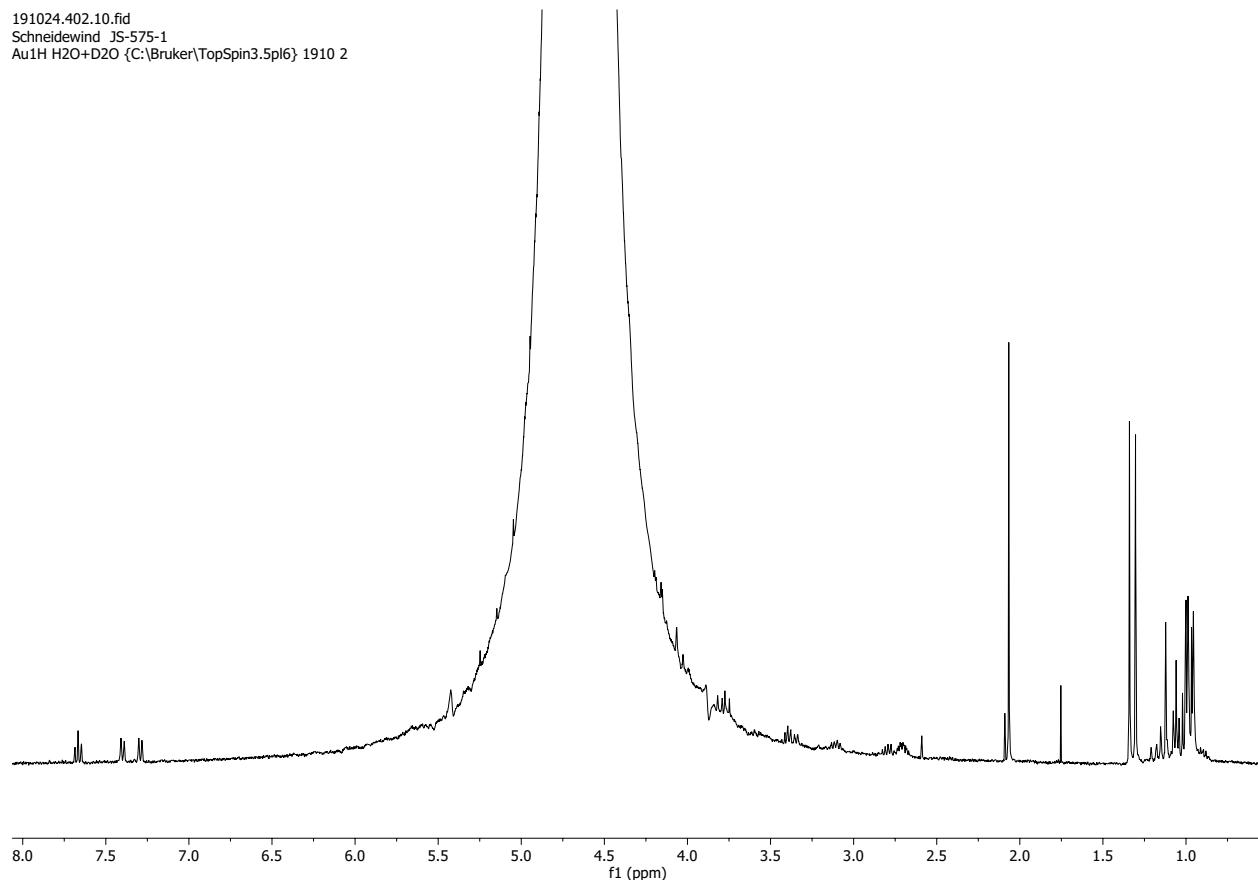


Figure 7.1-6 ¹H NMR spectrum of 1 in H₂O (298 K) synthesized using Ag₂O

191024_402.11.fid
Schneewind JS-575-1
Au31P|quant H2O+D2O {C:\Bruker\TopSpin3.5pl6} 1910 2

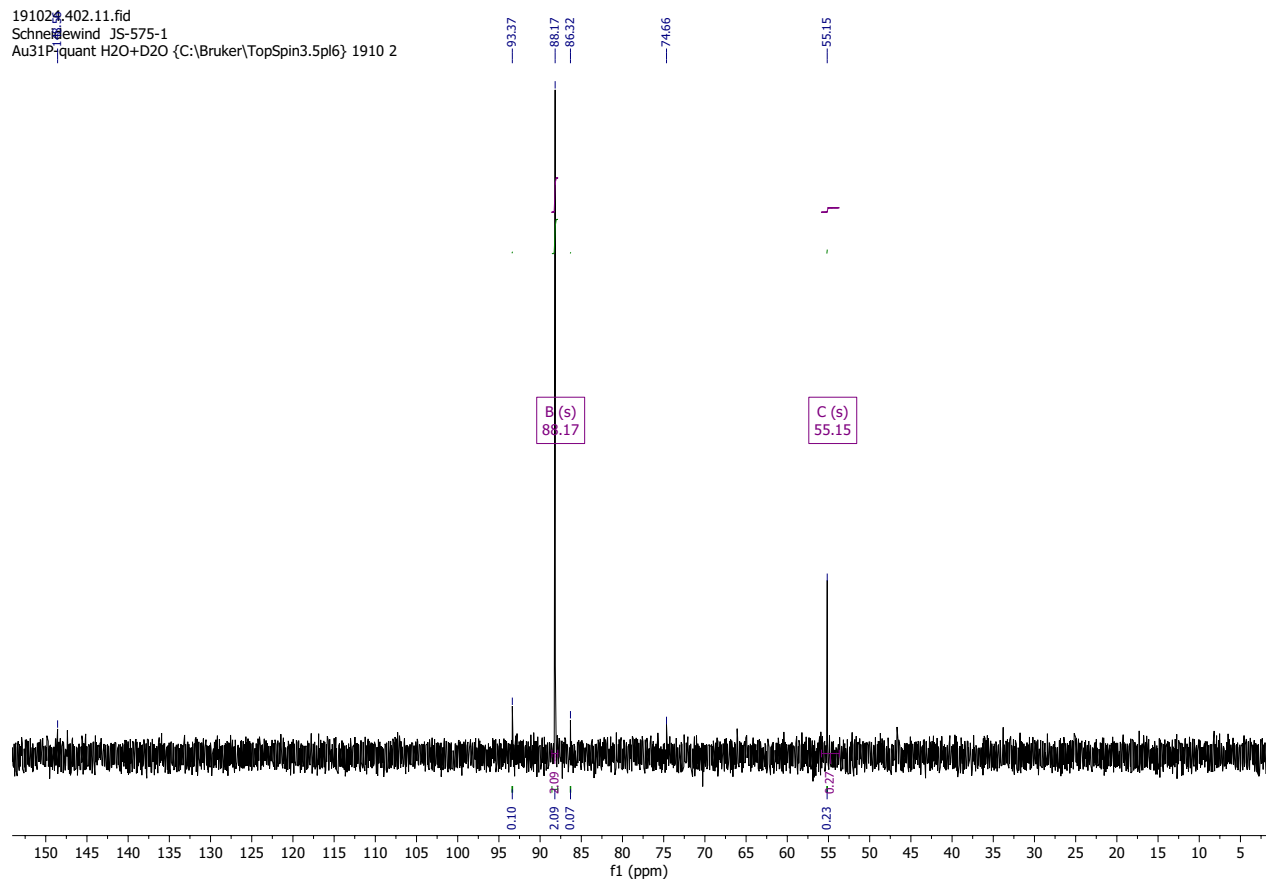


Figure 7.1-7 $^{31}\text{P}\{\text{H}\}$ NMR spectrum of 1 in H_2O (298 K) synthesized using Ag_2O

190221.325.10.fid
Schneidewind JS-531-2
Au1H H2O+D2O (C:\Bruker\TopSpin3.6.0) 1902 25

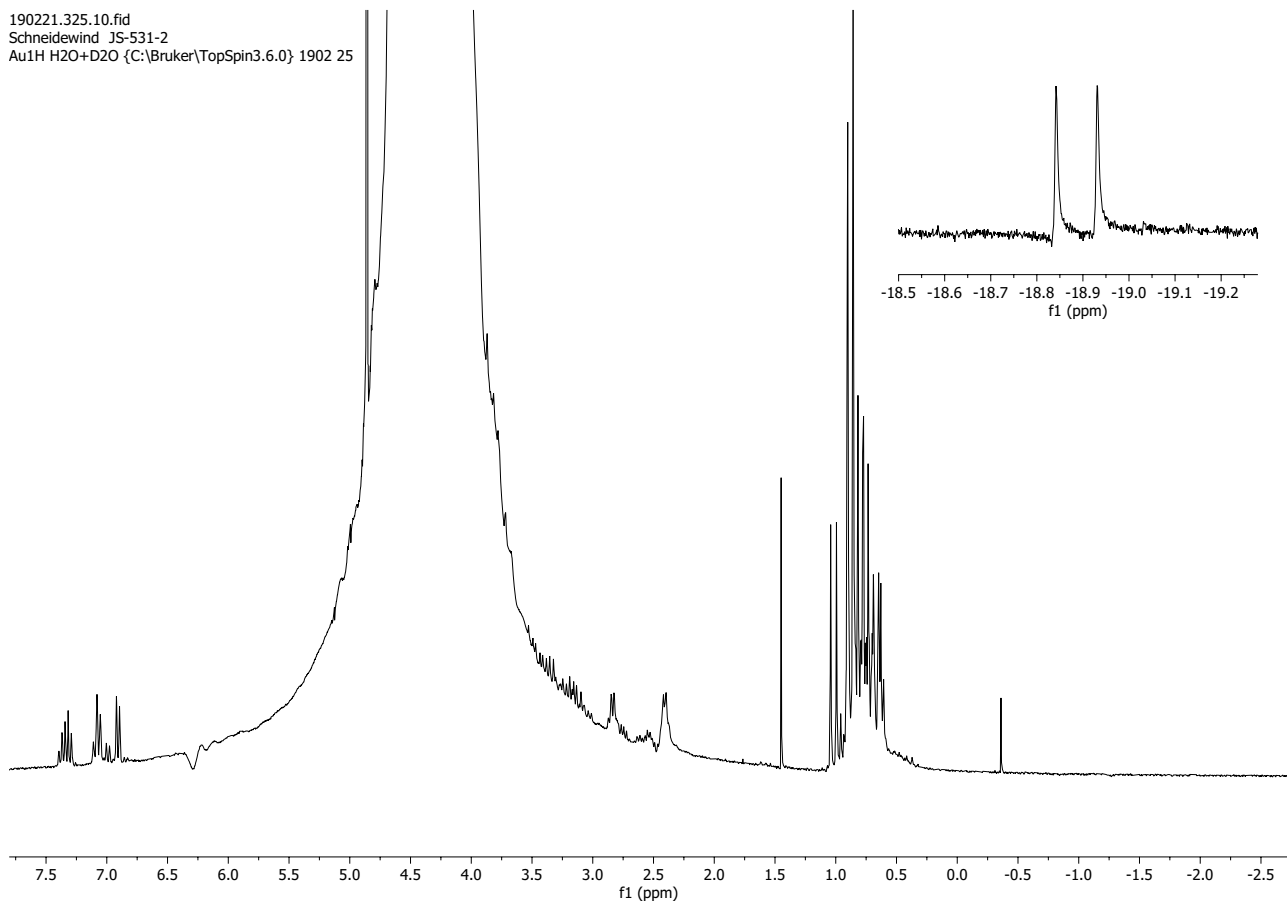


Figure 7.1-8 ¹H NMR of **2-trans** in H₂O (298 K) after three days of reflux, displaying formation of **1** (inlet showing hydride peak of residual **2-trans**)

190221.325.11.fid
Schneidewind JS-53123
Au31P-quant H₂O+D₂O {C:\Bruker\TopSpin3.6.0} 1902 25

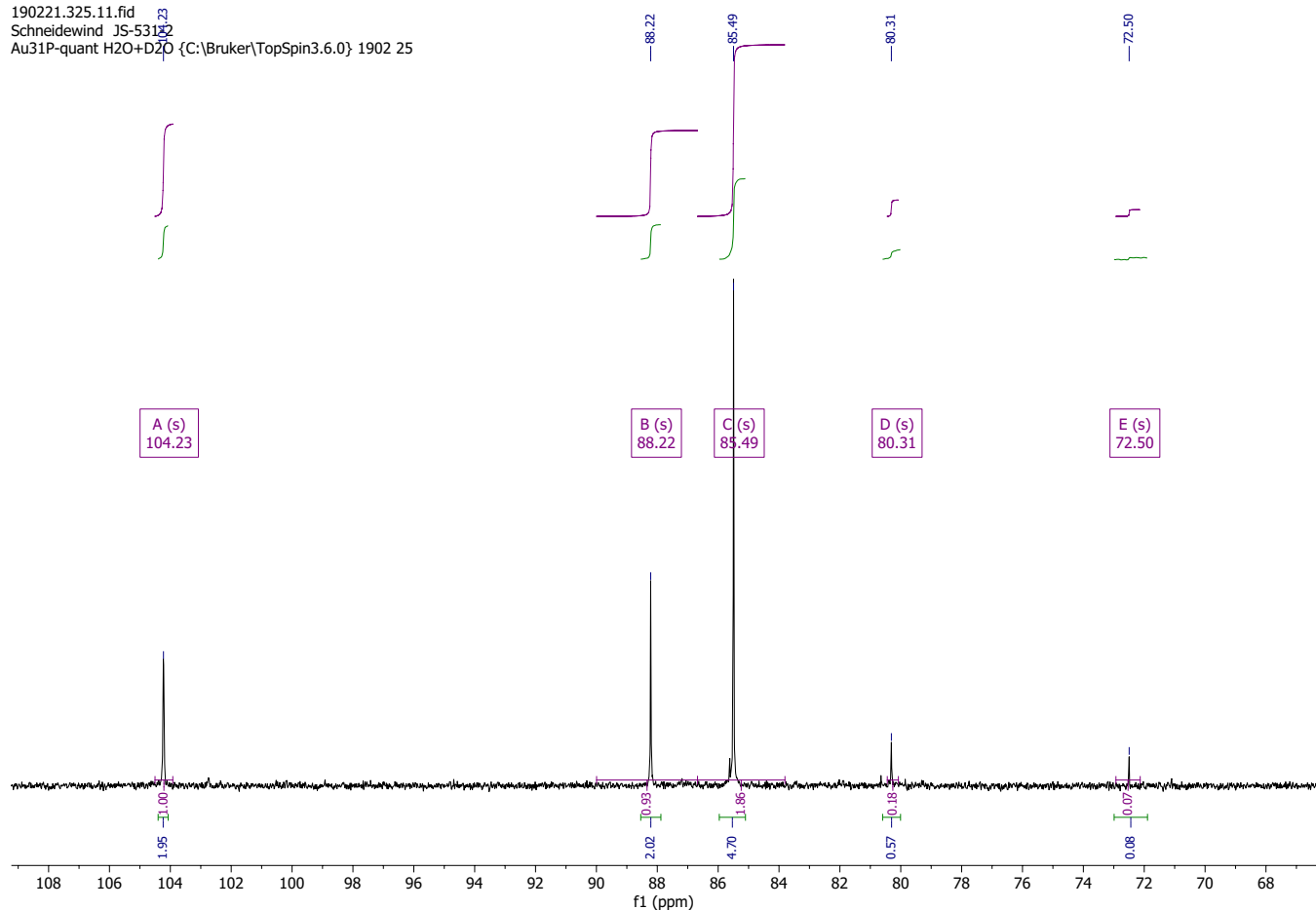


Figure 7.1-9 ³¹P{¹H} NMR of 2-trans in H₂O (298 K) after three days of reflux, displaying formation of 1

7.2 Characterization of 2-trans

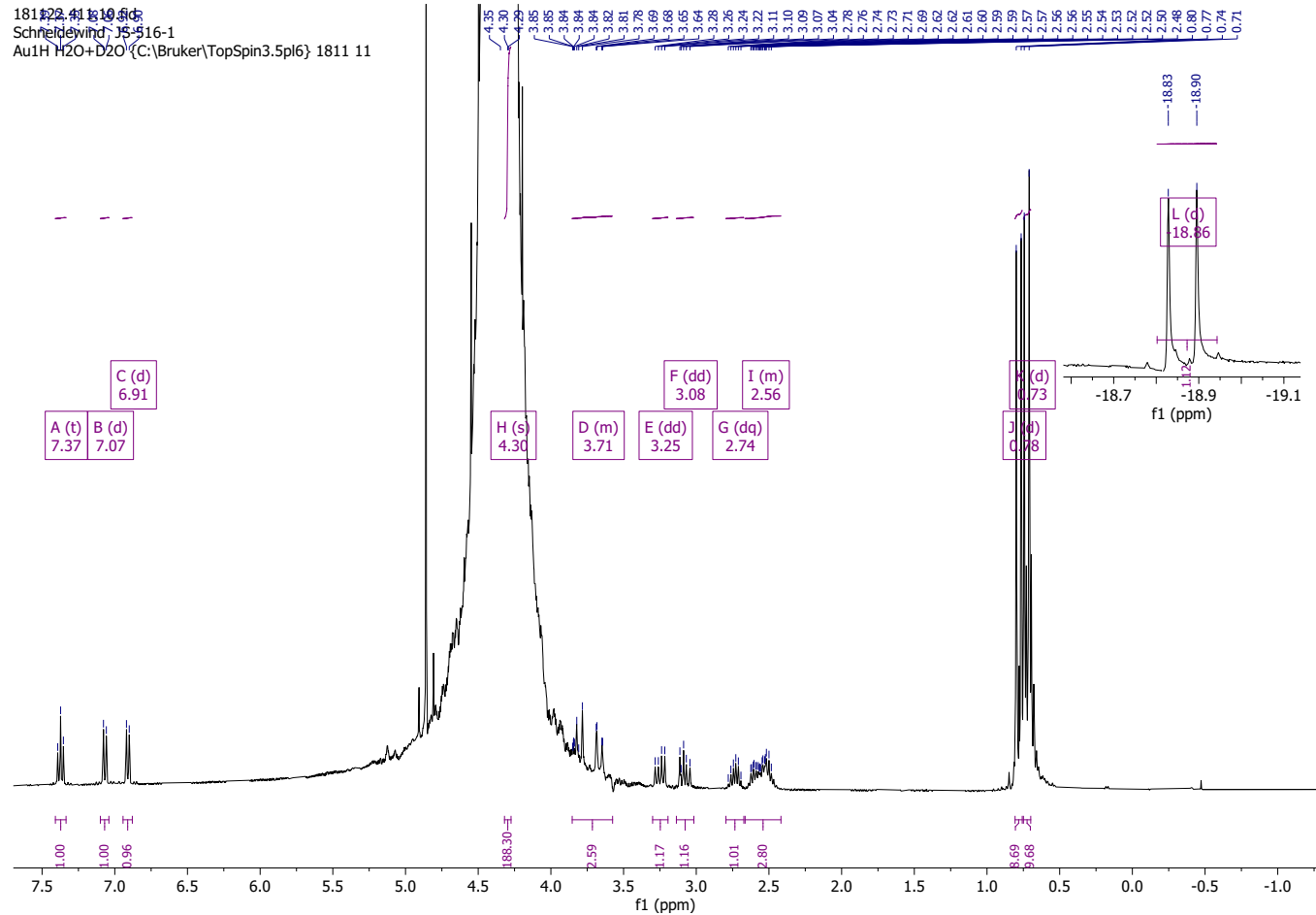


Figure 7.2-1 ^1H NMR spectrum of 2-trans in H_2O (298 K)
(inlet showing hydride peak)

181122.411.11.fid
Schneidewind JS-516-1
Au31P-quant H2O+D2O {C:\Bruker\TopSpin3.5pl6} 1811 11

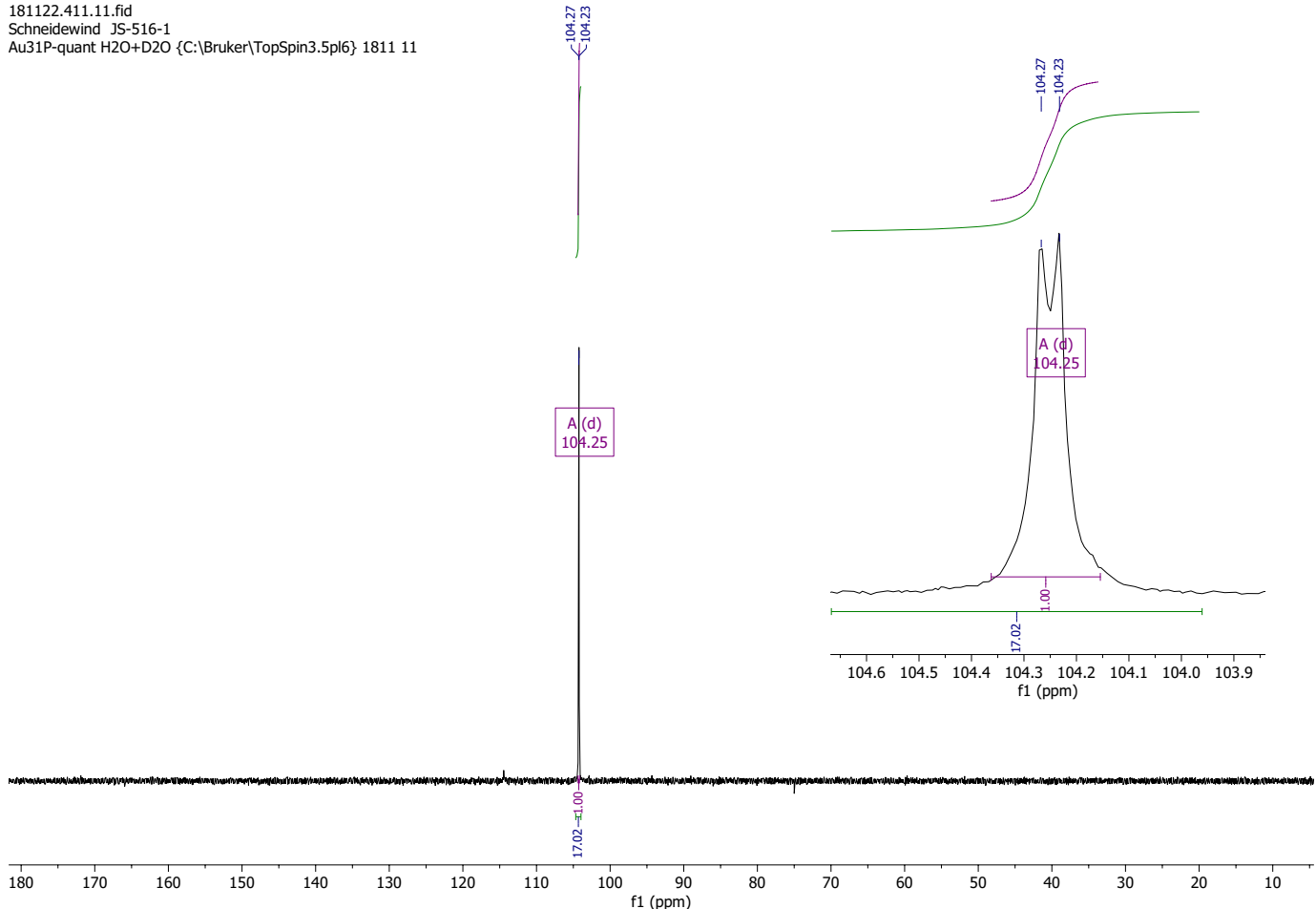


Figure 7.2-2 $^{31}\text{P}\{\text{H}\}$ NMR spectrum of 2-trans in H_2O (298 K)
(inlet shows splitting of ^{31}P signal due to coupling to hydride ligand, which is outside of decoupler range)

7.3 Characterization of (p-cymene)RuCl₂(CO)

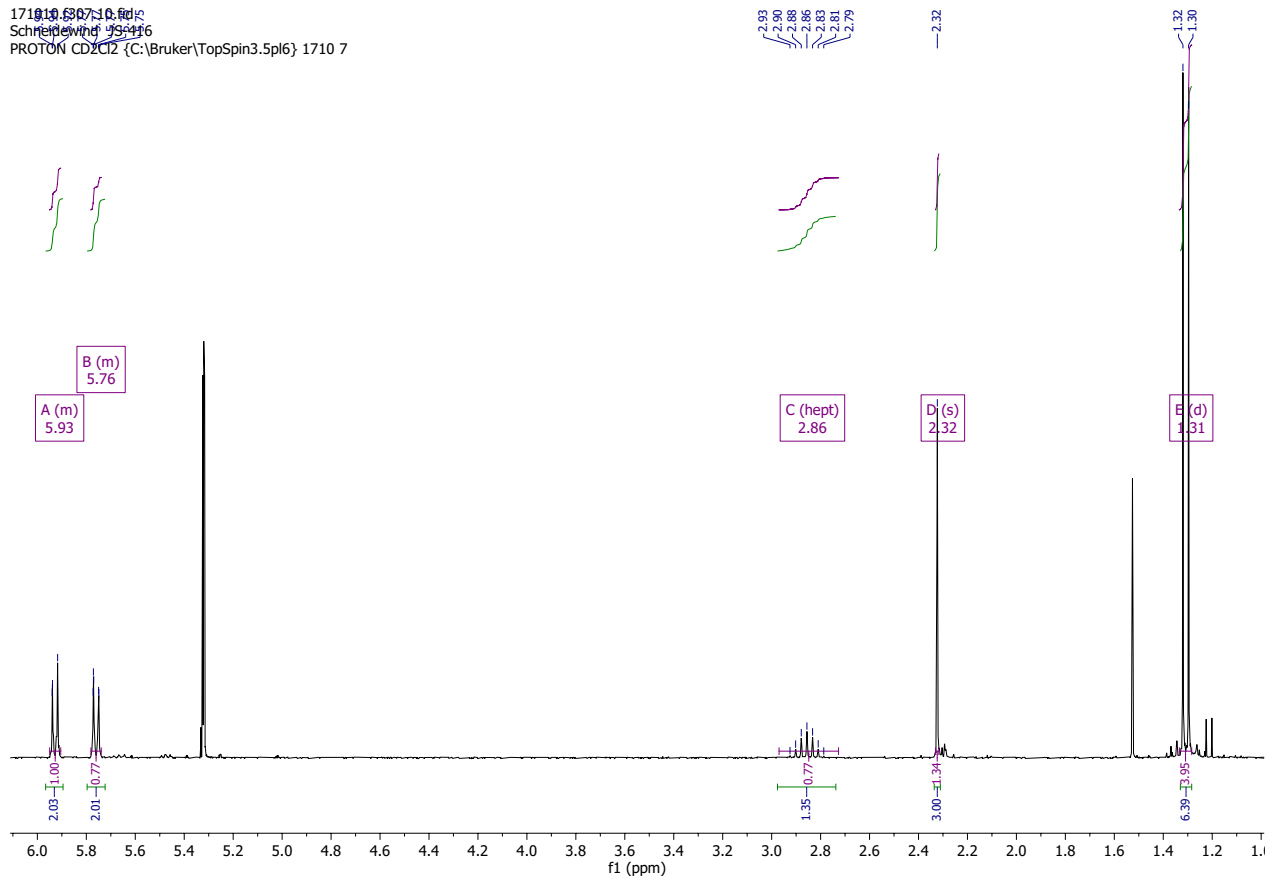


Figure 7.3-1 ¹H NMR spectrum of (p-cymene)RuCl₂(CO) in CD₂Cl₂ (298 K)

7.4 Characterization of (PNN)RuCl₂(CO)

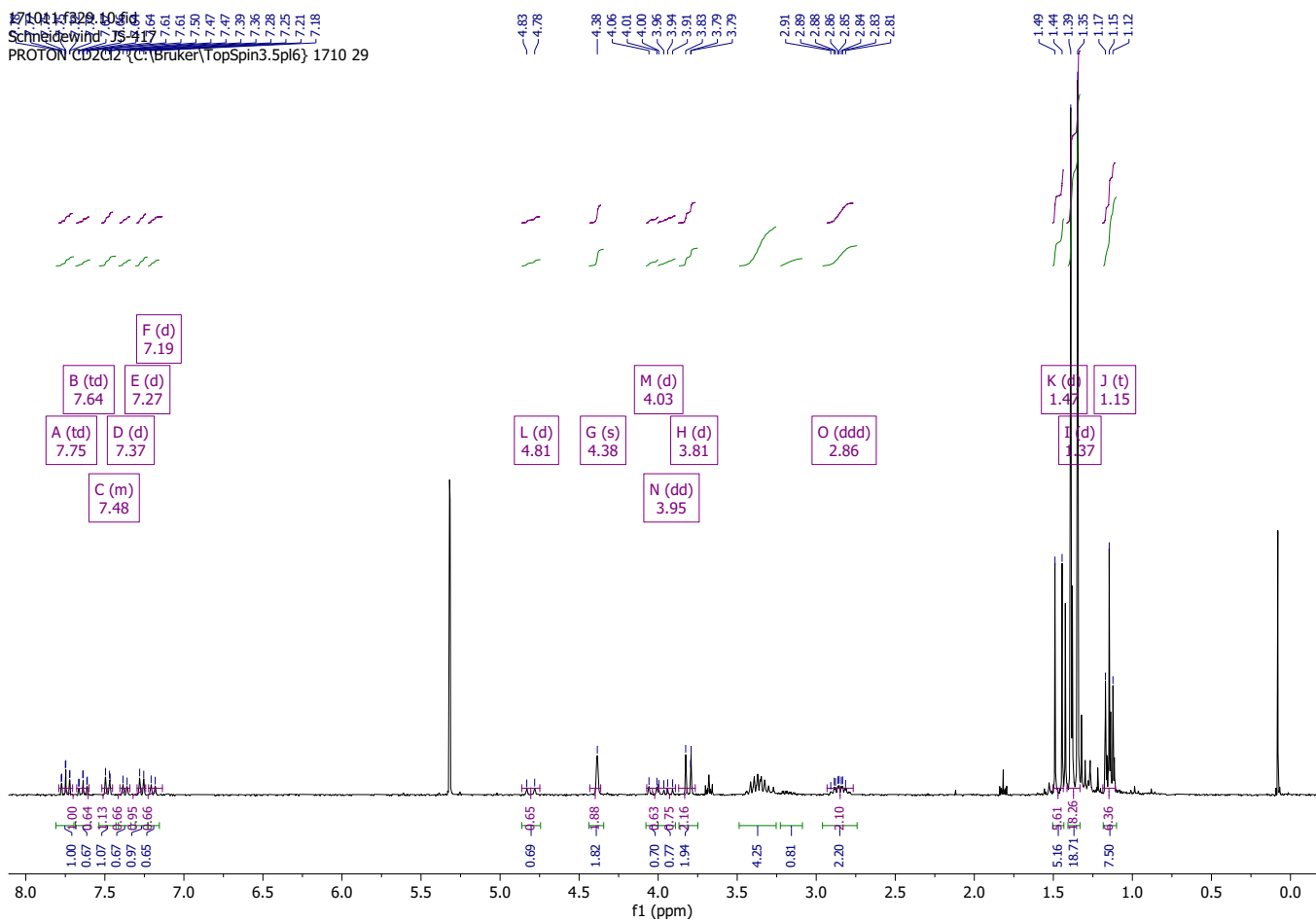


Figure 7.4-1 ¹H NMR spectrum of (PNN)RuCl₂(CO) in CD₂Cl₂ (298 K)
(mixture of cis and trans isomers)

171011.f329.11.fid
Schneidewind JS-417
P31quant CD₂Cl₂ {C:\Bruker\TopSpin3.5pl6} 1710 29

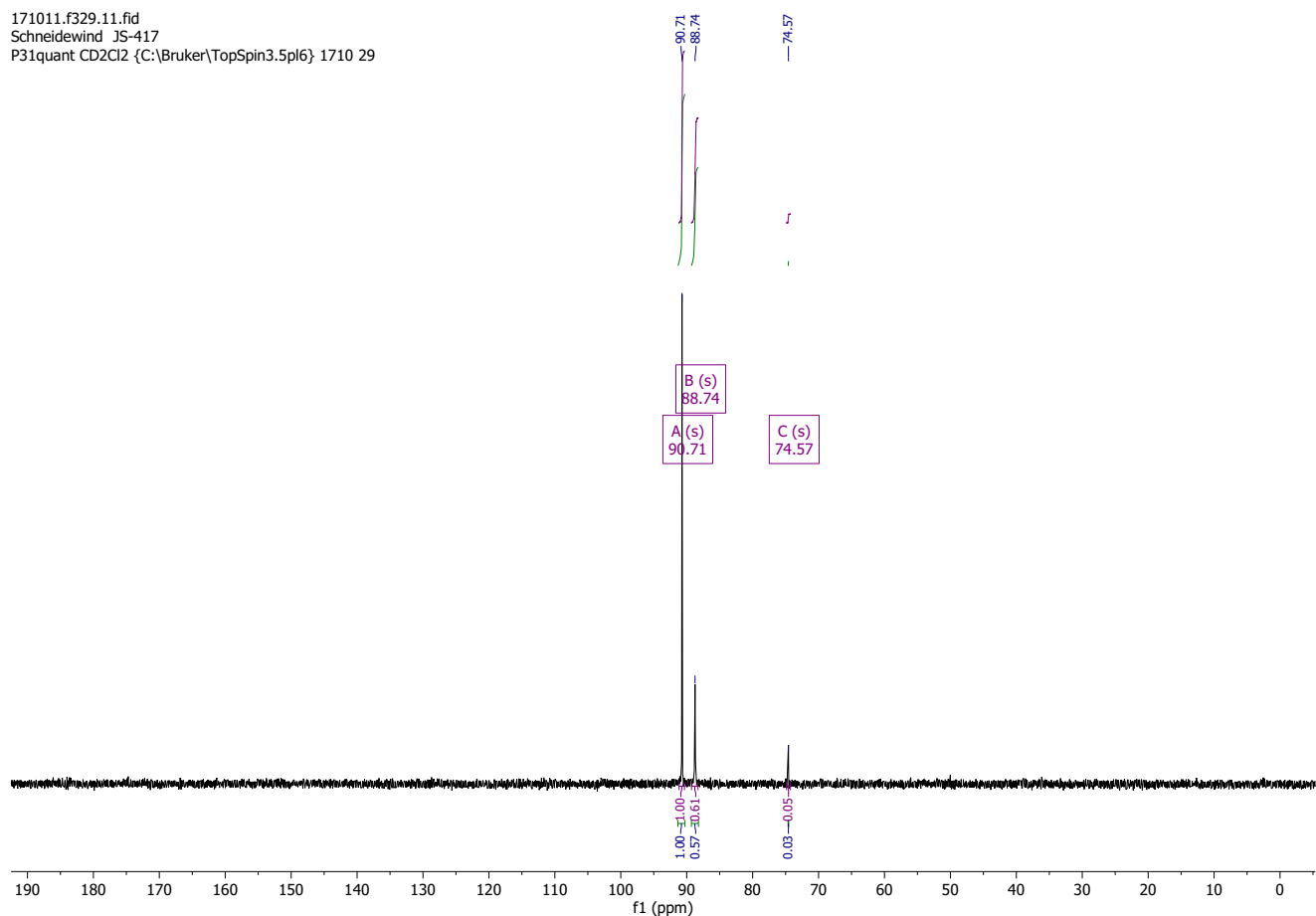


Figure 7.4-2 ³¹P{¹H} NMR spectrum of (PNN)RuCl₂(CO) in CD₂Cl₂ (298 K)
(mixture of cis and trans isomers)

7.5 Data for Irradiated Samples

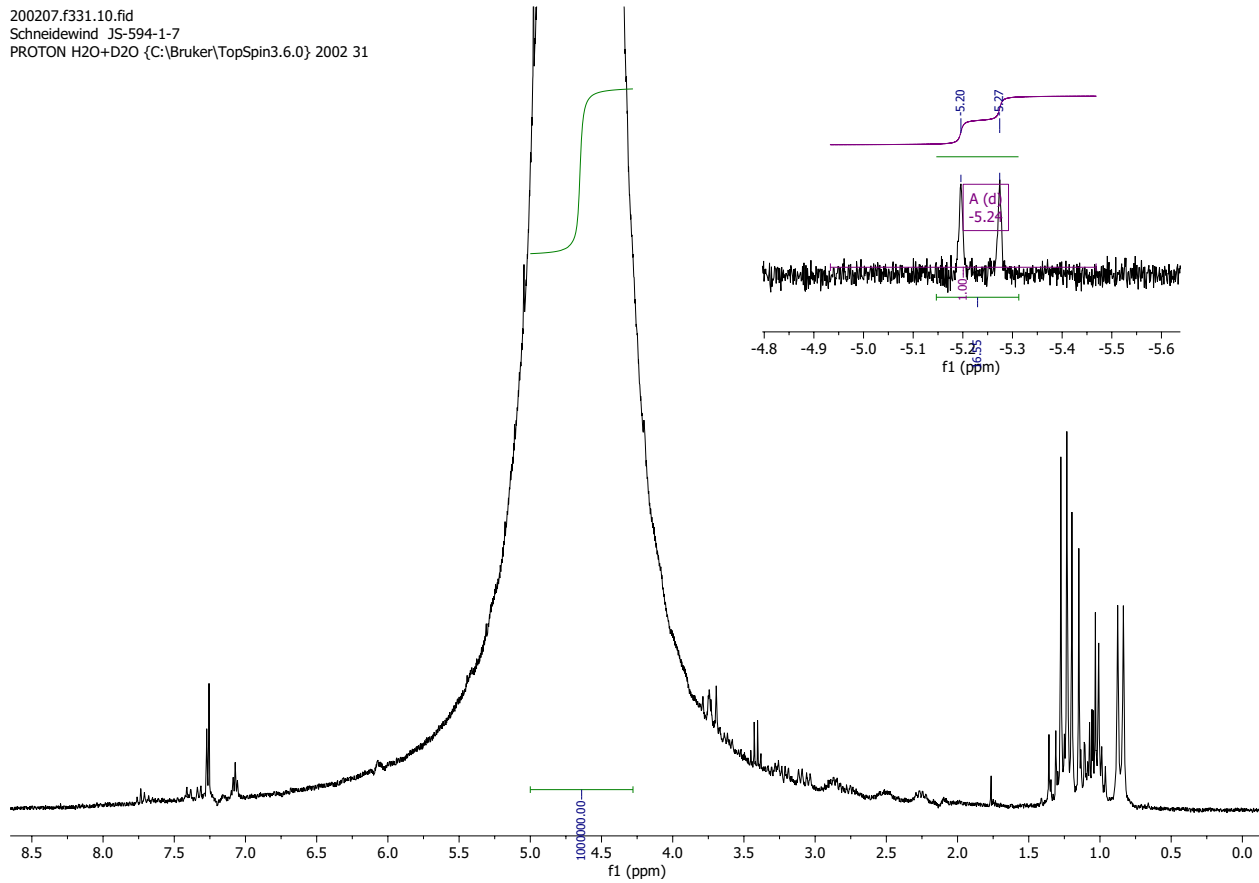


Figure 7.5-1 ¹H NMR spectrum of 1 (in H_2O , 298 K) after irradiation with QTH light source for 46h (irradiation without longpass filters, inlet showing hydride peak for 2-cis)

200207.f331.11.fid
Schneidewind JS-594-1-7
P31quant H2O+D2O {C:\Bruker\TopSpin3.6.0} 2002 31

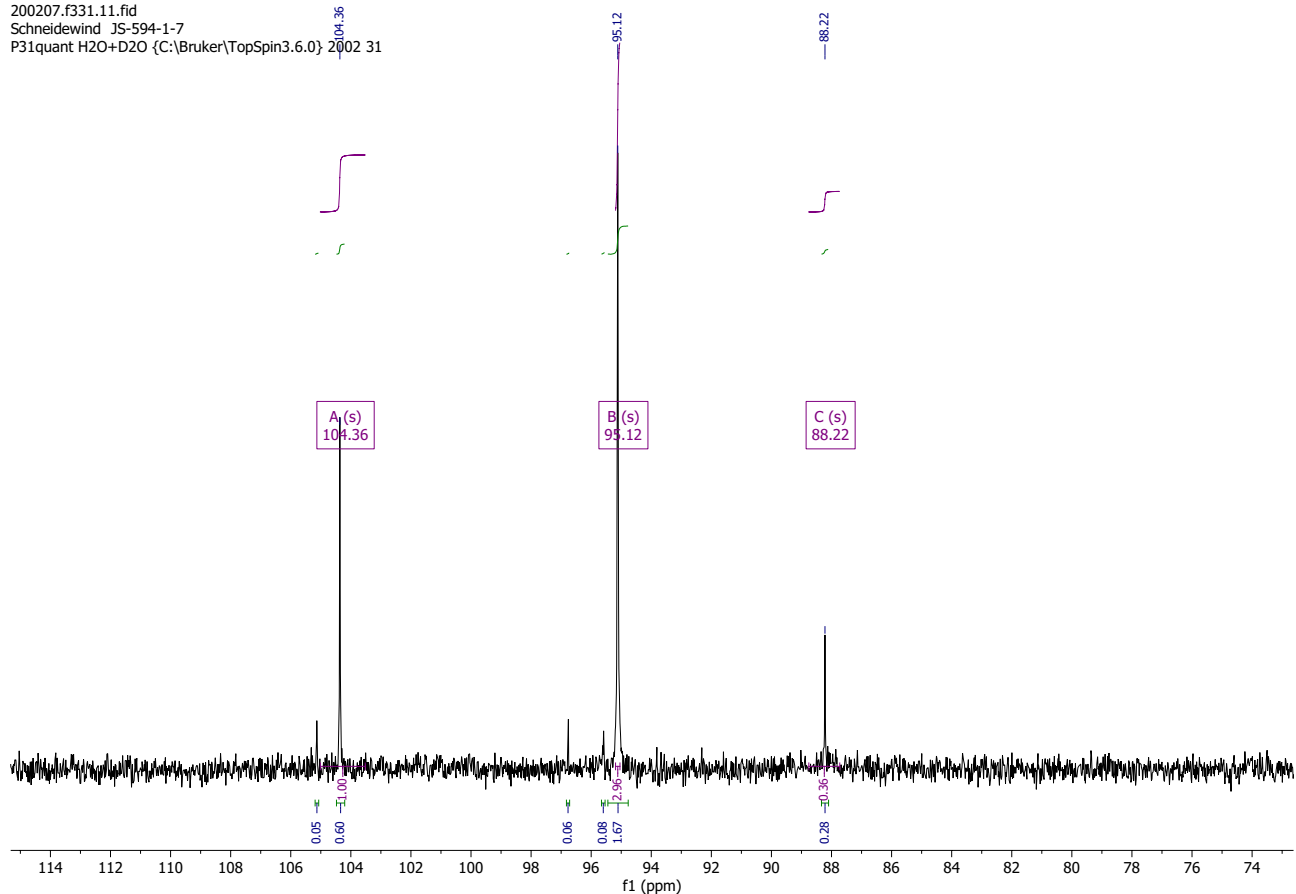
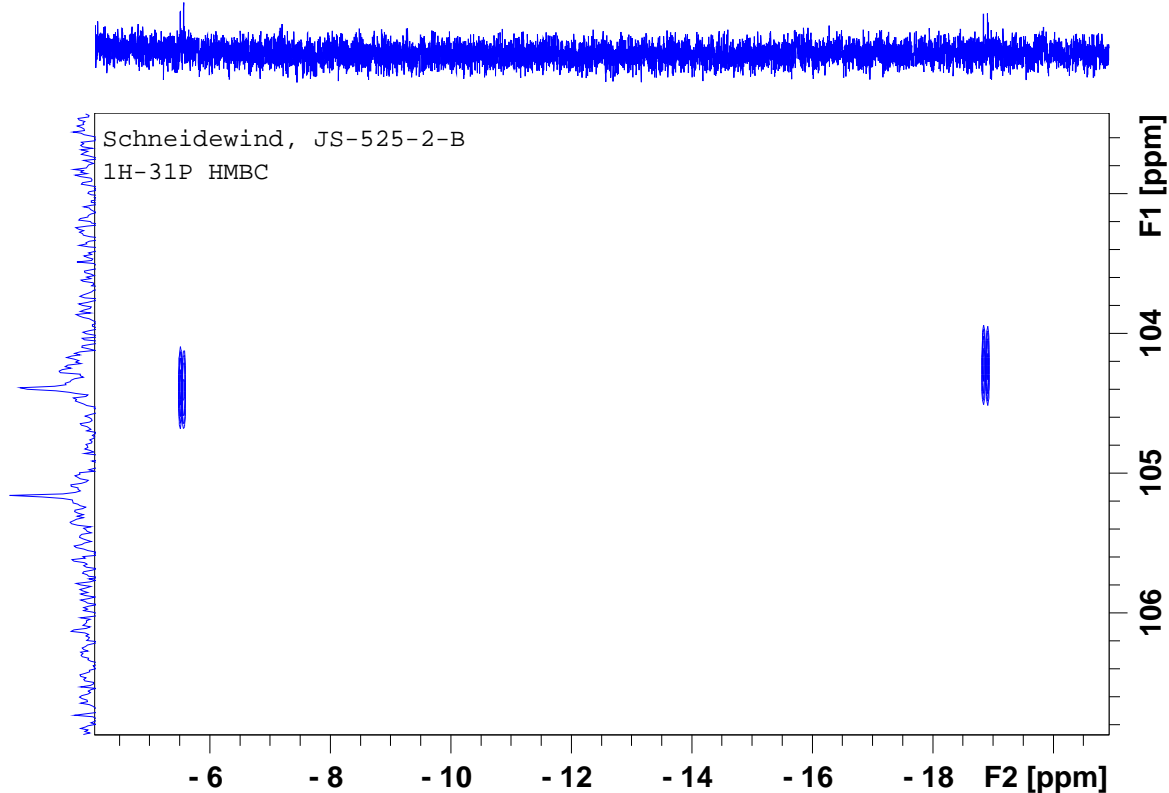
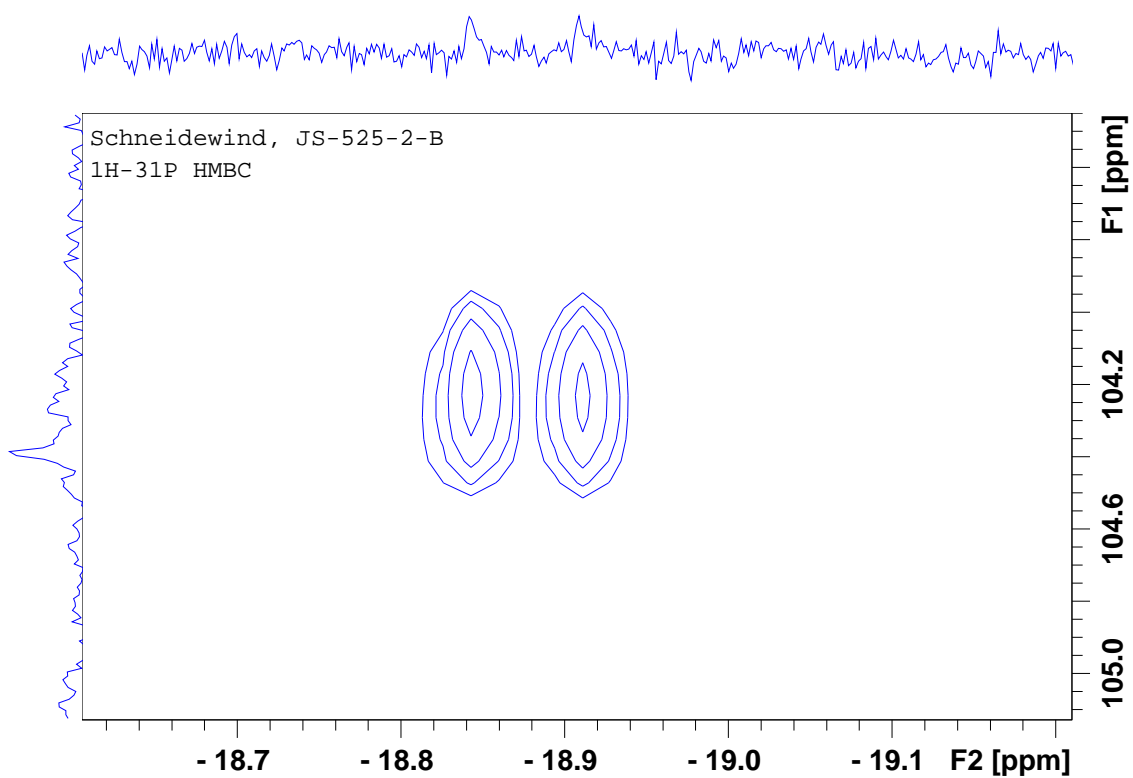


Figure 7.5-2 $^{31}\text{P}\{\text{H}\}$ NMR spectrum of 1 (in H_2O , 298 K) after irradiation with QTH light source for 46h (irradiation without longpass filters)

190130.40a 4 1 K:\nmr\AV400\data\1901\nmr



190130.40a 4 1 K:\nmr\AV400\data\1901\nmr



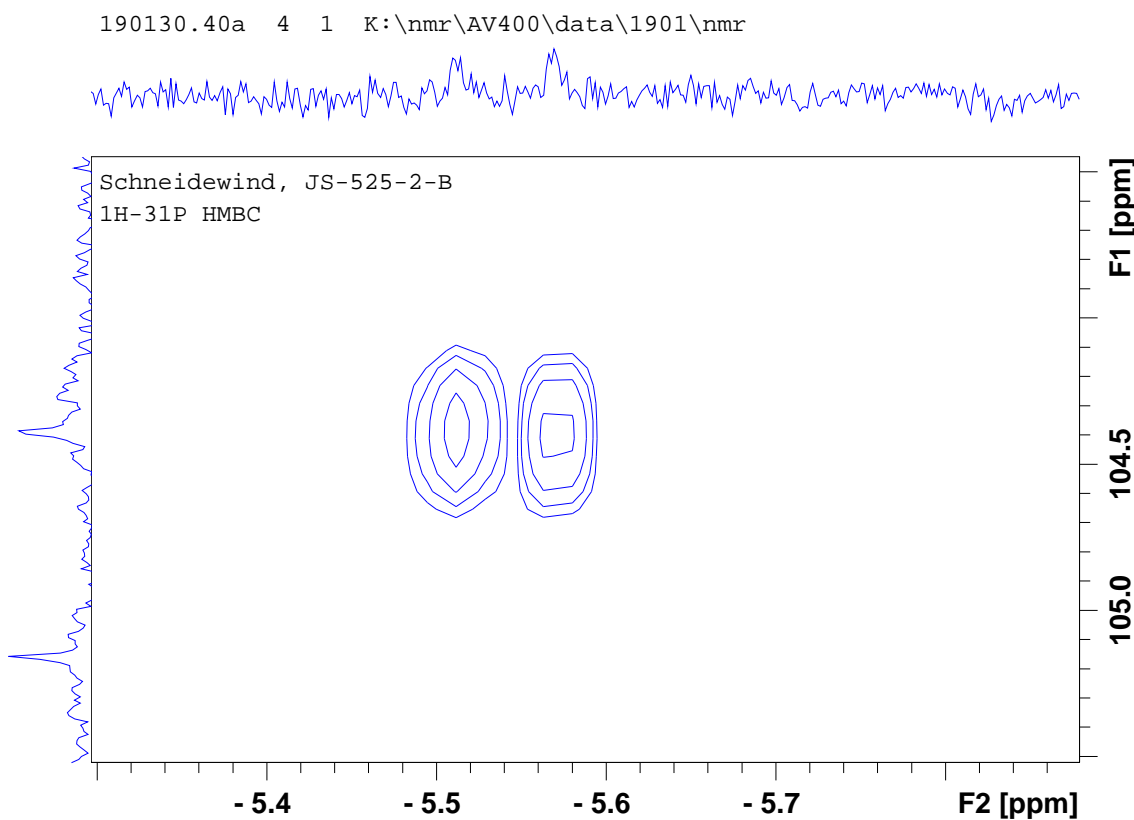


Figure 7.5-3 ^1H - ^{31}P HMBC (hydride region) NMR spectrum of 1 (in H_2O , 298 K) after irradiation
 Top: overview of entire ^1H - ^{31}P spectrum. Middle: Zoom showing coupling of $\delta(^{31}\text{P}) = 104.25 \text{ ppm}$ with $\delta(^1\text{H}) = -18.86 \text{ ppm}$, corresponding to **2-trans**. Bottom: Zoom showing coupling of $\delta(^{31}\text{P}) = 104.36 \text{ ppm}$ with $\delta(^1\text{H}) = -5.24 \text{ ppm}$ corresponding to **2-cis**. Note that **2-trans** is present in this sample since the HMBC measurement was performed five days after irradiation, allowing for partial isomerization of **2-cis** to **2-trans**.

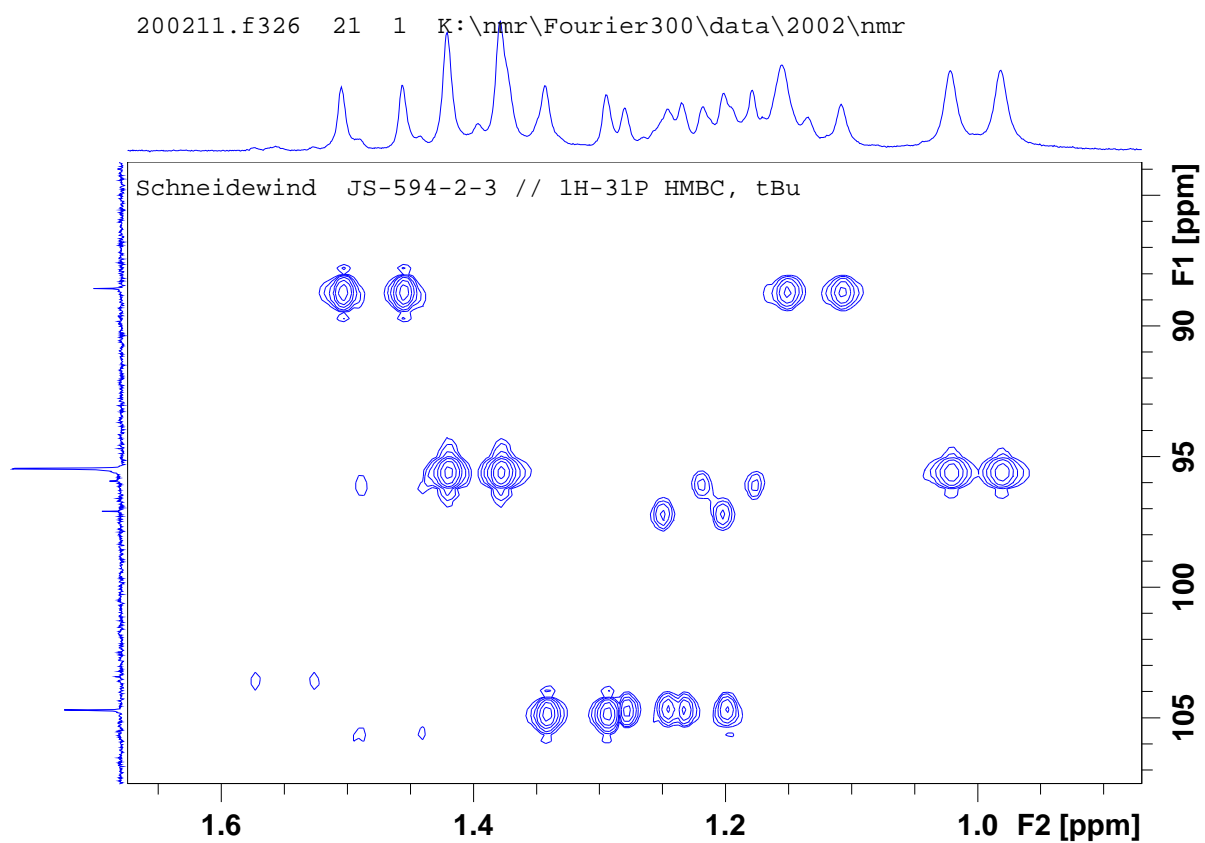


Figure 7.5-4 ^1H - ^{31}P HMBC (aliphatic region) NMR spectrum of **1** (in H_2O , 298 K) after irradiation

Note that this spectrum was measured directly after irradiation hence no **2-trans** is present. The $\delta(^{31}\text{P}) = 95.12$ ppm signal couples with two doublets at $\delta(^1\text{H}) = 1.4$ ppm and $\delta(^1\text{H}) = 1.0$, which correspond to the two tBu groups of the PNN ligand. This shows that the tBu groups in this species are not equivalent and hence this species has no symmetry.

190311.306.d0.fid
Schneidewind AS-531-5-2
Au1H H2O+D2O {C:\Bruker\TopSpin3.6.0} 1903 6

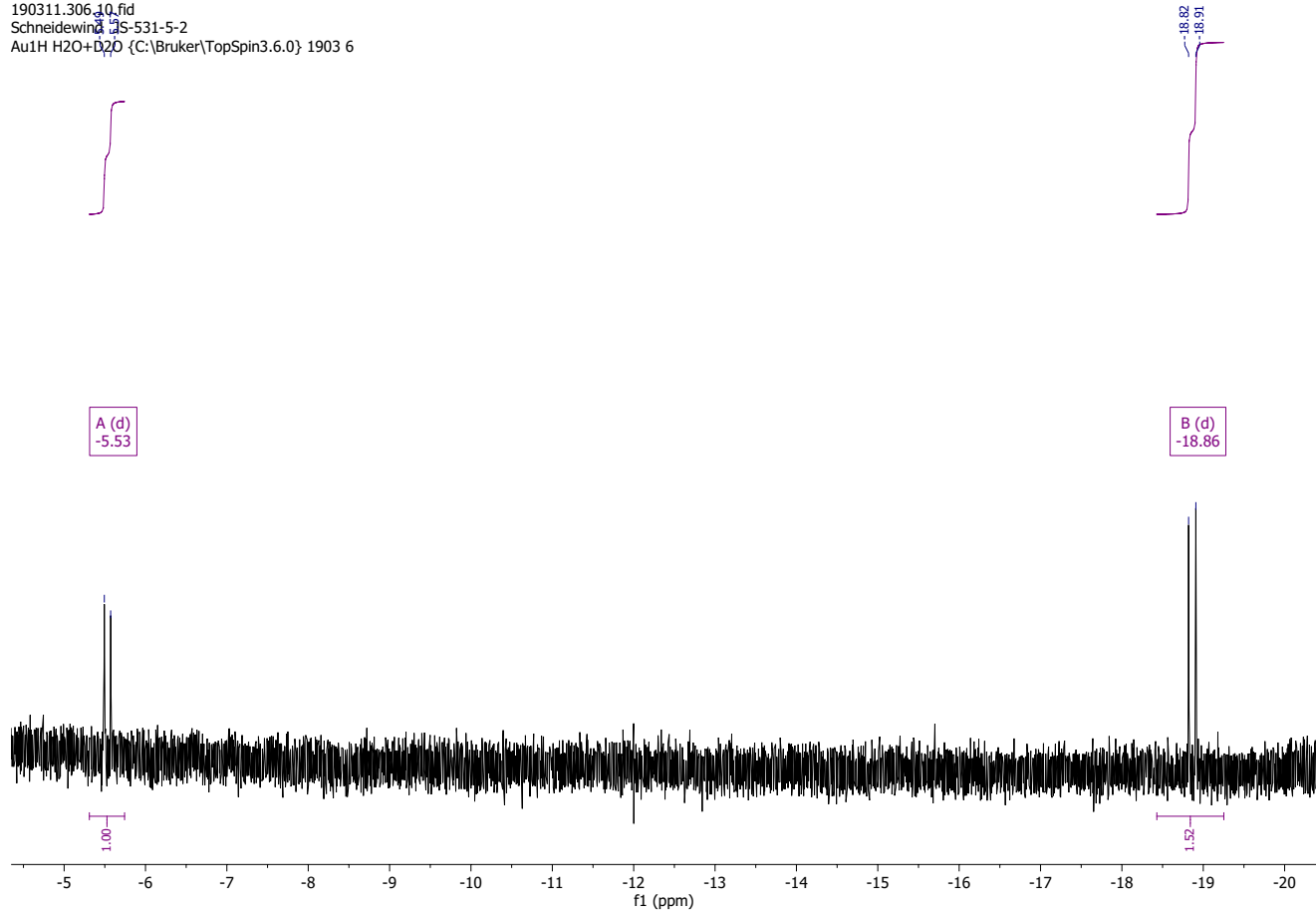


Figure 7.5-5 ${}^1\text{H}$ NMR spectrum of 2-trans (in H_2O , 298 K) after irradiation (320 – 500 nm, 4h) in presence of O_2

190311.306.11.fid
Schneidewind JS-531-5-2
Au31P-quant H2O+D2O {C:\Bruker\TopSpin3.6.0} 1903 6

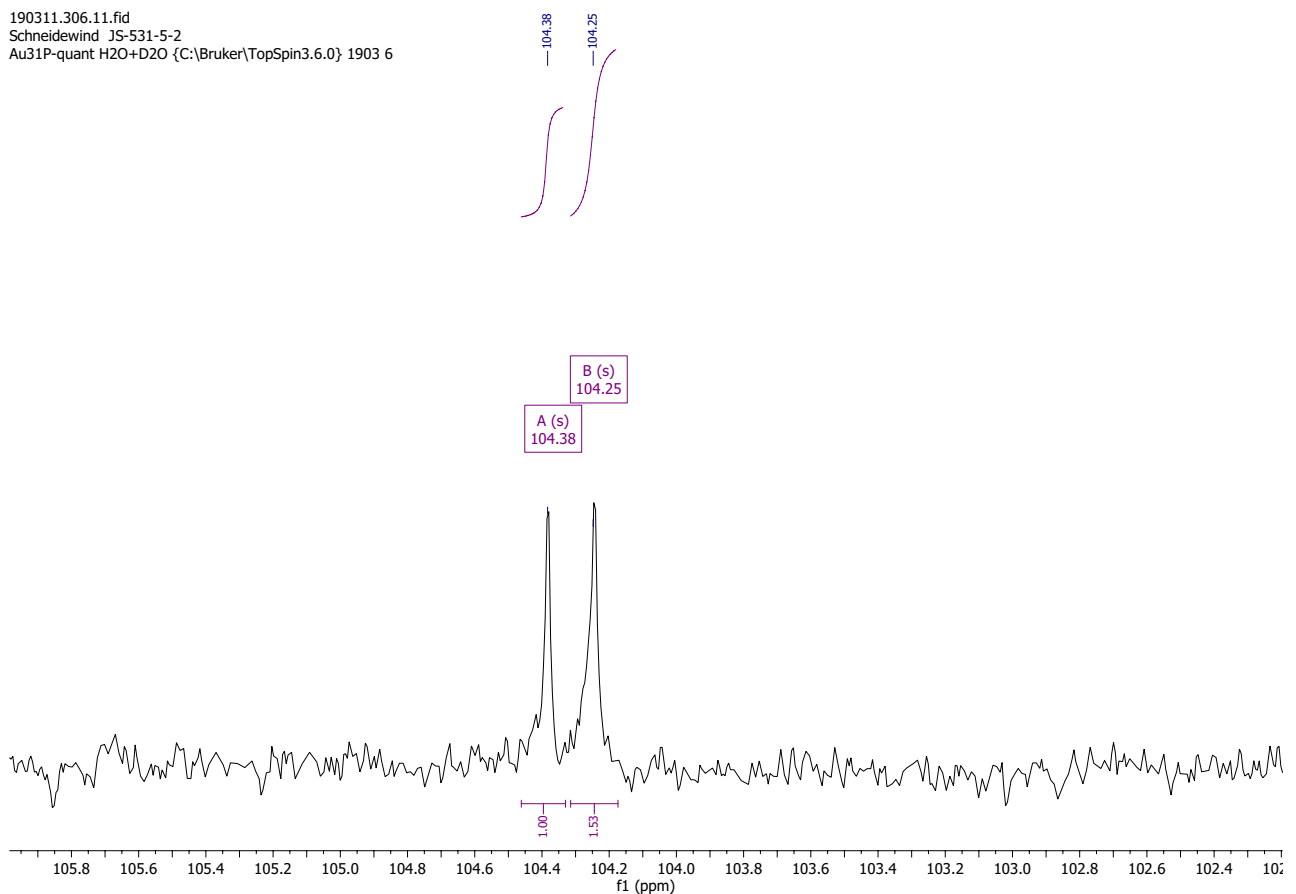


Figure 7.5-6 $^{31}\text{P}\{\text{H}\}$ NMR spectrum of 2-trans (in H_2O , 298 K) after irradiation (320 – 500 nm, 4h) in presence of O_2

200129.326.10.fid
Schneidewind JS-575-2-2
Au1H H2O+D2O {C:\Bruker\TopSpin3.6.0} 2001 26

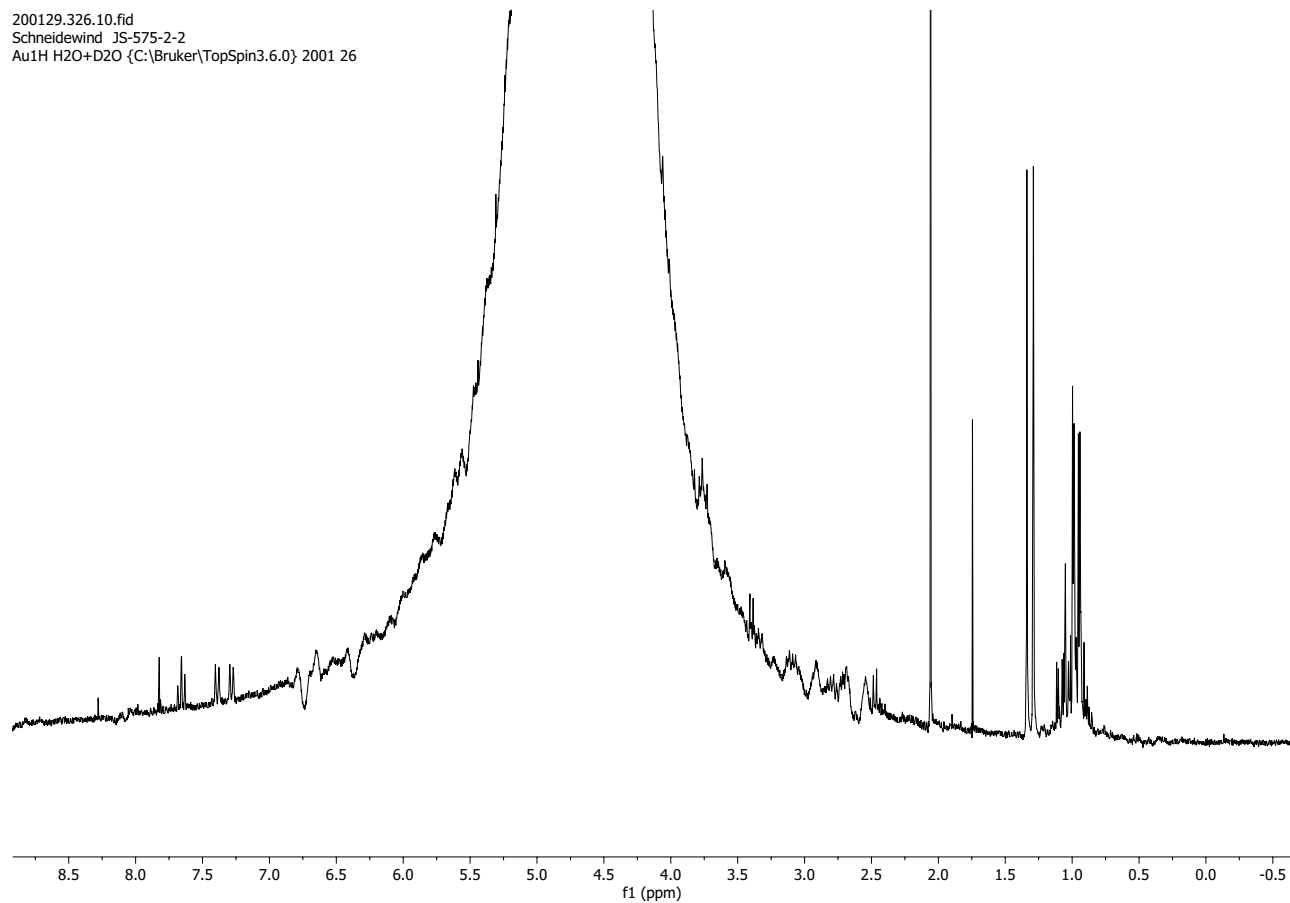


Figure 7.5-7 ¹H NMR spectrum of 1 (in 52 mM KOH aq., 298 K, Ag₂O synthesis route) in air before irradiation.

200129.326.11.fid
Schneidewind JS-575-2-2
Au31P-quant H2O+D2O {C:\Bruker\TopSpin3.6.0} 2001 26

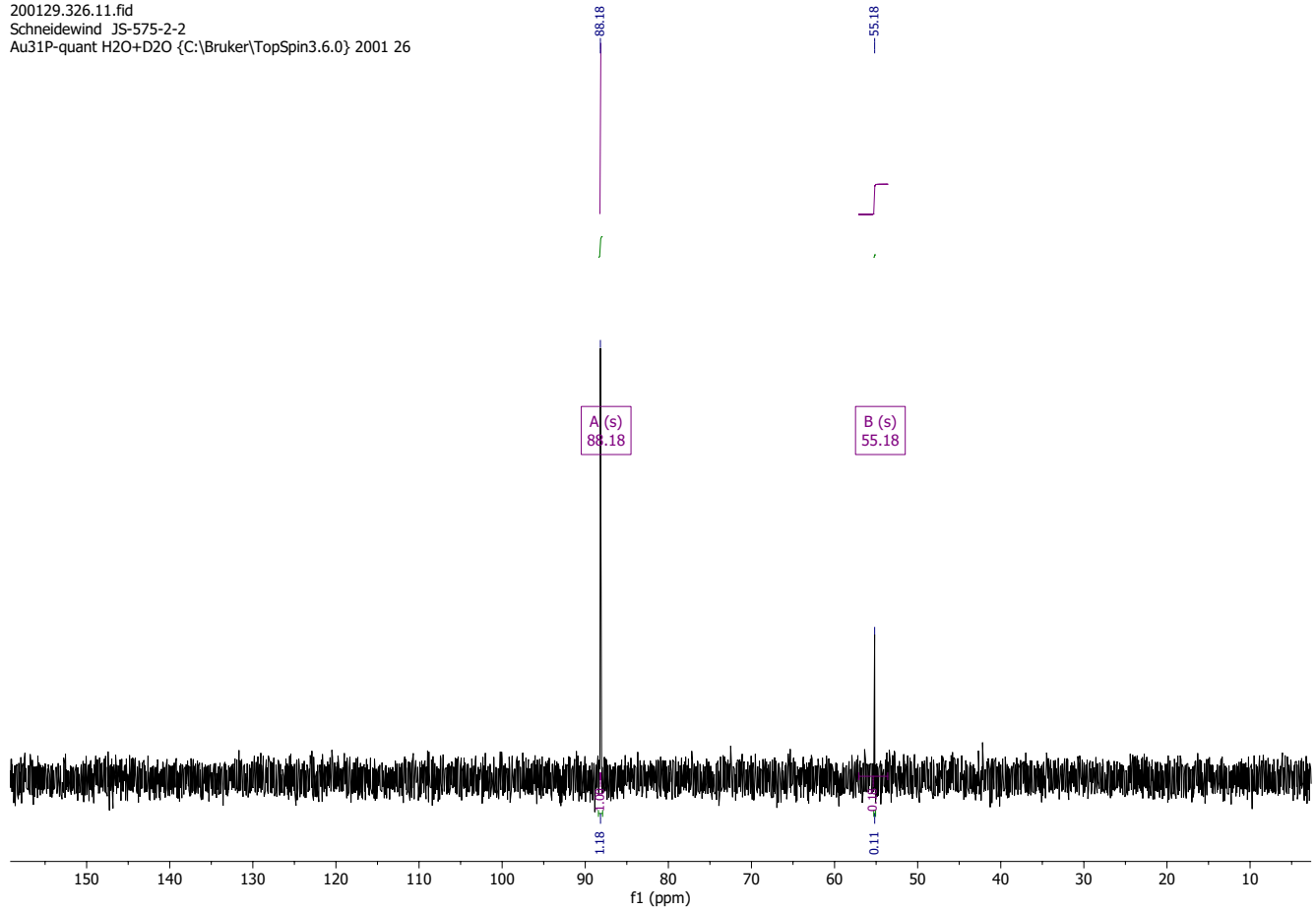


Figure 7.5-8 $^{31}\text{P}\{\text{H}\}$ NMR spectrum of **1** (in 52 mM KOH aq., 298 K, Ag_2O synthesis route) in air before irradiation.

Integrals are relative to H_3PO_4 capillary standard.

200130.301.10.fid
Schneidewind JS-575-2-3
Au1H H2O+D2O {C:\Bruker\TopSpin3.6.0} 2001 1

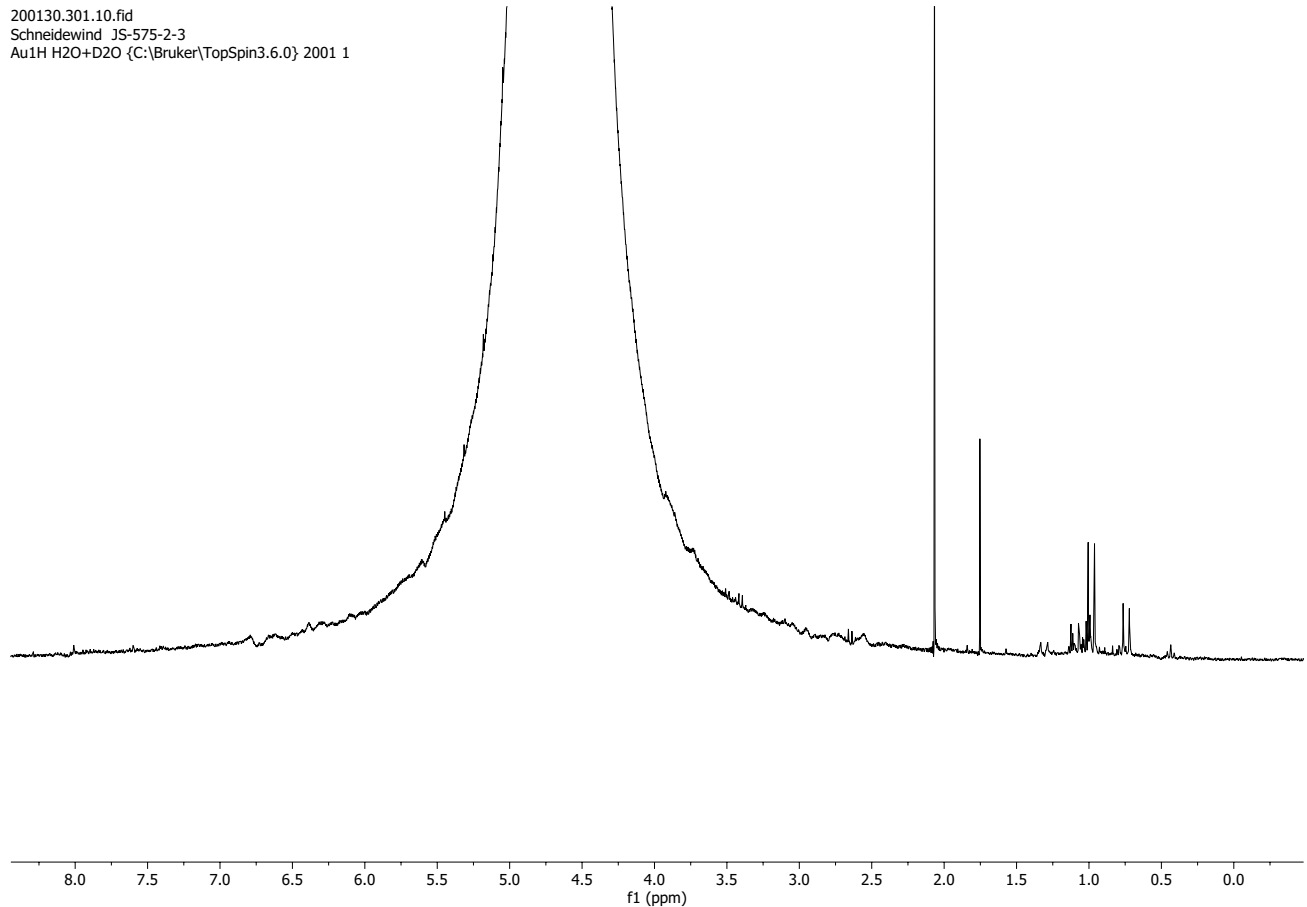


Figure 7.5-9 ¹H NMR spectrum of **1** (in 52 mM KOH aq., 298 K, Ag₂O synthesis route) in air after irradiation (QTH, 16h)

200130.301.11.fid
Schneidewind JS-575-2-3
Au31P-quant H2O+D2O (C:\Bruker\TopSpin3.6.0) 2001 1

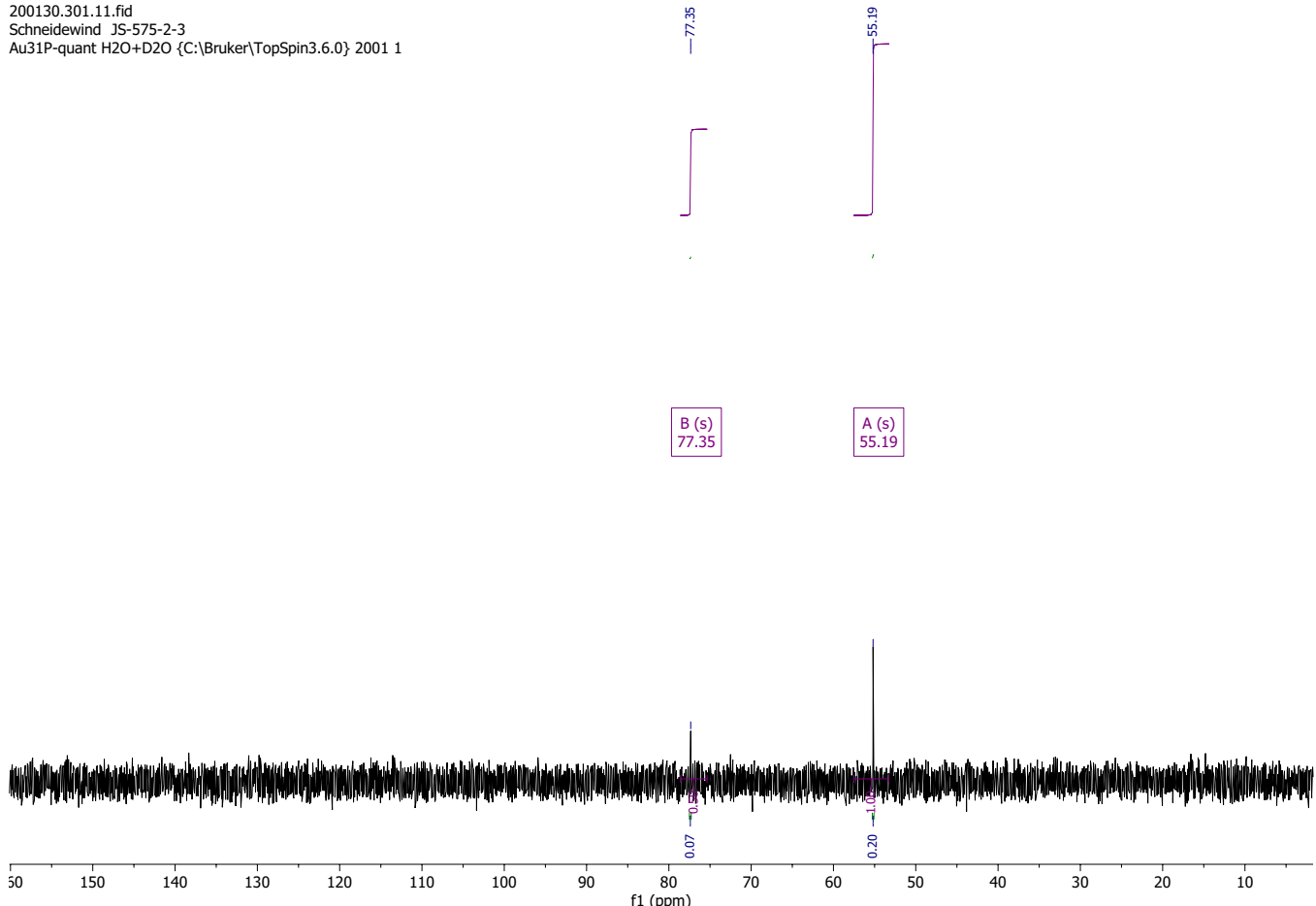


Figure 7.5-10 $^{31}\text{P}\{\text{H}\}$ NMR spectrum of 1 (in 52 mM KOH aq., 298 K, Ag_2O synthesis route) in air after irradiation (QTH, 16h)
Integrals are relative to H_3PO_4 capillary standard.

7.6 Isomerization Reactions in the Dark

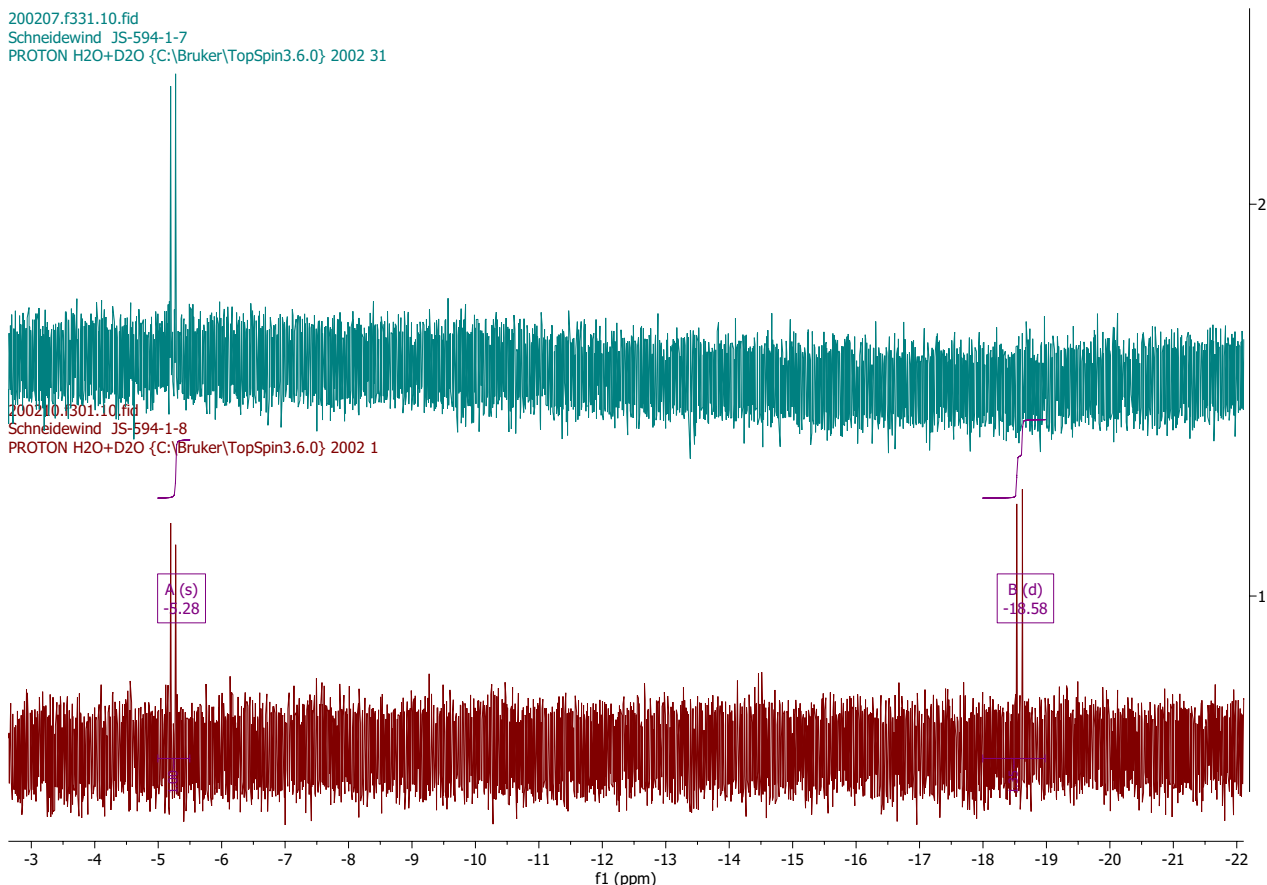


Figure 7.6-1 Stacked ^1H NMR spectra of 1 (in H_2O , 298 K) immediately after irradiation (top, green) and same sample after two more days in the dark (bottom, red)

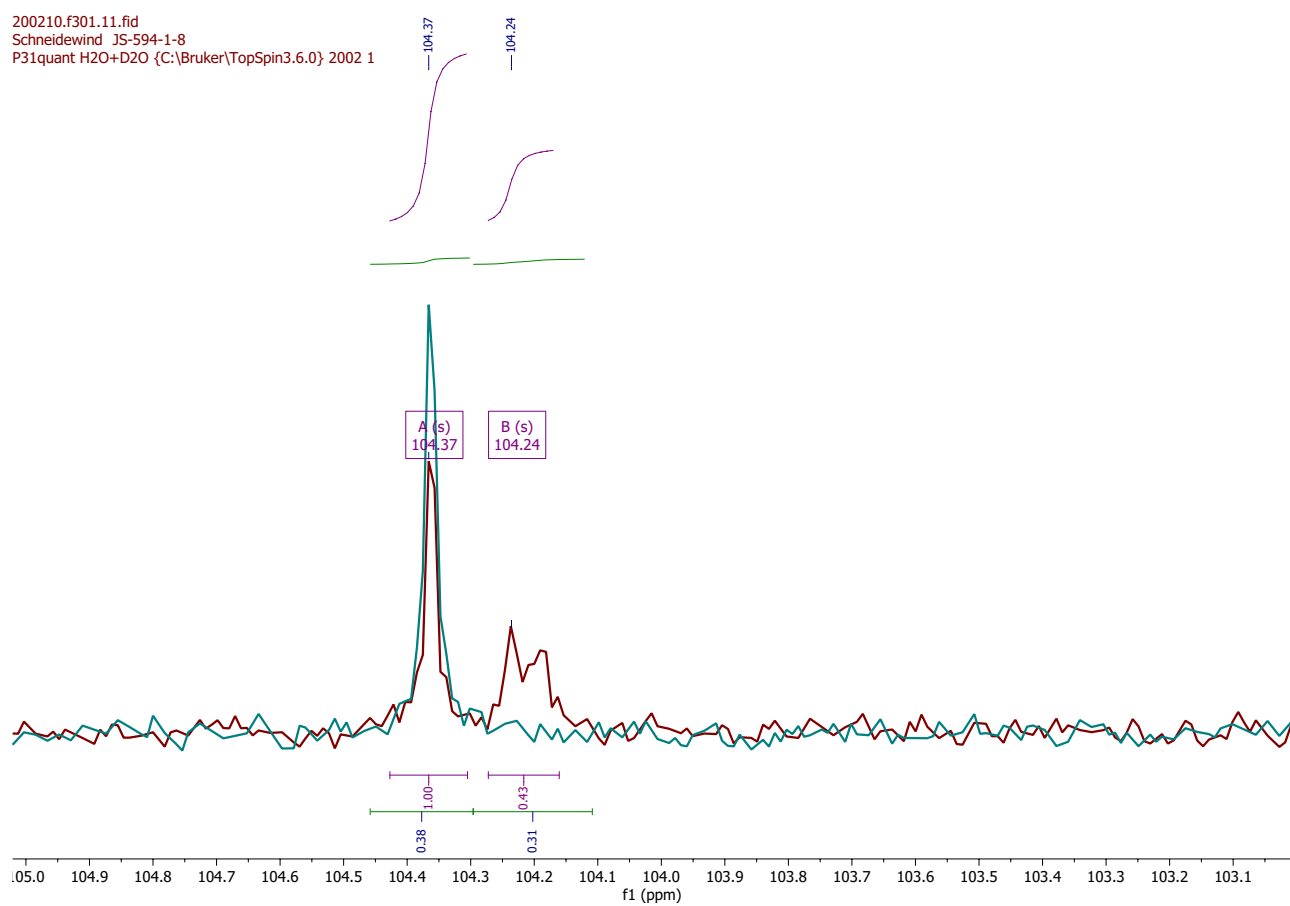


Figure 7.6-2 Superimposed $^{31}\text{P}\{\text{H}\}$ NMR spectra of 1 (in H_2O , 298 K) immediately after irradiation (green) and same sample after two more days in the dark (red)

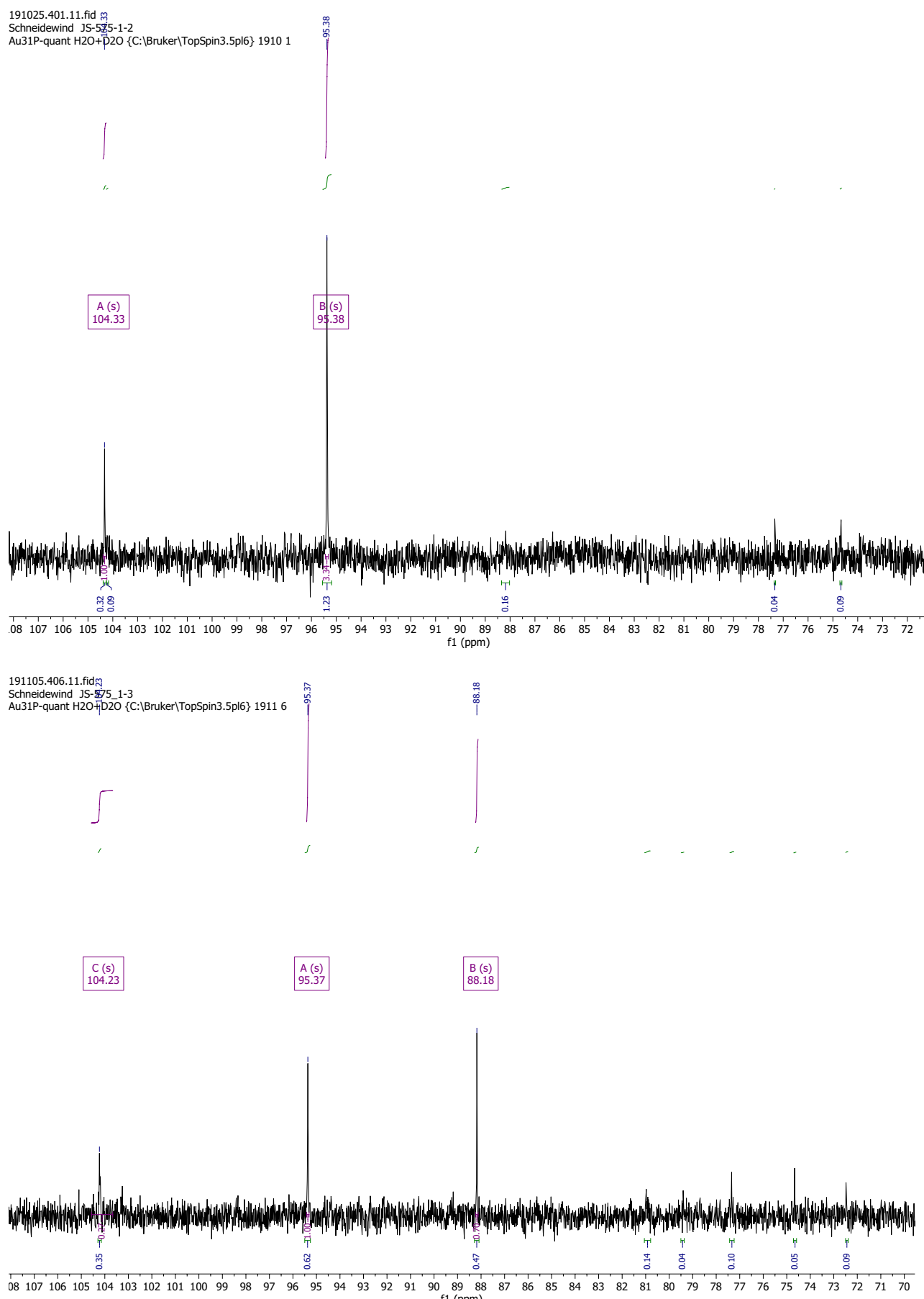


Figure 7.6-3 $^{31}\text{P}\{^1\text{H}\}$ NMR spectrum of 1 (in 52 mM KOH aq., 298 K, Ag_2O synthesis route) immediately after irradiation (top) and the same sample after twelve more days in the dark

7.7 Data for $\partial(^3\text{P}) = 86$ ppm Product

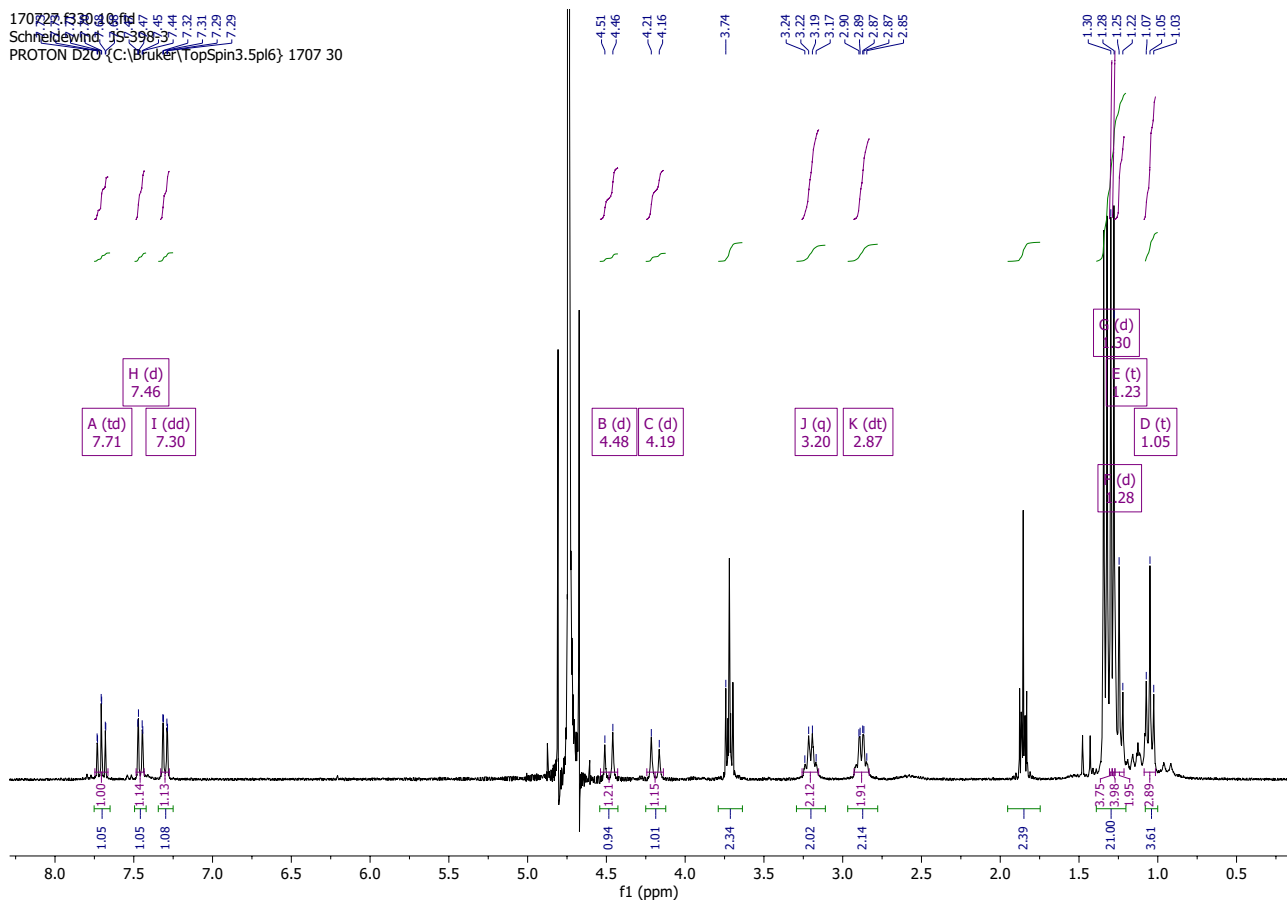


Figure 7.7-1 ^1H NMR spectrum of raw product (in D_2O , 298 K) after reaction of 2-trans with N_2O for 20h in presence of 83 equivalents of H_2O

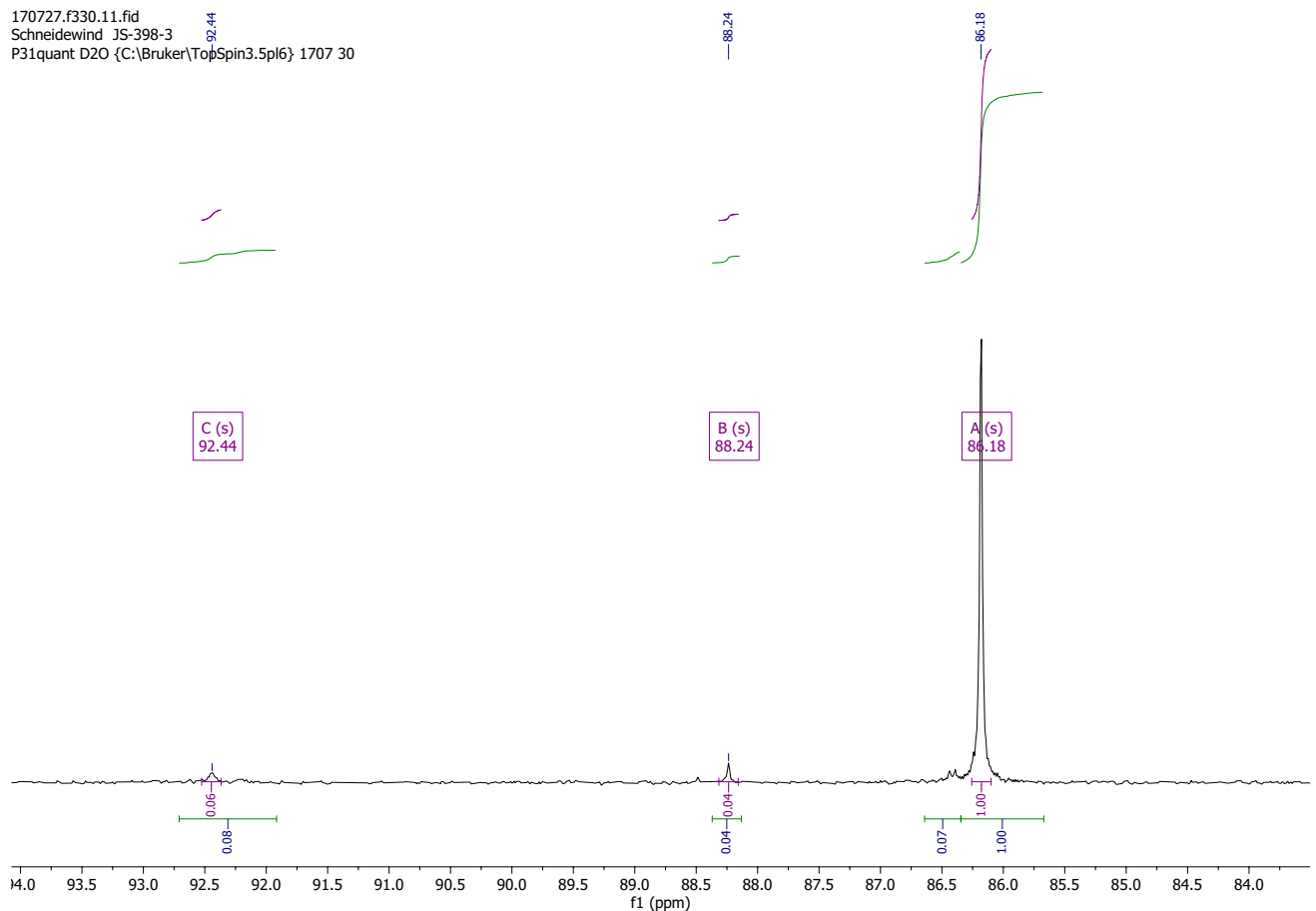


Figure 7.7-2 $^{31}\text{P}\{\text{H}\}$ NMR spectrum of raw product (in D_2O , 298 K) after reaction of 2-trans with N_2O for 20h in presence of 83 equivalents of H_2O

8 Other Analytical Data

8.1 IR Spectrum of Complex 1

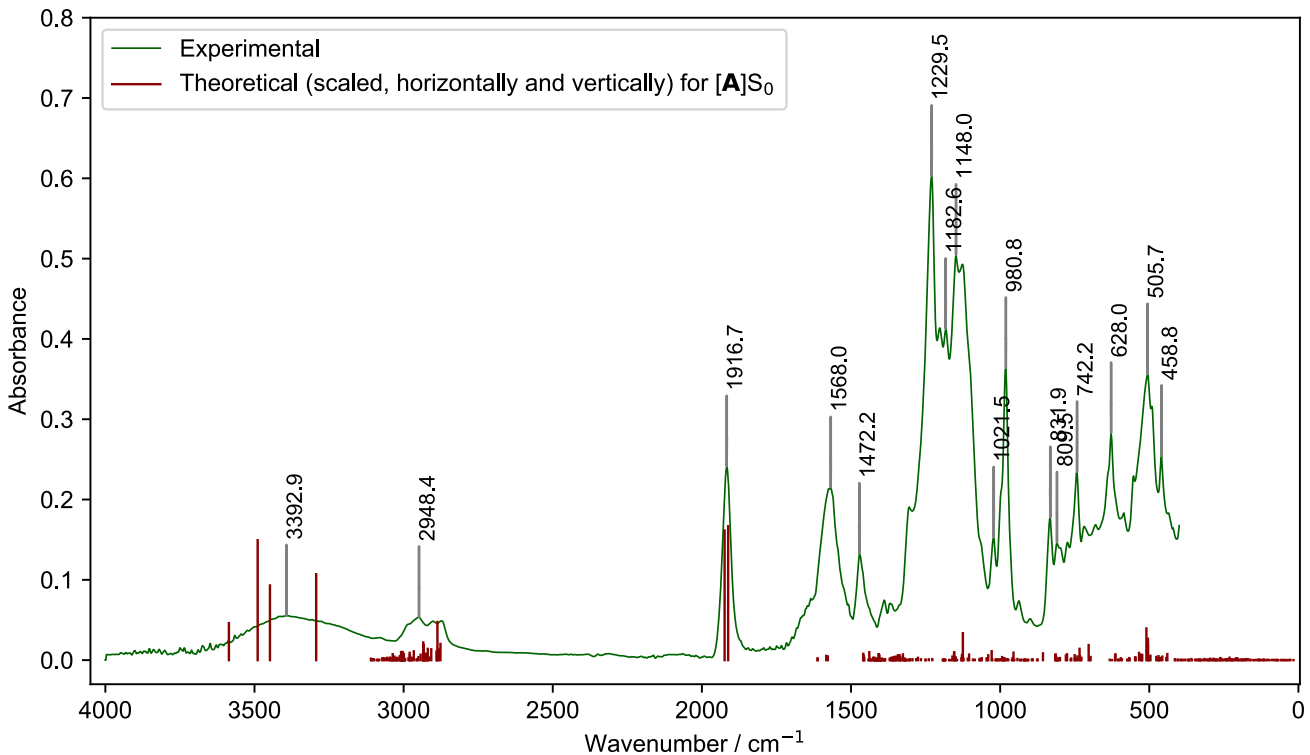


Figure 8.1-1 IR Spectrum (ATR) of complex 1 along with theoretical spectrum for $[A]S_0$

Note: theoretical spectrum is shown as vertical lines for each transition. The theoretical spectrum has been scaled horizontally by a factor of 0.96 and has been scaled vertically.

8.2 EPR Spectrum of Complex 1 Synthesis Raw Product

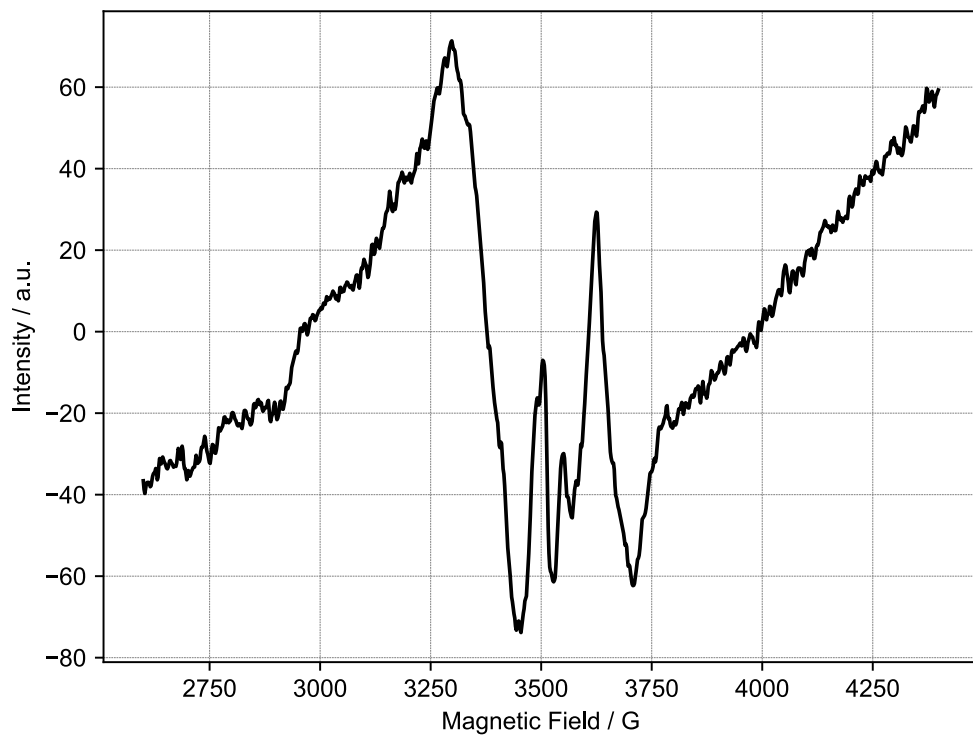


Figure 8.2-1 EPR spectrum of green raw product obtained via reaction of 2-trans with N₂O

N₂O reaction of **2-trans** was carried out as described in 3.1.1, but after the reaction, the solvent was completely removed under vacuum and the dark green solid residue was washed with Et₂O and pentane. The residue was then dissolved in DCM, yielding a green solution, which was transferred to a capillary and measured.

9 Ultrafast Pump-Probe Spectroscopy

9.1 Experimental Procedure and Analysis

Transient absorption spectra were recorded with a time resolution of ca. 200 fs by means of a pump-probe setup based on a Ti:sapphire laser system (Spectra-Physics, Spitfire Pro) operating at a centre wavelength of 800 nm and a repetition rate of 1 kHz. Pump pulses at a centre wavelength of 400 nm were generated by frequency doubling a part of the output of the Ti:sapphire system using a BBO-crystal. The energy of the pump pulses was between 0.8 and 1 μ J. A white light continuum for probing was obtained by focussing a small fraction of the Ti:sapphire output into a CaF₂-crystal. Pump and probe beam were focussed into the sample so that their overlapping spots had an effective diameter of 360 μ m for the pump and 210 μ m for the probe. Measurements were performed with the polarizations of the pump and probe beam set to parallel, perpendicular, and in magic-angle (54.7°). After passing through the sample, the probe beam was dispersed by a prism and transient absorption changes were recorded by an array detector in a spectrally resolved fashion.

Complex **1** was dissolved in oxygen-free water and the sample solution was transferred into a 1 mm fused silica cuvette under inert conditions. The optical density at 400 nm was ca. 0.7 to obtain transient spectra with a good signal to noise ratio (concentration \approx 0.007 M). The cuvette was mounted and measured on a rotation stage. A rotation frequency of about 1 Hz resulted in a sufficiently fast refreshing of the sample in the interaction region to avoid degeneration of the signal during the measurements. Transient absorption data was analyzed by global fitting of a sum of exponential decays revealing time constants and the corresponding decay associated spectra (DAS). To describe the ultrafast dynamics with sufficient accuracy, two exponential decay components are necessary and a long lived one with an “infinite” lifetime (>> 2 ns) much longer than the time range of 2 ns covered by our setup.

9.2 Results and Interpretation

Decay associated spectra for the two detected species ($\tau = 6$ ps and $\tau = 150$ ps) are shown in Figure 9.2-1. The $\tau = 6$ ps species can likely be attributed to an emissive S_n state of **1**, since the positive mΔOD between 450 and 650 nm agrees well with the measured fluorescence of **1**, suggesting that this feature is due to stimulated emission. The short lifetime of only 6 ps can also explain the weak nature of **1**’s fluorescence.

The experimental DAS for the $\tau = 150$ ps species agrees well with the computed DAS for [B-Trans]T₀ (see 11.4.2 for details on computed DAS spectra). The lifetime of this species, however, is too short to explain the observed reaction rates based on the kinetic model (see 10.3), which predicts a minimum lifetime of $\tau \approx 10$ ns for the second-photon absorbing intermediate. We propose that [B-Trans]T₀ might partially isomerize to [B]T₀ or [B]T₀ might be formed directly from [A]S_n, but in amounts which are below the detection limit of the used experimental set-up (TD-DFT calculations predict that [B]T₀ absorbs 400 – 700 nm light more weakly compared to [B-Trans]T₀, see Figure 11.2-1, further complicating direct detection). [B]T₀ and [B-Trans]T₀ might have different relaxation channels, especially because Ru-O bond formation can lead to **Oxo Dimer** formation for [B-Trans]T₀ but not for [B]T₀. The lifetime of [B]T₀ might therefore be longer than the lifetime of [B-Trans]T₀, explaining why [B]T₀ can act as the second-photon absorbing intermediate.

As can be seen in Figure 9.2-2, [A]T₀ yields a theoretical DAS which is inconsistent with experimental data, suggesting that it is not the species corresponding to $\tau = 150$ ps.

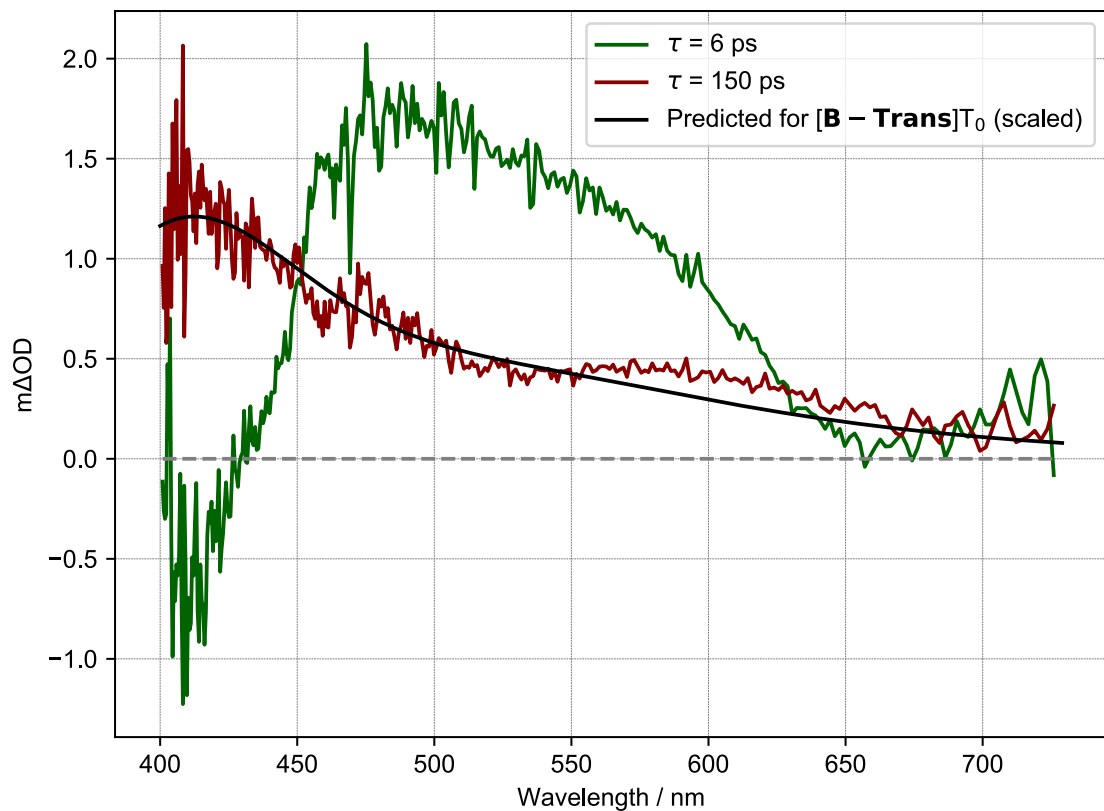


Figure 9.2-1 Decay associated spectra (magic angle polarization) and predicted DAS for $[B\text{-Trans}]T_0$
 Predicted DAS for $[B\text{-Trans}]T_0$ was computed as the difference spectrum between $[A\text{-Mono}]S_0$ and $[B\text{-Trans}]T_0$. For the structure of $[B\text{-Trans}]T_0$ see Figure 11.5-11.

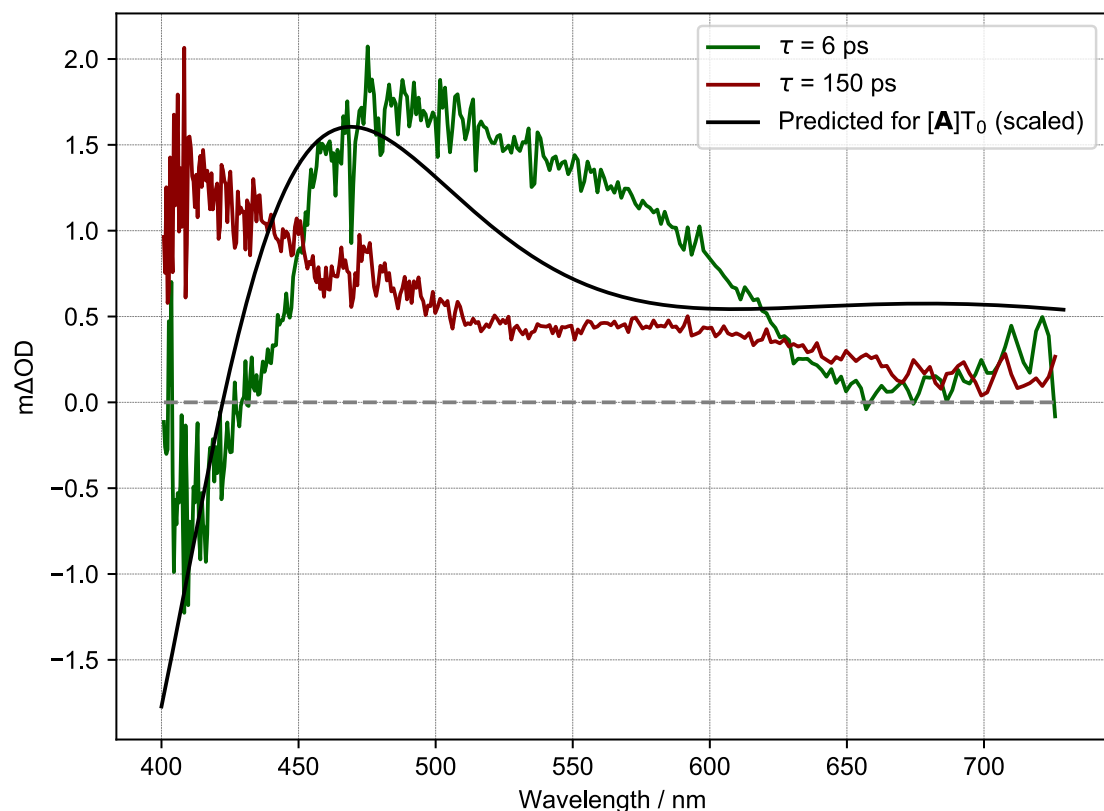


Figure 9.2-2 Decay associated spectra (magic angle polarization) and predicted DAS for $[A]T_0$
 Predicted DAS for $[A]T_0$ was computed as the difference spectrum between $[A\text{-Mono}]S_0$ and $[A]T_0$.

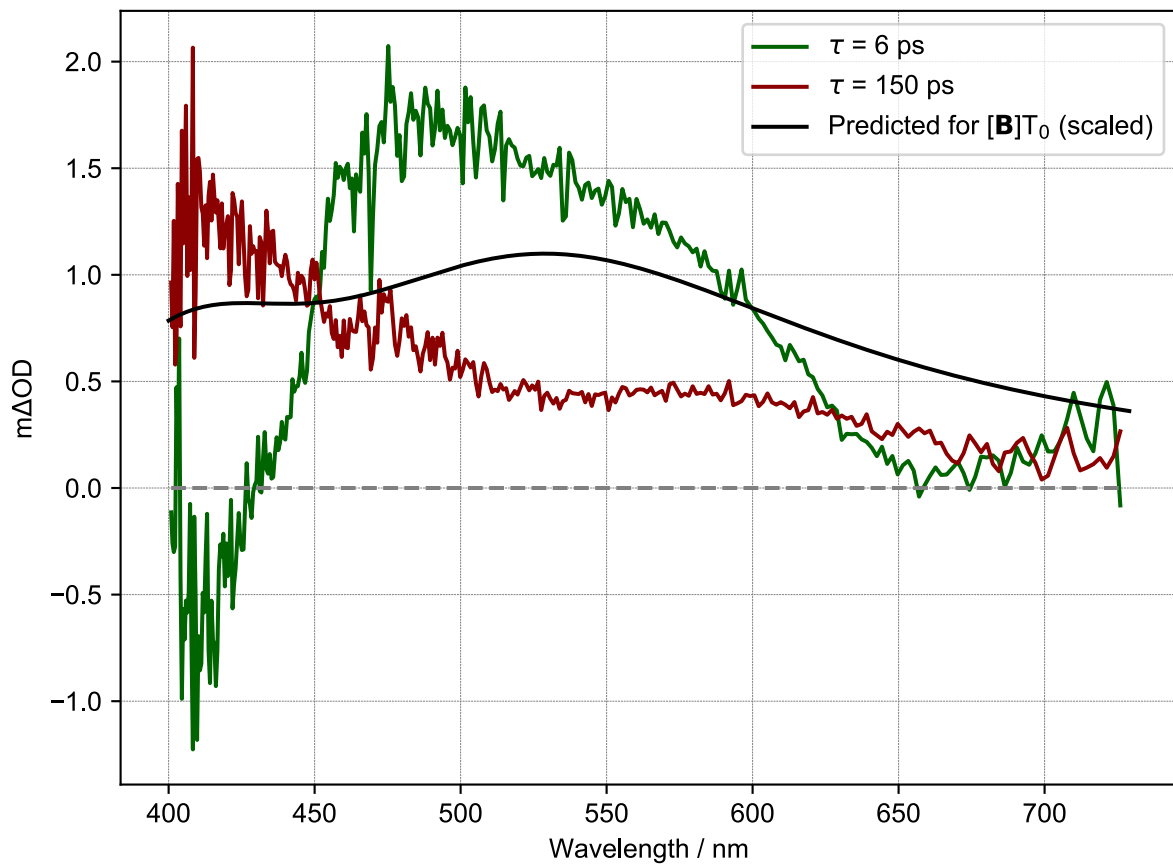


Figure 9.2-3 Decay associated spectra (magic angle polarization) and predicted DAS for $[\mathbf{B}]T_0$
 Predicted DAS for $[\mathbf{B}]T_0$ was computed as the difference spectrum between $[\mathbf{A-Mono}]S_0$ and $[\mathbf{B}]T_0$.

10 Photochemical Kinetic Model

10.1 Description of Kinetic Model

A simple kinetic model to describe the two-photon water splitting reaction was developed using the reaction sequence shown in Table 10.3-1. In this reaction sequence, starting complex **A** absorbs a photon to form transient intermediate **B**. **B** decays back to **A** with a lifetime of τ . Furthermore, **B** can absorb a second photon to form O_2 (+ corresponding complex, which is not part of this kinetic model). O_2 can then be consumed by a third reaction (forming **X**), which also requires photon absorption (see 4.3.2). This reaction sequence is therefore a simplified version of the water splitting mechanism determined using DFT and CASSCF calculations, combined with the experimentally observed, O_2 consuming reaction.

The reaction sequence can be described using the following system of differential equations:

$$\frac{d[A]}{dt} = \frac{1}{\tau}[B] - q_1 c_{abs} Flux [A] \quad \text{Equation (4)}$$

$$\frac{d[B]}{dt} = -\frac{1}{\tau}[B] + q_1 c_{abs} Flux [A] - q_2 c_{abs} Flux [B] \quad \text{Equation (5)}$$

$$\frac{d[C]}{dt} = q_2 c_{abs} Flux [B] - q_3 c_{abs} Flux [C] \quad \text{Equation (6)}$$

$$\frac{d[D]}{dt} = q_3 c_{abs} Flux [C] \quad \text{Equation (7)}$$

Wherein q_n are the respective quantum efficiencies for each reaction step, *Flux* is the photon flux and c_{abs} is the absorption cross-section. For simplicity, it was assumed that absorption cross sections are the same for each step ($1.15E-17 \text{ cm}^2$, which corresponds to an extinction coefficient of $3000 \text{ M}^{-1} \text{ cm}^{-1}$). Furthermore, it was assumed that *Flux* is the same for each reaction step.

The kinetic model was fitted to experimental data from the intensity dataset. For this, all experiments with the same photon flux were averaged. Afterwards, the data was normalized to express the amount of O_2 as a fraction of the initial amount of **1** (based on 0.005 M concentration of **1**). This gave the averaged and normalized experimental data shown in Figure 10.3-1A. For the photon flux = $3.3e+17$ data, Gaussian noise with the same standard deviation as the experimental data was appended from 240 s , since the experimental data was only available up to this time. Fitting was performed by numerically solving the system of differential equations with an updated guess for τ , q_1 , q_2 and q_3 at each optimization step, with *Flux* being the corresponding photon flux for each data series. Updated guesses were generated using the Nelder-Mead algorithm. This was done until convergence was reached. It should be noted that only one set of optimization parameters (τ , q_1 , q_2 and q_3) describes all experiments with different photon flux values. The resulting fit is shown in Figure 10.3-1A. Optimized parameters are shown in Table 10.3-1.

10.2 Relationship between Initial Rate and Photon Flux

The described kinetic model was also used to explore the relationship between initial rate of O_2 formation and photon flux. For this, the optimized parameters shown in Table 10.3-1 were used, unless noted otherwise. With these parameters and within the photon flux range of the intensity dataset, a square relationship between initial rate of O_2 formation and photon flux is obtained (just like it was observed experimentally). In other words, fitting a function of the form $f(x) = ax^b$ (optimizing a and b) to the initial rate/photon flux data gives a value of 2 for power b .

We were interested to see how the relationship between initial rate and photon flux would change for increasing lifetimes τ of **B**. Thus, keeping q_1 , q_2 and q_3 constant, τ was changed over several orders of magnitude, and for each τ value, power b was determined within the intensity dataset photon flux range. Corresponding results are shown in Figure 10.3-1. It can be seen that starting at

$\tau = 10^{-2}$ s, the relationship of initial and photon flux starts to transition to linear one, meaning that power b changes gradually from 2 to 1.

10.3 Interpretation of Results

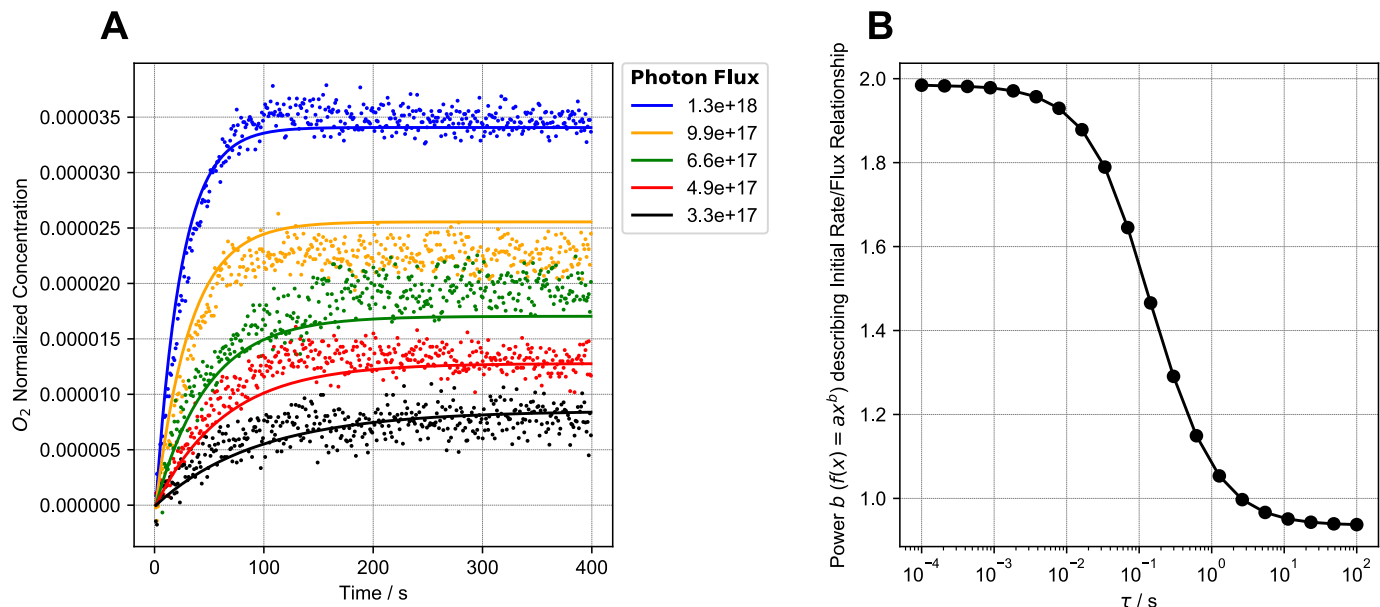
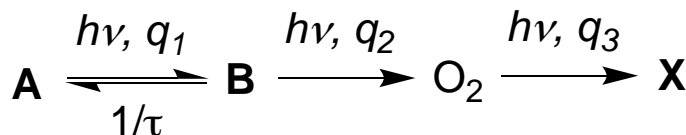


Figure 10.3-1 Photochemical kinetic model used to describe the two-photon water splitting reaction

A Fit of photochemical kinetic model to experimental data. Experimental data is for irradiation with different photon fluxes (intensity dataset) and for each flux value, all measurements with this flux were averaged and converted to normalized O_2 concentration, yielding the shown data. For the photon flux = $3.3e+17$ data, Gaussian noise with the same standard deviation as the experimental data was appended from 240 s, since the experimental data was only available up to this time. Fit of the kinetic model is shown as solid lines.

B Dependence of power b on the lifetime of the intermediate in the two-photon mechanism. Power b describes the relationship between initial rate and photon flux. A value of 2 for b indicates a square dependence of the initial rate on photon flux (as observed experimentally), while a value of 1 indicates a linear relationship. It can be seen that for increasing lifetimes, the relationship of initial rate and photon flux transitions from a square to a linear one. For this modeling, the optimized parameters from **A** were used, changing only τ . The flux level range of the intensity dataset was used to determine b .

Table 10.3-1 Optimized parameters for photochemical kinetic model^[a]



Lifetime τ / ns	Quantum Efficiency q_1	Quantum Efficiency q_2	Quantum Efficiency q_3
65	0,661	0,145	0,0028

[a] Note that there are multiple solutions giving identical fits and only one solution is shown here.

When interpreting the optimized parameters obtained via fitting of the kinetic model to experimental data it should be noted that there is no unique solution. For example, keeping q_1 and q_3 the same, $\tau = 6.5 \mu\text{s}$ and $q_2 = 0.00145$ would give the same result as the parameters shown in Table 10.3-1. This model therefore only provides a rough idea for the underlying lifetime and quantum efficiencies operative in the system. However, through examination of the initial rate/photon flux relationship (Figure 10.3-1), we can see that the lifetime of intermediate **B** must be below $\tau = 10^{-1} \text{ s}$ to explain the experimentally observed square relationship between initial rate and photon flux. In turn, this provides us with lower bound for q_2 , although the lifetime of **B** is probably significantly shorter than $\tau = 10^{-1} \text{ s}$ (given its high energy, see DFT results), with q_2 thus being significantly higher than its lower bound. The lower bound for τ is $\tau \approx 10 \text{ ns}$, which would correspond to $q_2 \approx 1$.

10.4 Comparison of Experimental Dual Irradiation Rates with Kinetic Model

To further assess the validity of the kinetic model, an approximate comparison between the excess initial rate observed in dual irradiation experiments and the prediction by the kinetic model was made.

For this comparison it is necessary to know the 455 – 630 nm photon flux used during dual irradiation experiments. Since chemical actinometry cannot be used in this wavelength region (see 6.3), the flux has to be approximated using power meter measurements.

For the Hg light source (320 – 400 nm), a power of 76 mW was measured in place of the liquid phase O₂ reactor (photon flux of 4.15E+17 s⁻¹ in this position). Based on the mean photon wavelength (360 nm) and the measured flux, the theoretical power is 229 mW. Therefore, measurements using this power meter have to be corrected by a factor of 3.01 to reflect the power received by the reactor.

Using the same power meter, powers of 471 mW and 359 mW were measured for the QTH light source using 455 nm and 630 nm longpass filters, respectively (in place of the liquid phase O₂ reactor). The power in the wavelength range 455 – 630 nm is therefore 112 mW. Using the correction factor of 3.01, one obtains a corrected power of 337 mW. Based on a mean photon wavelength of 542.5 nm, the 455 – 630 nm photon flux is therefore roughly 9.23E+17 s⁻¹.

In dual irradiation experiments, an excess initial rate of ca. 0.001 μmol l⁻¹ s⁻¹ was observed when the 455 nm longpass filter was used. Based on a reaction volume of ca. 550 μl, this corresponds to ca. 3.3E+11 O₂ forming reactions per second. Given a 455 – 630 nm photon flux of ca. 9.23E+17 s⁻¹, this means that the probability of inducing an O₂ forming reaction is ca. 3.59E-07 per 455 – 630 nm photon.

To calculate the theoretical reaction probability we will assume the same absorbance for the second-photon absorbing intermediate as used in the kinetic model (3000 M⁻¹ cm⁻¹). Based on this absorbance, an intermediate lifetime of 65 ns (see Table 10.3-1) and a 455 – 630 nm photon flux of 9.23E+17 s⁻¹, we can calculate that there is a probability of 6.93E-07 for the intermediate to absorb a photon in its lifetime. Multiplying this absorption probability by a quantum yield for the second absorption of 0.145 (see Table 10.3-1) gives us a predicted reaction probability of 1.01E-07 per 450 – 630 nm photon.

Table 10.4-1 Comparison of experimental and predicted reaction probabilities

Experimental reaction probability per 455 – 630 nm photon	Predicted reaction probability per 455 – 630 nm photon
3.59E-07	1.01E-07

Experimental and predicted reaction probabilities are in the same order of magnitude, which we consider to be a rather good agreement, given the simplicity of the kinetic model. Through this comparison it can also be seen that the rather low experimental reaction probability per 455 – 630 nm photon is likely due to a short life time of the absorbing intermediate, making second photon absorption less probable. Increasing the lifetime could therefore significantly increase both reaction rate and overall quantum yield.

11 Computational Section

11.1 Computational Methods

11.1.1 DFT Methods

All DFT calculations were performed using the PBE0 (PBE1PBE) hybrid functional, along with Grimme D3 dispersion with Becke-Johnson damping (GD3BJ). For all calculations, the SDD basis set and effective core potential was used for ruthenium, while all other atoms were described using the indicated basis set. Closed shell calculations (singlet) were performed as restricted (RHF), while open shell (doublet and triplet) calculations were performed as unrestricted (UHF) calculations. Calculations were performed using three different model chemistries:

1. Dimeric model of two ruthenium complexes interacting via non-covalent bonds. This model was used for [A], [B], [C], TS-[CD] and [D] [F] (dimer model).
2. Monomeric model, in which only the ruthenium complex on which O-O bond formation takes place (or [F]) is modeled. This model was used for [A-Mono], [B-Mono], [C-Mono], [D], [E] and [F].
3. In some cases, a simplified version of the monomeric model was used, in which the ligand *t*Bu and Et groups were replaced by methyl. Use of this model is indicated by "Me model".

Use of the “-Up” designation indicates opposite (relative to the normal models) PNN ligand conformation. Geometry optimizations and frequency calculations (298 K, 1 atm) were performed in the gas phase using the cc-pVDZ basis set. Structures were confirmed to be minima or first-order saddle points by having either zero (minima) or one (first-order saddle points) imaginary frequencies. Reported gas phase Gibbs free energies are based on Gibbs free energies obtained using frequency calculations.

Single point energy calculations were performed using the cc-pVTZ basis set and SMD solvation (the solvent being water). Reported solution phase Gibbs free energies are based on singlet point energy calculations, corrected by using the thermal correction to Gibbs free energy obtained using frequency calculations.

Electronic excitations and theoretical UV/Vis spectra were calculated using TD-DFT, using the cc-pVDZ basis set and SMD solvation (in water). Typically, the 25 lowest energy transitions were computed. Theoretical UV/Vis spectra were constructed using the calculated transition wavelengths and oscillator strengths. Furthermore, transitions were broadened using Gaussian curves with a half-width at half-height of 0.333 eV. To visualize excitations, natural transition orbitals were computed, and the resulting hole-particle pairs with the highest contribution (typically > 1.7) are shown.

Scans were performed as relaxed potential energy surface scans using the cc-pVDZ basis set in the gas phase. For Scan-[DE]T₀, single point energy calculations using cc-pVTZ and SMD solvation (water) were performed for all optimized geometries along the scan. Since frequency calculations are not meaningful for scan geometries, only relative energies instead of Gibbs free energies (either gas phase or solution phase) are reported.

NMR calculations were performed using the cc-pVTZ basis set and SMD solvation (water). Reported chemical shifts are relative to tetramethylsilane (¹H) or H₃PO₄ (³¹P).

All calculations were performed using Gaussian 16, Revision A.03.(10) Structures were prepared and visualized using Avogadro.(11) Furthermore, surfaces for closed shell molecules were also visualized using Avogadro. Surfaces for open shell molecules were visualized using Gabedit.(12) Simplified structures were visualized using PyMOL.(13) Visualizations were rendered using POV Ray.(14) In all visualizations, ruthenium is shown in turquoise, phosphorous in orange, oxygen in red, nitrogen in blue, carbon in grey and hydrogen in white. For surfaces: orbitals are shown in yellow/magenta and spin densities are shown in green.

11.1.2 CASSCF Methods

All CASSCF calculations were performed as state averaged (SA)-CASSCF calculations, using the five lowest energy states weighed equally. An active space consisting of 13 electrons in 11 orbitals, CAS(13,11), was used (see Figure 11.3-2). The active space consists of two Ru-OH σ and σ^* , four pyridine π and π^* , two Ru-CO π and π^* (combining with oxygen lone pair orbitals), two OH and O lone pair and the singly occupied O lone pair orbitals.

The ANO-RCC-VDZ all-electron basis set was used for all atoms (which includes relativistic effects). To improve computational performance, the resolution of identity Cholesky decomposition (RICD) method was used.(15, 16) For computational tractability, the simplified monomeric model using methyl groups instead of *t*Bu and ethyl on the ligand (Me model) was used for all CASSCF calculations.

For **[B-Mono]** and **[C-Mono]**, geometries obtained using DFT geometry optimization were used. The geometries of conical intersections (**[BC]** D_2/D_1 MECI and **[BC]** D_1/D_0 MECI) were optimized using CASSCF with analytical gradients in the gas phase.(17) Gas phase energies are reported relative to the energy of **[B-Mono]** D_0 root 1.

Solvation was taken into account by performing single point calculations for all intermediates with the PCM conductor version and water as the solvent. For **[B-Mono]**, equilibration solvation based on root 1 was used for root 1, while non-equilibrium solvation based on root 3 was used for all other roots (modeling vertical excitation from root 1 to root 3). For **[BC]** D_2/D_1 MECI, equilibrium solvation based on root 3 was used for all roots. For **[BC]** D_1/D_0 MECI, equilibrium solvation based on root 2 was used for all roots. For **[C-Mono]**, equilibrium solvation based on root 1 was used. Solution phase energies are reported relative to the energy of **[B-Mono]** D_0 root 1.

All calculations were performed using OpenMolcas version 19.11.(18, 19) Visualizations were performed using Pegamoid. In all visualizations, ruthenium is shown in turquoise, phosphorous in orange, oxygen in red, nitrogen in blue, carbon in grey and hydrogen in white. For surfaces: orbitals are shown in yellow/magenta, spin densities are shown in green and transition difference densities are shown in red/blue.

11.2 DFT Results

11.2.1 Relative Energies of [A] and [B] Isomers, Oxo Dimer, $[F]S_0 \rightarrow [A\text{-Mono}]S_0$

Table 11.2-1 Relative energies of $[A]S_0$ and $[A\text{-Mono}]S_0$

	$[A]S_0$	$[A\text{-Mono}]S_0$
$\Delta G^\circ(\text{SMD}) / \text{kcal/mol}$	8.05	0.00
$\Delta G^\circ(\text{Gas Phase}) / \text{kcal/mol}$	0.00	2.5

In Table 11.2-1 it can be seen that while dimeric $[A]S_0$ is predicted to be more stable in the gas phase compared to monomeric $[A\text{-Mono}]S_0$, it is predicted to be less stable in solution. However, the lower stability in solution might be attributed to the challenging description of hydrogen bonding energies using DFT.(20)

Table 11.2-2 Relative energies of [A] isomers

	$[A]S_0$	$[A\text{-RR}]S_0$	$[A\text{-RS-1}]S_0$	$[A\text{-RS-2}]S_0$	$[A]T_0$
$\Delta G^\circ(\text{SMD}) / \text{kcal/mol}$	0.00	0.49	1.05	1.88	21.91

Different isomers of $[A]S_0$ were computed, varying in their configuration ($[A\text{-Mono}]S_0$ is chiral, therefore either a homo- or heterochiral dimer can be formed) and conformation of the ligand. Among the computed isomers, $[A]S_0$ was found to be the most stable, although the energy differences are small. $[A]T_0$ was found to be relatively low in energy, being only ca. 22 kcal/mol less stable than $[A]S_0$.

Table 11.2-3 Relative energies of $[B]T_0$ isomers

	$[B]T_0$	$[B\text{-Trans}]T_0$
$\Delta G^\circ(\text{SMD}) / \text{kcal/mol}$	8.56	0.00

Table 11.2-4 Relative energies of [B-Mono]D₀ isomers

	[B-Mono]D ₀	[B-Mono-Up]D ₀	[B-Mono-Trans]D ₀	[B-Mono-Trans-Up]D ₀
ΔG°(SMD) / kcal/mol	6.86	8.68	1.53	0.00

When comparing [B] and [B-Trans] in both the dimeric and monomeric model, [B-Trans] was found to be slightly more stable.

Table 11.2-5 Relative energy of [B-Alt]T₀

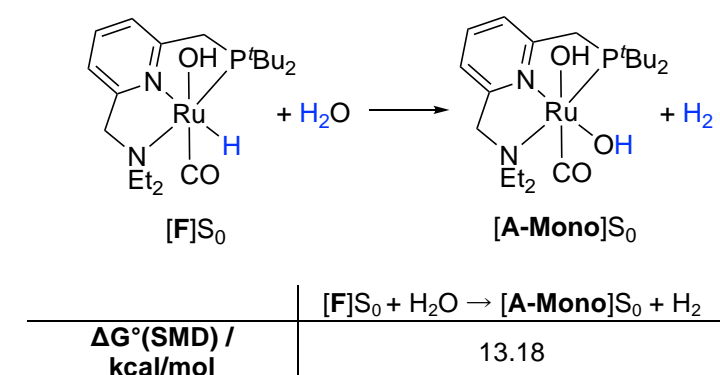
	[B-Alt]T ₀
ΔG°(SMD) / kcal/mol	7.96 ([B-Alt]T ₀ + H ₂ O + [F]S ₀ relative to [B]T ₀) 16.5 ([B-Alt]T ₀ + H ₂ O + [F]S ₀ relative to [B-Trans]T ₀)
ΔG°(Gas Phase) / kcal/mol	39.1 ([B-Alt]T ₀ + H ₂ O + [F]S ₀ relative to [B-Trans]T ₀)

[B-Alt]T₀ would be an alternative reaction intermediate, obtained via two consecutive proton-coupled electron transfers from [A] (forming one equivalent of [F]S₀ in the process). It is, however, less stable than either [B]T₀ or [B-Trans]T₀.

Table 11.2-6 Relative energy of Oxo Dimer

	[Oxo Dimer]S ₀
ΔG°(SMD) / kcal/mol	12.2 (relative to [A-Mono]S ₀) 4.2 (relative to [A]S ₀)

Table 11.2-7 Reaction Energy for [F]S₀ + H₂O → [A-Mono]S₀ + H₂



Considering the energy change for [F]S₀ + H₂O → [A-Mono]S₀ + H₂ (13.18 kcal/mol) and [A]S₀ → 2 [F]S₀ + O₂ (82.73 kcal/mol), as well as the relative stability of [A]S₀ vs. [A-Mono]S₀ (8.05 kcal/mol), one arrives at an energy change of 117.11 kcal/mol. This value is identical with the energy change of 2 H₂O → O₂ + 2 H₂ when using our DFT methodology, which is in good agreement with the thermodynamical value (4-electron 1.23 V, 113.46 kcal/mol).

11.2.2 TD-DFT Computed UV-Vis Spectra

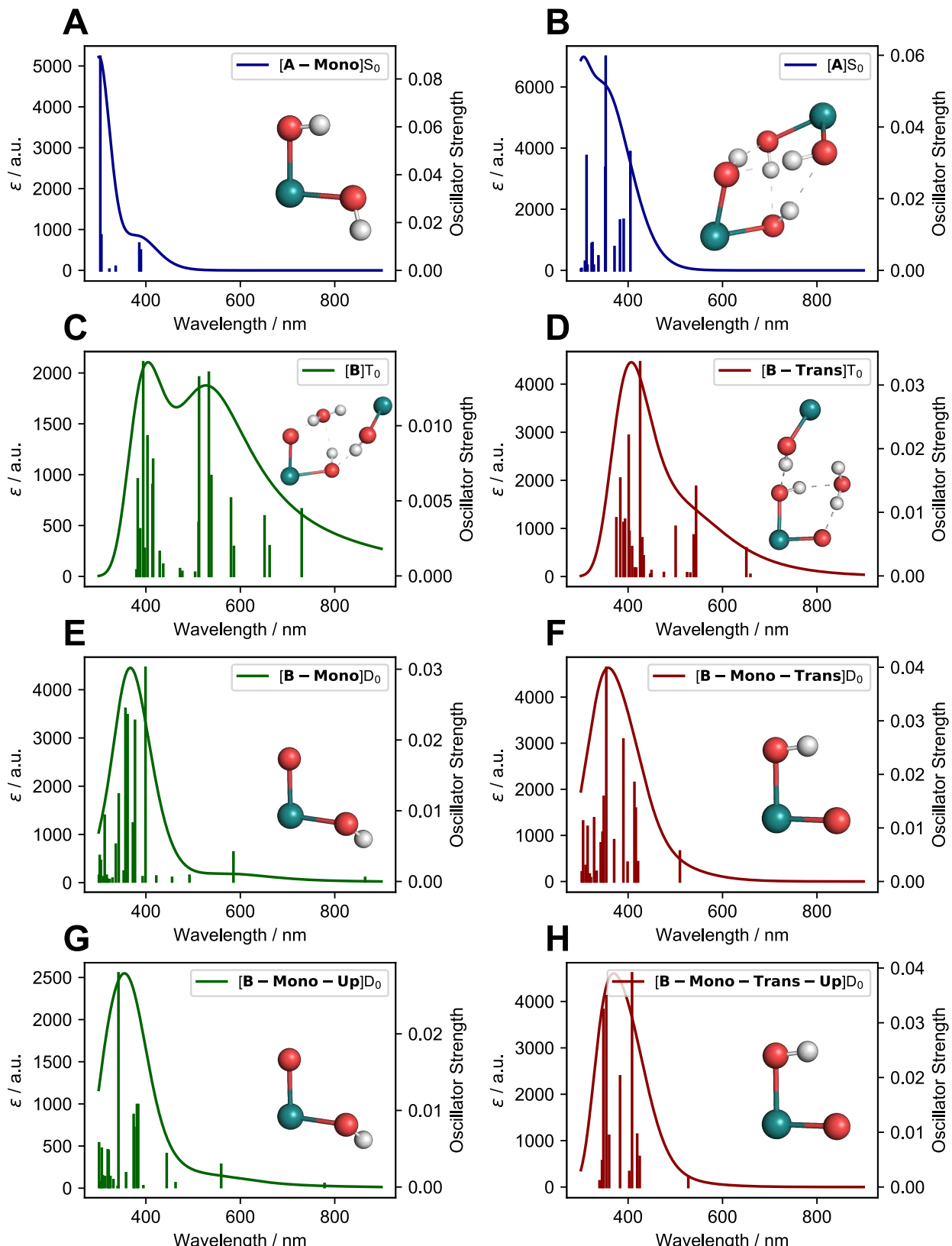


Figure 11.2-1 UV-Vis spectra computed for $[A]S_0$ and $[B]T_0$ along with isomers/monomers

Spectra for **[A]** are shown in blue, **[B]** in green and **[B-Trans]** in red. Vertical lines indicate individual transitions (oscillator strength for these transitions are shown on the right). Smooth curves show the UV-Vis spectrum, which was computed using the sum of Gaussian curves with a half-width half-maximum of 0.333 eV. Insets show the simplified, corresponding molecular structures. “-Up” indicates opposite PNN ligand conformation. Up to 25 transitions between 300 nm and 900 nm are shown.

11.2.3 Natural Transition Orbitals for [A]S₀

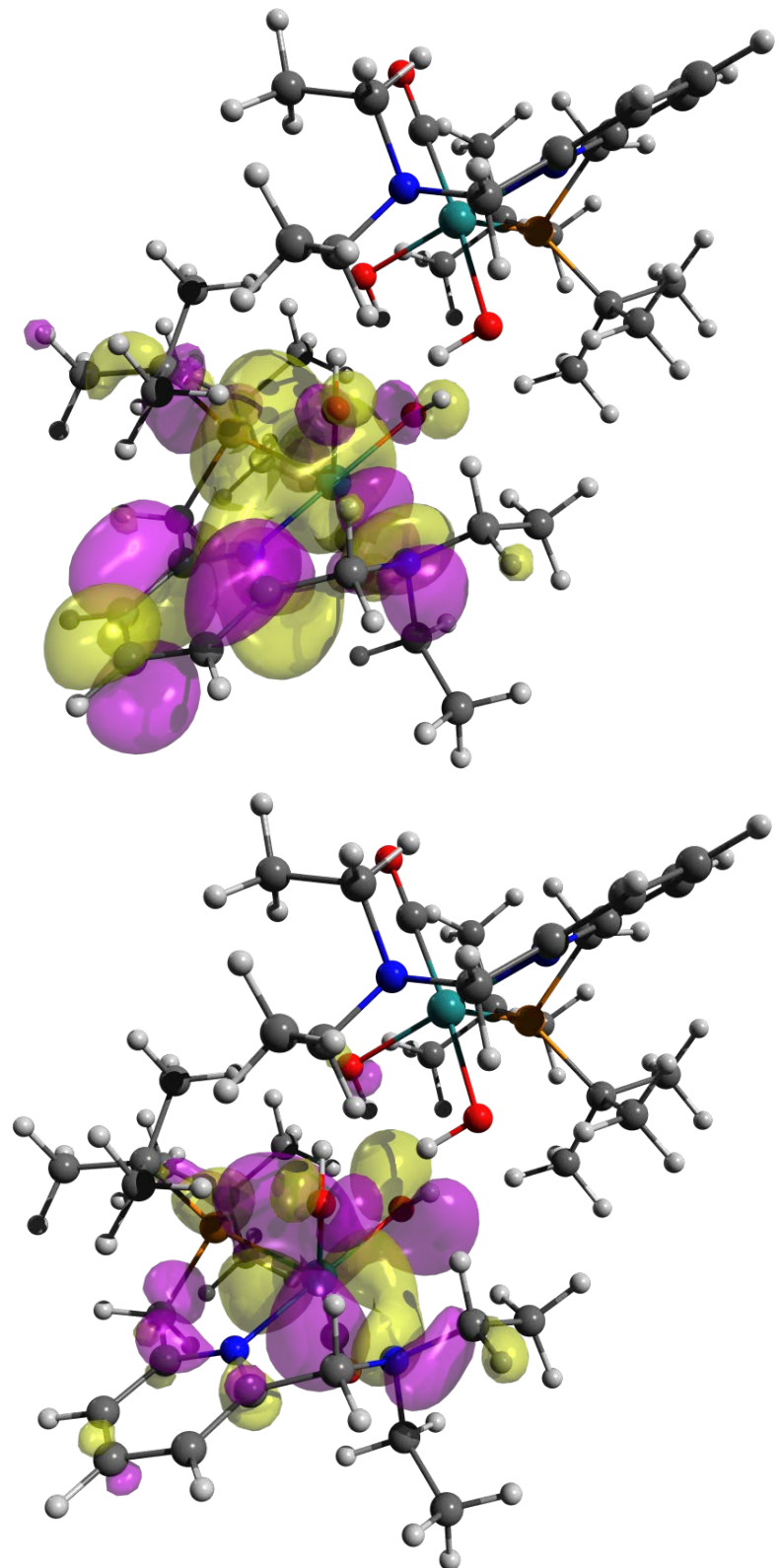


Figure 11.2-2 Transition 1 (405 nm, $f = 0.033$) for [A]S₀, particle (top) and hole (bottom), isovalue = 0.02

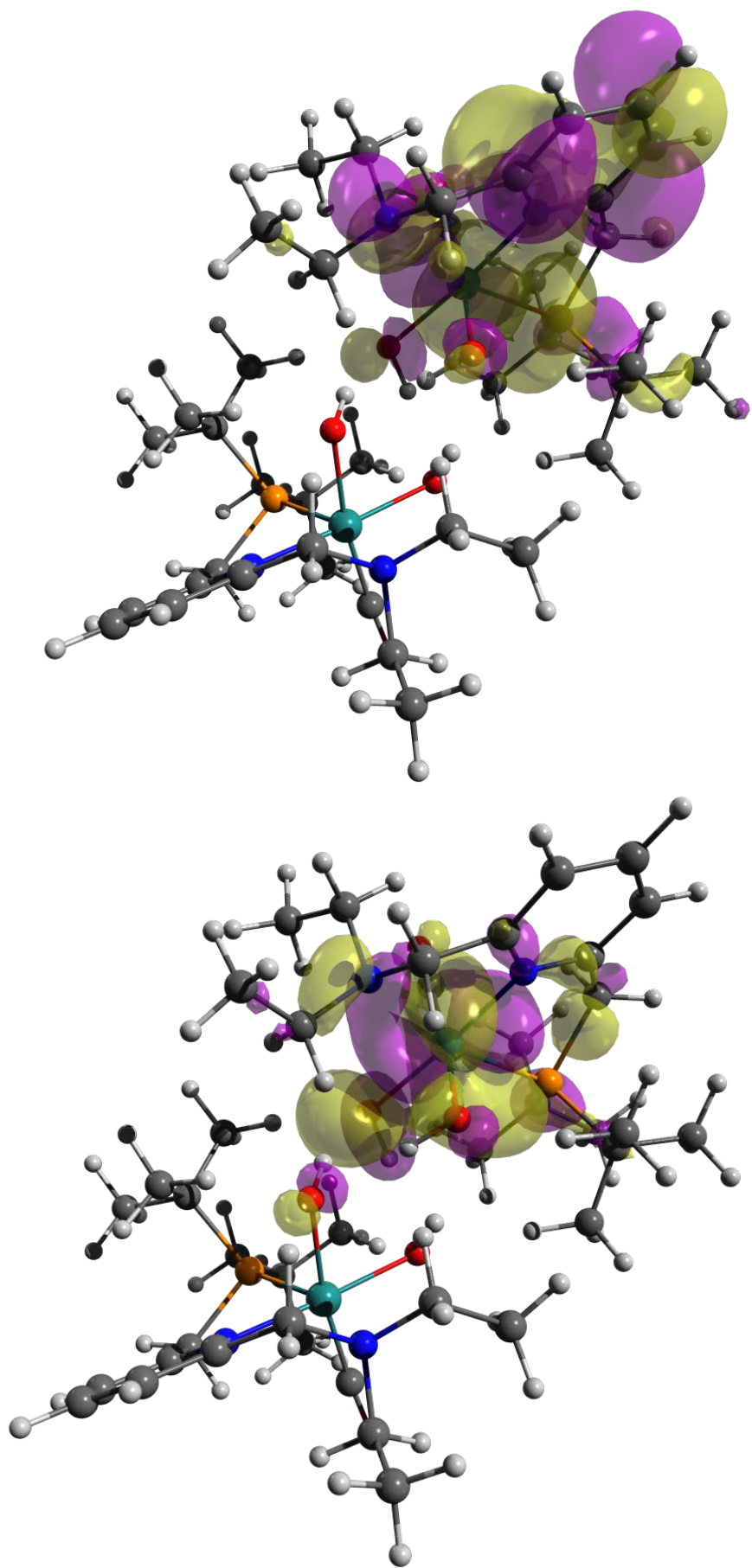


Figure 11.2-3 Transition 2 (391 nm, $f = 0.0141$) for $[A]S_0$, particle (top) and hole (bottom), isovalue = 0.02

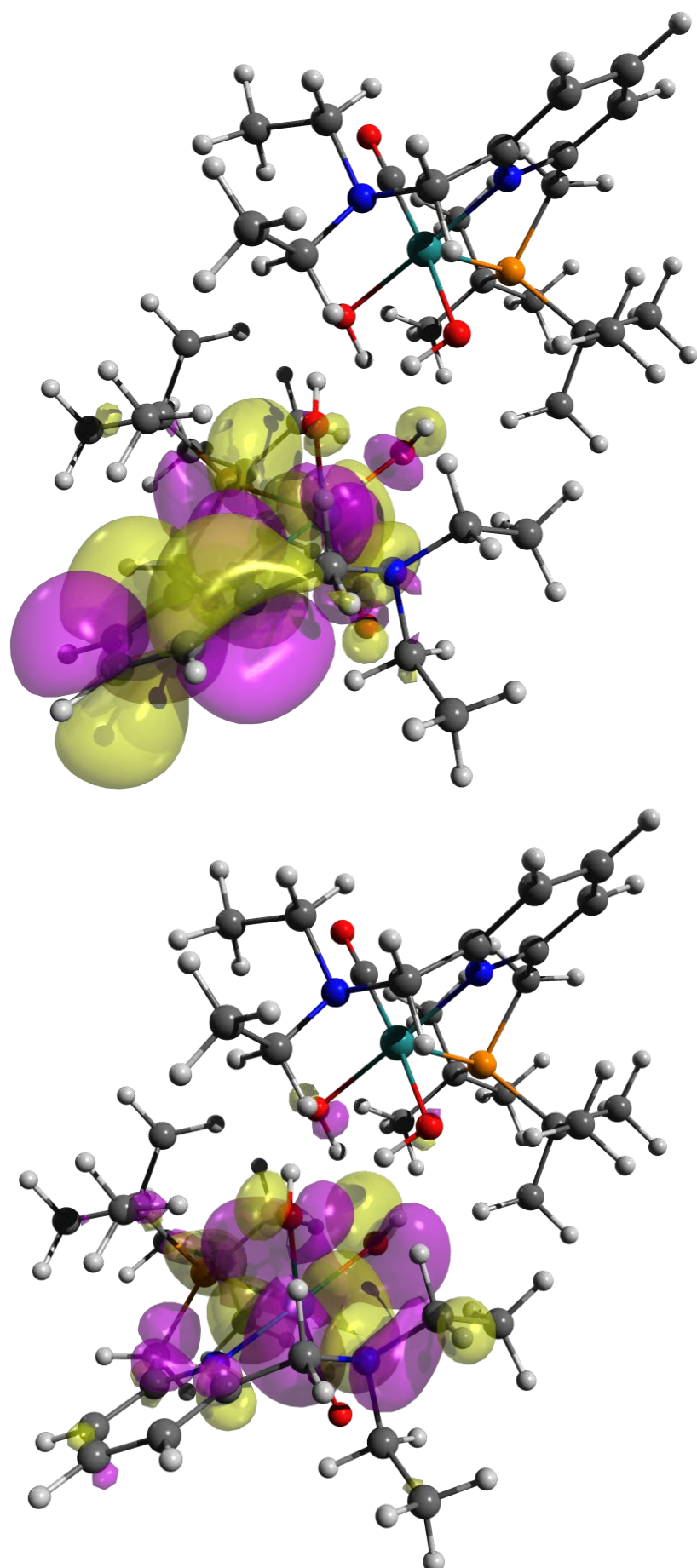


Figure 11.2-4 Transition 3 (383 nm, $f = 0.014$) for $[A]S_0$, particle (top) and hole (bottom), isovalue = 0.02

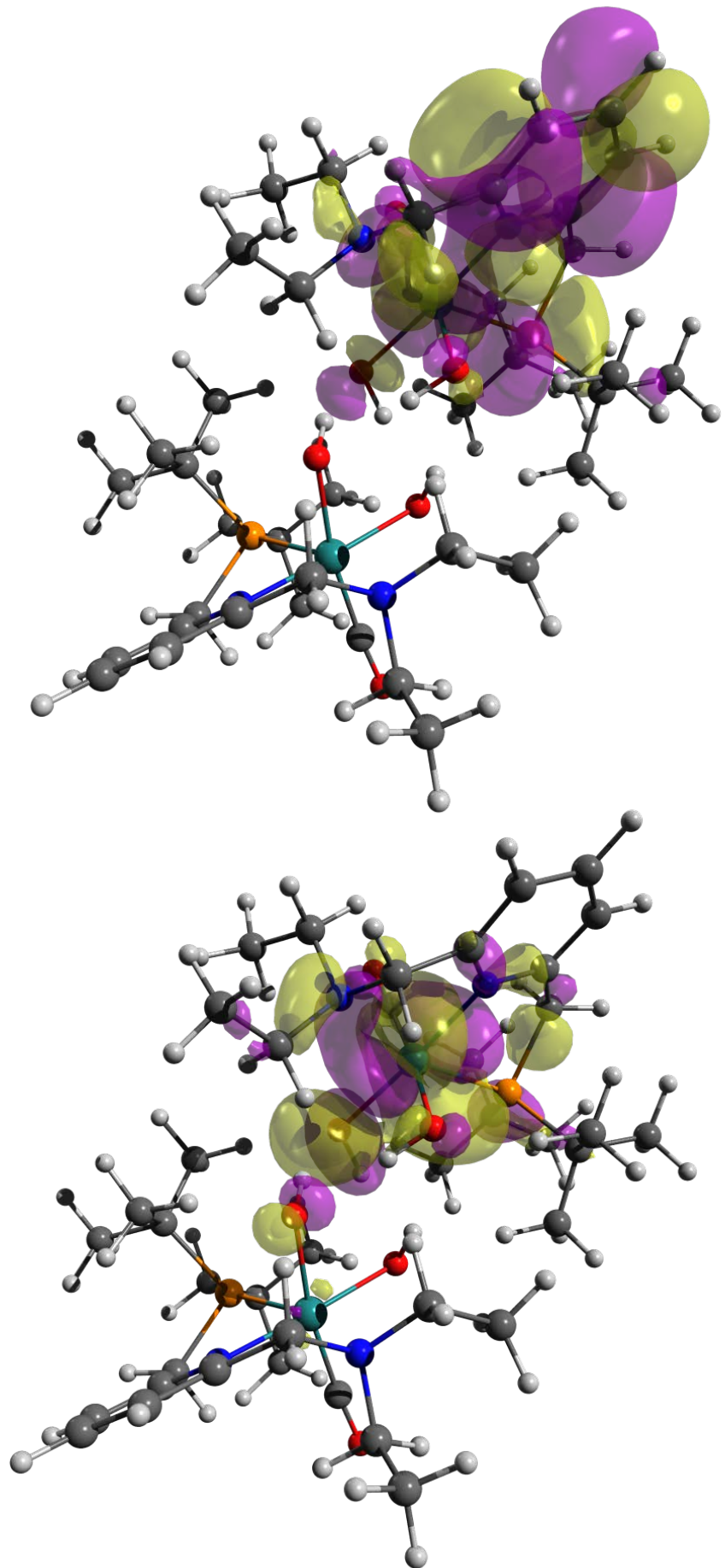


Figure 11.2-5 Transition 4 (371 nm, $f = 0.0065$) for $[A]S_0$, particle (top) and hole (bottom), isovalue = 0.02

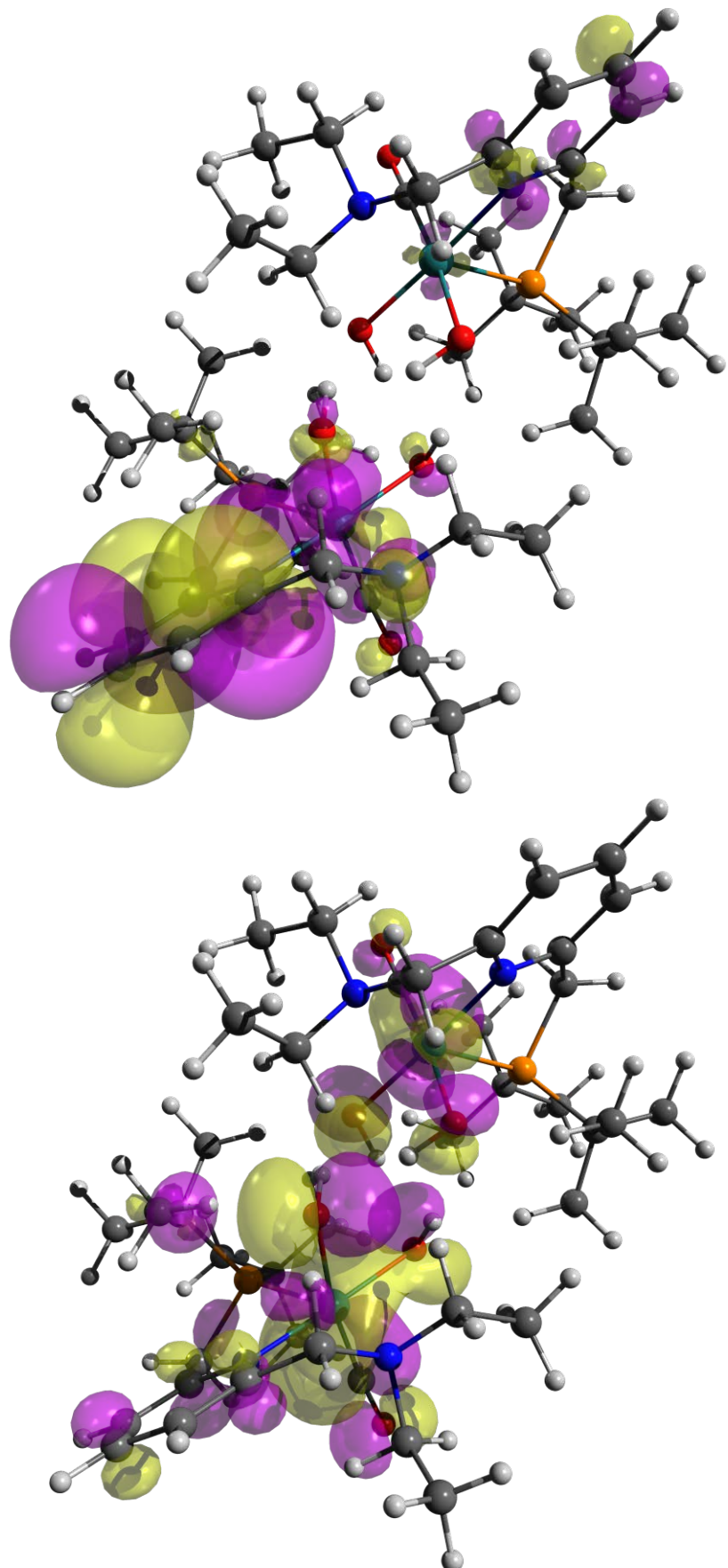


Figure 11.2-6 Transition 5 (353 nm, $f = 0.0596$) for $[A]S_0$, particle (top) and hole (bottom), isovalue = 0.02

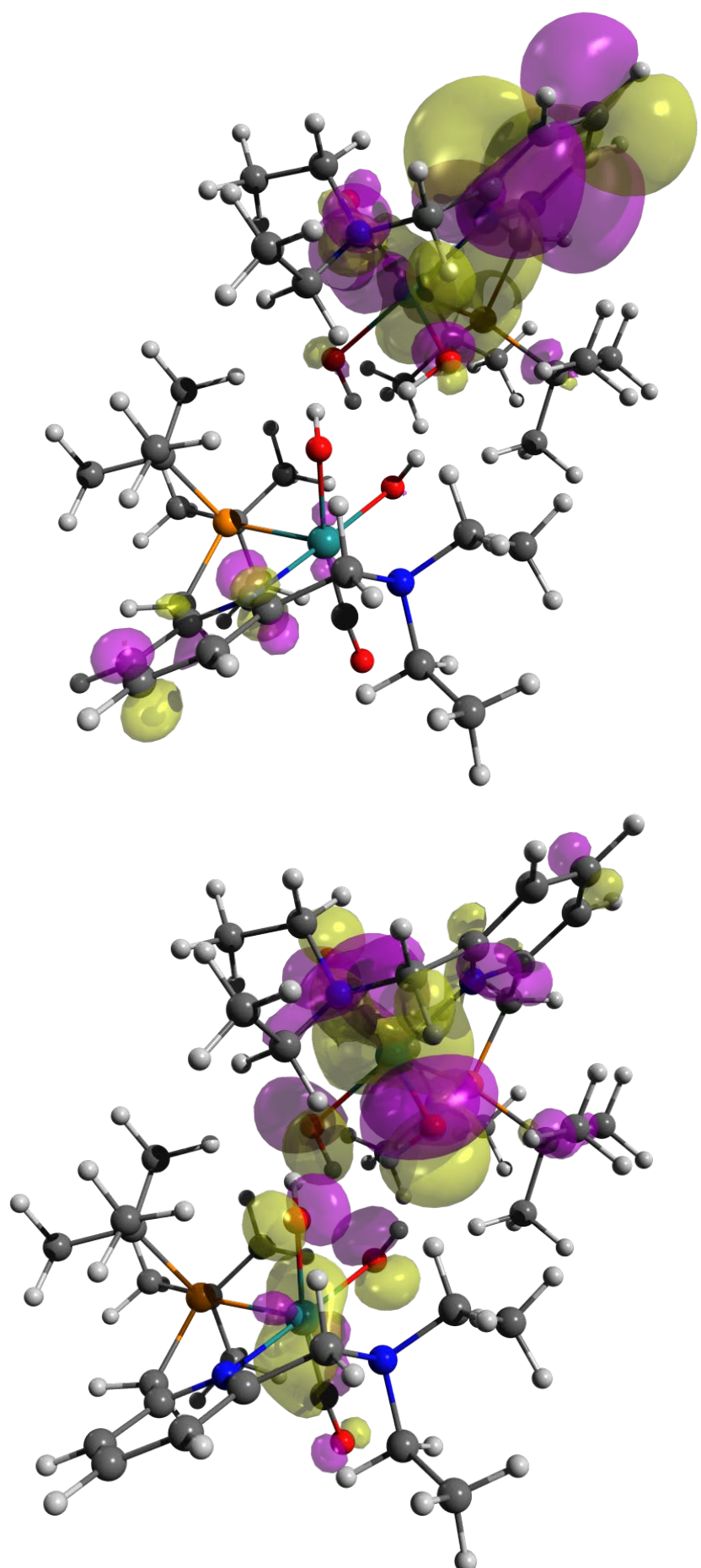


Figure 11.2-7 Transition 6 (352 nm, $f = 0.0287$) for $[A]S_0$, particle (top) and hole (bottom), isovalue = 0.02

11.2.4 Natural Transition Orbitals for $[B]T_0$

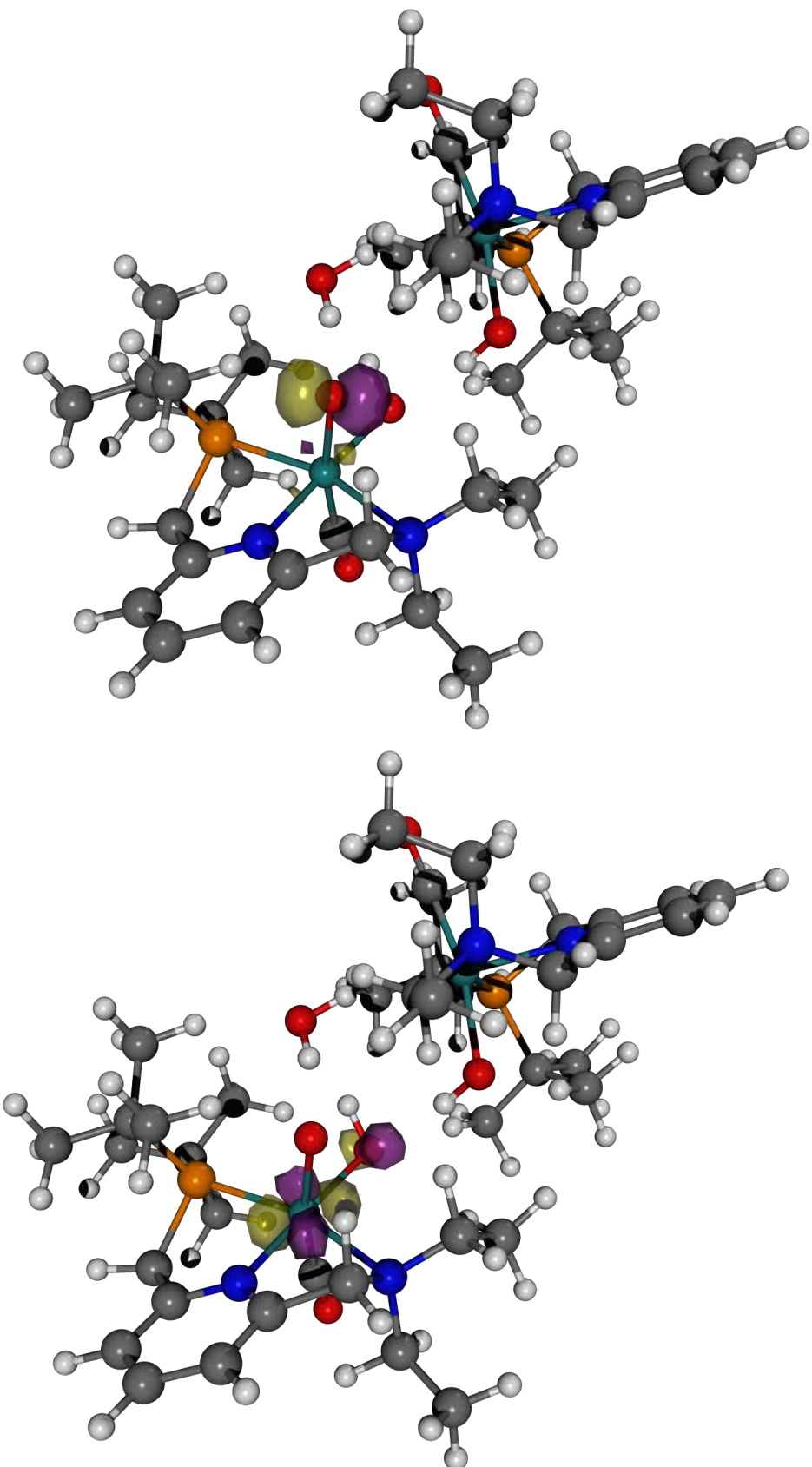


Figure 11.2-8 Transition 2 (933 nm, $f = 0.0029$) for $[B]T_0$, particle (top) and hole (bottom), isovalue = 0.1

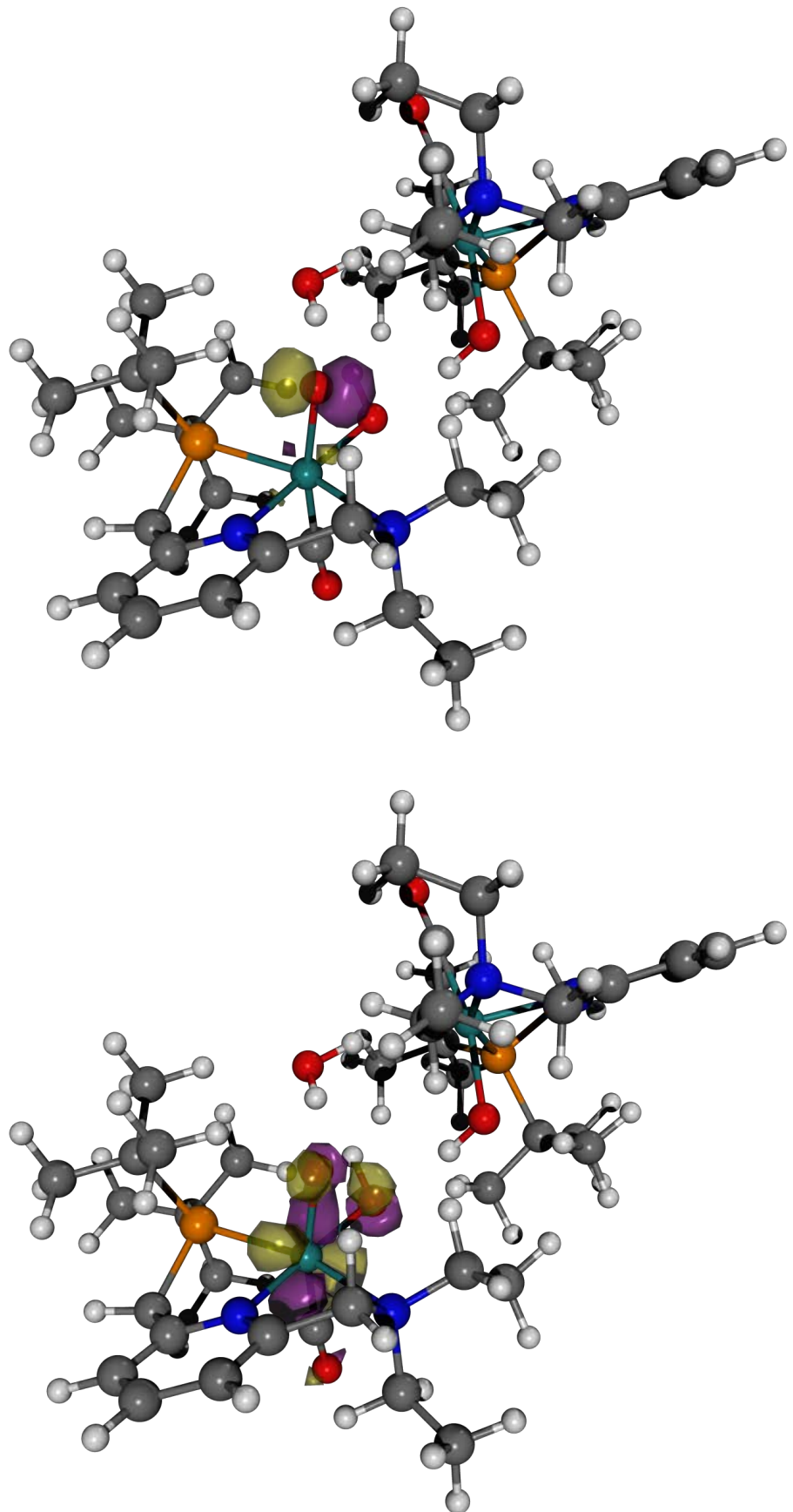


Figure 11.2-9 Transition 8 (539 nm, $f = 0.0066$) for $[B]T_0$, particle (top) and hole (bottom), isovalue = 0.1

11.2.5 Natural Transition Orbitals for [B-Mono]D₀ (Me Model)

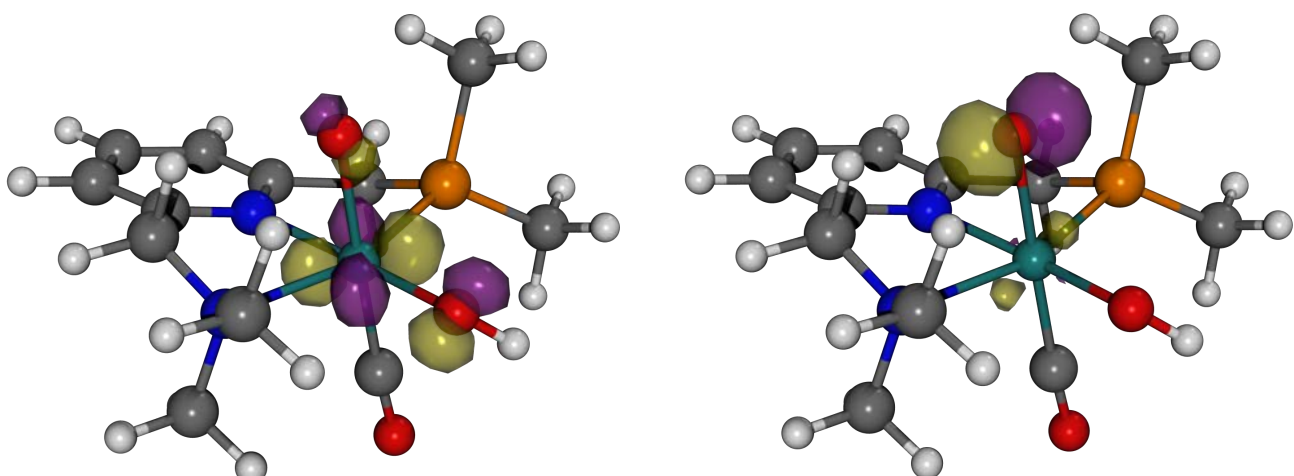


Figure 11.2-10 Transition 2 (804 nm, $f = 0.0004$) for [B-Mono]D₀ (Me model), hole (left) and particle (right), isovalue = 0.1

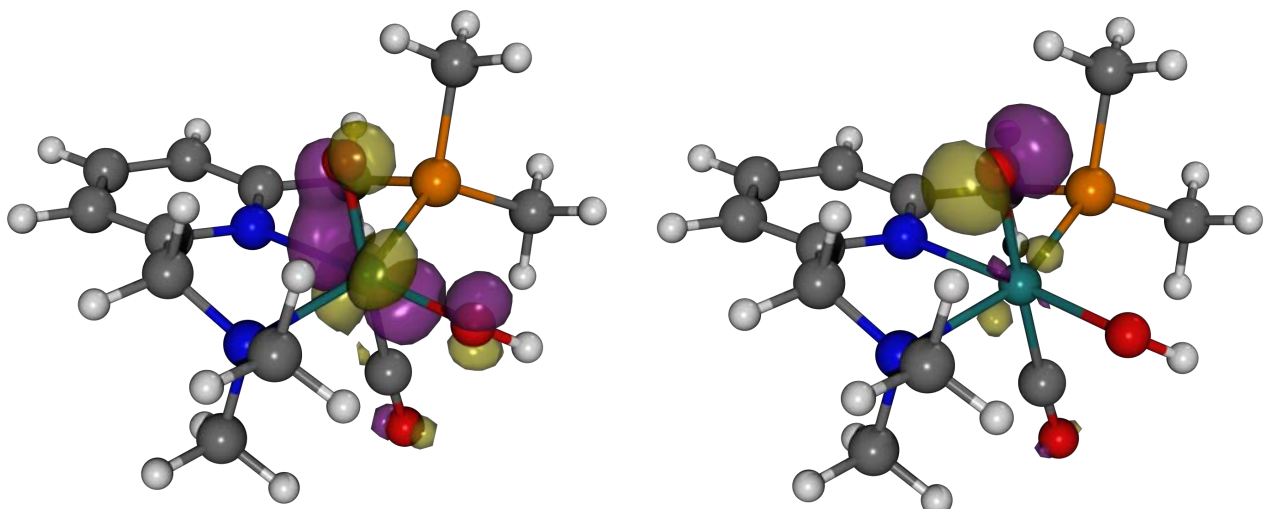


Figure 11.2-11 Transition 4 (495 nm, $f = 0.0027$) for [B-Mono]D₀ (Me model), hole (left) and particle (right), isovalue = 0.1

11.2.6 Spin Density Plots

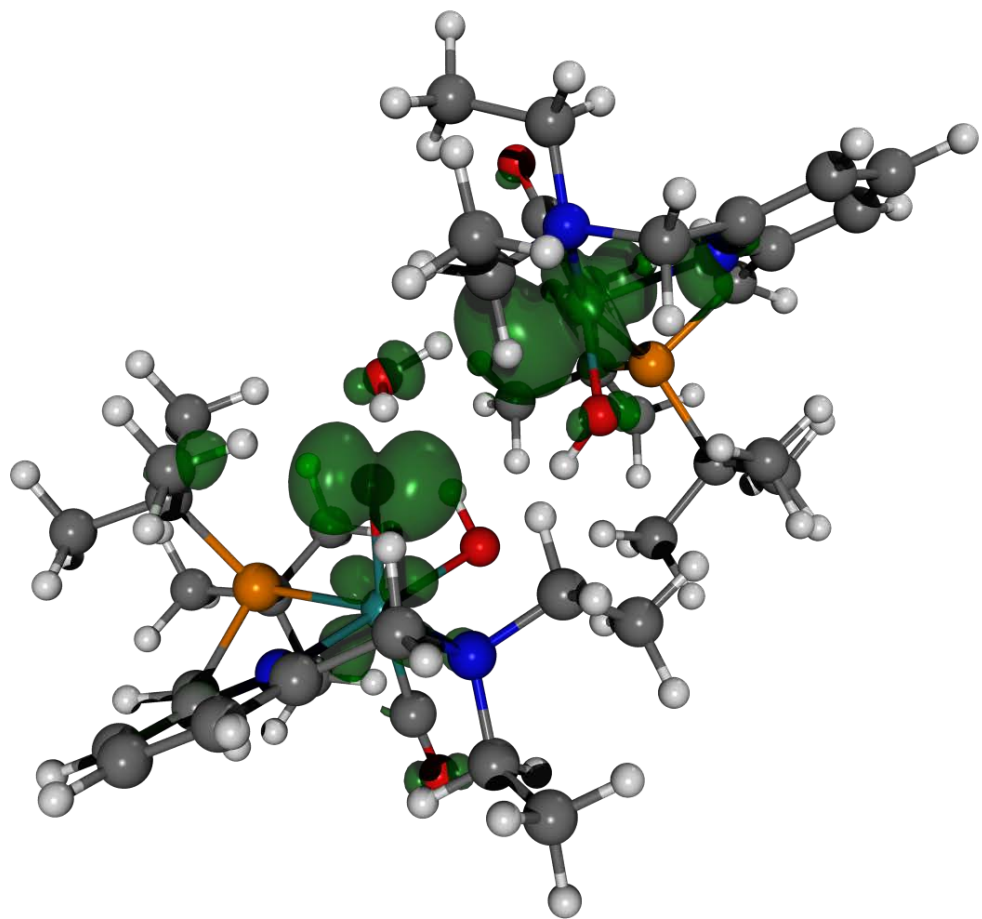


Figure 11.2-12 Spin density (isovalue = 0.004) for $[B]T_0$

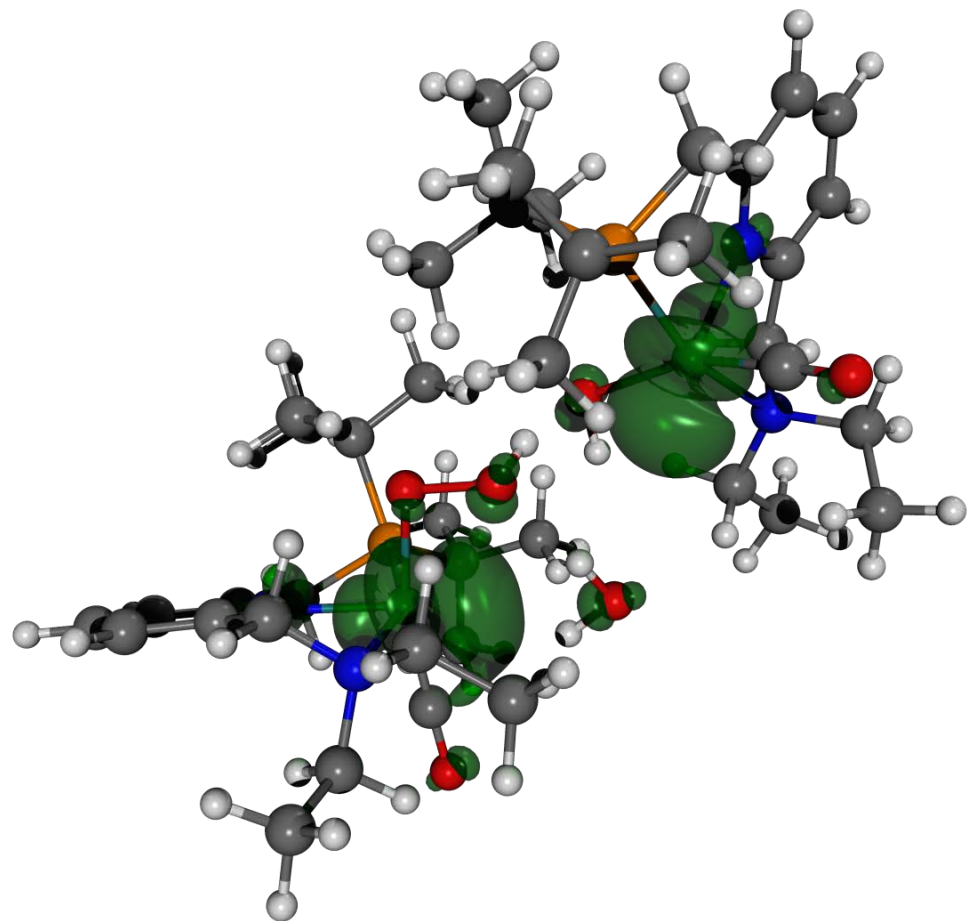


Figure 11.2-13 Spin density (isovalue = 0.004) for $[C]T_0$

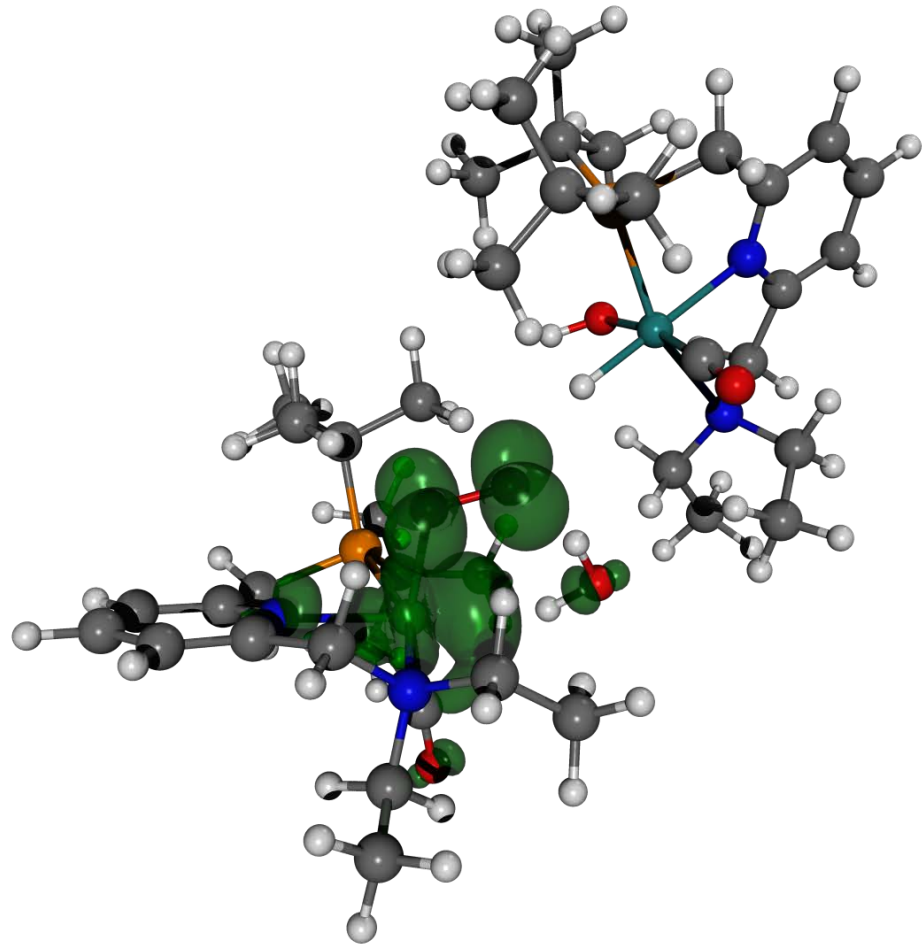


Figure 11.2-14 Spin density (isovalue = 0.004) for $[D]T_0[F]S_0$ (Dimer Model)

11.2.7 Scan-[DE]T₀

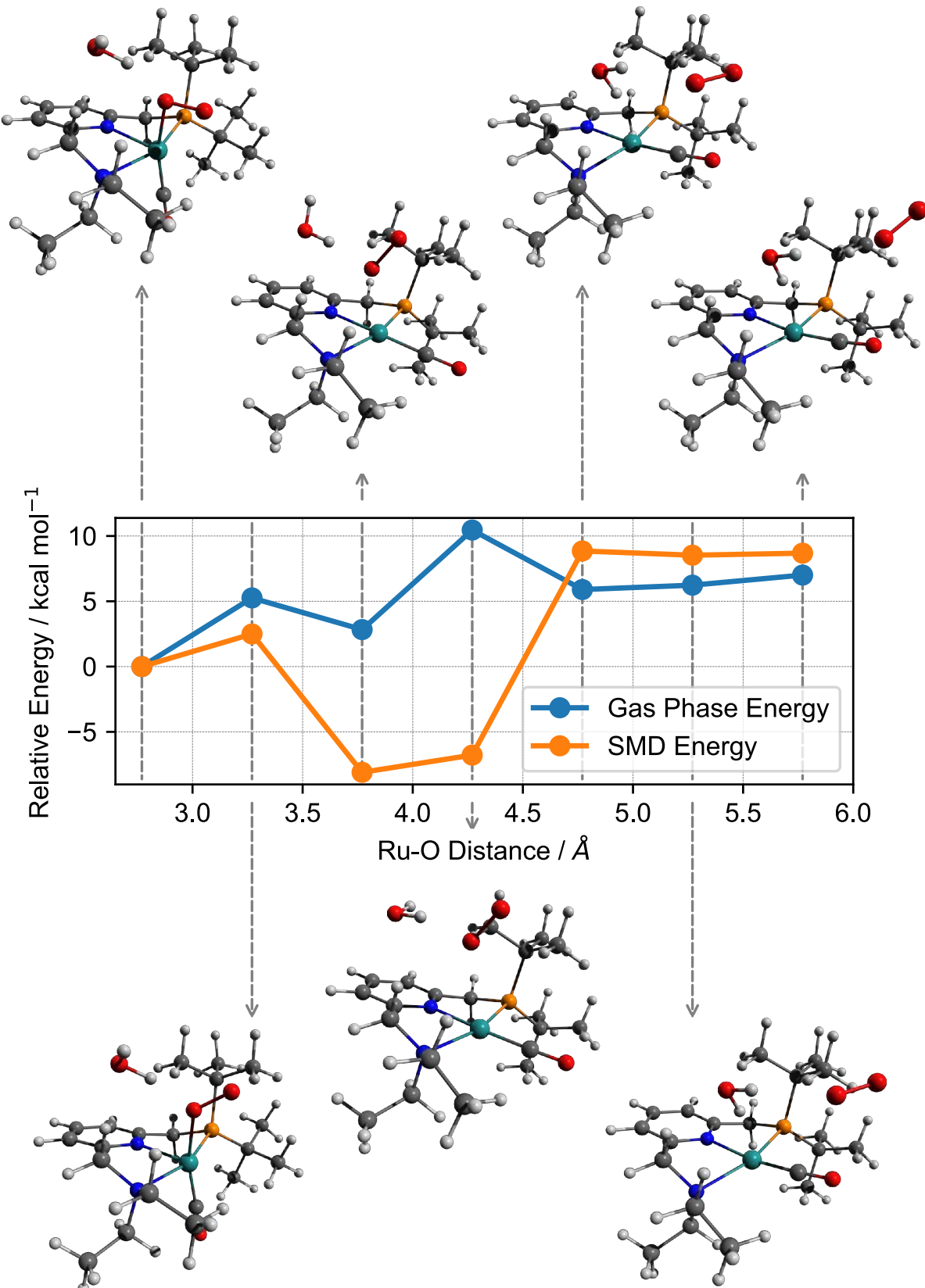


Figure 11.2-15 Energy profile for relaxed PES Scan-[DE]T₀ (gas phase and SMD energies)

Ru-O distance refers to the distance between the ruthenium center and the most distant oxygen atom of the superoxo ligand. Structures corresponding to the different points along the scan are shown outside of the plot. The decrease in energy for the third scan geometry can be attributed to movement of the CO ligand from an axial to an equatorial position.

11.2.8 O-O Bond Formation Scans

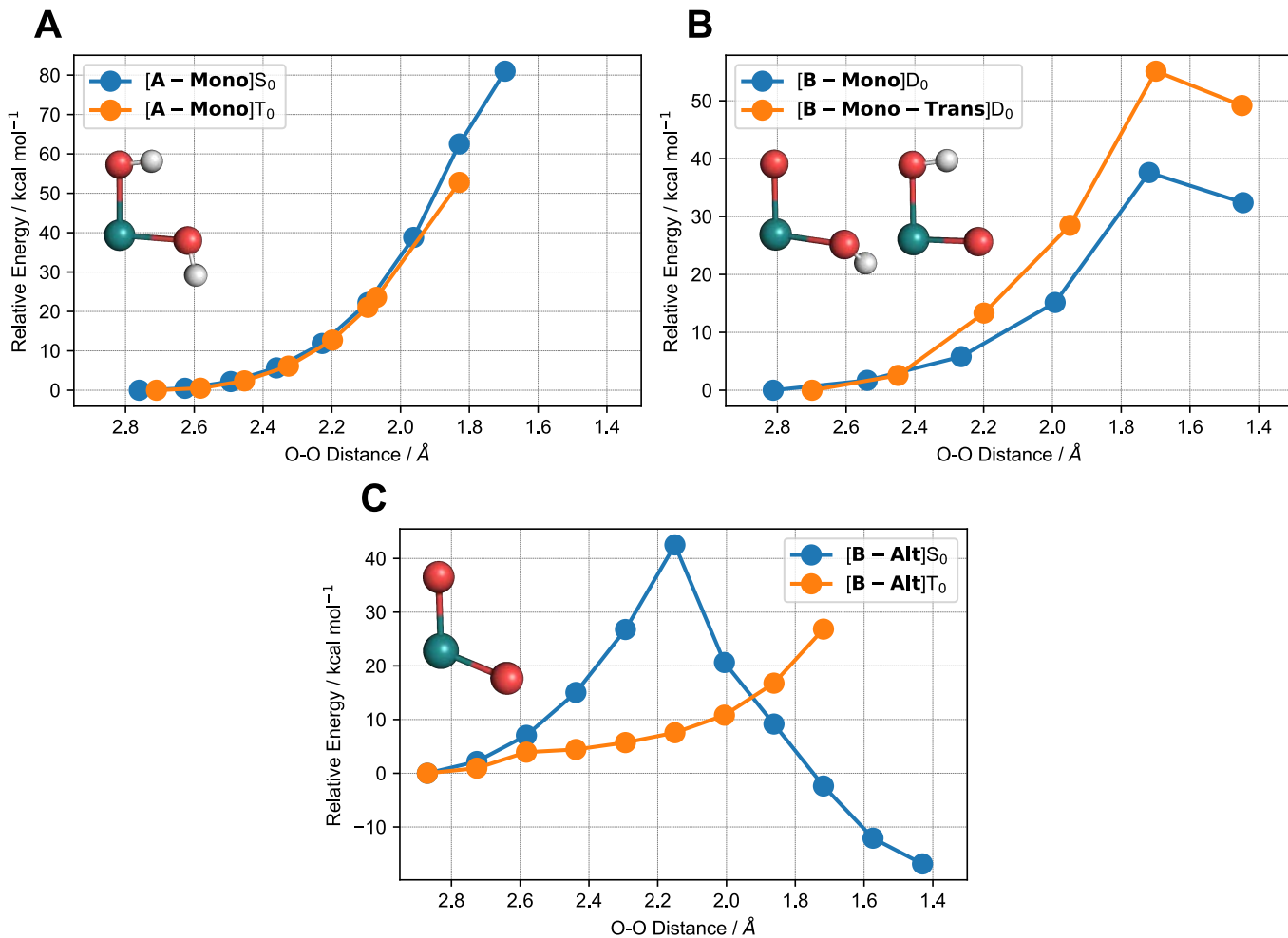


Figure 11.2-16 Energy profiles for relaxed PES scans of O-O bond formation

A Scan of O-O distance for [A-Mono] in singlet and triplet state. Inlet shows [A-Mono] S_0

B Scan of O-O distance for [B-Mono] D_0 (Me model) as well as [B-Mono-Trans] D_0 (Me model). Note that for these scans, the same methyl substituted models were used that were also used for CASSCF calculations. Insets show [B-Mono] D_0 (left) and [B-Mono-Trans] D_0 (right).

C Scan of O-O distance for [B-Alt] in singlet and triplet state ([B-Alt] would be the hypothetical result of a second PCET preceding O-O bond formation). Inlet shows [B-Alt] T_0 .

Energy of starting point for each scan is set to 0 kcal/mol.

Relaxed potential energy surface scans were performed to investigate potential O-O bond formation for six different reaction intermediates. These intermediates span the various possibilities of intramolecular O-O bond formation (fully protonated, singly deprotonated and doubly deprotonated). For [A] and [B-Alt], calculations were performed in the singlet or triplet ground state, while calculations for [B-Mono] and [B-Mono-Trans] were performed in the duplet ground state. These scans therefore provide an estimate for the lower bound of O-O bond formation for each intermediate.

For [A-Mono] in both the singlet and triplet state, no O-O bond formation could be observed (see Figure 11.2-16A). For [A-Mono] T_0 , constrained geometry optimizations for O-O distances smaller than 1.83 Å were unsuccessful. These results are consistent with previous findings on the lack of O-O bond formation starting from [A].(21, 22)

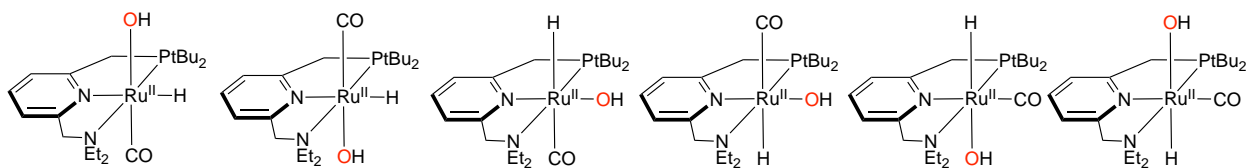
When comparing [B-Mono] D_0 and [B-Mono-Trans] D_0 , it can be seen that the barrier for O-O bond formation is significantly lower for [B-Mono] D_0 (by more than 15 kcal/mol, see Figure 11.2-16B).

For [B-Alt], potential O-O bond formation was studied in both the singlet and triplet state. For [B-Alt] S_0 , O-O bond formation can be observed, although with a barrier of over 40 kcal/mol (in comparison, the barrier for O-O bond formation in [B-Mono] D_0 is 37.6 kcal/mol). Furthermore, it is

questionable whether **[B-Alt]S₀** is even a feasible intermediate. This is based on the observation that **[B]S₀** was found to be unstable during geometry optimizations, reverting back to **[A]S₀**. Such instability can be attributed to the fact that in the S₀ state, there is no charge separation between the two ruthenium centers (as is the case in the T₀ state, see Figure 11.2-12). Therefore, proton transfer from one complex to another is less favorable, explaining why **[B]S₀** reverts back to **[A]S₀**. The same reasoning can be applied to **[B-Alt]S₀**, which would likely not be formed. Hence, **[B-Alt]T₀** was also investigated, but no O-O bond formation was found in this case (constrained geometry optimizations failed for short O-O bond lengths).

11.2.9 Theoretical NMR Data for [F]S₀ Isomers

Table 11.2-8 Relative energies and theoretical NMR data for [F]S₀ isomers



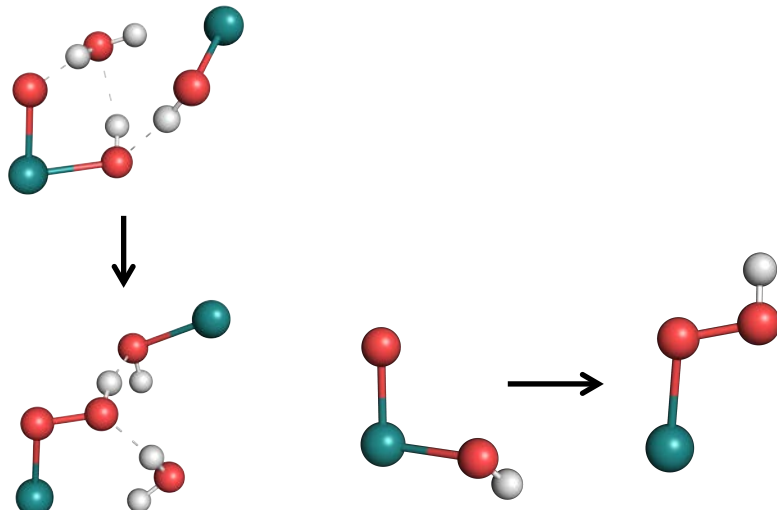
	[F]S ₀	[F-Up]S ₀	[F-Cis]S ₀	[F-Cis-Up]S ₀	[F-Trans]S ₀	[F-Trans-Up]S ₀
ΔG°(SMD) / kcal/mol	4.62	3.17	13.27	13.93	2.46	0.00
δ(¹ H, hydride) / ppm	-9.28	-7.98	0.13	0.08	-10.02	-10.22
δ(³¹ P) / ppm	125.28	108.47	112.55	106.05	110.59	109.14
Experimental	/		δ(¹ H) = -5.5 ppm δ(³¹ P) = 104.3 ppm		δ(¹ H) = -18.9 ppm δ(³¹ P) = 104.2 ppm	

It can be seen that **[F-Trans-Up]S₀** is the most stable isomer of **[F]**, with the cis isomers being significantly less stable. While theoretical hydride chemical shifts are somewhat overestimated, the relative experimental difference between cis and trans isomers of 13.4 ppm is well reproduced (10.2 ppm). **[F]S₀** is only slightly less stable than the trans isomers.

11.3 CASSCF Results

11.3.1 Comparison of DFT and CASSCF Energies and Absorption Wavelengths

Table 11.3-1 Comparison of DFT and CASSCF reaction energies for $[B] \rightarrow [C]$ and absorption wavelengths for $[B\text{-Mono}]D_0$



Method	Parameter	$[B]T_0 \rightarrow [C]T_0$	$[B\text{-Mono}]D_0 \rightarrow [C\text{-Mono}]D_0$	$[B\text{-Mono}]D_0 \rightarrow [C\text{-Mono}]D_0$ (Me model)
DFT	$\Delta G^\circ / \text{kcal/mol}^{[a]}$	35.0 (35.9)	33.5	31.9
	Transition Wavelength / nm ^[b]	539 (Trans. 8)	/	495 (Trans. 4)
CASSCF	$\Delta E / \text{kcal/mol}^{[c]}$	/	/	29.8 (36.3)
	Transition Wavelength / nm ^[d]	/	/	482

[a] Gas phase ΔG° (SMD ΔG° in parentheses). [b] Transition corresponding to second lowest energy transition of CASSCF model of $[B\text{-Mono}]D_0$, calculated using SMD solvation. [c] Gas phase ΔE (PCM ΔE in parentheses). [d] Second lowest energy transition of $[B\text{-Mono}]D_0$, calculated in gas phase.

Table 11.3-1 assesses the agreement between different model chemistries as well as between DFT and CASSCF for O-O bond formation from $[B]$ to $[C]$ as well excitation of $[B]$.

For DFT, it can be seen that there is good agreement for reaction Gibbs free energies between the different model chemistries, with all of them being within 3 kcal/mol. This validates the use of either $[B\text{-Mono}]D_0$ or $[B\text{-Mono}]D_0$ (Me model) to describe O-O bond formation in $[B]T_0$. Also, relative energies of $[B\text{-Mono}]D_0$ to $[C\text{-Mono}]D_0$ (Me model) calculated using CASSCF reproduces the DFT results well.

Furthermore, excitation of $[B]$ was compared between the different model chemistries/methods. In all cases, the lowest energy transition (< 0.4 eV) is an excitation of an electron from the fully occupied to the singly occupied oxo ligand lone pair. Due to its low excitation energy, this transition is likely not photochemically active.

Given the selected active space, CASSCF predicts the second lowest transition to be an excitation from a Ru d_{xz} /OH lone pair orbital to the singly occupied oxygen lone pair (see Figure 11.3-4), with a transition wavelength of 482 nm.

Corresponding transitions can be found in the TD-DFT results for $[B]T_0$ (transition 8, see Figure 11.2-9) and $[B\text{-Mono}]D_0$ (Me model, transition 4, see Figure 11.2-11), with similar transition wavelengths (see Table 11.3-1). It should be noted that the corresponding transition wavelength for $[B]T_0$ is red-shifted by ca. 45 nm. TD-DFT also predicts other, lower energy transitions: in case of $[B\text{-Mono}]D_0$ (Me model), the second lowest energy transition involves a Ru- d_{xy} /OH lone pair orbital

(see Figure 11.2-10), while the third lowest energy transition involves an oxo p_z orbital. For $[\mathbf{B}]T_0$, in addition to these, transitions involving the second ruthenium complex can be found. The reason that these lower energy transitions predicted using TD-DFT for $[\mathbf{B}\text{-Mono}]D_0$ are not found using CASSCF is due to the selection of the active space, which does not include orbitals which would be necessary to describe them. This limitation has to be accepted, as inclusion of more electrons and orbitals in the active space would make calculations computationally infeasible. However, as can be seen below, it was found that the second lowest energy transition in CASSCF does indeed lead to O-O bond formation.

Overall, good agreement between DFT and CASSCF results for reaction energies and excitation of $[\mathbf{B}]$ was found, justifying the applied CASSCF methodology.

11.3.2 Energy Profile including PCM Solvation

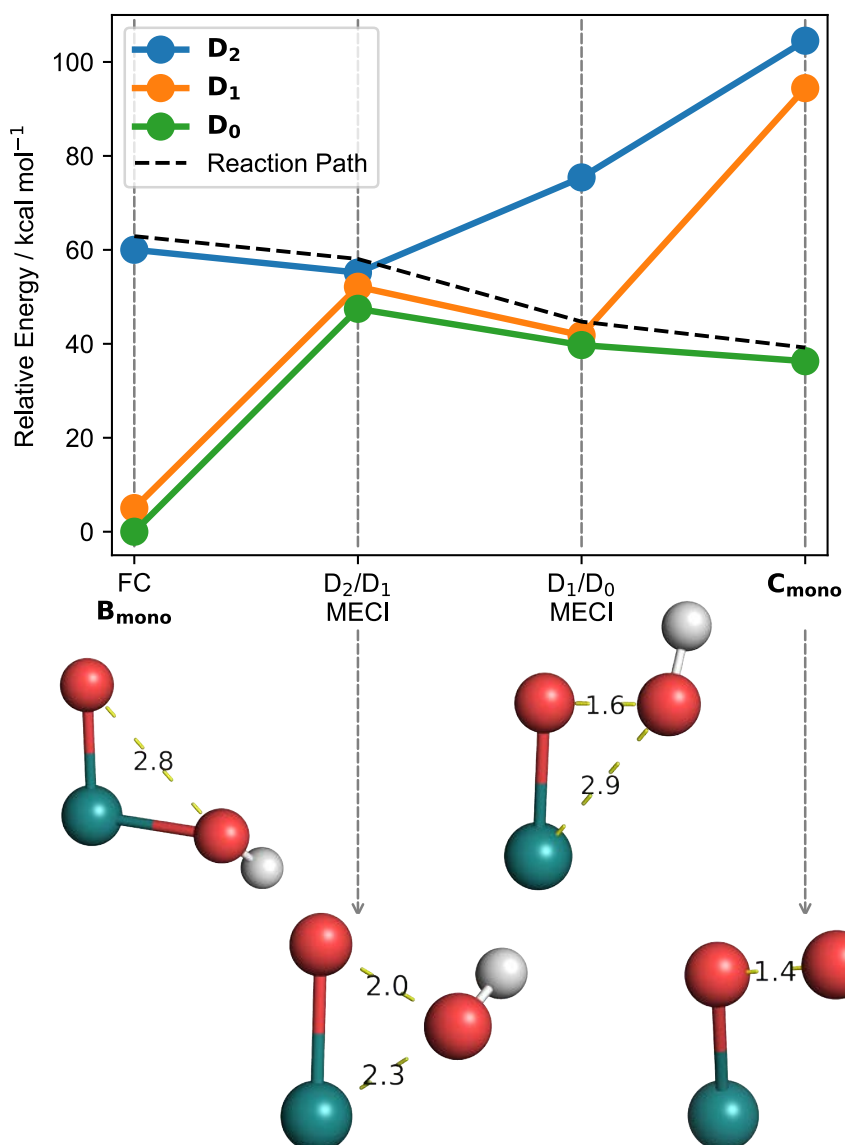
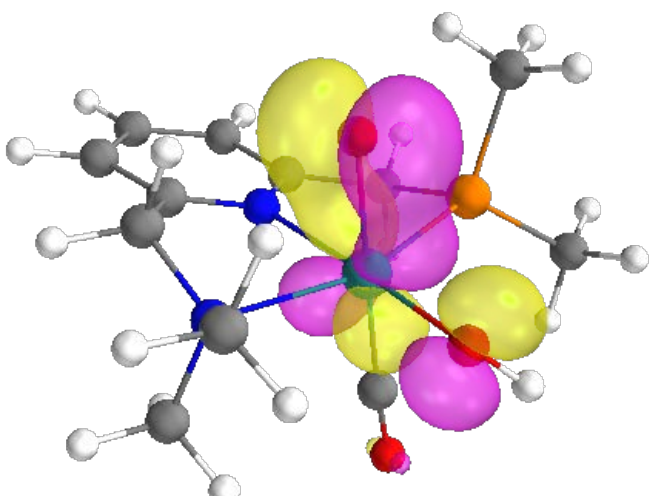
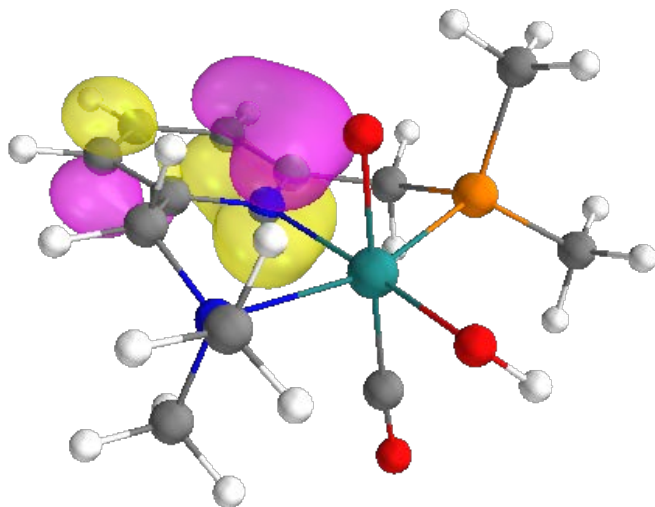
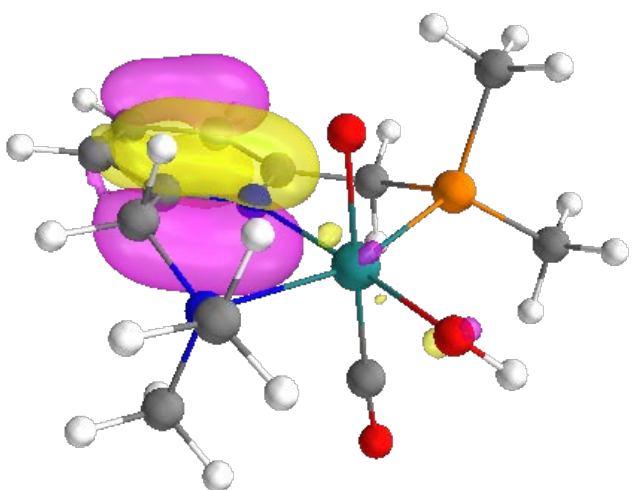
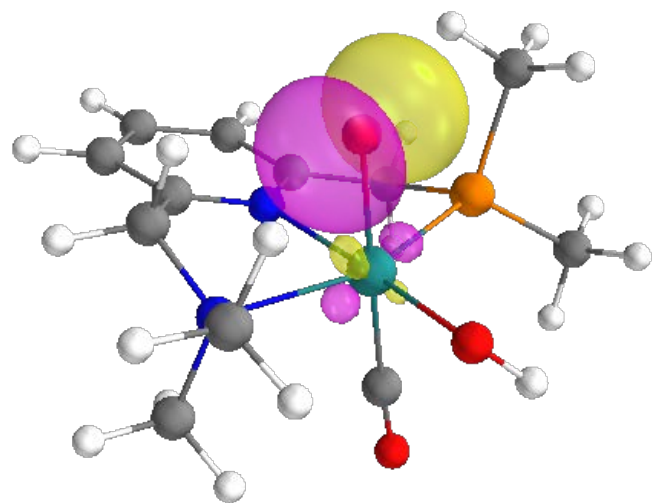
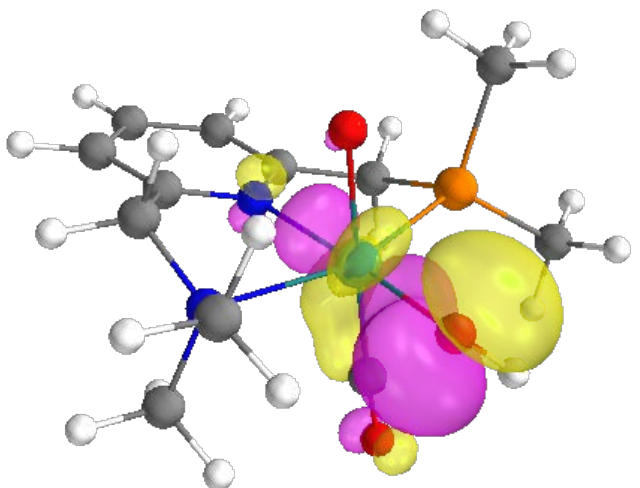
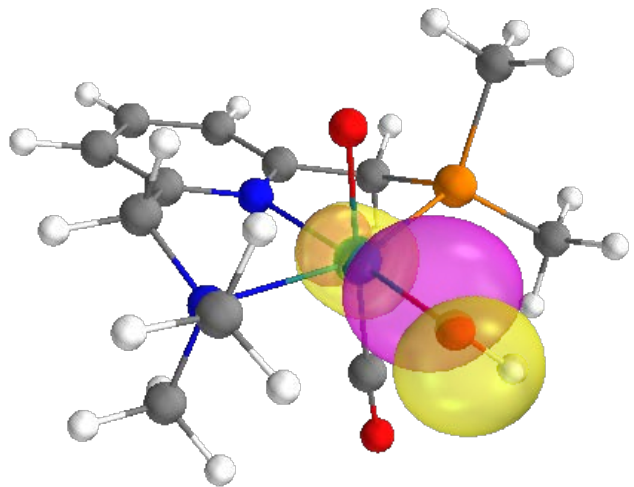


Figure 11.3-1 CASSCF energy profile including PCM solvation

Corresponding structures are shown below the plot, with bond lengths shown in Ångström. Note that degeneracy for conical intersections is slightly lost, since geometries were optimized in the gas phase.

11.3.3 Active Space Orbitals



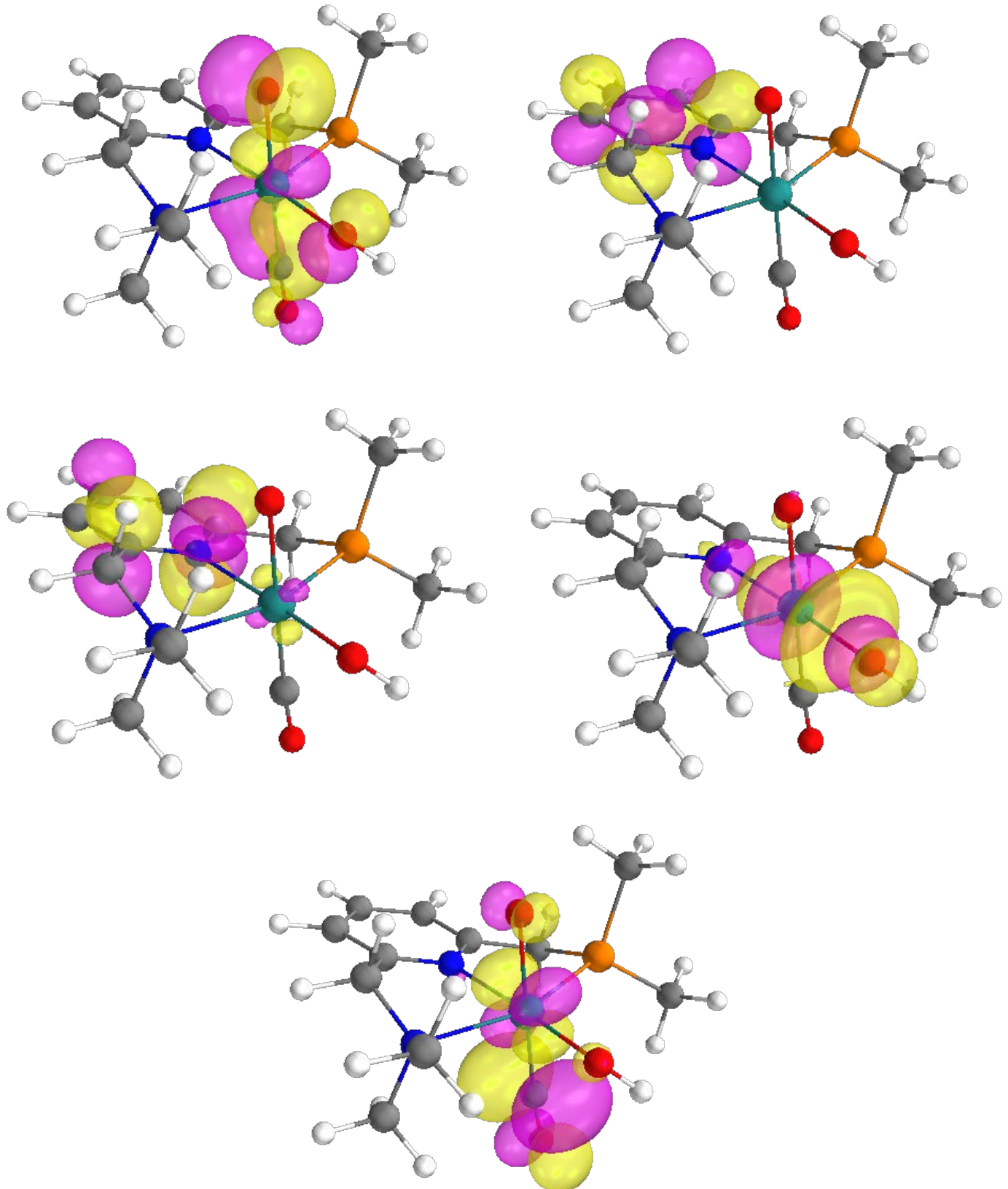


Figure 11.3-2 Active space orbitals of $[B\text{-Mono}]D_0$ used for CASSCF(13,11) calculations (isovalue = 0.05)
(average orbitals from SA-CASSCF(13,11) calculation for five lowest energy states are shown)

11.3.4 Surfaces for [B-Mono]D_n

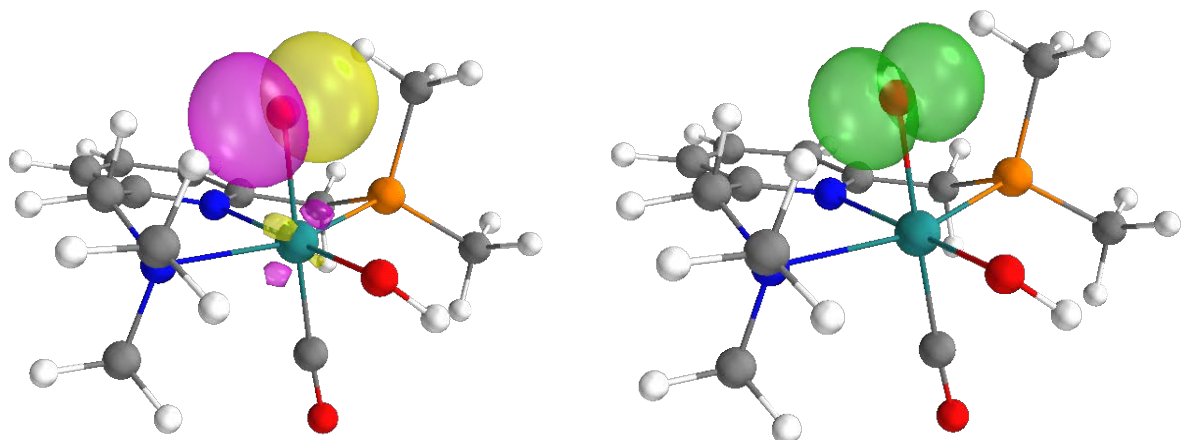


Figure 11.3-3 Singly occupied MO (left, isovalue = 0.05) and spin density (right, isovalue = 0.006) for [B-Mono]D₀

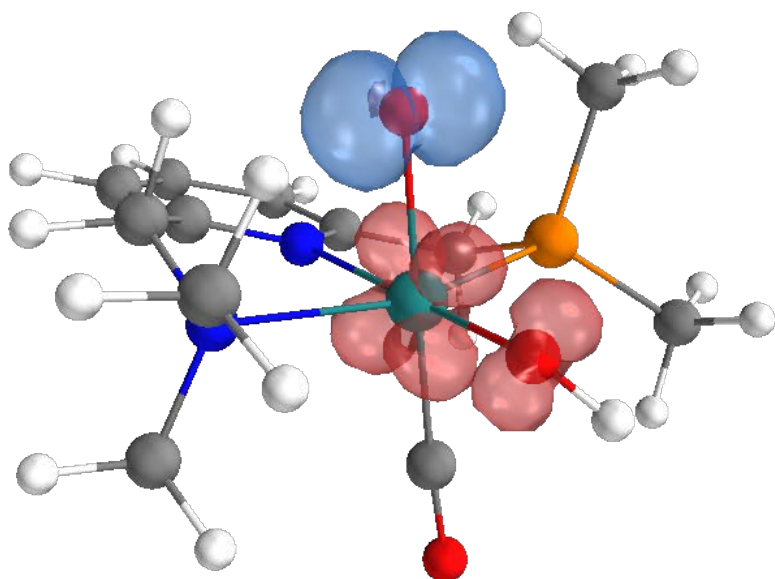


Figure 11.3-4 Unrelaxed transition difference density for [B-Mono]D₀ → [B-Mono]D₂ (detachment density in red, attachment density in blue, isovalue = 0.0005)

11.3.5 Difference Orbitals for Conical Intersections

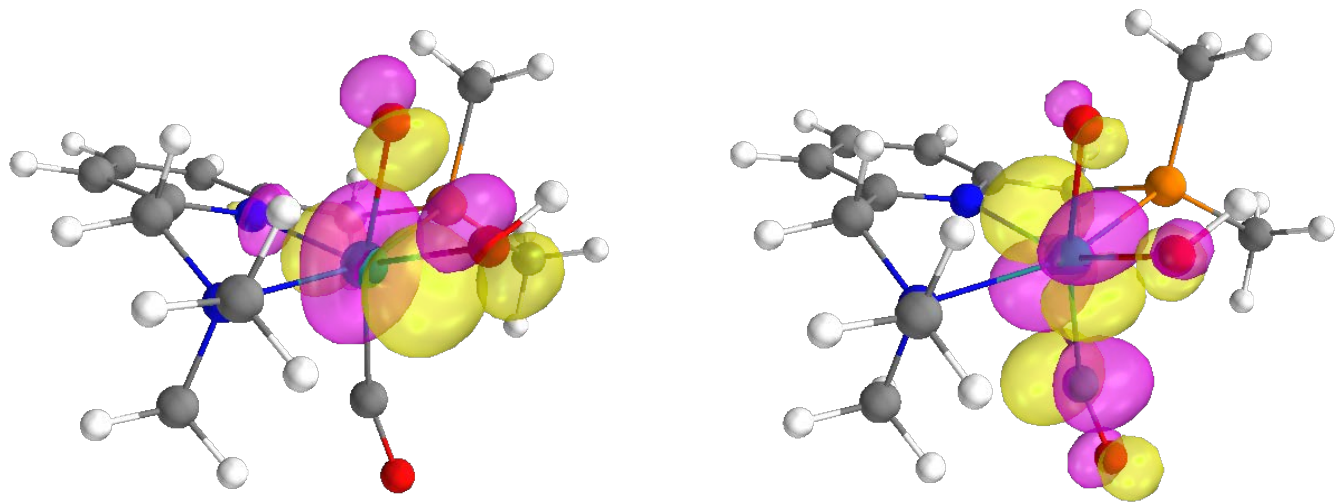


Figure 11.3-5 Difference orbitals for [BC] D_2/D_1 MECI with largest population changes (isovalue = 0.05)
(population change left: -0.8269, population change right: 0.9811)

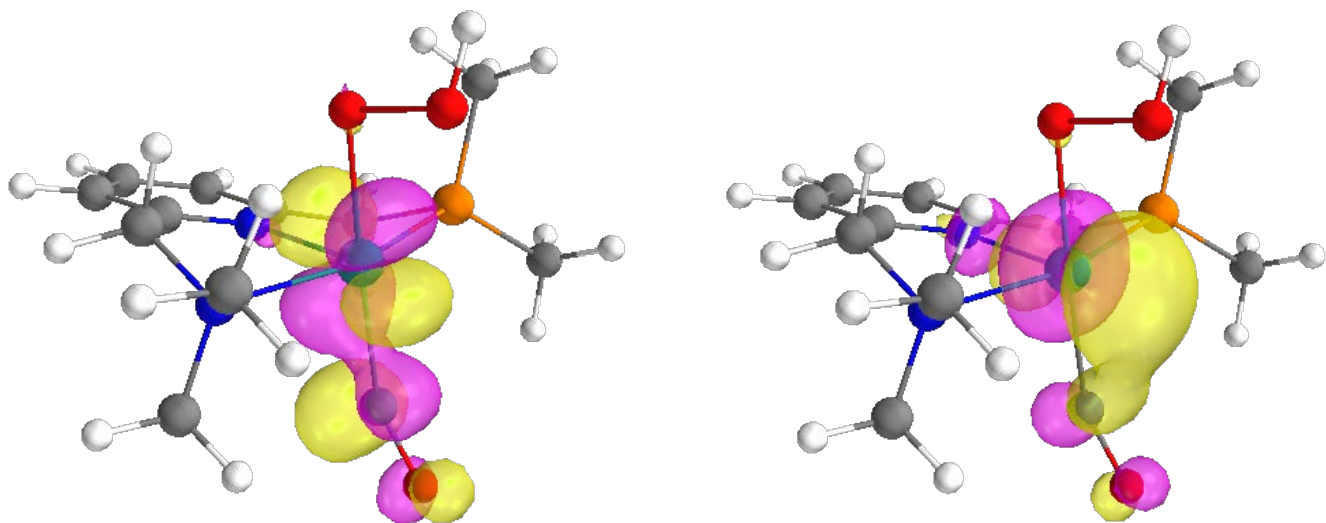


Figure 11.3-6 Difference orbitals for [BC] D_1/D_0 MECI with largest population changes (isovalue = 0.05)
(population change left: -0.8193, population change right: 0.7764)

11.3.6 Surfaces for [C-Mono]D₀

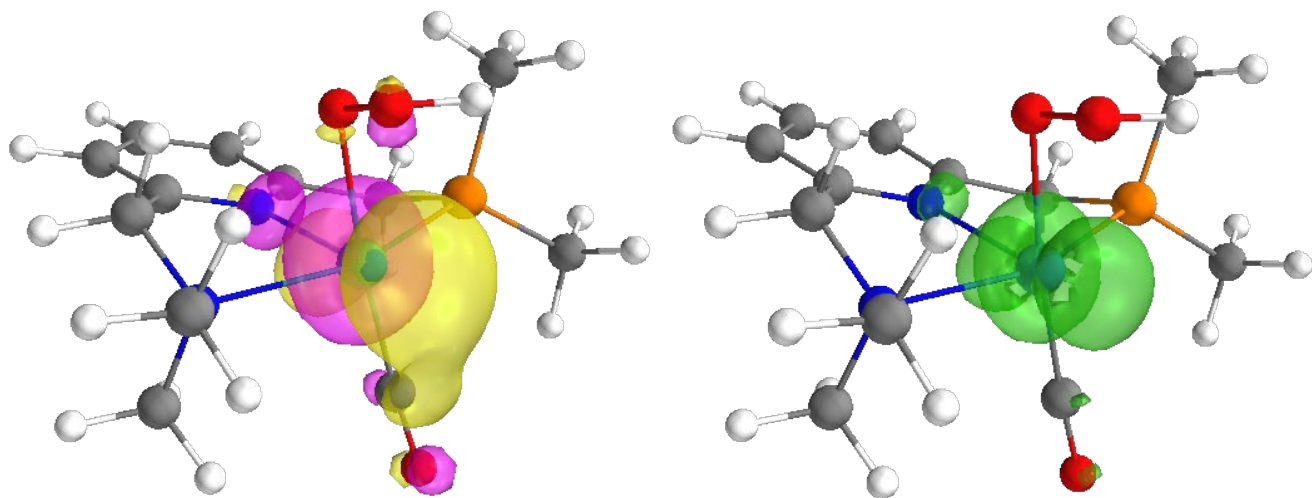


Figure 11.3-7 Singly occupied MO (left, isovalue = 0.05) and spin density (right, isovalue = 0.006) for [C-Mono]D₀

11.4 Integration of Computational and Experimental Results

11.4.1 Dual Irradiation Experiments

The liquid phase O₂ dual irradiation experiments can be seen as a way to probe the absorption characteristics of the second-photon absorbing intermediate. We developed a model convert to theoretical UV/Vis spectra into predicted dual irradiation behavior. This allows for the comparison of experimental dual irradiation data with predicted behavior of various computed intermediates.

Conversion of theoretical UV/Vis spectra to predicted dual irradiation behavior takes place in the following steps:

1. The QTH light source spectrum is described as an ideal blackbody (see Figure 6.1-2) using Planck's law with a blackbody temperature of 3400 K. The spectral power distribution is converted to a spectral photon distribution through division of the power distribution by respective photon energies.
2. For a given longpass filter wavelength (e.g. 630 nm) the corresponding intervals of the theoretical UV/Vis spectrum and spectral photon distribution are selected. Interval end is determined by the cut-off wavelength of the water filter (1000 nm for these calculations), resulting e.g. in [630 nm, 1000 nm] intervals.
3. To calculate the excess reaction rate corresponding to this longpass filter wavelength, the overlap of spectral photon distribution and theoretical UV/Vis spectrum is calculated by multiplying the corresponding intervals and then taking the sum of the resulting vector.
4. This procedure was repeated for each desired longpass filter wavelength. To obtain smooth curves, calculations were performed in 1 nm steps.
5. Resulting curves were scaled vertically through multiplication with a scaling factor to give the best possible fit to experimental data (since it is not trivial to perform this calculation to obtain accurate absolute reaction rates).

In the following, dual irradiation plots with experimental data (black dots) and thus calculated predicted behavior for different potential intermediate are shown.

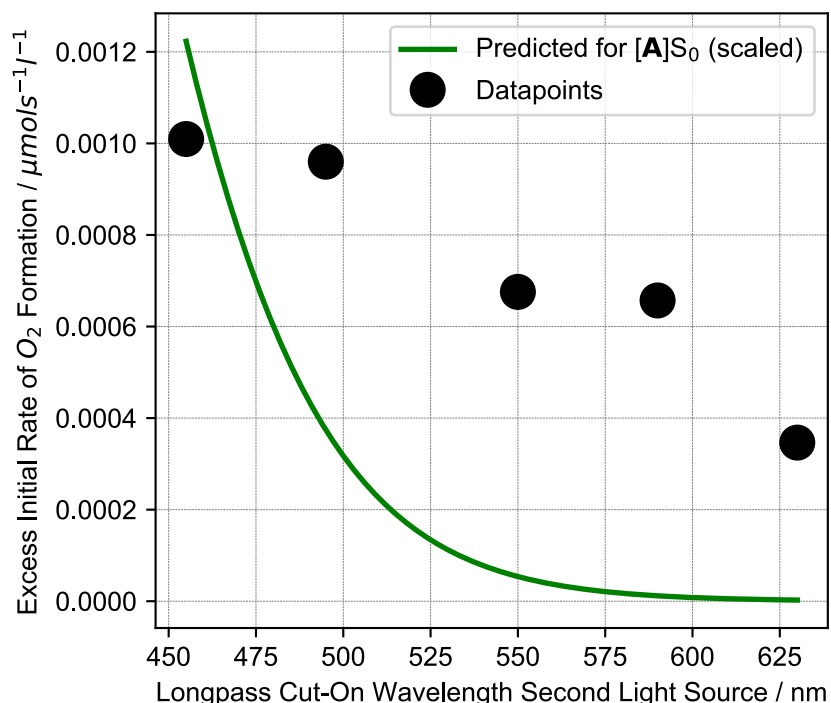


Figure 11.4-1 Dual irradiation data and predicted behavior of [A]S₀ (scaled)

As can be seen in Figure 11.4-1, predicted behavior for $[A]S_0$ is not consistent with experimental data. This is because $[A]S_0$ does not significantly absorb any wavelengths longer than 500 nm, although experimental data shows that these wavelengths already contribute to O_2 formation. Therefore, it can be ruled out that both photons involved in water splitting are absorbed by $[A]S_0$.

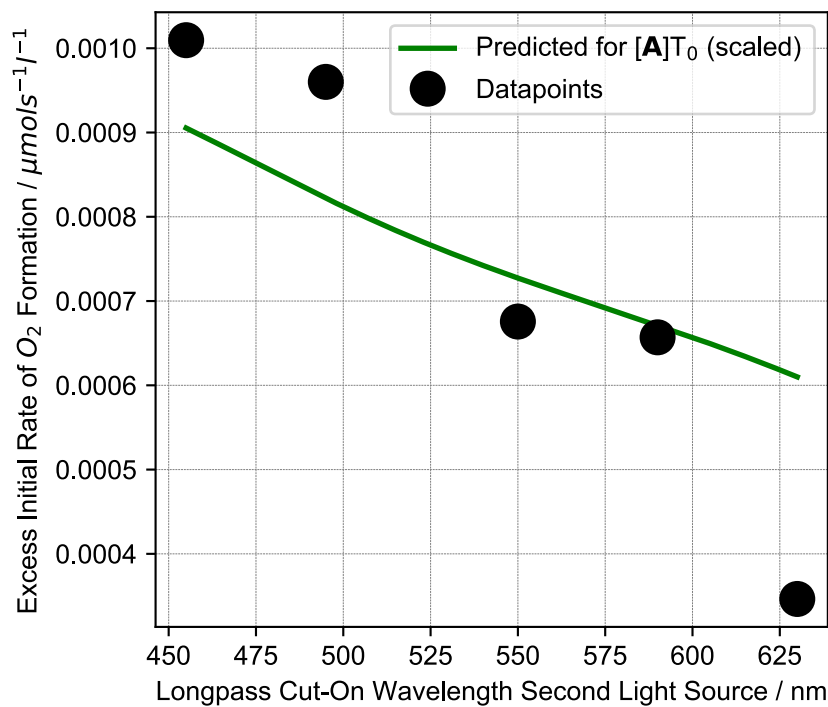


Figure 11.4-2 Dual irradiation data and predicted behavior of $[A]T_0$ (scaled)

The triplet state of $[A]$, $[A]T_0$, could be considered another candidate for the second-photon absorbing intermediate. However, in this case poor agreement is obtained as well. This is due to the fact that $[A]T_0$ absorbs longer wavelengths only very weakly, giving a slope for longpass filter wavelength/reaction rate which is smaller than the one observed experimentally. These results showing that $[A]T_0$ is likely not the second-photon absorbing intermediate are also consistent with DFT calculations showing that O-O bond formation at $[A]T_0$ is unlikely.

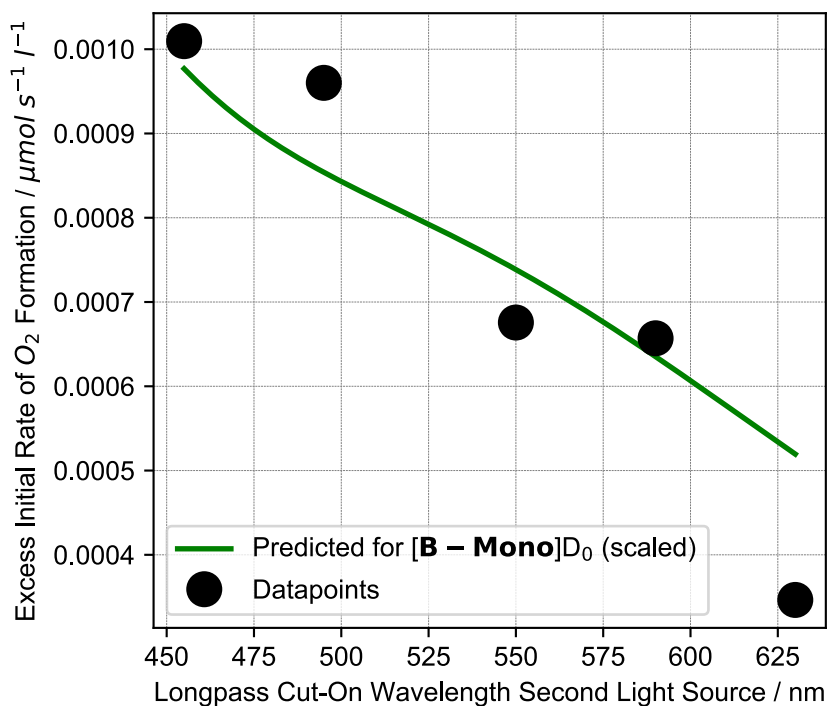


Figure 11.4-3 Dual irradiation data and predicted behavior of $[B\text{-Mono}]D_0$ (scaled)

As can be seen in Figure 11.4-3, $[B\text{-Mono}]D_0$ gives an acceptable fit for the dual irradiation data, although it is slightly inferior compared to the fit of $[B\text{-Mono-Up}]D_0$. As the ligand conformation does not have a significant effect on the obtained energies (see 11.2.1), the choice of ligand conformation does not have a major impact on computations. Calculations studying O-O bond formation were performed using $[B\text{-Mono}]D_0$.

11.4.2 Decay Associated Spectra

Theoretical decay associated spectra (DAS) were computed using theoretical UV/Vis spectra for a reference and an intermediate of interest. Theoretical UV/Vis spectra were used as reference (instead of experimental UV/Vis spectra) so as to allow for error cancellation between theoretical UV/Vis spectra.

DAS were computed using the following formula:

$$DAS = (p_{pop} \text{ } Abs_{int} + (1 - p_{pop}) \text{ } Abs_{ref}) - Abs_{ref} \quad \text{Equation (8)}$$

Wherein Abs_{int} is the absorption spectrum of the intermediate of interest, Abs_{ref} is the absorption spectrum of the reference and p_{pop} is the population of the intermediate of interest after excitation. p_{pop} was assumed to be 0.1, although p_{pop} only effects the DAS magnitude and not its shape.

Thus calculated DAS were scaled vertically by multiplication with a scaling factor to yield the best fit to experimental data.

11.5 Structures and Coordinates for Computed Species

Figure 11.5-1 [A]S₀ Structure and Coordinates

128		Energy: -1951573.6088386
H	0.45669	-1.41554 -3.91019
C	-0.60849	-1.19121 -3.76131
H	-1.11536	-1.29884 -4.73276
H	-0.68914	-0.14799 -3.42124
H	-0.74297	0.90882 2.57857
O	-0.73313	0.99069 -1.30811
H	-0.86407	3.10316 1.53230
O	-1.30655	-1.17052 0.32709
H	-0.11798	0.23950 -1.31847
C	-1.15605	-2.12135 -2.70053
H	-1.34189	0.63234 4.24389
H	-1.19394	-3.16363 -3.07447
C	-1.54956	1.15446 3.29347
H	-1.17142	2.92058 -0.19928
H	-1.50205	2.23282 3.50526
H	-0.49457	-2.11224 -1.82445
C	-1.48683	3.46582 0.70359
H	-1.28687	4.54268 0.57069
H	-2.17348	-2.85488 -0.51445
Ru	-2.51776	0.09058 -0.76873
H	-2.32615	-1.22677 2.00794
N	-2.49410	-1.72633 -2.21407
C	-2.97419	-2.74821 -1.26400
C	-2.93493	0.72547 2.80365
H	-2.70322	-1.17497 3.7243
H	-2.82644	3.73565 3.11401
C	-2.98864	-0.80829 2.77427
O	-2.21626	3.26957 0.97402
P	-3.21371	1.18224 1.02207
H	-3.15200	-3.72018 -1.75468
C	-3.41191	4.01555 2.29562
H	-3.11689	0.67633 3.90443
H	-2.77234	-3.04860 -4.74444
H	-3.24914	5.00319 2.05928
C	-3.46221	-1.53612 -3.31726
H	-3.76709	0.77330 4.77624
C	-3.33499	1.14602 -1.98472
C	-4.00916	1.20050 3.78848
H	-3.48450	3.39830 -1.16373
C	-3.76998	3.84199 -0.20428
H	-4.05874	2.28811 3.90782
H	-3.54789	4.92029 -0.26501
C	-4.20392	-2.27738 -0.54802
N	-4.18814	-0.97126 -0.21953
C	-3.69183	-2.73052 -4.23152
H	-4.02129	-1.17123 2.58909
H	-4.41501	-1.23043 -2.86054
H	-4.48087	3.87829 2.45436
H	-4.10485	-3.60071 -3.69946
C	-5.04785	1.04374 0.77758
H	-4.42084	-2.44844 -5.00597
H	-5.01097	0.83045 3.52344
C	-5.21189	-0.41068 0.46124
C	-5.27900	-3.08726 -0.20149
H	-4.85906	3.74404 -0.07432
H	-5.27592	-4.14092 -0.48292
H	-5.32999	1.63204 -0.11068
H	-5.69471	1.35408 1.60901
C	-6.31091	-1.17896 0.83734
C	-6.34379	-2.53021 0.50361
H	-7.12815	-0.71577 1.39103
H	-7.19795	-3.14636 0.78976
O	-3.88678	1.76908 -2.83721
C	0.53409	-3.71739 2.88972
H	1.03191	1.20848 -2.61109
O	0.65050	0.63916 1.17066
H	1.12549	3.11974 -1.16533
O	1.44261	-1.31103 -0.69485
H	0.26065	1.02485 0.36109
C	0.80054	-2.40419 2.17077
H	1.68202	1.04433 -4.26091
C	1.88201	1.46254 -3.26027
H	1.45188	2.85330 0.54886
H	1.90016	2.55632 -3.36662
C	1.77392	3.42698 -0.33278
H	1.60977	4.50161 -0.14530
H	2.21320	-3.13261 0.23384
Ru	2.48771	-0.14715 0.67409
H	2.42528	-1.08233 -2.29685
N	2.22014	-2.03548 1.98131
C	2.88466	-3.01696 1.10162
C	3.21523	0.90739 -2.75460
H	3.06562	-0.85253 -3.97218
H	3.14665	3.90086 -2.70611
C	3.21891	-0.61872 -2.90429
C	3.25842	3.18559 -0.62318
P	3.07743	1.18422 -0.89528
H	3.03776	-3.99536 1.00302
C	3.72389	4.05880 -1.78770
H	3.93789	-1.53805 3.05434
H	1.86008	-0.15924 3.86531
H	3.59703	5.11498 -1.49697
C	2.93991	1.94814 3.26960
H	4.16382	1.16053 -4.65719
C	3.31771	0.77390 2.01601
C	4.36497	1.44823 -3.61143
H	3.80161	3.07199 1.51083
C	4.07551	3.61023 0.59852
H	4.47194	2.53768 -3.58867
H	3.87932	4.67998 0.78110
C	4.18485	-2.51032 0.55399
N	4.19730	-1.20307 0.23710
C	2.23139	-1.09489 4.30517
H	4.19048	-1.05275 -2.61958
H	3.09882	-2.96832 3.67033
H	4.79216	3.92068 -2.01152
H	1.37686	-1.62062 4.75467
C	5.18533	0.84532 -0.56671
H	2.93276	-0.83914 5.11222
H	5.33086	0.99479 -3.34259
C	5.28552	-0.62889 -0.31867
C	5.29319	-3.31376 3.08082
H	5.15955	3.50693 0.43450
H	5.26682	-4.37010 0.57750
H	5.44504	1.36565 0.36985
H	5.89468	1.17571 -1.33728
C	6.41479	-1.39237 -0.60461
C	6.41695	-2.74787 -0.28829
H	7.28349	-0.91982 -1.06390
H	7.29594	-3.35964 -0.49892
H	0.51938	-1.28667 -0.38188
O	3.84337	1.29469 2.91844
H	-0.55554	-3.85917 2.95147
H	0.92613	-3.74051 3.91838
H	0.94292	-4.58591 2.35026
H	0.33909	-2.42001 1.17789
H	0.32431	-1.56825 2.69632
H	-0.67343	-0.57507 0.79032

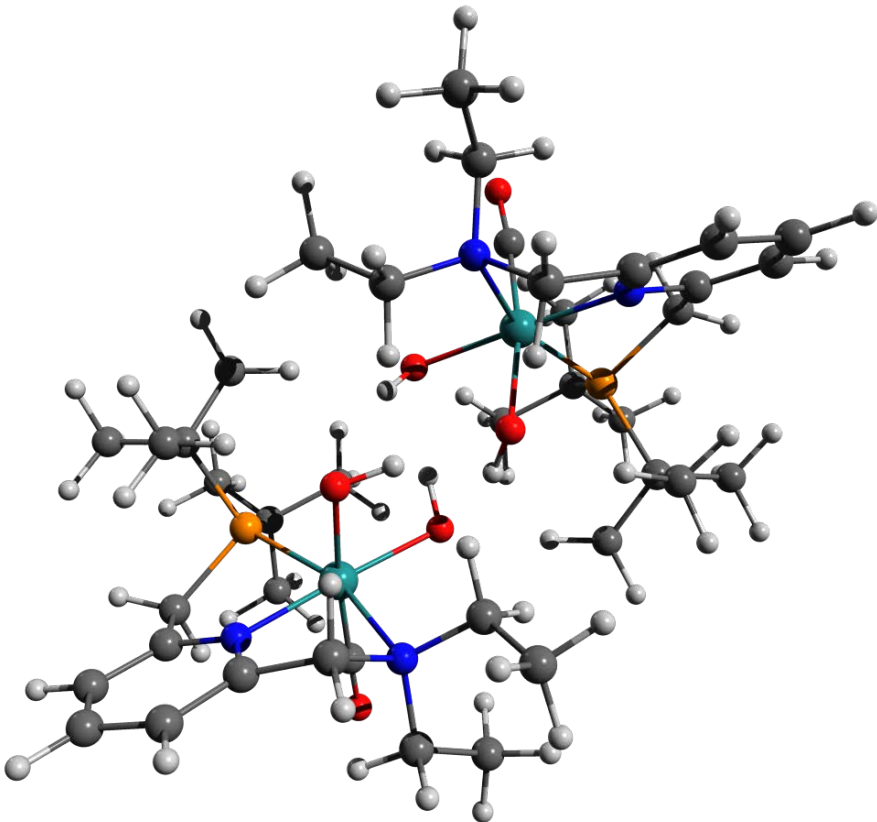


Figure 11.5-2 [A-RR]S₀ Structure and Coordinates

128

Energy: -1951572.9167082

C	-1.33476	1.62962	3.69683
H	-0.26977	-1.45456	-1.99998
O	-1.00000	-0.94847	1.55613
H	-0.69418	-3.51808	-0.61782
O	-1.16182	0.99921	-0.43577
C	-1.63792	2.42574	2.44563
H	-0.43706	-1.55601	-3.77219
C	-0.88137	-1.87525	-2.81475
H	-1.36512	-2.97340	0.92589
H	-0.80142	-2.97152	-2.77187
C	-1.50682	-3.69045	0.10226
H	-1.41068	-4.72148	0.48355
H	-2.11655	2.78328	-0.01923
Ru	-2.60257	-0.08485	0.60240
H	-1.90018	0.68200	-2.25402
N	-2.83716	1.95014	1.72806
C	-3.06271	2.80387	0.54647
C	-2.33492	-1.40393	-2.76955
H	-1.86051	0.28270	-4.00954
H	-2.24788	-4.41338	-2.45745
C	-2.38522	0.10267	-3.05592
C	-2.88702	-3.52920	-0.54760
P	-3.00905	-1.68496	-1.00600
H	-3.30498	3.84415	0.82365
C	-3.04458	-4.50892	-1.70925
H	-3.85094	1.17903	3.37948
H	-3.64271	3.64614	3.90445
H	-2.98825	-5.53336	-1.30402
C	-4.03307	1.92951	2.60067
H	-2.70959	-1.81161	-4.83771
C	-3.71958	-0.90744	1.79395
C	-3.14948	-2.09636	-3.86696
H	-3.90230	-3.25753	1.38718
C	-3.96162	-3.87414	0.48495
H	-3.13803	-3.18967	-3.81289
H	-3.81069	-4.92111	0.79619
O	-4.13030	2.22111	-0.32930
N	-4.09753	0.68019	-0.99999
C	-4.42734	3.25143	3.24266
H	-3.41925	0.45853	-3.14656
H	-4.40174	4.14718	1.99693
H	-4.01792	-4.41009	-2.21348
H	-4.67408	4.02796	2.50298
C	-4.83154	-1.27709	1.21853
H	-5.32631	3.09131	3.85669
H	-4.19637	-1.75785	-3.88610
C	-4.98710	0.21414	-1.19742
C	-5.08534	2.96481	-1.01727
H	-4.97961	-3.80540	0.07074
H	-5.10111	4.05079	-0.91839
H	-5.32519	-1.69300	-0.32500
H	-5.30741	-1.72040	-2.10386
C	-5.95975	0.90972	-1.91117
C	-6.00672	2.29855	-1.82227
H	-6.66897	0.36131	-2.53192
H	-6.76286	2.85910	-2.37469
H	-0.42438	0.37664	-0.58526
O	-4.37127	-1.37026	2.64145
C	1.30359	-1.37352	3.78803
H	0.29481	1.58800	-1.99894
O	1.03826	1.02511	1.61441
H	0.88996	3.59972	-0.60082
O	1.09120	-0.88920	-0.40805
C	1.55019	-2.25202	2.58013
H	0.43562	1.60929	-3.77068
C	0.91906	1.93554	-2.83465
H	1.62411	3.10560	0.93434
H	0.91009	3.03531	-2.83283
C	1.74815	3.77187	0.06532
H	1.71600	4.82376	0.39669
H	1.98309	-2.72548	0.11055
Ru	2.60225	0.12276	0.61552
H	1.74851	-0.65907	-2.22066
N	2.75934	-1.86762	1.82092
C	2.92848	-2.78423	0.67748
C	2.33958	1.37024	-2.79326
H	1.76399	-0.31898	-3.98372
H	2.40859	4.37481	-2.55388
C	2.28703	-0.14409	-3.02839
C	3.08265	3.51160	-0.64424
P	3.06784	1.64973	-1.05231
H	3.11897	-3.82273	0.99687
C	3.23871	4.44917	-1.84065
H	3.84335	-1.07408	3.41866
H	3.51821	-3.49458	4.06914
H	3.25147	5.48578	-1.46371
C	3.97091	-1.86838	2.67360
H	2.69610	1.69491	-4.87946
C	3.76844	0.93623	1.76348
C	3.17664	1.97283	-3.92616
H	4.19024	3.22897	1.23990
C	4.22682	3.82382	0.32206
H	3.24462	3.06520	-3.90259
H	4.14280	4.88270	0.61809
C	4.00795	-2.29506	-0.23921
N	4.03247	-0.95918	-0.40353
C	4.30793	-3.17694	3.37295
C	3.29447	-0.57481	-3.52622
H	4.14461	-1.55373	2.03888
H	4.18438	4.48658	-2.37953
H	4.04544	-4.00159	2.66992
C	4.85699	1.12496	-1.28099
H	5.22779	-3.03581	3.96020
H	4.19586	1.55927	-3.95705
C	4.03388	0.37027	1.21712
C	4.90832	-3.11179	-0.91452
H	5.21535	3.69907	-0.14678
H	4.87646	-4.19174	-0.76656
H	5.39407	1.54156	-0.42312
H	5.33725	1.51112	-2.20034
C	5.85550	-1.14217	-1.92095
C	5.83838	-2.52595	-1.76976
H	6.57610	-0.65667	-2.57971
H	6.55364	-3.14599	-2.31319
H	0.38008	-1.02765	0.25693
O	4.44257	1.39800	2.59466
H	-1.75243	3.50226	2.68089
H	-0.80012	2.33087	1.74631
H	-2.02715	1.84874	4.52480
H	-0.31432	1.86984	4.02428
H	-1.36384	0.55228	3.47461
H	1.62589	-3.31834	2.87075
H	0.69051	-2.14886	1.90309
H	2.03483	-1.52819	4.59704
H	0.30462	-1.60278	4.18461
H	1.30428	-0.31685	3.48018
H	-0.38513	-0.22179	1.78772
H	0.41886	1.21775	0.88892

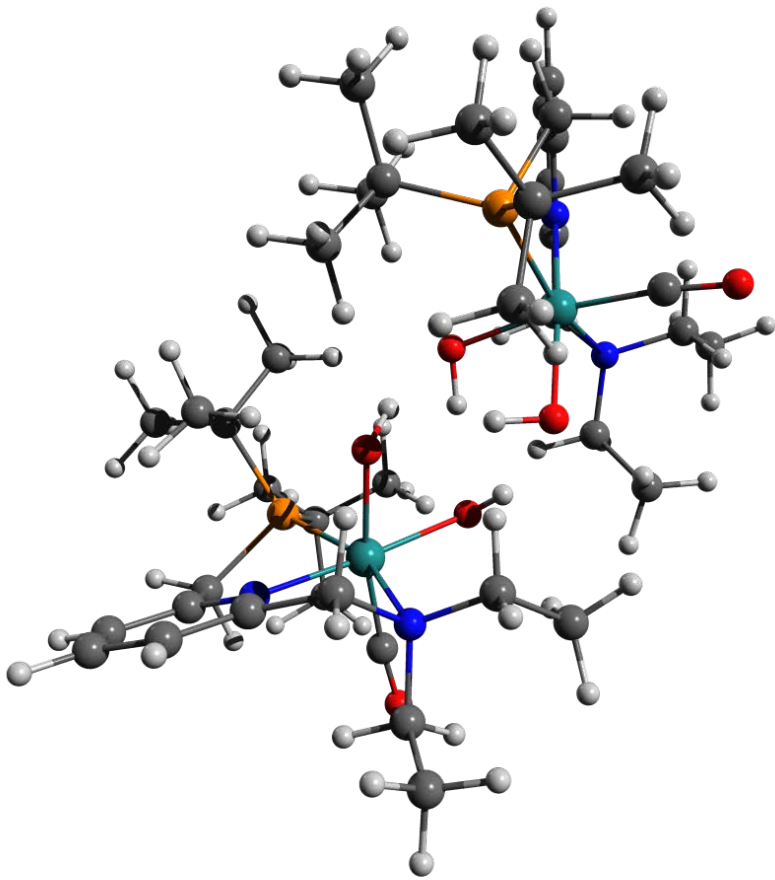


Figure 11.5-3 [A-RS-1]S₀ Structure and Coordinates

128 Energy: -1951573.3041640

C	0.44944	1.22488	-3.77639
H	0.85001	-1.78901	2.23509
O	0.88713	-1.26790	-1.44493
H	1.57788	-3.69098	0.87899
O	0.98095	0.88491	0.39954
C	0.79921	2.22961	-2.69815
H	1.26570	-1.62533	3.95664
H	0.64403	3.26790	-3.05872
C	1.65776	-1.92898	2.97132
H	1.93112	-3.16660	-0.77294
H	1.88358	-3.00310	3.03292
H	0.12105	2.06733	-1.84896
C	2.32505	-3.74865	0.07538
H	2.42815	-4.80718	-0.21773
H	1.57306	2.83785	-0.37216
Ru	2.44962	-0.09044	-0.75468
H	1.79048	0.71994	2.13147
N	2.16494	2.06545	-2.18577
C	2.41038	2.98380	-1.07523
C	2.90298	-1.09150	2.67002
H	2.20094	0.53729	3.87486
H	3.52988	-4.02953	2.56215
C	2.56397	0.39387	2.84285
C	3.69327	-3.21981	0.52014
P	3.42989	-1.36334	0.85447
H	2.44494	4.04258	-1.39333
C	4.21952	-4.02271	1.70965
H	3.05995	1.30047	-3.90411
H	2.34497	3.63209	-4.57434
H	4.34614	-5.06930	1.38574
C	3.20642	2.14589	-3.21895
H	3.61586	-1.23656	4.68387
C	3.53938	-0.75838	-2.05805
C	4.01472	-1.42166	3.67240
H	4.38662	-2.90712	-1.54788
C	4.69148	-3.40826	-0.02637
H	4.35525	-2.97777	3.64201
H	4.75181	-4.48659	-0.84501
C	3.91212	2.63839	-0.31581
N	3.87236	1.14886	-0.07070
C	3.27034	3.44640	-4.00884
H	3.45930	1.03171	2.72334
H	4.17171	1.96408	-2.72147
H	5.20328	-3.66674	2.05212
H	3.45657	4.32098	-3.36660
C	5.12282	-0.55440	0.79579
H	4.09598	3.39154	-4.73430
H	4.88796	-0.76266	3.55393
C	4.95773	0.92694	0.62682
C	4.54049	3.60455	0.16296
H	5.70742	-3.07897	-0.35564
H	4.34930	4.65660	-0.05122
H	5.59454	-0.95183	-0.11779
H	5.77818	-0.79507	1.64343
C	5.86173	1.85499	1.13857
C	5.64754	3.20948	0.90675
H	6.72471	1.50940	1.70833
H	6.34577	3.95253	1.29638
H	0.16102	0.80024	-0.13289
O	4.15621	-1.09821	-2.98708
C	-1.19301	-3.84473	-1.18152
H	-0.26419	2.42261	1.01026
O	-0.73798	-1.41373	0.85327
H	-0.39436	1.23053	3.13584
O	-1.36411	0.39594	-1.19688
H	-0.16417	-0.63117	0.95056
C	-1.71073	-2.77480	-2.11892
H	-0.62877	4.16044	0.81622
C	-0.94210	3.23229	1.32537
H	-1.01484	-0.42043	2.99262
H	-0.79963	3.39421	2.40359
C	-1.12835	0.52400	3.54629
H	-0.88319	0.35518	4.60876
H	-2.46759	-0.43411	-2.77867
Ru	-2.53285	-0.62460	0.18044
H	-2.00588	2.17779	-1.04332
N	-2.90366	-2.07190	-1.59740
C	-3.34620	-1.07479	-2.59111
C	-2.40466	2.95723	0.96836
H	-2.18292	3.96727	-0.91269
H	-2.01998	3.12487	3.94360
C	-2.56224	2.99352	-0.55736
C	-2.56286	1.05027	3.43758
P	-2.88694	1.20278	1.56571
H	-3.68593	-1.54294	-3.53017
C	-2.72345	2.33878	4.24338
H	-3.66771	-3.63450	-0.44206
H	-3.69938	-4.57063	-2.77946
H	-2.52085	2.10771	5.30280
C	-4.00430	-3.01267	-1.28002
H	-2.94425	5.02381	1.12511
C	-3.41776	-1.74699	1.32201
C	-3.29761	4.06429	1.53923
H	-3.44520	-0.96318	3.57207
C	-3.51212	0.01888	4.05009
H	-3.26800	4.14975	2.63062
H	-3.23062	-0.01510	5.07633
C	-4.40472	-0.19363	-2.01841
N	-4.47751	0.14522	-0.72650
O	-4.49518	-3.90181	-2.41606
H	-3.61973	2.93371	-0.85771
H	-4.84222	-2.41181	-0.89722
H	-3.74677	2.74021	4.18807
H	-4.88329	-3.32890	-3.26859
C	-4.75401	1.23729	1.35488
H	-5.30745	-4.53433	-2.04271
H	-4.34603	3.95500	1.22413
C	-5.07513	0.96578	-0.08390
C	-5.48543	0.32174	-2.73305
H	-4.56123	0.35307	4.03718
H	-5.62270	0.04053	-3.77768
H	-5.11703	0.37291	1.94924
H	-5.25224	2.13269	1.72618
C	-6.16943	1.50670	-0.75472
C	-6.37327	1.18280	-2.09319
H	-6.85123	2.17357	-0.22620
H	-7.22639	1.59603	-2.63427
H	-6.61046	-0.19239	-1.42034
O	-3.91652	-2.56087	1.99078
H	-6.62551	1.30058	-3.99399
H	0.64812	0.20444	-3.41292
H	0.99685	1.39251	-4.71719
H	-1.00677	-3.40740	-0.18877
H	-0.23452	-4.21439	-1.57202
H	-1.87164	-4.70722	-1.08997
H	-0.92118	-2.02245	-2.25956
H	-1.94765	-3.19941	-3.11412
H	0.39291	-1.52961	-0.63555

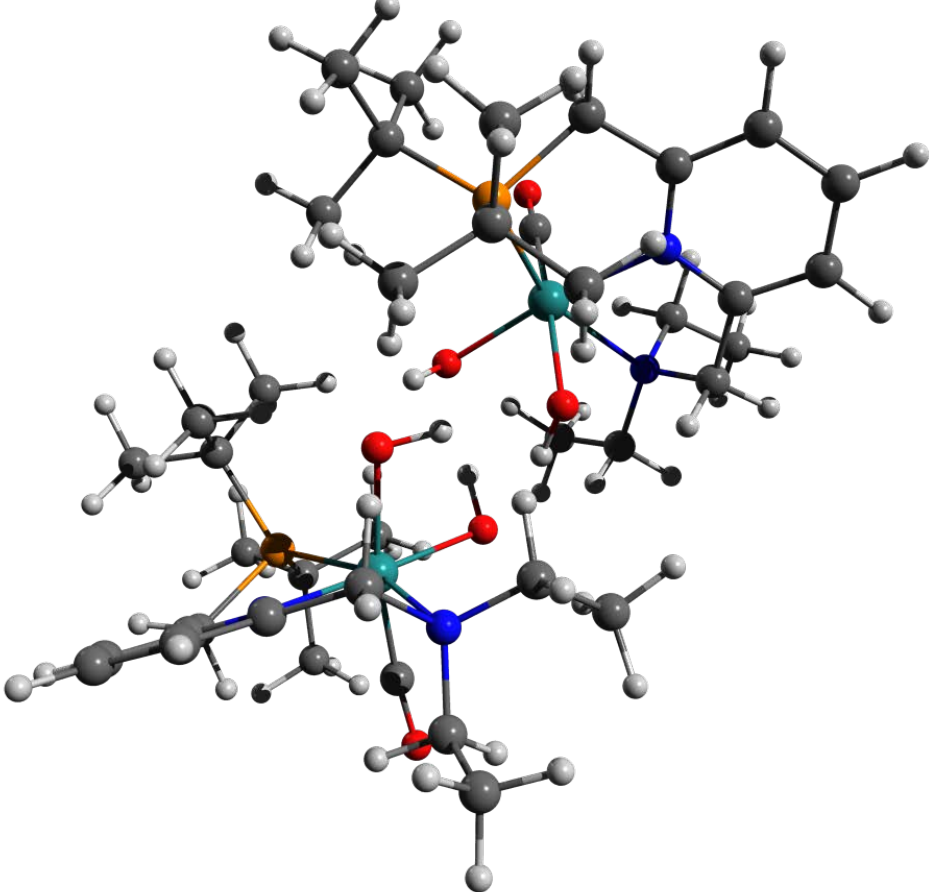


Figure 11.5-4 [A-RS-2]S₀ Structure and Coordinates

128 Energy: -1951572.5055138

C	-1.16194	-3.96254	0.55818
H	-0.28547	2.55698	-0.56699
O	-0.71633	-1.22947	-1.04323
H	-0.41574	1.72517	-2.90022
O	1.37263	0.25431	1.25590
H	-0.14262	-0.44333	-0.99728
C	1.67727	-3.05591	1.65360
H	0.64876	4.24417	-0.11099
C	-0.95882	3.40685	0.76038
H	-1.04447	0.07567	-3.01956
H	-0.80424	3.73235	-1.79927
C	-1.15597	1.09668	-3.41404
H	-0.91646	1.09973	-4.49107
H	-2.46097	-0.86938	2.68486
Ru	-2.52248	-0.57308	-0.26885
H	-2.04005	1.99190	1.39806
N	-2.87838	-2.29591	1.25096
C	-3.33258	-1.47943	2.39246
C	-2.42515	3.08378	-0.46455
H	-2.22018	3.77888	1.55552
H	-2.02347	3.73102	-3.37496
C	-2.59537	2.87446	1.04586
C	-2.58569	1.60700	-3.21317
P	-2.89982	1.44898	-1.33940
H	-3.66860	-2.09820	3.24145
C	-2.73620	3.01159	-3.79611
H	-3.62358	-3.65750	-0.14564
H	-3.64930	-4.96047	2.02194
C	-2.53836	2.95472	-4.87985
C	-3.96814	-3.18351	0.78104
H	-2.97044	5.14641	-0.27862
C	-3.38552	-1.50789	-1.58371
C	-3.31123	4.27088	-0.85685
H	-3.49938	-0.34703	-3.66603
C	-3.54712	0.69940	-3.98296
H	-3.26008	4.54057	-1.91680
H	-3.26225	0.72878	-5.04784
C	-4.39988	-0.51775	1.97028
N	-4.21716	0.01900	0.74920
C	-4.44520	-4.24977	1.75605
H	-3.65521	2.76763	1.32441
H	-4.81111	-2.53646	0.49757
H	-3.75507	3.40879	-3.67224
H	-4.85141	-3.82674	2.68713
C	-4.76609	1.42433	-1.12500
H	-5.25455	-4.82416	1.28070
H	-4.36541	4.10888	-0.58674
C	-5.08332	0.92583	0.25017
C	-5.48466	-0.14662	2.75743
H	-4.59044	1.04577	-3.92042
H	-5.61757	-0.59610	3.74205
H	-5.12379	0.67768	-1.85267
H	-5.27147	2.37505	-1.34127
C	-6.18240	1.33887	0.99957
C	-6.38195	0.79836	2.26671
H	-6.87085	2.07685	0.58688
H	-7.23854	1.10900	2.86765
H	-0.60569	-0.38424	1.38092
O	-3.86464	-2.21004	-2.38127
H	-0.53829	0.45268	4.17835
C	0.52979	0.40724	3.92102
H	1.11249	0.42470	4.49359
H	0.70910	-0.54051	3.39085
H	0.79342	-1.13444	-2.52605
O	0.91432	-1.37723	1.29448
H	1.46971	-3.38523	-1.45868
O	1.03384	0.96896	-0.20626
C	0.84882	1.56909	3.00435
H	1.21054	-0.84276	-4.19128
H	0.72861	2.53646	3.52091
C	1.59831	-1.32480	-3.27797
H	1.90942	-3.21844	0.24600
H	1.80927	-2.37257	-3.53444
H	0.13824	1.55332	2.16730
C	2.24561	-3.62799	-0.71930
H	2.31753	-4.72653	-0.64710
H	1.58278	2.70824	0.86890
Ru	2.48862	-0.13997	0.78538
H	1.77452	1.12681	-1.96506
N	2.20456	1.49639	2.42021
C	2.42865	2.68434	1.57538
C	2.85422	-0.57168	-2.83232
H	2.16359	1.25552	-3.72049
H	3.38851	-3.48871	-3.25647
C	2.53404	0.92498	-2.73502
C	3.61447	-3.05813	-1.10613
P	3.37383	-1.16762	-1.09234
H	2.45643	3.61660	2.16440
C	4.09113	-3.65269	-2.43111
H	3.12402	0.42379	3.95740
H	2.37123	2.55669	5.08958
H	4.18984	-4.74341	-2.29982
C	3.25511	1.39149	3.45879
H	3.55876	-0.36720	-4.84451
C	3.57726	-1.09645	1.89839
C	3.95888	-0.73043	-3.88287
H	4.37145	-3.13218	0.96251
C	4.63697	-3.46765	-0.04444
H	4.28934	-1.76320	-4.03702
H	4.67512	-4.56940	-0.01908
C	3.66953	2.53433	0.74934
N	3.88766	1.28977	0.28531
C	3.29696	2.50194	4.49834
H	3.43367	1.52044	-2.51419
H	4.22093	1.33666	2.93511
H	5.08006	-3.27043	-2.72699
H	3.48085	3.49358	4.05824
C	5.08766	-0.41751	-0.91673
H	4.12250	2.29925	5.19710
H	4.83902	-0.11051	-3.65529
C	4.95052	1.01411	-0.50029
C	4.52900	3.57781	0.42300
H	5.65342	-3.11756	-0.28298
H	4.33800	4.57849	0.81212
H	5.55431	-0.97211	-0.08606
H	5.73358	-0.52553	-1.79812
C	5.83620	2.02474	-0.86699
C	5.62030	3.31907	-0.40233
H	6.68607	1.79111	-1.50887
H	6.30554	4.12275	-0.67778
H	0.21147	0.79237	0.71037
O	4.16237	-1.67771	2.71045
H	-1.90771	-3.39843	2.56906
H	-0.89587	-2.33029	1.91152
H	-1.82472	-4.80355	0.32849
H	-0.19204	-4.38523	0.88638
H	-0.98821	-3.36937	0.35049
H	0.46736	-1.56382	0.44287

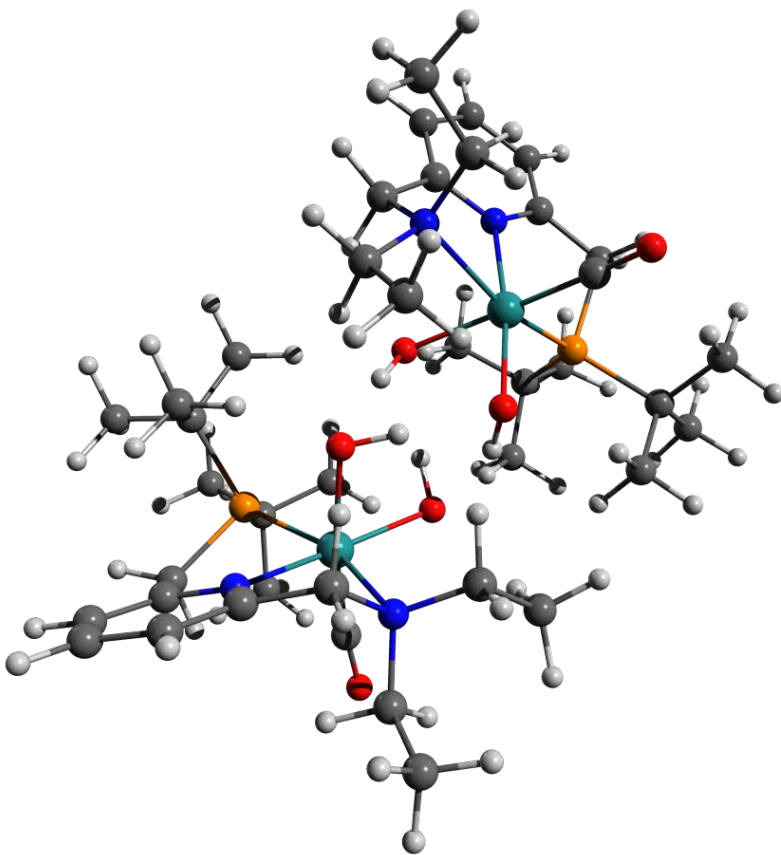


Figure 11.5-5 [A]T₀ Structure and Coordinates

128

Energy: -1951545.5657542

H	0.31863	-4.29565	-0.54368
C	-0.74782	-4.05620	-0.66007
H	-1.25666	-4.95812	-1.03476
H	-0.83424	-3.25902	-1.41383
H	-0.89863	2.85473	0.60480
O	-0.81090	-0.46520	-1.74247
H	-1.03805	3.35602	-1.86063
O	-1.24485	-0.42066	1.01348
H	-0.19731	-0.01036	-1.12069
C	-1.29305	-3.57816	0.66899
H	-1.52275	4.12018	1.69653
H	-1.26491	-4.40087	1.41479
C	-1.71674	3.57878	0.75441
H	-1.15604	1.73456	-2.60268
H	-1.68868	4.32026	-0.05772
H	-0.65852	-2.76439	1.04954
C	-1.58651	2.74850	-2.59407
H	-1.43788	3.20907	-3.58570
H	-2.24912	-1.89079	2.23744
Ru	-2.42361	-0.74411	-0.65979
H	-2.34600	1.11425	1.95336
N	-2.64389	-3.01925	0.56942
C	-3.08084	-2.50418	1.85122
C	-3.07295	2.87641	0.85781
H	-2.70549	2.56665	2.95908
H	-3.18995	4.76240	-1.58997
C	-3.03607	1.96444	2.09462
C	-3.08836	2.68472	-2.28609
P	-3.24831	1.72285	-0.65451
H	-3.31703	-3.29603	2.58922
C	-3.70208	4.08183	-2.28393
H	-3.31453	-4.05086	-1.10616
H	-2.95781	-5.89659	0.63487
H	-3.61235	4.51704	-3.29444
C	-3.62965	-3.89580	-0.06666
H	-4.02518	4.45554	1.97149
C	-3.36486	-1.34120	-2.25581
C	-4.19650	3.89629	1.03496
H	-3.37346	0.82330	-3.40463
O	-3.2114	1.85211	-3.30979
H	-4.25189	7.462811	0.21944
H	-3.51094	2.421281	-4.36297
C	-4.25781	-1.59700	1.69925
N	-4.21736	-0.72903	0.66500
C	-3.86878	-5.23942	0.61286
H	-4.03273	1.56862	2.34058
H	-4.57500	-3.33317	-0.12247
H	-4.77282	4.06406	-2.02686
H	-4.22593	-5.12822	1.64853
C	-5.03521	1.18702	-0.58544
H	-4.63688	-5.80115	0.05987
H	-5.17972	3.41023	1.13140
C	-5.19506	0.18768	0.51919
C	-5.31278	-1.58449	2.60864
H	-4.84681	1.83379	-3.30016
H	-5.31214	-2.30225	3.42990
H	-5.22278	0.68777	-1.54863
H	-5.75961	2.00674	-0.47589
C	-6.28110	0.23361	1.39299
C	-6.34423	-0.66720	2.44904
H	-7.05858	0.98311	1.24109
H	-7.18533	-0.64836	3.14469
O	-3.95239	-1.78104	-0.03127
C	0.46634	0.92944	4.49928
H	1.05119	-1.86914	-1.77387
O	0.68245	1.25187	-0.04535
H	1.17504	0.58034	-3.03899
O	1.59054	-1.20381	0.91053
H	0.68848	1.87513	-0.77795
C	0.80149	0.86999	3.01811
H	1.58372	-3.34978	-2.61470
C	1.79147	-2.27601	-2.47557
H	1.80904	2.09388	-2.35449
H	1.63051	-1.78465	-3.44595
C	1.94625	1.35647	-3.15761
H	1.77585	1.87055	-4.11806
H	2.26759	-1.13380	2.93873
Ru	2.56684	0.54429	0.42633
H	2.69920	-2.51644	0.11657
N	2.23960	0.90872	2.67109
C	2.92162	-0.28578	3.20523
C	3.22067	-2.10962	-1.96357
H	3.14970	-3.95303	-0.87315
H	2.92299	-0.73598	-4.64067
C	3.38740	-2.89712	-0.65726
C	3.37353	0.79744	-3.12893
P	3.47221	-0.27104	-1.54417
H	3.06077	-0.22542	4.29811
C	3.64980	0.06049	-4.43884
H	3.92137	2.13685	2.74600
H	1.86747	3.41929	1.76505
C	3.57127	0.79015	-5.26218
C	2.90572	2.12915	3.17040
H	4.10409	-3.77616	-2.97141
C	3.37619	2.16288	0.15103
C	4.22365	-2.68001	-2.97180
H	4.28215	2.54675	-2.91537
C	4.36815	1.95830	-3.05241
H	4.08518	-2.33110	-3.99299
H	4.44426	2.74113	-3.89428
O	4.23212	-0.55244	2.52984
N	4.26066	-0.29347	1.20812
C	2.17837	3.41271	2.81830
H	4.42733	-2.87195	-0.29351
H	3.02487	2.05820	4.26026
H	4.66297	-0.36397	-4.47338
H	1.28096	3.55834	3.43643
C	5.26488	-0.21591	-0.98745
H	2.84597	4.27026	2.98512
H	5.26986	-2.47853	-2.69355
C	5.35194	-0.57317	0.46505
C	5.33575	-1.10622	3.16925
H	5.40872	1.61545	-3.16035
H	5.29714	-1.30072	4.24147
H	5.57622	0.83481	-1.10176
H	5.94760	-0.82993	-1.59141
C	6.47694	-1.14500	1.05423
C	6.46875	-1.41098	2.41990
H	7.34875	-1.37413	0.44085
H	7.34436	-1.85234	2.89915
H	0.63496	-1.05555	0.77572
O	3.87246	3.21300	0.03062
H	-0.62825	0.88816	4.60526
H	0.80880	1.85473	4.98886
H	0.87716	0.07545	5.06003
H	0.39995	-0.04647	2.56943
H	0.32600	1.69534	2.47519
H	-0.66325	0.32172	0.76362

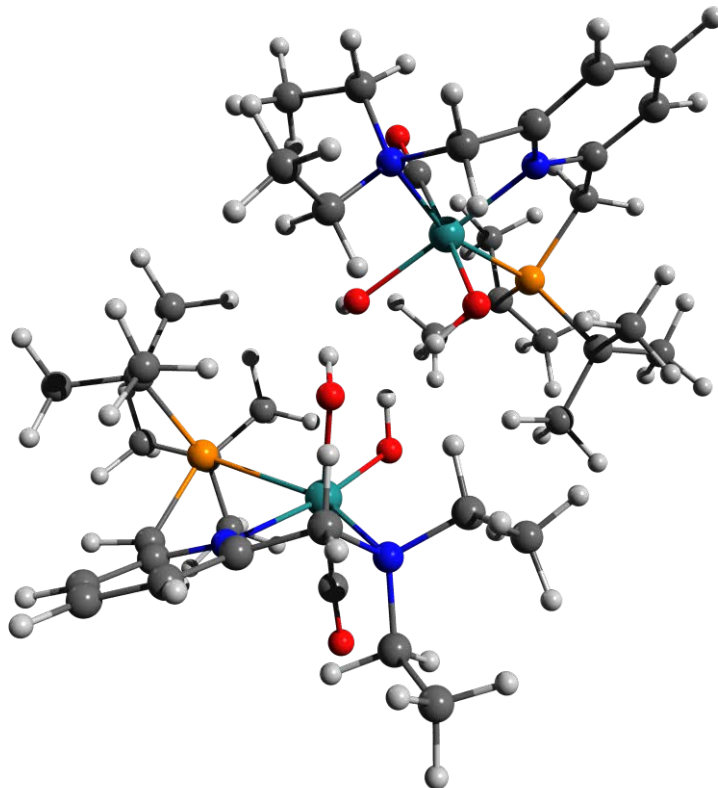


Figure 11.5-6 [A-Mono]S₀ Structure and Coordinates

64
 Energy: -975781.7288466
 N -0.71461 1.41145 -0.05552
 C -1.93725 1.87355 0.26183
 C 0.19459 2.20723 -0.65239
 C -2.28128 3.20265 0.05361
 C -1.33114 4.06030 -0.49717
 C -0.08773 3.55709 -0.86171
 C -2.85043 0.84429 0.85528
 H -3.27959 3.55437 0.31562
 H -1.56883 5.11248 -0.66341
 H 0.66192 4.19707 -1.32817
 C 1.45721 1.55183 -1.11784
 N -2.72411 -0.45534 0.16951
 H -3.89160 1.21043 0.86121
 H -2.55608 0.68653 1.90573
 H 1.24304 1.16737 -2.13027
 P 1.78985 -0.01998 -0.16505
 H 2.29722 2.25937 -1.16090
 Ru -0.39928 -0.61383 0.08172
 C -3.28283 -0.39340 -1.19918
 C 2.97324 -0.99546 -1.29362
 C -3.38475 -1.48595 1.00200
 C 2.72182 0.58988 1.38220
 C 2.11769 -1.74151 -2.32039
 C 3.72410 -2.04167 -0.46792
 C 3.96342 -0.09780 -2.03899
 C 1.86381 1.68472 2.02822
 C 4.09031 1.19356 1.06301
 C 2.89349 -0.54913 2.39174
 C -0.39429 -0.83617 1.89956
 O -0.45848 -1.02652 3.05049
 H -2.68999 0.34812 -1.75005
 C -4.77475 -0.11819 -1.30549
 H -3.03278 -1.34793 -1.67752
 H -2.85003 -1.49718 1.96295
 C -3.35227 -2.86901 0.38750
 H -4.42405 -1.16918 1.22102
 O -0.32453 -2.62404 -0.33069
 H 0.05403 -3.30148 0.30746
 O -0.53805 -0.41410 -1.96323
 H -0.31921 -1.34094 -2.23979
 H -2.32197 -3.10175 0.06512
 H -4.05251 -2.96053 0.47057
 H -3.67404 -3.60285 1.14184
 H -5.05270 -0.10914 -2.37017
 H -5.06413 0.86089 -0.89282
 H -5.38839 -0.88876 -0.81452
 H 2.78956 -2.35108 -2.94866
 H 1.55854 -1.05021 -2.96420
 H 1.38471 -2.39095 -1.81685
 H 4.25560 -2.71733 -1.15807
 H 3.03302 -2.65720 0.12777
 H 4.47476 -1.60264 0.20341
 H 4.59861 -0.73497 -2.67721
 H 4.62793 0.47120 -1.37696
 H 3.44808 0.60833 -2.70613
 H 4.81061 0.44266 0.71220
 H 4.50493 1.63794 1.98338
 H 4.03158 1.99636 0.31245
 H 3.57490 -1.32971 2.03359
 H 1.93780 -1.01914 2.65161
 H 3.32255 -0.13633 3.32020
 H 2.33188 1.98025 2.98143
 H 0.84386 1.34147 2.24529
 H 1.79979 2.58622 1.40116

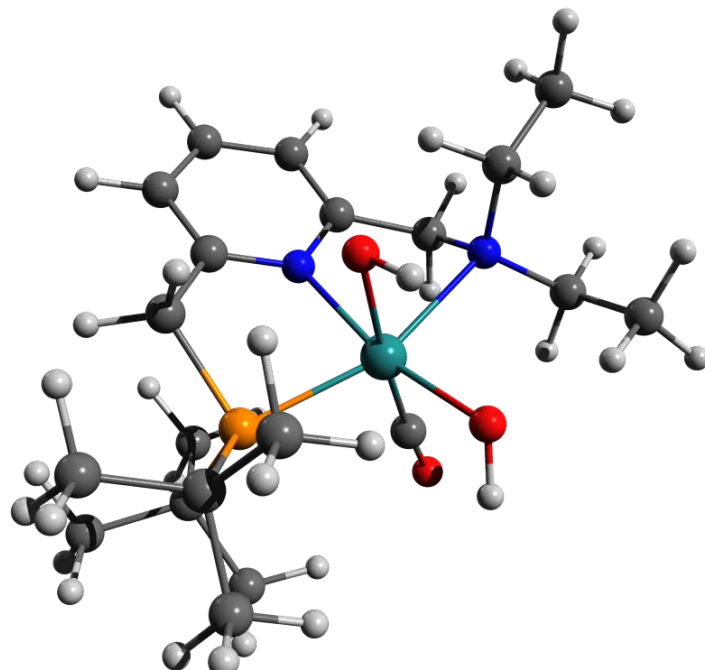


Figure 11.5-7 [B]T₀ Structure and Coordinates

128 Energy: -1951514.6685434

H	0.84052	-2.25311	-2.78417
C	-0.23016	-2.03744	-2.88605
H	-0.57102	-2.40557	-3.86621
H	-0.34157	-0.94451	-2.83707
H	-1.64170	1.80046	2.89472
O	-0.72294	0.62491	-1.06975
H	-1.47959	3.47385	1.34965
O	-1.68143	-1.00834	0.89192
H	-0.59535	0.16002	1.52690
C	-0.95291	-2.67994	-1.72274
H	-2.72120	1.84010	4.31167
H	-0.92044	-3.78459	-1.80117
C	-2.64606	2.08586	3.23880
H	-1.25654	2.94128	-0.32533
H	-2.75935	3.17491	3.15115
H	-0.44556	-2.38791	-0.79259
C	-1.83479	3.61673	0.32271
H	-1.62574	4.65797	0.02470
H	-2.39869	-2.96096	0.34173
Ru	-2.59566	-0.16092	-0.64776
H	-2.65270	-0.58334	2.49333
N	-2.36315	-2.24342	-1.59784
C	-3.03659	-3.03916	-0.55326
C	-3.74898	1.31946	2.50435
H	-3.64812	-0.26873	3.94669
H	-3.94625	4.28929	2.05223
C	-3.60773	-0.16651	2.84936
C	-3.33511	3.34700	0.15613
P	-3.59593	1.52157	0.59701
H	-3.14219	-4.09816	-0.84126
C	-4.18056	4.31654	0.98119
H	-2.63361	-1.64826	-3.57898
H	-2.17894	-4.14639	-3.71682
H	-3.98034	5.34225	0.62908
C	-3.10242	-2.34818	-2.87765
H	-5.10749	1.73192	4.11432
C	-3.10209	0.56386	-2.27223
C	-5.11937	1.16407	3.1304
H	-3.02838	2.96955	-1.97683
O	-3.67618	3.55659	-1.77979
H	-5.36574	2.07755	2.73822
H	-3.37638	4.62220	-1.55798
C	-3.67820	-2.43769	4.21014
N	-4.38113	-1.09200	0.21354
C	-3.17526	-3.73298	-3.50339
H	-4.42527	-0.77276	2.43364
H	-4.11879	-1.96813	-2.69623
H	-5.26952	4.13419	0.85440
H	-3.72043	-4.45666	-2.87920
C	-5.34568	1.09320	0.04616
H	-3.71432	-3.66016	-4.45984
H	-5.93331	1.12663	2.67327
C	-5.49449	-0.39610	0.10003
C	-5.50907	-3.15651	0.12748
H	-4.72847	3.34280	-1.55912
H	-5.48528	-4.24674	0.12427
H	-5.39920	1.41082	-1.00804
H	-6.14654	1.60481	0.59464
C	-6.66267	-1.06745	0.45377
C	-6.66638	-2.45986	0.46973
H	-7.55649	-0.49909	0.71248
H	-7.57298	-3.00206	0.74405
O	-3.40404	0.96102	-3.33181
C	0.89904	-3.73171	2.71449
H	1.01359	1.04158	-2.29506
O	-0.12798	0.98651	1.82267
H	1.24131	3.20125	-0.85621
O	1.51852	-1.13690	-0.49408
H	0.82336	0.81278	1.65421
C	1.17691	-2.34510	2.15621
H	1.49211	1.02732	-4.01085
C	1.75687	1.42185	-3.01446
H	1.76771	3.00575	0.82090
H	1.64899	2.51591	-3.06415
C	1.97639	3.54475	-0.11382
H	1.81802	4.62383	0.05364
H	2.53022	-3.00441	0.15890
Ru	2.76648	-0.04139	0.73767
H	2.67561	-1.03155	-2.07911
N	2.60090	-1.98701	1.95836
C	3.23282	-2.92416	1.00403
C	3.19079	1.00164	-2.68368
H	2.99687	-0.79961	-3.83875
H	2.98925	4.01912	-2.61904
C	3.31565	-0.52190	-2.81920
C	3.41729	3.30850	-0.58173
P	3.54254	1.42138	-0.85356
H	3.38858	-3.91959	1.45565
C	3.70547	4.17978	-1.80325
H	4.35562	-1.54072	2.98214
H	2.38435	-0.23237	4.03344
H	3.62357	5.23765	-1.50059
C	3.37597	-1.98434	3.21683
H	3.94360	1.20083	-4.67999
C	3.49418	0.94625	2.09061
C	4.16731	1.62428	-3.66610
H	4.29331	3.15174	1.43832
C	4.38621	3.74748	0.52040
H	4.08575	2.12427	-3.71794
H	4.16500	4.79133	0.7893
O	4.01613	-2.40174	0.4993
N	4.51001	-1.09843	0.14339
C	2.72102	-1.22694	4.35416
H	4.35911	-0.85558	-2.70433
H	3.56560	3.03025	3.52098
H	4.72349	4.02930	-2.19144
H	1.85839	-1.76843	4.76853
C	5.37414	0.99133	-0.69100
H	3.45166	-1.08927	5.16455
H	5.21502	1.36975	-3.46452
C	5.54851	-0.48094	-0.44195
C	5.65844	-3.17209	0.18390
H	5.43282	3.70979	0.17958
H	5.67600	-4.23157	0.44358
H	5.70147	1.52347	0.21738
H	6.00622	1.33539	-1.52244
C	6.69878	-1.20598	-0.75386
C	6.75075	-2.56054	-0.43242
H	7.54228	-0.71178	-1.23800
H	7.64639	-3.14154	-0.66061
H	0.78527	-0.56025	-0.78993
O	3.92481	1.54918	3.00268
H	-0.18949	-3.84641	2.83096
H	1.35456	-3.90128	3.70334
H	1.23928	-4.53427	2.04175
H	0.71188	-2.20240	1.17126
H	0.74400	-1.57738	2.80962
H	-0.43434	0.98733	-0.21631

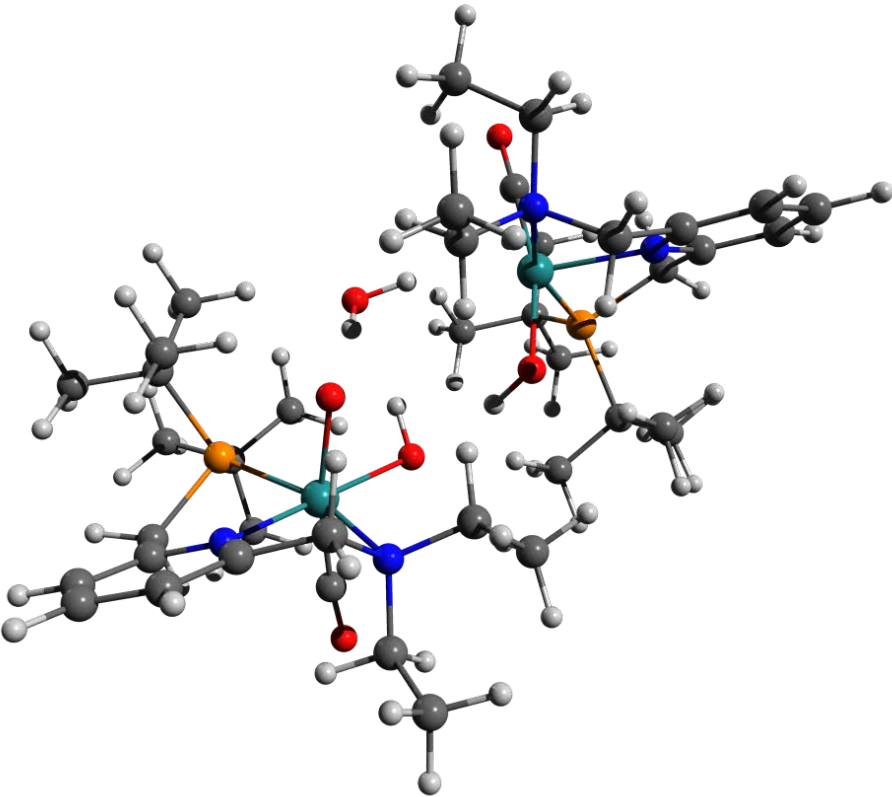


Figure 11.5-8 [B-Mono]D₀ (Me Model) Structure and Coordinates

39 Energy: -778002.1873236

O	-0.55505	-2.76423	-0.44723
O	0.12508	-0.53954	-0.02669
C	2.33494	-2.33026	-0.93340
H	2.32532	0.00079	-1.74955
N	2.03471	-1.17743	-0.07897
C	2.56292	0.06059	-0.67376
C	-2.66050	0.70913	-1.96705
C	-3.66291	-0.22283	0.57254
P	-2.13697	0.26299	-0.27867
H	3.65817	0.13929	-0.54726
C	2.57390	-1.37539	1.26528
C	-0.47743	-1.05726	1.74030
C	1.86506	1.29245	-0.16828
N	0.54935	1.13551	0.08192
C	-1.69729	1.88636	0.55815
C	-0.24327	2.19517	0.34859
C	2.46033	2.54481	-0.08112
H	3.52962	2.65191	-0.26713
H	-1.87475	1.70669	1.63369
H	-2.33600	2.73055	0.25599
C	0.29836	3.47682	0.41385
C	1.66531	3.64977	0.21585
H	-0.35016	4.32785	0.62448
H	2.10798	4.64516	0.28014
O	-0.72992	-1.22961	2.86076
H	-3.43464	1.49046	-1.96458
H	-3.04101	-0.20175	-2.45134
H	-1.76103	1.01476	-2.51817
H	-3.45978	-0.44094	1.62671
H	-4.05811	-1.14273	0.10074
H	-4.45366	0.55989	0.50619
H	1.84660	-3.21136	-0.49936
H	3.42719	-2.48162	-1.02251
H	1.87627	-2.14584	-1.91327
H	2.34751	-0.50001	1.89028
H	3.67065	-1.52383	1.23530
H	2.10148	-2.25869	1.71336
Ru	-0.17204	-0.78748	-0.06391
H	-1.30296	-3.07172	0.07743

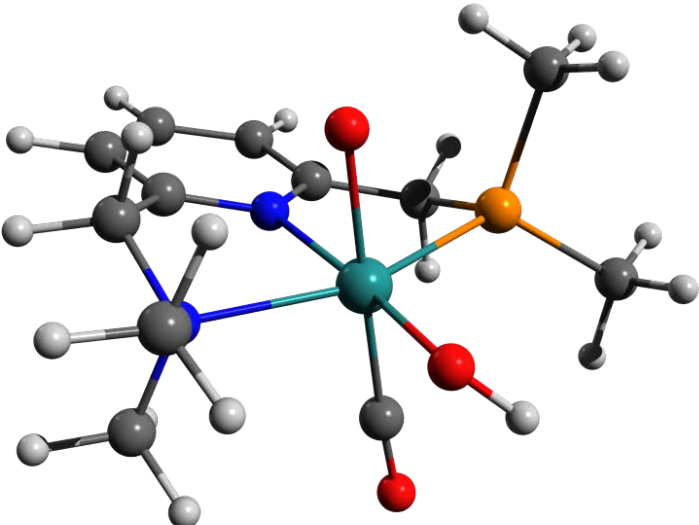


Figure 11.5-9 [B-Mono]D₀ Structure and Coordinates

63

	Energy: -975165.8829902		
H	-3.59713	-3.37011	1.85732
C	-3.30686	-2.75815	0.99015
H	-4.05420	-2.93520	0.20058
H	-2.30651	-3.08263	0.65924
H	1.49110	-0.73473	2.72708
O	-0.25026	-2.58975	0.68320
H	4.33842	-1.68068	0.66041
O	-0.48413	-0.19782	2.04727
C	-3.23487	-1.31048	1.42488
H	2.87147	0.05398	3.54960
H	-4.22373	-0.93932	1.76129
C	2.52841	-0.39289	2.60092
H	2.86422	-2.66213	0.46270
H	3.17429	-1.25419	2.38812
H	-2.52682	-1.20764	2.26099
C	3.65433	-2.11887	-0.07818
H	4.22969	-2.85168	-0.66789
H	-2.32081	0.92236	1.90782
Ru	-0.39555	-0.61368	0.13394
H	0.70178	1.55765	2.11987
N	-2.70573	-0.40463	0.37971
C	-2.75145	0.97496	0.89198
C	2.59529	0.67938	1.50764
H	2.14556	2.24447	2.90814
H	4.76596	0.33218	-0.95365
C	1.74084	1.87352	1.95171
C	3.06317	-1.07233	-1.02616
P	1.79654	-0.02448	-0.06751
H	-3.78161	1.36308	0.96435
C	4.17182	-0.23927	-1.67502
H	-3.20025	-1.51011	-1.31426
H	-5.43814	-1.02666	-0.23633
H	4.85933	-0.91938	-2.20537
C	-3.41984	-0.51442	-0.90804
H	4.35612	1.64830	2.25763
C	-0.57405	-1.06302	-1.67230
C	4.03188	1.16178	1.10044
H	1.56834	-2.50274	-1.74182
C	2.32624	-2.50274	-2.14048
H	4.03188	0.71495	1.11946
H	3.06007	-2.41065	-2.70890
C	-1.88057	1.90873	0.10674
N	-0.69360	1.38892	0.25425
C	-4.92463	-0.29089	-0.87206
H	1.77858	2.70973	1.23656
H	-2.95208	0.20869	-1.59418
H	3.77213	0.46010	-2.42482
H	-5.19915	0.71495	-0.51997
C	1.54856	1.47139	-1.17724
H	-5.32498	-0.39766	-1.89143
H	4.12562	1.91569	0.52060
C	0.25002	2.15170	-0.85440
C	-2.18830	3.23851	-0.15518
H	1.83157	-1.13894	-2.85135
H	-3.15904	3.63838	0.13975
H	1.48976	1.05781	-2.19907
H	2.38389	2.18731	-1.16170
C	-0.00188	3.49525	-1.12311
C	-1.23569	4.04003	-0.77988
H	0.76850	4.10418	-1.59729
H	-1.45156	5.08839	-0.99284
O	-0.79262	-1.32801	-2.78212
H	0.34645	-3.05966	0.08963

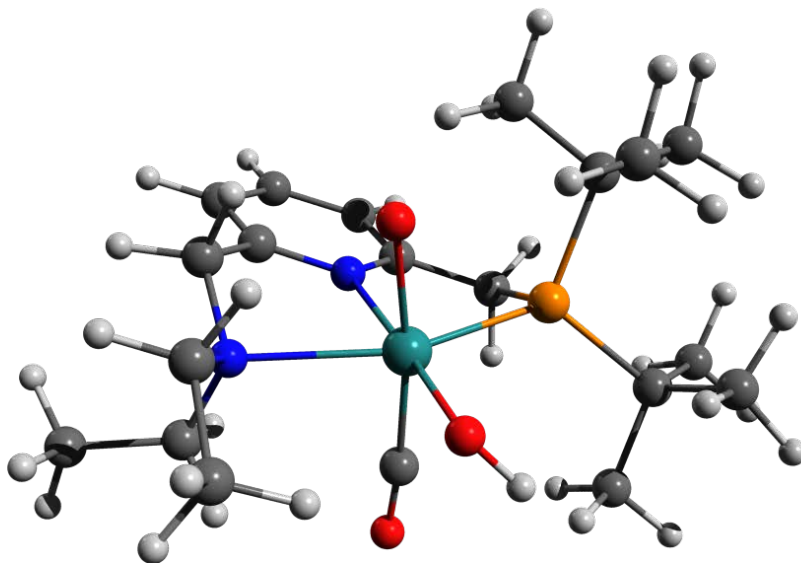


Figure 11.5-10 [B-Mono-Up]D₀ Structure and Coordinates

63

```

Energy: -975164.6396053
N   -0.74074   1.42138  -0.09733
C   -1.96289   1.88374   0.22032
C    0.17622   2.21737  -0.68254
C   -2.30204   3.21558   0.02029
C   -1.34598   4.07348  -0.52001
C   -0.10169   3.56952  -0.88257
C   -2.88430   0.85097   0.80217
H   -3.30015   3.56986   0.28000
H   -1.57919   5.12778  -0.67888
H    0.65212   4.21228  -1.33854
C    1.44448   1.56307  -1.13985
N   -2.70439  -0.46230   0.15473
H   -3.93071   1.19911   0.74917
H   -2.63964   0.72630   1.86984
H    1.25253   1.19198  -2.16066
P    1.78133  -0.01008  -0.18518
H   2.28303   2.27367  -1.16965
Ru  -0.39601  -0.59869   0.12102
C   -3.20909  -0.43591  -1.23905
C    2.85648  -1.04703  -1.35491
C   -3.36843  -1.49999   0.97491
C    2.78394   0.59230   1.31399
C    1.90070  -1.73018  -2.33764
C    3.55725  -2.14341  -0.55043
C    3.87599  -0.21711  -2.13684
C    1.99413   1.73965   1.95477
C    4.16940   1.11761   0.93685
C    2.92947  -0.53336   2.34160
C   -0.40004  -0.68686   1.97617
O   -0.47562  -0.77910   3.13527
H   -2.68179   0.38306  -1.74960
C   -4.71270  -0.28445  -1.40559
H   -2.83982  -1.34707  -1.72405
H   -2.87188  -1.48262   1.95655
C   -3.26382  -2.88646   0.77377
C   -4.42473  -1.21021   1.47300
O   -0.18170  -2.04943  -0.04358
H    0.14649  -3.01157   0.76766
O   -0.54564  -0.56134  -1.85533
H    2.1126  -3.09138  -0.16760
H   -3.89543  -3.00367  -0.51592
H   -3.60245  -3.62393  -1.11892
H   -4.94265  -0.24441  -2.48080
H    5.10743   0.64145  -0.95834
H   -5.27286  -1.13184  -0.98342
H    2.49969  -2.36903  -3.00935
H    1.34662  -1.00652  -2.95296
H    1.16093  -2.34476  -1.80028
H    4.02159  -2.85217  -1.25567
H    2.83394  -2.70824  -0.05660
H    4.35550  -1.75779   0.09962
H    4.42435  -0.89100  -2.81628
H    4.61745   0.28340  -1.50127
H    3.38880   0.54168  -2.76701
H    4.83845   0.31922   0.58911
H    4.63419   1.56882   1.82951
H    4.12758   1.89776   0.16160
H    3.52590  -1.37251   1.96409
H    1.95694  -0.92246   2.66522
H    3.44126  -0.13502  -3.23371
H    2.49440   2.03236   2.89242
H    0.96381   1.44847   2.19949
H    1.95863   2.63050   1.31020

```

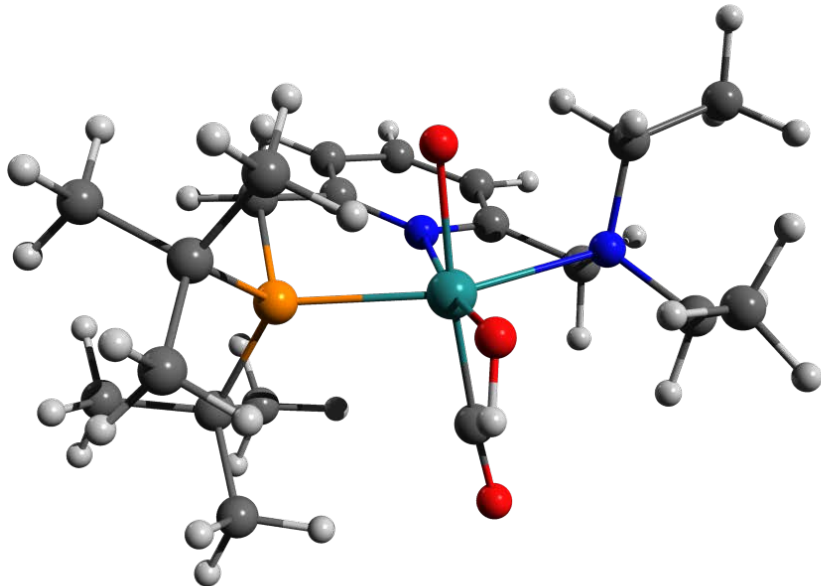


Figure 11.5-11 [B-Trans]T₀ Structure and Coordinates

128 Energy: -1951524.2043341

H	-0.03271	1.60418	4.13717
C	0.93903	1.19234	3.83039
H	1.55757	1.10677	4.17375
H	1.40931	1.90677	3.14666
H	1.16667	1.59848	2.33818
O	1.86714	2.11966	1.09547
H	3.26370	3.58976	-1.40532
O	1.13720	-0.21512	-0.12088
H	0.67013	2.31303	-0.01713
C	0.70514	-0.13262	3.14136
H	1.65072	1.13562	-4.04736
H	0.23184	-0.85739	3.83074
C	2.20339	1.42983	-3.13929
H	3.78233	3.29263	0.25363
H	2.69252	2.39138	-3.35541
H	0.01209	-0.01986	2.29622
C	4.15143	3.47733	-0.76538
H	4.70769	4.42922	-0.78539
H	0.74442	-1.81454	1.29101
Ru	2.84345	0.41858	0.84464
H	1.84130	-0.99793	-1.75221
N	1.94541	-0.73808	2.59715
C	1.60894	-2.01774	1.94199
C	3.21917	0.33453	-2.80832
H	1.88886	-1.17928	-3.54147
H	4.74593	2.90047	-3.37196
C	2.49751	-1.00907	-2.63714
C	5.06992	2.35683	-1.26636
P	4.03937	0.75614	-1.14019
H	1.31415	-2.78482	2.67687
C	5.56579	2.70422	-2.66978
H	3.29420	0.02463	4.00180
H	1.72024	-1.32990	5.41648
H	6.15948	3.63055	-2.59746
C	2.96490	-0.96123	3.65394
H	3.65865	-0.29099	-4.80620
C	4.23993	0.99765	1.88691
C	4.20926	0.16512	-3.96646
H	6.07936	1.98017	0.66517
C	6.30687	2.25095	-0.37099
H	4.63229	1.10637	-4.32961
H	6.79448	3.23921	-0.34468
C	2.74500	-2.50792	1.09336
N	3.49427	-1.54532	0.52592
C	2.53635	-1.79930	4.84880
H	3.21037	-1.84541	-2.56623
H	3.83516	-1.42327	3.16440
H	6.22003	1.92761	-3.09094
H	2.22104	-2.81646	4.57277
C	5.23604	-0.66838	-0.89074
H	3.39534	-1.89987	5.52898
H	5.03647	-0.52011	-3.72437
C	4.50474	-1.84421	-0.31228
C	3.00870	-3.85068	0.84361
H	7.04318	1.53799	-0.77358
H	2.39588	-4.62062	1.31359
H	5.96418	-0.30988	-0.14538
H	5.79248	-0.94732	-1.79631
C	4.80936	-3.17184	-0.60228
C	4.05194	-4.18314	-0.1677
H	5.62666	-3.40435	-1.28555
H	4.24449	-5.23441	-0.60002
O	5.05375	1.38425	2.62202
C	-0.17524	-3.30764	-1.34667
H	-1.24587	1.94143	3.62104
O	0.05950	2.34163	-0.80701
H	-2.09722	3.65271	-0.87619
O	-1.42466	-0.63826	0.77242
H	-0.74161	1.85095	-0.54158
C	-0.72051	-2.49274	1.60285
H	-1.71046	2.83297	3.09142
C	-2.00864	2.60120	2.05539
H	-2.73850	2.72199	-2.23269
H	-2.00637	3.54772	1.49496
C	-2.98459	3.51026	-1.50902
H	-3.16278	4.44821	-2.06195
H	-1.89005	-2.72701	0.59986
Ru	-2.72275	-0.16773	-0.79566
H	-2.56150	-0.09991	2.23946
N	-2.17984	-2.34650	-1.40602
C	-2.59716	-3.05718	-0.18043
C	-3.37671	1.92043	2.06136
H	-2.87080	0.75163	3.79098
H	-3.78661	4.67535	0.82229
C	-3.25875	0.56585	2.77370
C	-4.24013	3.16238	-0.70340
P	-3.83908	1.54269	0.24875
H	-2.55567	-4.15280	-0.31104
C	-4.61001	4.36190	0.16717
H	-4.00259	-2.53275	-2.38774
H	-2.33659	-1.32998	-3.95335
H	-4.83577	5.21175	-0.49896
C	-2.96552	-2.86448	-2.54726
H	-4.14001	2.67516	3.91761
C	-3.52292	0.24424	-2.37986
C	-4.38657	2.76361	2.84614
H	-5.27115	2.04492	-2.30541
C	-5.40753	2.92610	-1.66678
H	-4.35929	3.82863	2.59535
H	-5.48364	3.80019	-2.33498
C	-3.96012	-2.64603	0.30186
N	-4.22295	-1.33845	0.18289
C	-2.48161	-2.41610	-3.91157
H	-4.24057	0.07946	2.89004
H	-2.97449	-3.97228	-2.50949
H	-5.50385	4.17952	0.78007
H	-1.54098	-2.90786	-4.19977
C	-5.50898	0.68212	0.44494
H	-3.23887	-2.67937	-4.66455
H	-5.42152	2.40630	2.72913
C	-5.34408	-0.79136	0.67597
C	-4.86654	-3.49958	0.92281
H	-6.36742	2.84197	-1.13418
H	-4.65076	-4.56583	1.00540
H	-6.00520	0.80826	-0.53016
H	-6.16164	1.13571	1.20551
C	-6.28211	-1.59085	1.33036
C	-6.03973	-2.95704	1.44578
H	-7.19058	-1.14560	1.73742
H	-6.76658	-3.60086	1.94491
H	-0.51848	-0.41630	0.7013
O	-3.9873	0.84862	-3.49393
H	0.11129	-3.83345	-1.90240
H	-0.61189	-4.45486	-2.57866
H	-0.32861	-4.49142	-0.82007
H	-0.24340	-1.96131	0.76500
H	-0.46742	-1.89627	2.49584
H	0.80147	0.56698	-0.59067

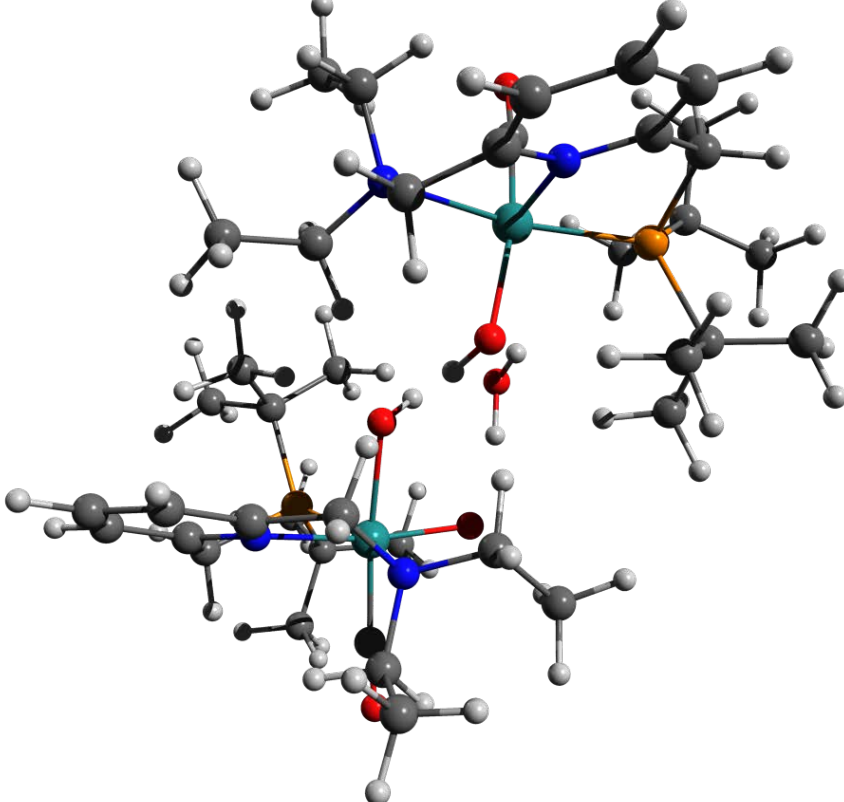


Figure 11.5-12 [B-Mono-Trans]D₀ Structure and Coordinates

63
 Energy: -975172.0784791
 H -3.52147 -3.33180 1.91476
 C -3.21273 -2.73924 1.04103
 H -3.90599 -2.97992 0.22015
 H -2.19116 -3.04629 0.76397
 H 1.93926 -0.66358 2.66178
 O -0.16459 -2.37754 0.90223
 H 2.96531 -2.60730 0.75502
 O -0.51143 -0.09534 2.16923
 C -3.22818 -1.27357 1.41611
 H 3.26996 -0.29760 3.34665
 H -4.25213 -0.93762 1.66951
 C 2.88237 -0.19169 2.43768
 H 1.61419 -2.86521 -0.35016
 H 3.61834 -0.94831 2.12774
 H -2.58714 -1.09775 2.29149
 C 2.68130 -2.59912 -0.30746
 H 3.27598 -3.37303 -0.82088
 H -2.30473 0.98017 1.86228
 Ru -0.40986 -0.62255 0.17304
 H 0.70035 1.43941 2.15670
 N -2.67307 -0.38667 0.36774
 C -2.74464 1.00794 0.85003
 C 2.64564 0.86733 1.36016
 H 2.10188 2.34881 2.81099
 H 4.81260 -0.98398 0.21233
 C 1.66058 1.91369 1.89823
 C 2.97237 -1.24134 -0.95698
 P 1.80265 0.00325 -0.10829
 H -3.78248 1.37546 0.90262
 C 4.46192 -0.92727 -0.82616
 H -3.12810 -1.53856 -1.31205
 H -5.39232 -1.04930 -0.30824
 H 5.02152 -1.68584 -1.39840
 C -3.35946 -0.53418 -0.93590
 H 4.21857 2.22703 1.87501
 C -0.54036 -1.26267 -1.54368
 C 3.94788 1.59477 1.01331
 H 1.59523 -1.50593 -2.66402
 C 2.65159 -1.30784 -2.45228
 H 4.79263 0.92558 0.82327
 H 3.22919 -2.13934 -2.88826
 C -1.88127 1.92541 0.03882
 N -0.70686 1.38778 -0.33782
 C -4.86498 -0.31800 -0.93794
 H 1.51175 2.74169 1.18775
 H -2.87726 0.17266 -1.62817
 H 4.72653 0.05722 -1.23858
 H -5.15359 0.69064 -0.60641
 C 1.50175 1.40498 -1.31722
 H -5.23715 -0.44030 -1.96609
 H 3.83783 2.26939 0.14977
 C 0.23022 2.12364 -0.96564
 C -2.18126 3.25278 -0.24505
 H 2.95743 -0.39133 -2.98035
 H -3.14183 3.67075 0.05806
 H 1.36662 0.92202 -2.29851
 H 2.34420 2.10582 -1.40654
 C -0.00850 3.46423 -1.25873
 C -1.22962 4.03010 -0.90145
 H 0.75780 4.05357 -1.76333
 H -1.4305 5.07689 -1.13027
 O -0.71029 -1.72257 -2.59914
 H -0.30740 -0.97807 2.52158

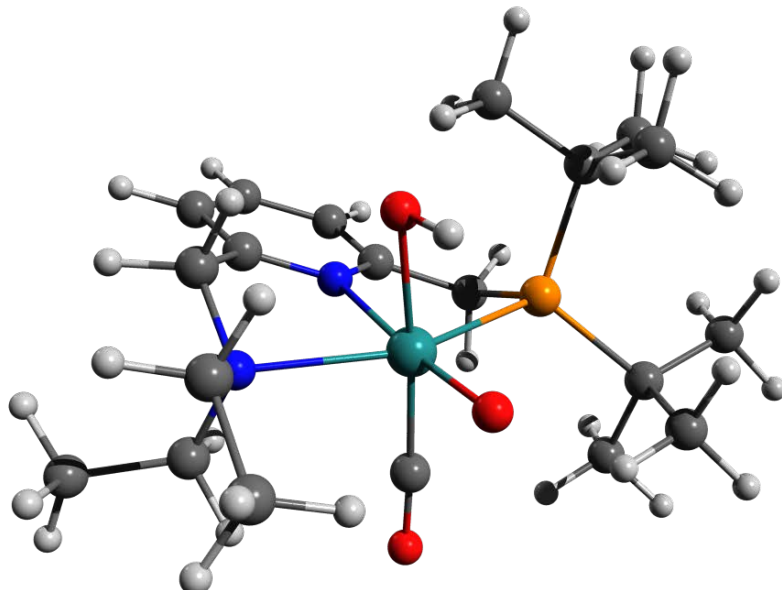


Figure 11.5-13 [B-Mono-Trans-Up]D₀ Structure and Coordinates

```

63          Energy: -975173.7263503
N   -0.73550  1.42125  -0.02208
C   -1.96750  1.86456  0.28053
O   0.17340  2.23170  -0.59528
O   -2.32652  3.19045  0.08017
C   -1.37399  4.06578  0.44217
C   -0.11894  3.59115  -0.79053
C   -2.86501  0.81117  0.85662
C   -3.33302  3.52853  0.32880
H   -1.62190  5.11719  -0.59060
H   0.63046  4.23614  -1.23640
C   1.44263  1.58998  -1.06790
N   -2.69846  -0.48240  0.16027
H   -3.91549  1.14707  0.85267
H   -2.57625  0.65027  1.90818
H   1.23589  1.24028  -2.09463
P   1.78869  -0.00874  -0.17117
H   2.28334  2.29787  -1.08076
Ru  -0.41448  -0.64096  0.07272
C   -3.25948  -0.42483  -1.21093
C   2.95262  -0.96472  -1.33095
C   -3.33235  -1.54129  0.98082
C   2.72034  0.54474  1.39552
C   2.10182  -1.66971  -2.38906
C   3.68224  -2.04466  -0.52984
C   3.95300  -0.04857  -2.03970
C   1.85805  1.61627  2.07491
C   4.08721  1.16238  1.09591
C   2.89745  -0.62801  2.36501
C   -0.39102  -0.90857  1.88917
O   -0.43996  -1.10599  3.03685
H   -2.69139  0.34337  -1.75061
C   -4.75996  -0.20438  -1.31443
H   -2.97355  -1.36336  -1.70059
H   -2.84433  -1.50672  1.96523
C   -3.19827  -2.93071  0.39736
H   -4.39647  -1.28329  1.14499
O   -0.22382  -2.50500  -0.32104
O   -0.53886  -0.35007  -1.97302
H   -2.14096  -3.15136  0.17157
H   -3.79382  -3.05995  -0.51852
H   -3.56282  -3.66199  1.13397
H   -5.03187  -0.17514  -2.38023
H   -5.08940  0.75050  -0.87617
H   -5.34650  -1.01228  -0.85134
H   2.78023  -2.24866  -3.03846
H   1.53741  -0.95722  -3.00423
H   1.37671  -2.35037  -1.91752
H   4.20178  -2.71174  -1.23693
H   2.97485  -2.65965  0.04710
H   4.44129  -1.63469  0.15033
H   4.59219  -0.66907  -2.68980
H   4.61277  0.49757  -1.35440
H   3.44634  0.67926  -2.69033
H   4.80829  0.42454  0.71985
H   4.50075  1.57465  2.03148
H   4.02741  1.99115  0.37408
H   3.61500  -1.37036  1.99704
H   1.95320  -1.14306  2.57572
H   3.28477  -0.23823  3.32116
H   2.32646  1.88437  3.03586
H   0.83963  1.26333  2.28304
H   1.76947  2.53610  1.47544
H   -0.52085  -1.27160  -2.26913

```

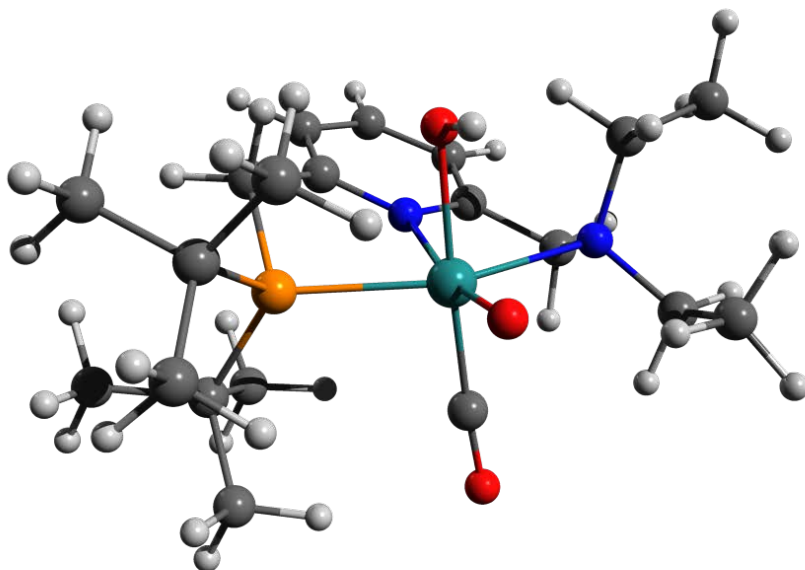


Figure 11.5-14 [B-Alt]T₀ Structure and Coordinates

62

```

Energy: -974727.8788646
H   -3.37170   -3.45409   1.93521
C   -3.14617   -2.83166   1.05673
H   -3.89627   -3.09852   0.28600
H   -2.14678   -3.11364   0.69908
H   1.43203   -0.73895   2.74140
O    0.00504   -2.50545   0.26301
H   4.24011   -1.78082   0.62515
O   -0.44643   -0.21944   1.93866
C   -3.15723   -1.37684   1.47382
C   2.86230   -0.05299   3.56056
H   -4.15576   -1.07734   1.84882
C   2.49277   -0.45756   2.60301
H   2.72915   -2.70038   0.34332
H   3.09225   -1.34501   2.36268
H   -2.41870   -1.21361   2.27597
C   3.55747   -2.16404   -0.14512
H   4.11907   -2.88988   -0.75579
H   -2.27115   0.85962   1.90665
Ru  -0.35462   -0.69712   0.13791
H   0.71569   1.51588   2.12337
N   -2.72905   -0.45400   0.40380
C   -2.76769   0.92147   0.91974
C   2.60744   0.64126   1.54098
H   2.14954   2.16794   2.97809
H   4.79589   0.24930   -0.92510
C   1.76287   1.83665   1.99980
C   3.02434   -1.06043   -1.06208
P   1.82004   0.00258   -0.05920
H   -3.79654   1.30265   1.03468
C   4.16657   -0.24589   -1.67315
H   -3.23597   -1.56796   -1.28232
H   -5.44523   -1.22885   -0.10792
H   4.81250   -0.92768   -2.25088
C   -3.48927   -0.59015   -0.84988
H   4.38508   1.54946   2.32069
C   -0.62707   -0.88215   -1.76209
C   4.05739   1.09118   1.37284
H   1.45359   -2.38214   -1.79420
C   2.24643   -1.73425   -2.19388
H   4.74174   0.25774   1.16261
H   2.95067   -2.35439   -2.77279
C   -1.92243   1.87476   0.12878
N   -0.71947   1.39723   -0.22866
C   -5.00080   -0.44809   -0.74224
H   1.83617   2.69550   1.31409
H   -3.09450   0.16548   -1.54675
H   3.79683   0.51719   -2.37522
H   -5.30680   0.53018   -0.34161
C   1.53853   1.52825   -1.10810
H   -5.44435   -0.54324   -1.74477
H   4.17855   1.85301   0.58630
C   0.21961   2.17956   -0.78374
C   -2.25559   3.20258   -0.12104
H   1.80126   -1.01000   -2.89205
H   -3.23994   3.57988   0.15842
H   1.51330   1.16638   -2.15038
H   2.36129   2.25550   -1.03714
C   -0.04789   3.52524   -1.03064
C   -1.30354   4.03277   -0.70786
H   0.01958   4.41773   -1.47237
H   -1.53725   5.00826   -0.90722
O   -0.86592   -0.86035   -2.90796

```

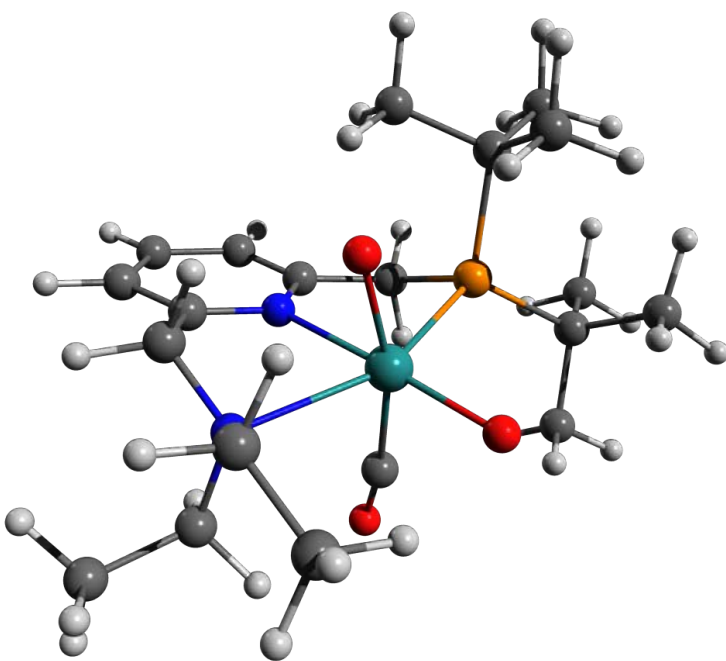


Figure 11.5-15 [BC] D₁/D₀ MECI Structure and Coordinates

```

39
-5668.6564319599938
O -0.34914799 -2.36258133 -2.38144151
O 0.11685657 -0.82199044 -2.03587137
C 2.45972115 -2.48770283 -0.59692125
H 2.47961778 -0.22805005 -1.63105341
N 2.16379531 -1.25231934 0.14256847
C 0.62880006 -0.09033524 -0.57055869
C -2.95592546 0.75130328 1.79018937
C -3.85195267 -0.02730160 0.89974336
P -2.30795928 0.27308186 -0.10621931
H 3.69309868 0.06167002 -0.37783977
C 2.62840602 -1.30970376 1.52619968
C -0.41490170 -1.04519197 2.19364736
C 1.88732904 1.20543682 -0.20269598
N 0.57933910 1.07344928 0.06366621
C -1.66417890 1.89964300 0.62849087
C -0.20953457 2.14595474 0.30032474
C 2.47868580 2.46568668 -0.22235894
H 3.52977925 2.55859074 -0.42706967
H -1.75784807 1.78995768 1.70762753
H -2.26840551 2.74654963 0.32032961
C 0.34078846 3.42118238 0.26751214
C 1.70205995 3.57535527 0.01007743
H -0.28345471 4.27631644 0.45043994
H 2.13906704 4.55889235 -0.00585560
O -0.73061464 -1.74610669 3.13055667
H -3.67933575 1.55973355 -1.72787910
H -3.42495100 -0.11461877 -2.24627638
H -2.12184913 1.04499984 -2.41770806
H -3.57230091 -0.26896885 1.91967123
H -4.38840515 -0.87507903 0.48484844
H -4.50670963 0.83997556 0.89817174
H 2.07210958 -3.34198547 -0.05431959
H 3.54399273 -2.58737731 -0.68353774
H 2.00477094 -2.45857026 -1.57612531
H 2.34624449 -0.41525499 2.06620993
H 3.71628435 -1.40166085 1.51688219
H 2.20065294 -2.16034732 2.03867858
Ru -0.11705731 -0.88144683 0.05896810
H -0.69487285 -2.18311611 -3.27277416

```

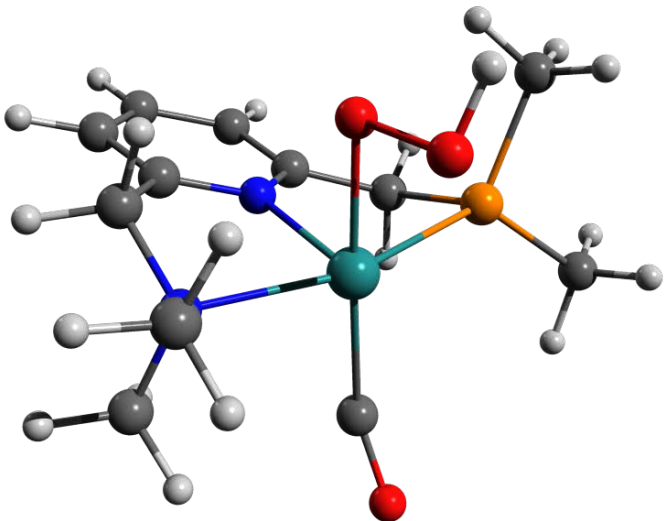


Figure 11.5-16 [BC] D₂/D₁ MECI Structure and Coordinates

```

39
-5668.6347902092621
O -0.49728033 -2.88986680 -1.22059513
O 0.01072006 -1.15926324 -2.16057615
C 2.54759921 -2.43747772 -0.70319219
H 2.44612775 -0.14246022 -1.70346216
N 2.12497170 -1.23114239 0.04303850
C 0.69047055 -0.00886238 -0.64091499
C -2.87559717 0.87962919 1.85659339
C -3.87797477 -0.02746943 0.75622607
P -2.29420613 0.29809104 -0.17808649
H 3.68994019 0.11231407 -0.47556600
C 2.63446526 -1.29572540 1.43245850
C -0.42517600 -1.11796295 2.03526966
C 1.88531427 1.24155372 -0.20809201
N 0.57880933 1.09855615 0.05344743
C -1.66441087 1.88021247 0.65687480
C -0.21056753 2.15434403 0.34797870
C 2.47760799 2.50106027 -0.16125789
H 3.52818477 2.60713109 -0.36260372
H -1.76355295 1.70866859 1.72754258
H -2.27528270 2.73776658 0.39383644
C 0.33884029 3.42996022 0.38761050
C 1.70049336 3.59590110 0.13645007
H -0.28294042 4.27462591 0.62127536
H 2.13843195 4.57847672 0.17568621
O -0.76941542 -1.65784233 3.06345115
H -3.61280414 1.67336524 -1.72222999
H -3.30868937 0.04220119 -2.39389968
H -2.02276168 1.22893868 -2.42838256
H -3.63710698 -0.33324758 1.76890258
H -4.41890407 -0.83703111 0.27598941
H -4.51302617 0.85388025 0.78345248
H 2.17775313 -3.31465047 -0.19503086
H 3.63727585 -2.48753836 -0.76820659
H 2.11698942 -2.41043829 -1.69912923
H 2.31779191 -0.42179048 1.98604882
H 3.72491453 -1.35349895 1.43491293
H 2.22794279 -2.16974797 1.92250448
Ru -0.11712086 -0.90963409 -0.04038537
H -1.23425376 -2.88666281 -1.78515039

```

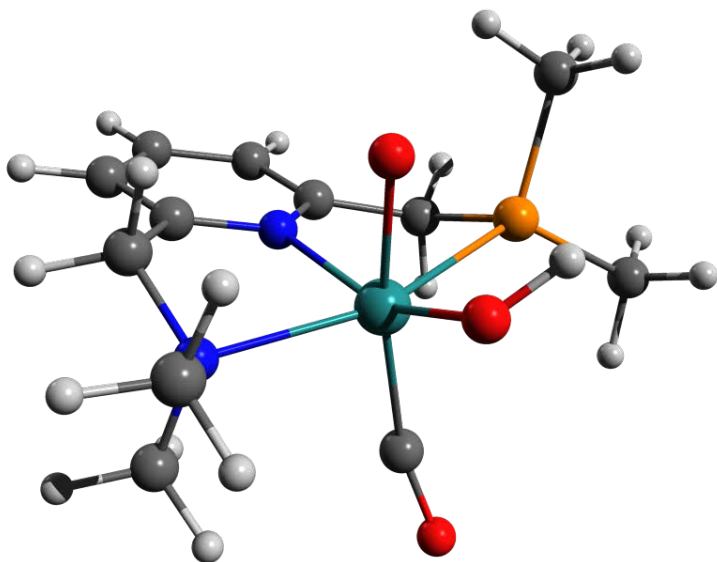


Figure 11.5-17 [C]T₀ Structure and Coordinates

128 Energy: -1951476.7711256

H	-0.89663	2.64286	3.71461
C	-1.82051	2.11644	3.43322
H	-2.52055	2.20160	4.27654
H	-1.56185	1.05758	3.90041
H	-0.94588	1.17047	1.92357
O	-1.54793	1.14940	0.35805
H	-0.46505	-3.21252	0.62748
O	-0.38495	1.09269	0.48860
H	-1.30571	-1.13414	2.37114
C	-2.35690	2.72304	2.15547
H	-0.42762	-1.22931	-3.69580
H	-2.65393	3.77688	2.32440
C	-0.84201	-1.63173	-2.75572
H	-1.18192	-2.88659	0.96029
H	-0.63509	-2.71240	-2.75244
H	-1.57419	2.71034	1.38621
C	-1.23079	-3.54977	0.08471
H	-0.97429	-4.57457	0.40376
H	-3.02154	2.81200	-0.24934
Ru	-2.93506	-0.05255	0.62261
H	-2.02696	0.77702	-2.20712
N	-3.49882	1.98143	1.57545
C	-3.93458	2.70522	0.36143
C	-2.34021	-1.32858	-2.71150
H	-2.10229	0.40060	-3.95847
H	-1.91428	-4.32214	-2.46486
C	-2.53641	0.17115	-2.96995
C	-2.63204	-3.54713	-0.53522
P	-3.01159	-1.72473	-0.96046
H	-4.32824	3.70825	0.59832
C	-2.68172	-4.52591	-1.70733
H	-4.26739	1.16253	3.33244
H	-4.46718	3.66488	3.69854
H	-2.49882	-5.54360	-1.32226
C	-4.62093	1.81899	2.52745
H	-2.60217	-1.77874	-4.79210
C	-3.82632	-1.03527	1.88254
C	-3.06671	-2.07353	-3.83578
H	-3.68005	-3.38462	1.39545
C	-3.62992	-4.03671	0.51621
H	-3.00493	-3.16488	-3.76707
H	-3.30884	-5.03384	0.86118
C	-4.92528	1.91027	-0.43937
N	-4.60825	0.61301	-0.54372
C	-5.20538	3.09470	3.11539
H	-3.60002	0.44820	-3.01407
H	-5.40405	1.25428	2.00043
H	-3.66651	-4.53633	-2.19830
H	-5.62643	3.76339	2.34944
C	-4.87492	-1.67125	-1.24538
H	-6.02607	2.82598	3.79731
H	-4.12726	-1.78721	-3.89992
C	-5.34574	-0.24586	-1.26668
C	-6.04579	2.42206	-1.08448
H	-4.64439	-4.15039	0.10438
H	-6.29998	3.47895	-0.99280
H	-5.30252	-2.14906	-0.34836
H	-5.22703	-2.22986	-2.12386
C	-6.47205	0.21034	-1.95158
C	-6.82062	1.55588	-1.89563
H	-7.06783	-0.48277	-2.54710
H	-7.06785	1.14093	-2.70145
O	-4.36895	-1.59430	2.76199
C	-2.25169	-4.23309	2.27755
H	0.39593	1.33942	-1.78486
O	-0.36653	-0.90501	2.48840
H	0.73781	3.27401	-0.09012
O	1.22609	-0.75221	-0.35429
H	-0.31008	-0.13011	1.88696
C	2.07281	-2.87484	1.76462
H	0.50681	1.61081	-3.53587
C	0.94319	1.88673	-2.56096
H	1.64615	2.93677	1.37694
H	0.75294	2.95909	-2.41240
C	1.58882	3.61533	0.51389
H	1.38245	4.63756	0.87464
H	3.15971	-2.92964	-0.49344
Ru	2.95689	0.02827	0.59441
H	2.12087	-0.58001	-2.18738
N	3.30918	-2.12648	1.41908
C	3.95399	-2.77327	0.25460
C	2.43551	1.55263	-2.57945
H	2.13359	-0.10388	-3.91191
H	2.01166	4.50714	-2.06629
C	2.60575	0.06800	-2.92953
C	2.90834	3.61726	-0.26354
P	3.17228	1.81398	-0.83471
H	4.37478	-3.75778	0.52349
C	2.85567	4.65771	-1.38144
H	5.09599	-1.45939	2.25320
H	3.06137	-0.67203	3.66314
H	2.72919	5.65276	-0.92212
C	4.25634	-2.10181	2.55628
H	2.66689	2.10298	-4.63927
C	3.93524	0.88083	1.86610
C	3.13950	2.35789	-3.67561
H	4.19371	3.31588	1.50469
C	4.03763	4.02757	0.68557
H	3.05890	3.44287	-3.55122
H	3.76725	4.99536	1.13992
C	5.01008	-1.92268	-0.38787
N	4.65226	-0.63829	-0.54253
C	3.63809	-1.59024	3.84198
H	3.66631	-0.21033	-3.02644
H	4.66912	-3.11774	2.71260
H	3.78625	4.68663	-1.96801
H	2.96626	-2.32853	4.30224
C	5.01901	1.67387	-1.14702
H	4.43318	-1.35802	4.56463
H	4.20379	2.09398	-3.76710
C	5.47119	0.24205	-1.14904
C	6.23062	-2.39505	-0.85291
H	4.99148	4.17700	0.15630
H	6.50582	-3.44076	-0.70779
H	5.48192	2.15371	-0.26885
H	5.37597	2.21375	-2.03570
C	6.69276	-0.17940	-1.67161
C	7.07707	-1.50981	-1.52099
H	7.34110	0.53679	-2.17869
H	8.03652	-1.85275	-1.91166
H	0.79955	-1.32491	0.29707
O	4.41514	1.39386	2.73121
H	1.25374	-4.912684	2.04173
H	2.78425	-4.33160	3.23914
H	2.77813	-4.94998	1.56809
H	1.48695	-2.91660	0.82732
H	1.48877	-2.26647	2.45624
H	0.21945	0.42705	0.02318

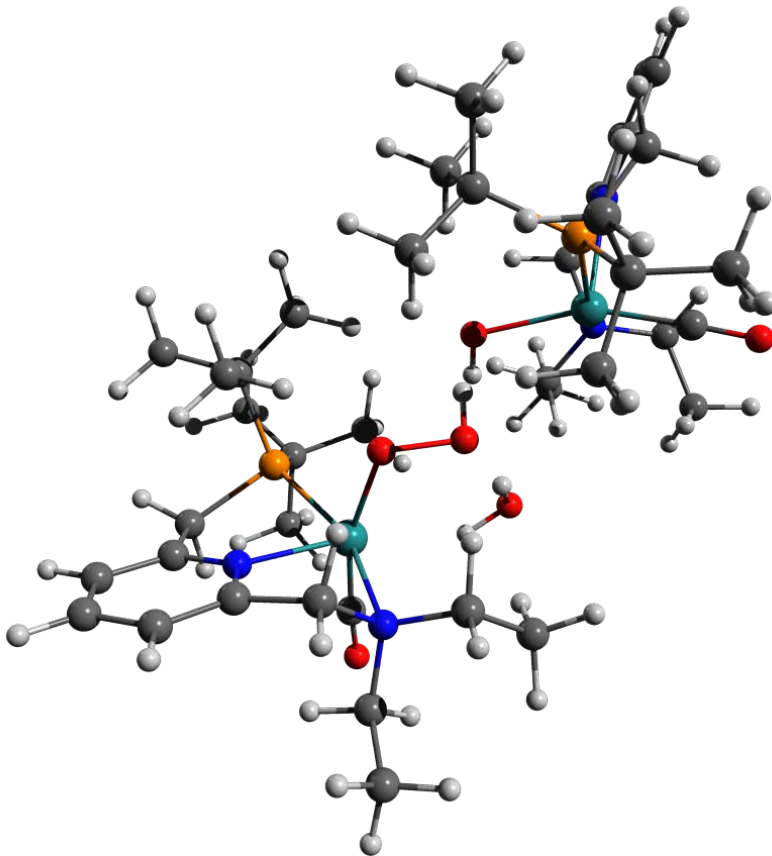


Figure 11.5-18 [C-Mono]D₀ Structure and Coordinates

63
 Energy: -975022.8334593
 H -3.38754 -3.53397 1.53840
 C -3.08449 -2.85544 0.72800
 H -3.69964 -3.09181 -0.15375
 H -2.02893 -3.06009 0.48536
 H 1.99577 -1.06227 2.50906
 O -0.60729 -0.32762 2.13706
 H 2.91476 -2.67415 0.32376
 O -0.29406 -1.59179 2.77994
 C -3.23558 -1.42286 1.19263
 H 3.29360 -0.11419 3.30022
 H -4.29666 -1.18668 1.40319
 C 2.92046 -0.49241 2.33282
 H 1.67766 -2.81774 -0.93524
 H 3.68266 -1.17982 1.93491
 H -2.65945 -1.27479 2.11627
 C 2.72113 -2.52891 -0.74944
 H 3.38511 -3.20716 -1.31153
 H -2.40630 0.82036 1.83739
 Ru -0.40306 -0.64584 0.07794
 H 0.71185 1.15314 2.25711
 N -2.68196 -0.44490 0.23274
 C -2.79962 0.91046 0.81070
 C 2.66361 0.68570 1.39125
 H 2.11002 1.99137 3.00737
 H 4.82850 -0.98794 0.00830
 C 1.67173 1.65167 2.05304
 C 2.98786 -1.08367 -1.18558
 P 1.78598 -0.00807 -0.15417
 H -3.84706 1.25313 0.85767
 C 4.47434 -0.77937 -1.00993
 H -3.05069 -1.46953 -1.54924
 H -5.36112 -1.12644 -0.59265
 H 5.04465 -1.43274 -1.69173
 C -3.32297 -0.50644 -1.09993
 H 4.21925 1.99983 2.06831
 C -0.46669 -1.34241 -1.60788
 C 3.95614 1.14144 1.13930
 H 1.60134 -1.06715 -2.90517
 C 2.85553 -0.93612 2.67536
 H 4.80198 0.13385 0.00603
 H 3.21495 -1.71607 -3.22845
 C -1.93808 1.91036 0.09217
 N -0.72432 1.44206 -0.24299
 C -4.83357 -0.32937 -1.13733
 H 1.50488 2.55053 1.43893
 H -2.83494 0.26308 -1.71691
 H 4.72459 0.26002 -1.26605
 H -5.16291 0.63819 -0.72947
 C 1.49998 1.54859 -1.18068
 H -5.16880 -0.37078 -2.18449
 H 3.83995 2.23298 0.35738
 C 0.20761 2.22244 -0.81205
 C -2.28018 3.23402 -0.15629
 H 3.00074 0.03562 -3.06956
 H -3.27064 3.60548 0.11039
 H 1.39644 1.18653 -2.21609
 H 2.33907 2.26030 -1.16633
 C -0.06943 3.56719 -1.06201
 C -1.32544 4.07116 -0.73425
 H 0.68993 4.20635 -1.51470
 H -1.56279 5.11805 -0.93256
 O -0.59256 -1.84912 -2.65857
 H 0.00586 -1.27580 3.64525

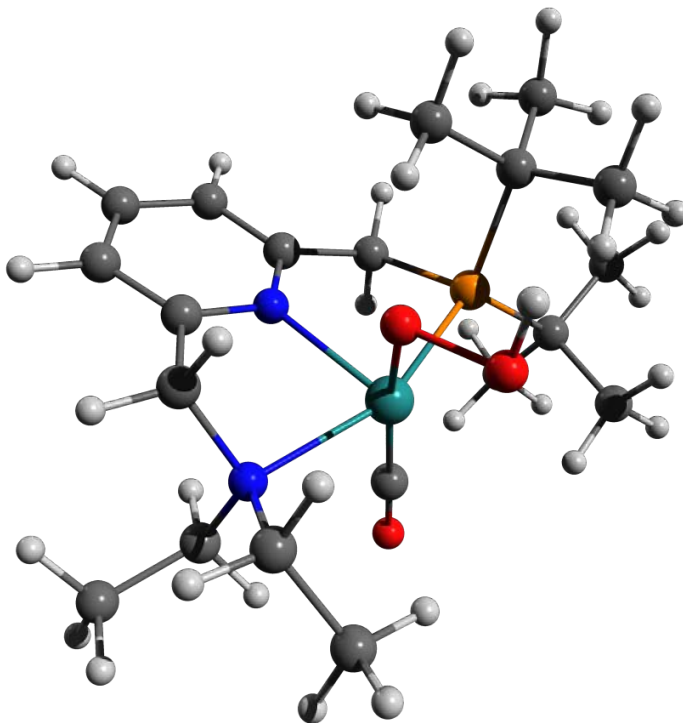


Figure 11.5-19 [C-Mono]D₀ (Me Model) Structure and Coordinates

39

O	-0.04819	-2.01605	-2.47646
O	0.05667	-0.67749	-1.94135
C	2.39625	-2.47917	-0.55239
H	2.24729	-0.24392	-1.65512
N	2.00393	-1.24720	0.14012
C	2.52464	-0.08266	-0.60105
C	-2.77035	0.64955	-1.70216
C	-3.70765	-0.11600	0.92180
P	-2.17257	0.20656	-0.02668
H	3.62423	-0.01324	-0.50776
C	2.53779	-1.24181	1.50431
C	-0.59321	-1.34333	1.86168
C	1.86066	1.20556	-0.19696
N	0.56759	1.08784	0.13363
C	-1.63830	1.86266	0.69978
C	-0.20747	2.16167	0.35840
C	2.46680	2.45591	-0.26299
H	3.52394	2.54288	-0.51795
H	-1.71414	1.71764	1.79252
H	-2.30447	2.69633	0.42805
C	0.33418	3.44392	0.27597
C	1.68706	3.58600	-0.02315
H	-0.29557	4.31693	0.45222
H	2.13311	4.58084	-0.07783
O	-0.87447	-1.61922	2.96363
H	-3.41804	1.53889	-1.69206
H	-3.33170	-0.20422	-2.11033
H	-1.88169	0.80270	-2.33215
H	-3.43984	-0.33107	1.96620
H	-4.19367	-1.00886	0.50298
H	-4.40554	0.73438	0.87989
H	2.04731	-3.33768	0.03619
H	3.49709	-2.54163	-0.66122
H	1.90799	-2.50833	-1.53414
H	2.24730	-0.31163	2.01051
H	3.64237	-1.32363	1.49550
H	2.11572	-2.08513	2.06483
Ru	-0.23290	-0.90538	0.11456
H	-1.00870	-2.14837	-2.48718

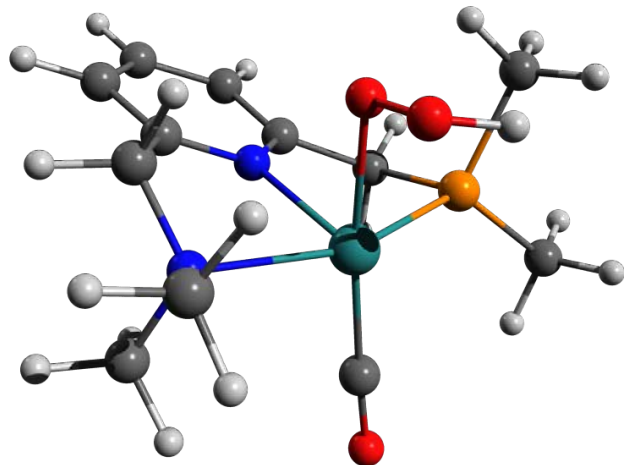


Figure 11.5-20 TS-[CD]T₀ Structure and Coordinates

```

128          Energy: -19514589.7937574
H   -1.35171  -0.17838  -4.75676
C   -2.22120  -0.15365  -4.08357
H   -3.12446  -0.09092  -4.70942
H   -2.19874  -0.76388  -3.47388
H   -0.31895  -1.20165  -1.26522
O   -1.25225  -0.74231  -0.30395
H   -2.04379  -3.71009  -0.57254
O   -0.24646  -0.24838  -1.03991
H   -1.89038  -2.23946  -1.47961
C   -2.19157  -1.38740  -3.20833
H   0.17655   1.42283  -2.96913
H   -2.24584  -2.30644  -3.82285
C   -0.64075  -1.60463  -2.25074
H   -3.45162  -3.48734  -0.48476
H   -0.79077  -2.69402  -2.21027
H   -1.24235  -1.41623  -2.65706
C   -3.13659  -3.81978  -0.51332
H   -3.37821  -4.89164  -0.60732
H   -2.03679  -2.65041  -1.06099
Ru  -3.10641  -0.23167  -0.59524
H   -1.38113  -0.99773  -1.65748
N   -3.26666  -1.41876  -2.18875
C   -3.09411  -2.63830  -1.37028
C   -1.88698  -0.85737  -2.72225
H   -0.74066  -0.85900  -3.31285
H   -2.51385  -3.83000  -3.15775
C   -1.61501  -0.65250  -2.67313
C   -3.86404  -3.04233  -1.61597
P   -3.27352  -1.22443  -1.46890
H   -3.29959  -3.55335  -1.95024
C   -3.58768  -3.72103  -2.95639
H   -4.75083  -0.40596  -3.25483
H   -4.29652  -2.41845  -4.70182
H   -4.01674  -4.73650  -2.92227
C   -4.62145  -1.39247  -2.79362
H   -1.44604  -0.71039  -4.81549
C   -4.52409  -1.17809  -1.24801
C   -2.20036  -1.20480  -4.18122
H   -5.69123  -2.59253  -0.45922
C   -5.37387  -3.11646  -1.36930
H   -2.15025  -2.27605  -4.39759
H   -5.65277  -4.17603  -1.24528
C   -3.91805  -2.60747  -0.11301
N   -4.00636  -1.40192  -0.46698
C   -4.93926  -2.47766  -3.81136
H   -2.45667  -1.23429  -3.0826
H   -5.33710  -1.43361  -1.95907
H   -4.05587  -3.19517  -3.79998
H   -4.85941  -3.49433  -3.39810
C   -4.69944  -0.19101  -2.14153
H   -5.97838  -2.34659  -4.14847
H   -3.18328  -0.83004  -4.50675
C   -4.63802  -1.22213  -1.63748
C   -4.49428  -3.72568  -0.47983
H   -5.94680  -2.72917  -2.22569
H   -4.42361  -4.70178  -0.00194
H   -5.60672  -0.65085  -1.71878
H   -4.79707  -0.22148  -3.23677
C   -5.21829  -2.30917  -2.29179
C   -5.14552  -3.56846  -1.02070
H   -5.72485  -2.16529  -3.24703
H   -5.39745  -4.42954  -2.00507
O   -5.30774  -1.77985  -1.74449
C   -1.95005  -4.47465  -0.60173
H   -1.76995  -0.90476  -2.80971
O   -1.00918  -2.26865  -1.89179
H   -0.60556  -2.82294  -0.89836
O   -2.64867  -1.23333  -1.58109
H   -0.64410  -1.39575  -1.61062
C   -1.82668  -3.27959  -0.42151
H   -2.44368  -1.76675  -4.22068
C   -2.29765  -1.81390  -3.12807
H   -0.76110  -2.18235  -0.73635
H   -1.65697  -2.68264  -2.91340
C   -0.98977  -3.05520  -0.10672
H   -0.44042  -3.93300  -0.48354
H   -3.88465  -2.90479  -0.89071
Ru  -2.74747  -0.27612  -0.27792
H   -4.03241  -0.24109  -2.49531
N   -2.97292  -2.46949  -0.91561
C   -4.19078  -2.85260  -0.16634
C   -3.65643  -1.90891  -2.43326
H   -4.59850  -0.68745  -3.92722
H   -2.27417  -4.56489  -1.74316
C   -4.51053  -0.69577  -2.82677
C   -2.48685  -3.37191  -0.08686
P   -3.34382  -1.78138  -0.55157
H   -4.57184  -3.83524  -0.49309
C   -2.71632  -4.63490  -0.74062
H   -3.99257  -1.91376  -2.64356
H   -1.46622  -1.56247  -3.03246
H   -2.21942  -5.47525  -0.22639
C   -3.22476  -2.65136  -2.36265
H   -4.74656  -2.97798  -3.93849
C   -2.63576  -0.38275  -1.96949
C   -4.40805  -3.15803  -2.90438
H   -2.87974  -2.81597  -2.18788
C   -2.95820  -3.67481  -1.51198
H   -3.79705  -4.06582  -2.91717
H   -2.31666  -4.47217  -1.92370
C   -5.28411  -1.82581  -0.23900
N   -4.86005  -0.55630  -0.19084
C   -1.99978  -2.49775  -3.23958
H   -5.53286  -0.77220  -2.42431
H   -3.67222  -3.65176  -2.52665
H   -3.78033  -4.89358  -0.83866
H   -1.28254  -3.31870  -3.10775
C   -5.09793  -1.84569  -0.13458
H   -2.31440  -2.48267  -4.29373
H   -5.31141  -3.35708  -2.30723
C   -5.71662  -0.47646  -0.14568
C   -6.64396  -2.12100  -0.26229
H   -3.99235  -4.05282  -1.53013
H   -6.98026  -3.15737  -0.31289
H   -4.98049  -2.16770  -1.18174
H   -5.75382  -2.57682  -0.36129
C   -7.09210  -0.24426  -0.14126
C   -7.55456  -1.06756  -0.20547
H   -7.78759  -1.08325  -0.09528
H   -8.62751  -1.26910  -0.21384
H   -1.12624  -1.05510  -1.40407
O   -2.50511  -0.06839  -3.06988
H   -1.03000  -5.23200  -0.22166
H   -2.06318  -5.09101  -1.65505
H   -2.79123  -5.21755  -0.03585
H   -1.73106  -3.00783  -0.62859
H   -0.92661  -2.92047  -0.94485
H   -1.08400  -0.09696  -0.35469

```

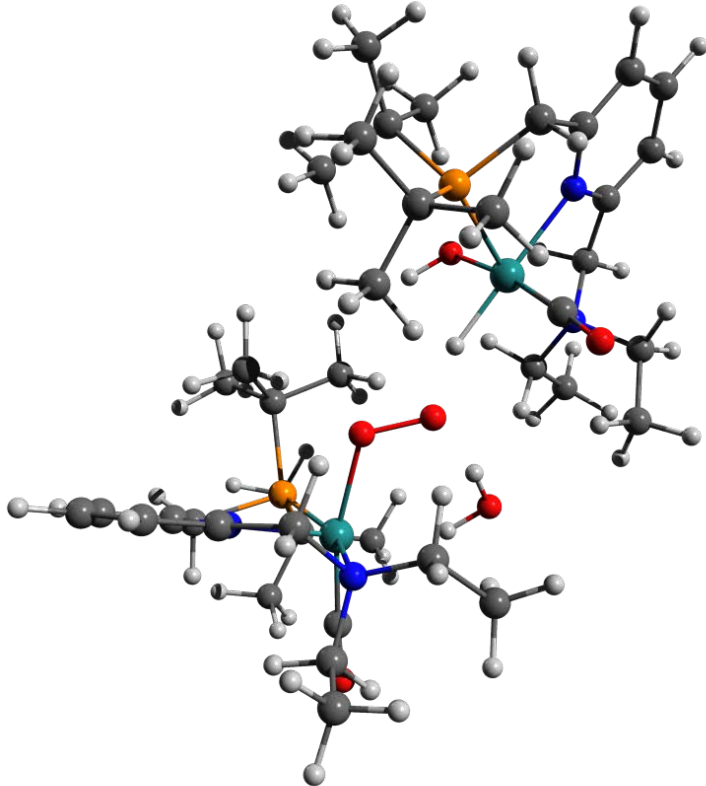


Figure 11.5-21 [D]T₀ [F]S₀ (Dimer Model) Structure and Coordinates

128

Energy: -1951474.5643316

H	2.21039	-2.23355	-4.32302
C	2.94020	-2.10065	-3.51092
H	3.76217	-2.79102	-3.70912
H	2.44399	-2.39608	-2.57405
H	0.20729	0.69700	0.93450
O	2.00197	0.89968	-1.11563
H	0.79753	-1.87017	2.19783
O	0.91009	0.32922	-1.54821
H	1.65613	-2.28902	0.30684
C	3.35522	-0.64652	-3.46822
H	0.28740	1.93394	2.06713
H	3.81547	-0.34125	-4.42738
C	0.39308	1.07378	1.96078
H	2.17595	-2.85811	1.70881
H	0.04202	0.28934	2.64875
H	2.46663	-0.01909	-3.31819
C	1.70714	-2.35054	2.56204
H	1.42251	-3.11900	3.30019
H	3.62475	1.64595	-2.49829
Ru	3.37129	-0.49295	-0.27560
H	2.20172	2.33336	0.26632
N	4.28549	-0.32083	-2.36027
C	4.59308	1.12622	-2.42419
C	1.82021	1.51701	2.27687
H	1.50189	3.46668	1.44084
H	1.06378	-0.50582	4.44736
C	2.22635	2.64419	1.31726
C	2.67215	-1.35764	3.21999
P	2.96471	0.03118	1.93490
H	5.18433	1.37831	-3.32006
C	2.07975	-0.90767	4.55421
H	5.27240	-2.15699	-2.21825
H	5.77660	-1.42642	-4.57931
H	2.01230	-1.78895	5.21372
C	5.53971	-1.11357	-2.42389
H	1.38104	3.07219	3.68524
C	4.29326	-2.00741	0.16757
C	1.90014	2.09943	3.69185
H	4.54301	-2.36849	2.62207
C	3.99571	-2.06566	3.52316
H	1.41175	1.48031	4.44974
H	3.77400	-2.98486	4.09033
C	5.27474	1.61909	-1.17756
N	4.80159	1.08031	-0.04426
C	6.33553	-1.03327	-3.71762
H	3.22071	3.05100	1.55899
H	6.15890	-0.78525	-1.57600
H	2.70644	-0.16287	5.06443
H	6.66552	-0.01184	-3.95952
C	4.66614	0.73279	2.33966
H	7.24174	-1.64741	-3.60772
H	2.93471	2.29472	4.01482
C	5.24957	1.46071	1.16314
C	6.26361	2.59505	-1.14450
H	4.65466	-1.44802	4.15262
H	6.64712	3.02303	-2.07160
H	5.29860	-0.14991	5.25265
H	4.69246	1.35254	3.24800
C	6.22637	2.45204	1.26262
C	6.73620	3.01873	3.03771
H	6.58475	2.76847	2.24044
H	7.04542	3.39870	0.36965
O	4.86915	-3.00676	0.96731
C	-1.67725	-4.45668	1.52902
H	-2.60178	2.18165	2.19599
O	0.83056	-2.38124	-0.81491
H	-1.09111	3.08609	-0.24809
O	-3.05347	-0.36368	1.91451
H	0.67780	-1.44550	-1.07669
C	-1.93640	-3.02562	1.01222
H	-3.38713	3.54642	2.92734
C	-3.08033	3.08788	1.97190
H	-0.98099	1.82862	-1.48757
H	-2.42915	3.80557	1.45027
C	-1.33266	2.85094	-1.29582
H	-0.75920	3.54442	-1.93434
H	-4.12042	-2.21994	1.93269
Ru	-2.98649	-0.33811	-0.18846
H	-4.60200	0.80015	2.14753
N	-3.08682	-2.59868	0.17864
C	-4.34181	-2.68580	0.95879
C	-4.32227	2.72502	1.15835
H	-5.40323	2.20156	2.93768
H	-2.90294	4.90516	-0.44755
C	-5.16594	1.73059	1.96779
C	-2.82692	3.02834	-1.58679
P	-3.73776	1.81492	-0.42011
H	-4.65609	-3.73378	1.10358
C	-3.19232	4.50319	-1.42759
H	-3.99955	-2.90770	-1.66592
H	-1.44430	-2.68958	-2.03879
H	-2.63751	5.07712	-2.18907
C	-3.24244	-3.41453	-1.04746
H	-5.65686	4.23734	1.88606
C	-2.67460	-0.47959	-1.97443
C	-5.18718	3.96793	0.92513
H	-2.91367	1.59427	-3.26355
C	-3.10729	2.65000	-3.04385
H	-4.62460	4.84203	0.58295
H	-2.43663	3.24323	-3.68784
C	-5.45941	-1.89036	0.34516
N	-5.07880	-0.71700	-0.17809
C	-1.97227	-3.62881	-1.84239
H	-6.12566	1.51303	1.47416
H	-3.67063	-4.39812	-0.76872
H	-4.26295	4.69503	-1.58765
H	-1.26561	-4.29481	-1.32963
C	-5.38276	1.41933	-1.25573
H	-2.23230	-4.08566	-2.80909
H	-6.00725	3.78417	0.21399
C	-5.96411	0.15525	-0.68740
C	-6.80155	-2.25763	0.36299
H	-4.13958	2.89557	-3.33875
H	-7.10272	-3.21866	0.78172
H	-5.12461	1.22841	-2.30996
H	-6.11529	2.23989	-1.23913
C	-7.32551	-0.14837	-0.68226
C	-7.74163	-1.36624	-0.5465
H	-8.04567	0.56181	-1.00229
H	-8.80221	-1.62728	-0.14874
H	-2.21835	0.01458	2.20818
O	-2.00511	-0.00538	-3.0932
H	-1.06114	-4.64178	2.10887
H	-2.00388	-5.20251	0.71828
H	-2.83017	-4.64733	2.19805
H	-1.92254	-2.30895	1.84537
H	-1.02934	2.85403	0.41687
H	-1.41111	-0.09993	-0.07392

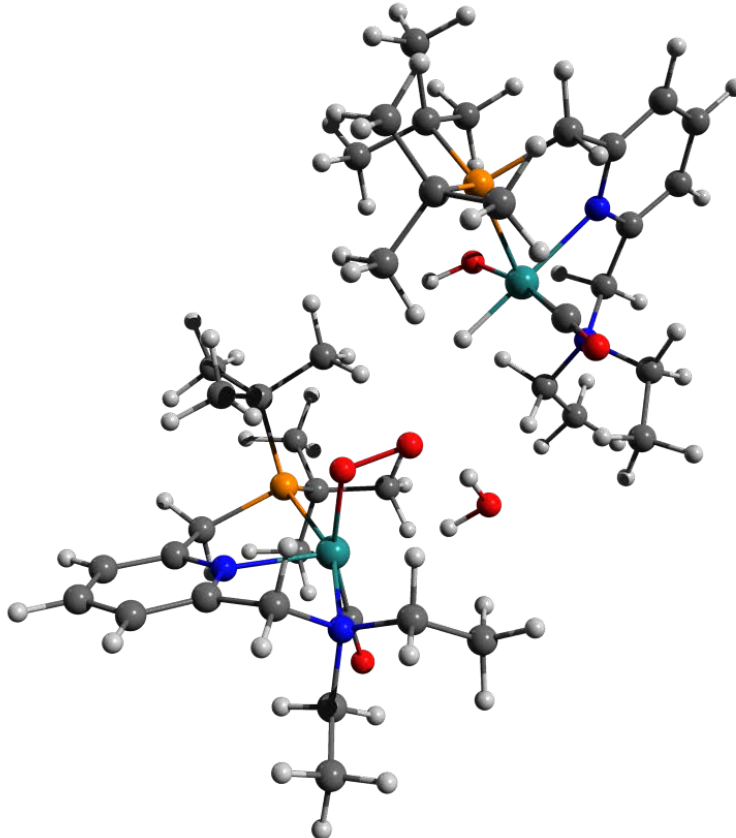


Figure 11.5-22 [D]T₀ Structure and Coordinates

65

```

Energy: -1022871.1899855
H   -3.38494   -3.31180   1.82737
C   -2.95112   -2.79277   0.95830
H   -3.38208   -3.24852   0.05218
H   -1.86643   -2.95916   0.96163
H   1.89851   -0.67840   2.70390
O   -0.53456   -0.35358   2.07755
H   3.01942   -2.52358   0.85085
O   -0.35394   -1.52334   2.63574
C   -3.25043   -1.31281   1.06133
H   3.09522   0.44848   3.41532
H   -4.34039   -1.12453   1.05618
C   2.80965   -0.08700   2.49421
H   1.90555   -2.89679   -0.47328
H   3.63051   -0.77775   2.24948
H   -2.86486   -0.91811   2.00937
C   2.92191   -2.54757   -0.24458
H   3.64858   -3.27877   -0.63668
H   -2.66408   1.08616   1.35598
Ru  -0.31837   -0.68828   -0.00504
H   0.53186   1.44950   2.04182
N   -2.60517   -0.51691   -0.00635
C   -2.83355   0.92076   0.27621
C   2.56533   0.92876   1.37589
H   1.84035   2.41943   2.74501
H   4.91382   -0.82138   0.45058
C   1.49019   1.92964   1.82129
C   3.19596   -1.17605   -0.87243
P   1.87279   -0.00911   -0.13540
H   -3.88007   1.20620   0.07627
C   4.65112   -0.78951   -0.61501
H   -2.77125   -1.86864   -1.59665
H   -5.17070   -1.52766   -0.94783
H   5.29862   -1.51901   -1.13009
C   -3.12403   -0.85838   -1.35592
H   4.01544   2.38917   1.98578
C   -0.23183   -1.57996   -1.59320
C   3.83591   1.74231   1.11081
H   1.97571   -1.47843   -2.68860
C   3.00900   -1.26566   -2.38964
H   4.73044   1.12740   0.97445
H   3.63245   -2.09289   -2.76752
C   -1.89906   1.81367   -0.48819
N   -0.64961   1.34073   -0.61557
C   -4.63079   -0.78598   -1.55459
H   1.33192   2.72272   1.07485
H   -2.61559   -0.18268   -2.05967
H   4.89859   0.20539   -1.01207
H   -5.05049   0.20694   -1.33435
C   1.64357   1.37017   -1.39287
H   -4.85289   -1.00424   -2.60984
H   3.73636   2.40888   0.24034
C   0.31283   2.05126   -1.22985
C   -2.24178   3.06770   -0.98206
H   3.34686   -0.34867   -2.89655
H   -3.26161   3.43938   -0.87459
H   1.62986   0.85885   -2.36903
H   2.46623   2.10001   -1.42016
C   0.03643   3.32619   -1.72152
C   -1.25326   3.83625   -1.59409
H   0.62291   3.90564   -2.20703
H   -1.49321   4.82932   -1.98022
O   -0.05641   -2.05583   -2.03553
O   -2.15763   1.34600   3.37545
H   -1.45833   0.73127   3.05377
H   -2.60547   0.82846   4.05496

```

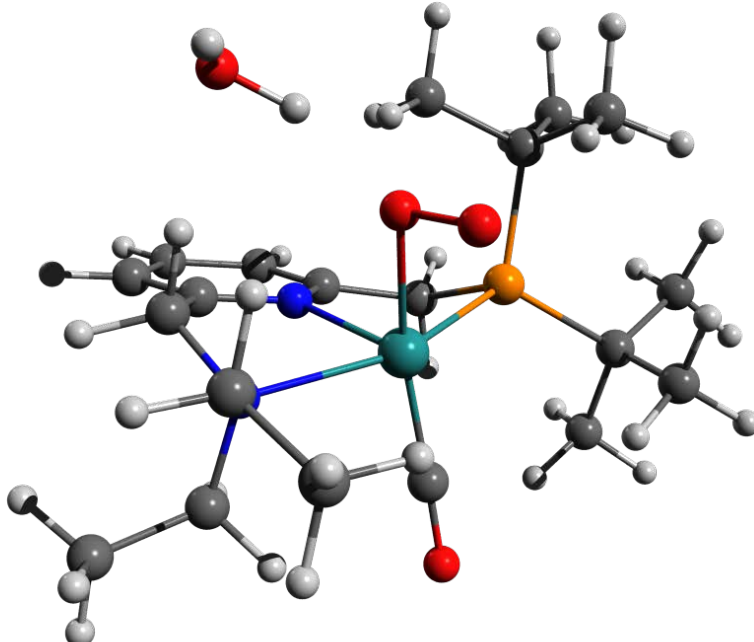


Figure 11.5-23 Scan-[DE]T₀ Geometry 5 Structure and Coordinates

65

```

Energy: -1022862.3366652
H   -3.52909   3.63066   0.69680
C   -3.14014   2.67577   1.07009
H   -3.70774   2.43237   1.98093
H   -2.08658   2.82131   1.34241
H   1.68759   1.14509   -1.72549
O   -0.13249   4.15116   -1.87917
H   4.21485   1.15428   0.97408
O   1.02322   4.35975   -1.65856
C   -3.28448   1.62227   -0.00542
H   3.21108   1.41790   -2.58285
H   -4.35763   1.46172   -0.23123
C   2.68412   1.24653   -1.62884
H   2.71787   1.87703   1.62409
H   3.19133   1.83450   -0.85194
H   -2.80464   1.95432   -0.93683
C   3.45799   1.07669   1.76795
H   3.96970   1.26101   2.72781
H   -2.73602   -0.06024   -1.72577
Ru  -0.40746   0.28477   0.36618
H   0.82599   -0.57996   -2.46733
N   -2.65529   0.31946   0.31333
C   -2.97713   -0.60257   -0.79572
C   2.66375   -0.25294   -1.32393
H   2.33072   -0.71345   -3.40479
H   4.61259   -1.38066   1.15940
C   1.86314   -0.94464   -2.43282
C   2.80169   -0.30485   1.80611
P   1.67304   -0.50435   0.28526
H   -4.05055   -0.86240   -0.81937
C   3.87043   -1.38738   1.96654
H   -2.68589   0.42603   2.39482
H   -5.14655   0.53499   1.74855
H   4.41231   -1.21646   2.91251
C   -3.09606   -0.23282   1.61775
H   4.51800   -0.71960   -2.31985
C   0.12668   1.97410   0.77974
C   4.08269   -0.81368   -1.31025
H   1.06471   0.39181   2.93114
C   1.86034   -0.36233   3.01447
H   4.74237   -0.26860   -0.62064
H   2.44092   -0.18706   3.93633
C   -2.13124   -1.83752   -0.76503
N   -0.88543   -1.64945   -0.28699
C   -4.59579   -0.41517   1.81058
H   1.85621   -2.04051   -2.32728
H   -2.57927   -1.19605   1.74069
H   3.43684   -2.39724   2.02516
H   -5.03675   -1.11348   1.08360
C   1.35159   -2.35785   0.29786
H   -4.77557   -0.83435   2.81187
H   4.10942   -1.88199   -1.04381
C   0.00997   -2.66200   -0.29230
C   -2.53968   -3.06661   -1.26824
H   1.37180   -1.34516   3.11201
H   -3.55523   -3.19103   -1.64581
H   1.33080   -2.64239   1.36285
H   2.14391   -2.95574   -0.17788
C   -0.33534   -3.90828   -0.80978
C   -1.62275   -4.14441   -1.29836
H   0.40247   -4.71444   -0.49102
H   -1.91814   -5.08799   -1.69942
O   0.00954   3.04000   1.09179
O   -1.02013   1.17283   -2.57593
H   -0.84821   2.12314   -2.80775
H   -0.64192   0.93092   -1.67189

```

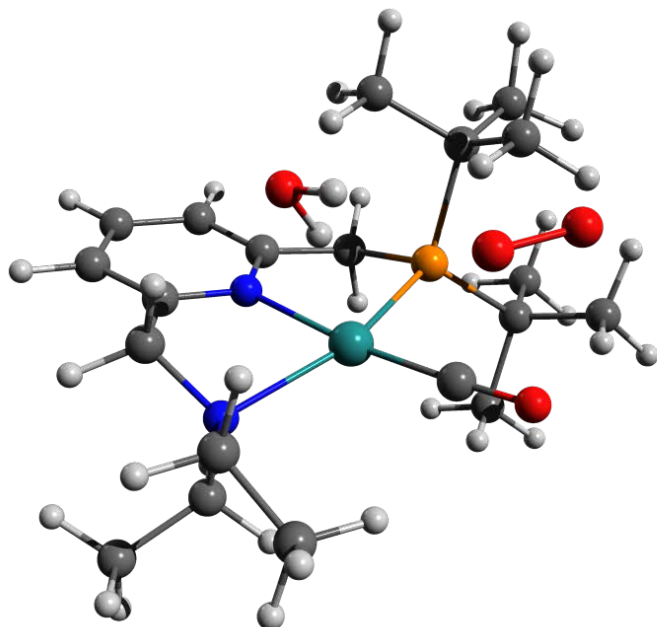


Figure 11.5-24 [E]S₀ Structure and Coordinates

```

63
Energy: -928588.5901943
N   -0.79133   1.42415   0.01683
C   -2.02380   1.84124   0.37017
C    0.19107   2.30928   -0.42940
C   -2.40595   3.17104   -0.25270
C    1.46999   4.09574   0.20893
C   -0.18941   3.66159   -0.54037
C    2.87907   0.77587   0.98864
C   -3.41494   3.47721   0.53136
H   -1.73711   5.14924   -0.30717
H    0.56365   4.36371   -0.89999
C    1.46351   1.74417   -0.81210
N   -2.65521   -0.55453   0.39254
H   -3.94471   1.06478   0.96488
H   -2.59052   0.70030   2.04990
H    1.44545   1.53749   -1.89569
P    1.70832   0.05142   -0.03024
H    2.27274   2.46679   -0.62445
Ru   -0.40599   -0.62089   0.15361
C    3.27363   -0.64358   -0.95219
C    2.97845   -0.74783   -1.20012
C    3.18949   -1.56064   1.33979
C    2.53410   0.45347   1.64701
C    2.19457   -1.27404   -2.40610
C    3.63932   -1.93931   -0.50368
C    4.04527   0.22764   -1.70266
C    1.63138   1.49050   2.32374
C    3.95281   1.01018   1.57578
C    2.49280   -0.81727   2.50075
H   -2.80880   0.13549   -1.57050
C   -4.79102   -0.53396   -1.01525
H   -2.93530   -1.59110   -1.39047
H   -2.55934   -1.48842   2.23915
C   -3.18632   -2.98500   0.83054
H   -4.21908   -1.27293   1.63398
C    0.03994   -2.38933   0.14073
H   -2.18198   -3.29149   0.51148
H   -3.88327   -3.13688   -0.00645
H   -3.50338   -3.65153   1.64617
H   -5.10318   -0.62787   -0.06600
H   -5.16787   0.43500   -0.65414
H   -5.29282   -1.32900   -0.44968
H   2.90715   -1.71394   -3.12478
H   1.62743   -0.48790   -2.92492
H   1.47710   -2.04963   -2.10743
H   4.23655   -2.49727   -1.24443
H   2.89196   -2.63300   -0.09153
H   4.32107   -1.63378   0.30265
H   4.74182   -0.31648   -2.36279
H   4.63926   0.67500   -0.89613
H   3.60801   1.04018   -2.30181
H   4.67507   0.27479   1.19572
H   4.28265   1.29668   2.58941
H   4.01533   1.91267   0.94747
H   3.13835   -1.61377   2.10810
H   1.46338   -1.20515   2.54493
H   2.83194   -0.58265   3.52443
H   1.98486   1.65715   3.35522
H   0.59120   1.13131   2.36546
H   1.64500   2.46423   1.09977
O   0.38651   -3.50621   0.09718
O   -0.68110   0.21173   -2.97203
H   -0.95813   1.08513   -2.86151
H   -0.52984   -0.26674   -2.11021

```

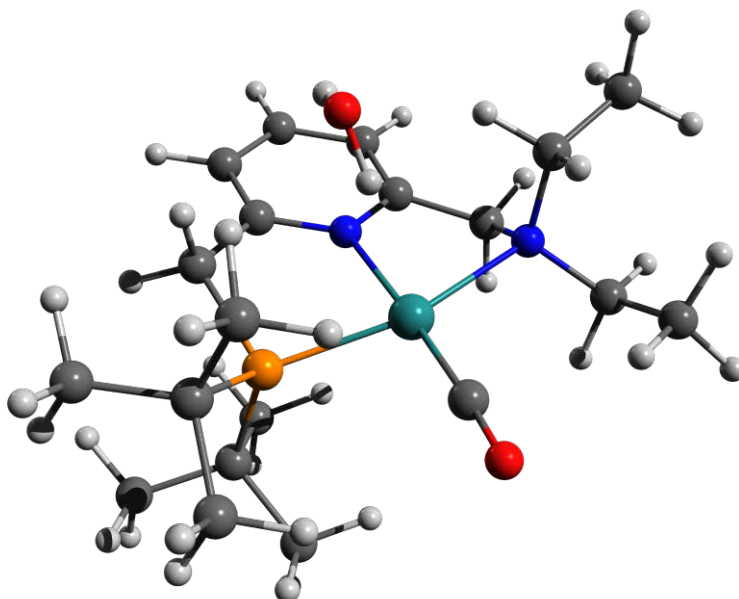


Figure 11.5-25 ³O₂ Coordinates

```

2
Energy: -94269.2503844
O   0.00000   0.00000   0.59806
O   0.00000   0.00000   -0.59806

```

Figure 11.5-26 [F]S₀ Structure and Coordinates

63 Energy: -928594.2432451

N	-0.74635	1.30730	-0.32033
C	-1.93878	1.84197	-0.01643
O	0.18858	2.01274	-0.97776
O	-2.25389	3.14457	-0.39308
C	-1.28825	3.08510	-1.07340
C	-0.06176	3.32937	-1.36675
C	-2.84308	0.97446	0.81471
H	-3.23108	3.56209	-0.14724
H	-1.51749	4.92094	-1.37588
H	0.70480	3.89705	-1.89563
C	1.48478	1.30907	-1.27073
N	-2.84341	-0.42575	0.38117
H	-3.85953	1.40663	0.85274
H	-2.41290	0.96630	1.83054
H	1.39796	0.81902	-2.25631
P	1.79947	-0.10207	-0.06444
H	2.31636	2.02663	-1.33554
Ru	-0.32175	-0.78130	0.27359
C	-3.46183	-0.59919	-0.94190
C	3.10916	-1.14527	-0.97707
C	-3.42210	-1.26670	1.43622
C	2.61156	0.77486	1.42558
C	2.39457	-2.02743	-2.00009
C	3.80009	-2.06975	0.02702
C	4.14004	-0.29775	-1.72864
C	1.69299	1.93832	1.81948
C	4.00605	1.33256	1.14447
C	2.66301	-0.19905	2.60550
H	0.01026	-2.25575	0.83530
H	-2.91836	0.06098	-1.63552
C	-4.95759	-0.32754	-1.02895
H	-3.24790	-1.62263	-1.27730
H	-2.81556	-1.05375	2.32917
C	-3.36080	-2.74585	1.11743
H	-4.46441	-0.95652	1.65455
C	-0.50126	-1.51406	-1.38531
O	-0.57986	-0.11284	2.25077
H	-0.37245	-0.84709	2.84019
H	-2.32717	-3.02846	0.86111
H	-4.02163	-3.03305	0.28531
H	-3.67211	-3.32484	1.99945
H	-5.29191	-0.47074	-2.06746
H	-5.21847	0.70230	-0.74089
H	-5.54132	-1.01426	-0.39748
H	3.15437	-2.60299	-2.55465
H	1.81938	-1.44712	-2.73550
H	1.71136	-2.73530	-1.51456
H	4.41226	-2.80230	-0.52475
H	3.06264	-2.62841	0.62341
H	4.46906	-1.53042	0.71081
H	4.86572	-0.97439	-2.21023
H	4.70470	0.38269	-1.08198
H	3.67478	0.29404	-2.53093
H	4.75838	0.54920	0.98004
H	4.32884	1.91247	2.02544
H	4.02144	2.01981	0.28437
H	3.31205	-1.06440	2.42213
H	1.64926	-0.54891	2.83581
H	3.05547	0.33489	3.48741
H	2.10639	2.40474	2.73046
H	0.68234	1.56615	2.08803
H	1.65235	2.72159	1.04725
O	-0.74696	-2.01597	-2.41088

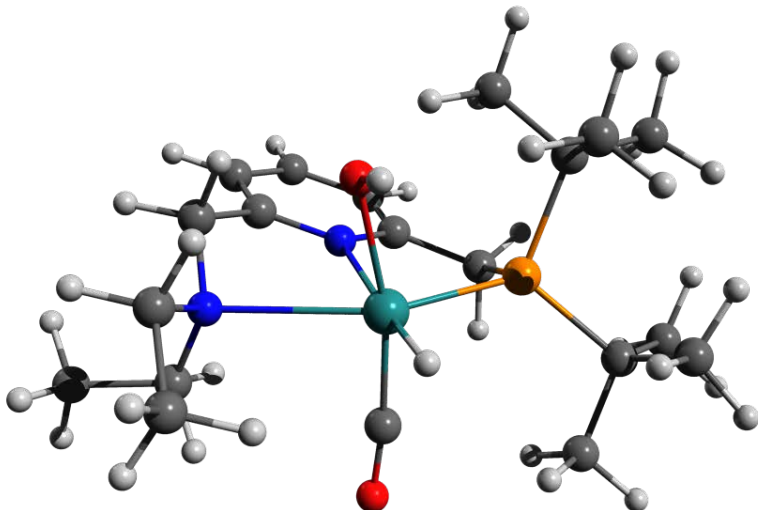


Figure 11.5-27 [F-Up]S₀

63 Energy: -928594.7107585
 N -0.76012 1.35702 0.06074
 C -1.98808 1.76019 0.41130
 O 0.14591 2.21168 -0.43933
 O -2.35911 3.09652 0.32530
 C -1.41501 4.01493 0.63117
 O -0.15550 3.57248 -0.52449
 C 2.86432 0.65143 0.91583
 H -3.36391 3.41035 0.61035
 H -1.66922 5.07414 -0.20352
 H 0.58703 4.27030 -0.91343
 C 1.42575 1.61298 -0.94035
 N -2.71088 -0.57889 0.10904
 H -3.91695 0.97807 0.97223
 H -2.54157 0.40295 1.94000
 H 1.24037 1.35471 -1.99701
 P 1.76437 -0.06514 -0.17220
 H 2.26264 2.32326 -0.88030
 Ru -0.40278 -0.73311 0.00089
 C -3.28097 -0.39488 -1.24605
 C 2.98529 -0.86036 -1.40368
 C -3.35596 -1.69012 0.84091
 C 2.68585 0.37918 1.43916
 C 2.16082 -1.50296 -2.52121
 C 3.76716 -1.97521 -0.70760
 C 3.94668 0.14893 -2.03561
 C 1.78330 1.34786 2.21325
 C 4.02979 1.07014 1.20419
 C 2.90333 -0.86685 2.30296
 H -0.17741 -2.28874 -0.35044
 H -2.67991 0.38194 -1.73612
 C -4.77086 -0.09912 -1.32183
 H -3.04599 -1.30790 -1.80675
 H -2.86129 -1.74689 1.82075
 C -3.24236 -3.02668 0.14065
 H -4.41803 -1.44218 1.03317
 C -0.36341 -1.29063 1.73384
 O -0.55241 -0.24421 -2.02943
 H -0.51954 -1.07146 -2.52109
 H -2.19154 -3.21571 -0.12667
 H -3.85742 -3.08026 -0.76983
 H -3.58479 -3.82187 0.81910
 H -5.05260 -0.00593 -2.38153
 H -5.04794 0.84874 -0.83522
 H -5.39256 -0.89811 -0.88922
 H 2.85351 -1.96637 -3.24406
 H 1.53388 -0.76769 -3.04204
 H 1.49724 -2.27858 -2.11355
 H 4.30778 -2.55843 -1.47151
 H 3.09393 -2.66558 -0.17658
 H 4.51440 -1.59451 0.00201
 H 4.62443 -0.38964 -2.71936
 H 4.57013 0.67690 -1.30360
 H 3.41141 0.89676 -2.63846
 H 4.77741 0.39768 0.76244
 H 4.42961 1.40719 2.17539
 H 3.94093 1.96074 0.56358
 H 3.62536 -1.56423 1.86222
 H 1.96971 -1.41019 2.48923
 H 3.30471 -0.55087 3.28072
 H 2.24443 1.55016 3.19394
 H 0.78337 0.92786 2.38544
 H 1.86994 2.31323 1.69793
 O -0.39707 -1.72073 2.82230

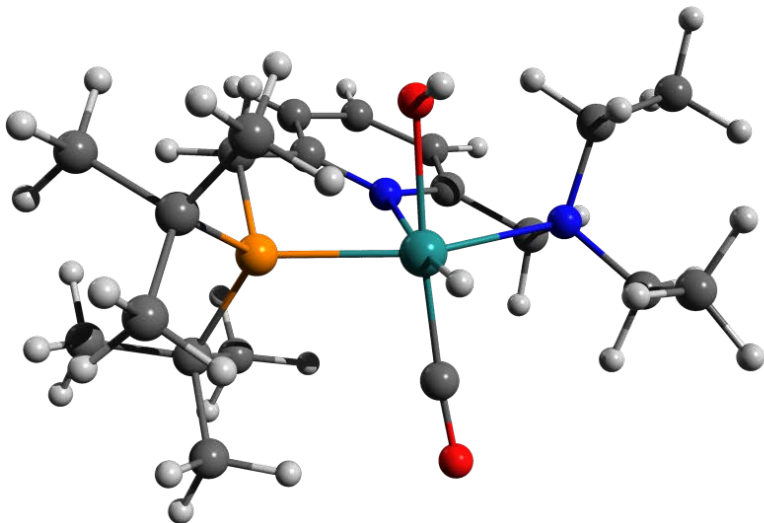


Figure 11.5-28 [F-Trans]S₀ Structure and Coordinates

```

63                                         Energy: -928595.0842646
N   -0.80008   1.42201   -0.04137
C   -2.01529   1.84205   0.33314
O    0.08710   2.25307   -0.61139
C   -2.40612   3.16389   0.15747
C   -1.49291   4.05389   -0.40659
C   -0.23606   3.59815   -0.79275
C   -2.83614   3.77931   0.98500
H   -3.40192   3.48854   -0.46079
H   -1.76456   5.10007   -0.55239
H   0.49999   4.27366   -1.24616
C   1.38015   1.63724   -1.04565
N   -2.67460   -0.52971   0.33005
H   -3.89593   1.07920   1.06179
H   -2.45228   0.65674   2.02086
H   1.20532   1.24514   -2.06318
P   1.72843   0.07619   -0.07604
H   2.20011   2.36921   -1.06618
Ru  -0.40440   -0.63417   0.12216
C   -3.31677   -0.52889   -1.00610
C   2.98840   -0.83483   -1.17047
C   -3.23884   -1.55482   1.23772
C   2.56798   0.66948   1.52673
C   2.19557   -1.57220   -2.25448
C   3.75077   -1.87787   -0.35107
C   3.96721   0.12336   -1.85464
C   1.66301   1.74844   2.13123
C   3.95882   1.26826   1.32423
C   2.62271   -0.50133   2.51198
H   -0.38438   -0.55794   1.74376
H   -2.72303   0.14852   -1.63637
C   -4.80382   -0.21466   -1.04423
H   -3.12800   -1.52055   -1.43586
H   -2.59533   -1.54706   2.12912
C   -3.29428   -2.95019   0.65467
H   -4.25429   -1.24594   1.55620
C   0.02966   -2.39316   0.33554
O   -0.62223   -0.36430   -0.01252
H   -0.67378   -1.23608   -2.41991
H   -2.32106   -3.24701   0.24091
H   -4.05502   -3.04876   -0.13346
H   -3.55292   -3.66121   1.45301
H   -5.15707   -0.32368   -2.08074
H   -5.03248   0.81782   -0.73872
H   -5.40541   -0.89516   -0.42114
H   2.90435   -1.96849   -3.00088
H   1.45853   -0.92112   -2.74563
H   1.64034   -2.41699   -1.82452
H   4.33695   -2.50636   -1.04223
H   3.06523   -2.54178   0.19634
H   4.45549   -1.43199   0.36428
H   4.69269   -0.46925   -2.43693
H   4.53709   0.74184   -1.15000
H   3.45345   0.78874   -2.56369
H   4.69663   0.52824   0.98659
H   4.31802   1.67091   2.28640
H   3.95127   2.10330   0.60632
H   3.31040   -1.29420   2.19136
H   1.62198   -0.93940   2.63946
H   2.97139   -0.13229   3.49119
H   2.06119   2.03045   3.11924
H   0.63871   1.37285   2.26559
H   1.63082   2.66104   1.51687
O   0.36196   -3.49890   0.50636

```

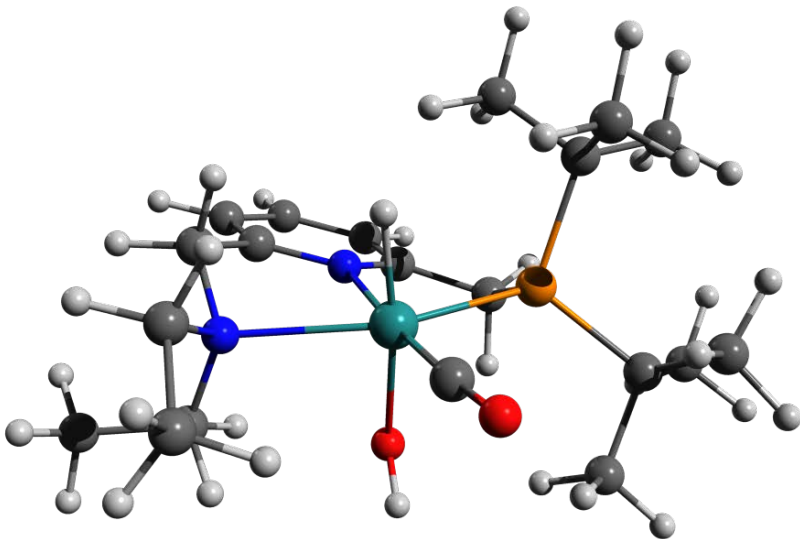


Figure 11.5-29 [F-Trans-Up]S₀ Structure and Coordinates

63

	Energy: -928597.8425390		
N	-0.80456	1.44495	-0.19829
C	-2.03468	1.86436	0.14891
O	0.12233	2.30384	-0.64514
O	-2.36507	3.20229	0.02647
C	-1.44432	4.11153	0.42708
C	-0.17108	3.66150	-0.59772
C	-2.90916	0.80031	0.72946
H	-3.40264	3.52229	0.29686
H	-1.69505	5.16956	-0.52185
H	0.59223	4.35144	-1.12469
C	1.43744	1.70691	-1.03843
N	-2.68203	-0.50943	0.08359
H	-3.97137	1.09596	0.70925
H	-2.57049	0.66141	1.77189
H	1.38751	1.45664	-2.11168
P	1.72097	0.06691	-0.17905
H	2.26188	2.42278	-0.90504
Ru	-0.41200	-0.61319	0.08095
C	-3.20203	-0.52723	-1.30271
C	2.89886	-0.81317	-1.38767
C	-3.30408	-1.53096	0.95651
C	2.63956	0.54327	1.41642
C	2.06909	-1.36145	-2.55174
C	3.56812	-1.99337	-0.67902
C	3.96741	0.12012	-1.96582
C	1.76616	1.61361	2.08406
C	4.05425	1.08518	1.22953
C	2.65974	-0.68229	2.33407
H	-0.43417	-0.78203	-1.52042
H	-2.66778	0.26567	-1.84531
C	-4.70588	-0.35856	-1.46514
H	-2.86686	-1.46983	-1.75382
H	-2.72796	-1.47327	1.89224
C	-3.29003	-2.93590	0.39539
H	-4.34571	-1.23050	1.18415
C	0.02049	-2.37940	0.20529
O	-0.76410	-0.17688	2.17309
H	-0.41080	-0.88374	2.72358
H	-2.27615	-3.24304	0.10712
H	-3.94853	-3.05374	-0.47837
H	-3.64559	-3.63190	1.16954
H	-4.95447	-0.40248	-2.53621
H	-5.06907	0.60960	-1.08879
H	-5.27648	-1.15404	-0.96304
H	2.75551	-1.82586	-3.27975
H	1.50507	-0.57340	-3.07289
H	1.34279	-2.11174	-2.21769
H	4.12018	-2.59036	-1.42402
H	2.83098	-2.65633	-0.20339
H	4.29185	-1.66865	0.08138
H	4.61776	-0.46331	-2.63891
H	4.60846	0.57207	-1.20033
H	3.52795	0.92880	-2.56855
H	4.75887	0.32382	0.86597
H	4.42910	1.43550	2.20622
H	4.08739	1.94673	0.54444
H	3.28052	-1.50000	1.94507
H	1.63860	-1.05754	2.48408
H	3.06554	-0.38893	3.31631
H	2.20182	1.84961	3.07021
H	0.73971	1.22947	2.23546
H	1.74397	2.55309	1.50940
O	0.35357	-3.49676	0.25197

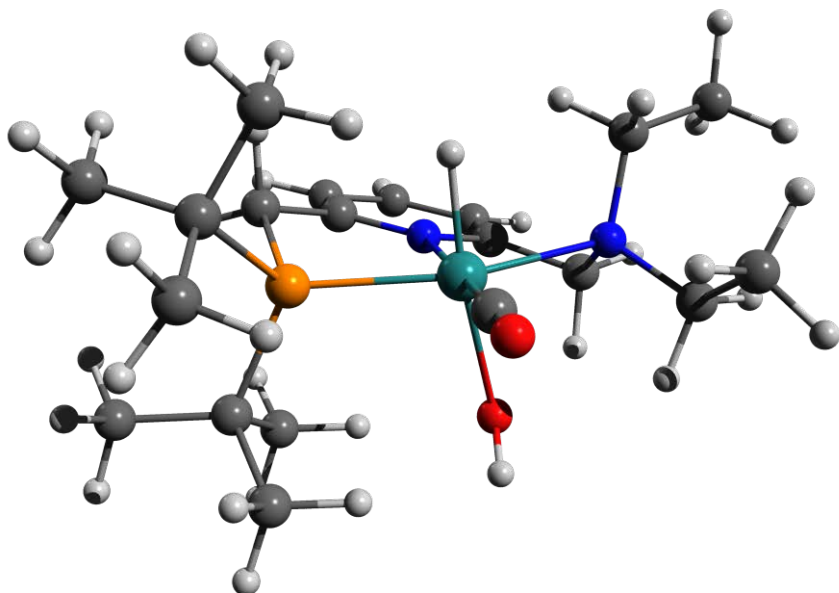


Figure 11.5-30 [F-Cis]S₀ Structure and Coordinates

63 Energy: -928584.1363893

N	0.71566	1.37102	0.24967
C	1.88601	1.90688	-0.14944
C	-0.22203	2.13284	0.85849
O	2.19695	3.23563	0.1033
C	1.26995	4.02858	0.76442
C	0.03258	3.47557	1.12704
C	2.73322	0.98067	-0.96914
H	3.15802	3.64155	-0.20754
H	1.47320	5.07710	0.98044
H	-0.73060	4.07916	1.62065
C	-1.51831	1.44743	1.18218
N	2.66800	-0.41382	-0.49369
H	3.77113	1.35162	-1.03319
H	2.30857	0.97872	-1.98663
H	-1.44297	0.99243	2.18545
P	-1.75656	-0.02386	0.03128
H	-2.35119	2.16642	1.20696
Ru	0.41346	-0.61138	-0.14255
C	3.42690	-0.55444	0.77262
C	-3.03865	-1.11267	0.91840
C	3.17947	-1.30585	-1.55970
C	-2.54199	0.74825	-1.53001
C	-2.28511	-1.92416	1.97289
C	-3.61065	-2.11050	-0.09137
C	-4.15196	-0.32493	1.61073
C	-1.68563	1.95376	-1.93209
C	-3.97745	1.23127	-1.32770
C	-2.47899	-0.26757	-2.67357
H	0.32804	-0.24845	-1.77202
H	2.99417	0.17132	1.47773
C	4.93463	-0.36535	0.69258
H	3.19723	-1.54836	1.17591
H	2.49649	-1.16511	-2.41000
C	3.19508	-2.76566	-1.16012
H	4.18443	-0.96125	-1.87714
C	0.60946	-1.12466	1.67406
O	0.15196	-2.61505	-0.66095
H	-0.04077	-2.60617	-1.60553
H	2.18267	-3.05345	-0.82169
H	3.93873	-2.98216	-0.37773
H	3.46261	-3.37173	-2.03913
H	5.35640	-0.47464	1.70297
H	5.22566	0.63128	0.32769
H	5.41672	-1.11829	0.05220
H	-3.00470	-2.58654	2.48267
H	-1.82336	-1.29010	2.74351
H	-1.50496	-2.54416	1.50536
H	-4.20342	-2.86484	0.45241
H	-2.79842	-2.63566	-0.61747
H	-4.27589	-1.63992	-0.82798
H	-4.82587	-1.03594	2.11799
H	-4.76170	0.26958	0.92036
H	-3.75465	0.34758	2.38635
H	-4.68328	0.40641	-1.16265
H	-4.30489	1.76218	-2.23745
H	-4.06683	1.93952	-0.48927
H	-3.11348	-1.14547	-2.49985
H	-1.44317	-0.60744	-2.81777
H	-2.82265	0.21757	-3.60270
H	-2.05120	2.33470	-2.00001
H	-0.63235	1.66355	-0.20528
H	-1.75400	2.77998	-1.20884
O	0.81361	-1.39650	2.78236

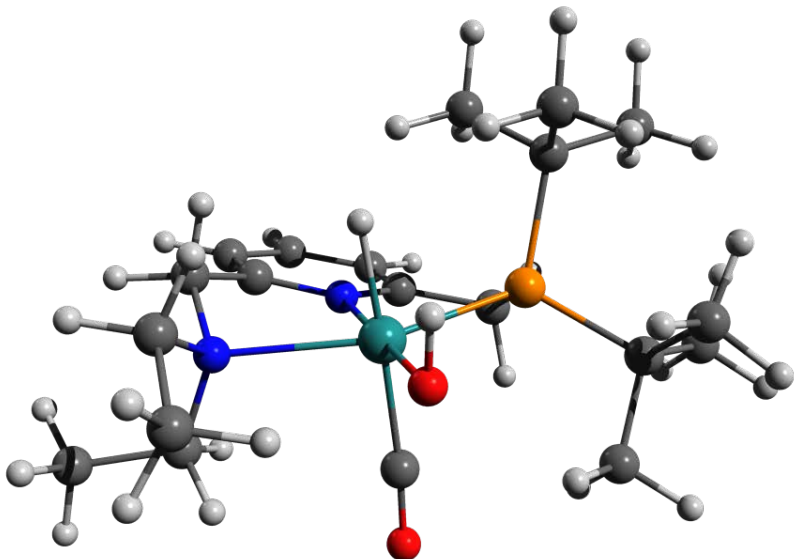


Figure 11.5-31 [F-Cis-Up]S₀

63

	Energy: -928583.3465243		
N	-0.76649	1.41843	-0.07154
C	-2.01036	1.85279	0.21670
O	0.14794	2.26376	-0.59987
C	-2.37124	3.16384	0.0272
C	-1.15168	4.06495	0.41404
C	-0.15168	3.61575	0.5320
C	-2.92299	0.78241	0.73207
H	-3.38574	3.50509	0.29284
H	-1.66577	5.14026	-0.52683
H	0.60447	4.28902	-1.15894
C	1.43193	1.64925	-1.06883
N	-2.68842	-0.50404	0.04480
H	-3.97678	1.10586	0.66433
H	-2.69735	0.61853	1.79906
H	1.29444	1.38772	-2.13247
P	1.73612	-0.00383	-0.23635
H	2.26951	2.35972	-1.00852
Ru	-0.40632	-0.58507	0.12753
C	-3.13183	-0.43630	-1.37016
C	2.76388	-0.97221	-1.51000
C	-3.38495	-1.57380	0.79678
C	2.81626	0.48715	1.25846
C	1.79173	-1.54530	-2.54607
C	3.42342	-2.15521	-0.79768
C	3.81352	-0.12407	-2.23086
C	2.06226	1.60909	1.98221
C	4.20708	1.00144	0.88987
C	2.94913	-0.70018	2.21525
H	-0.38263	-0.54300	-1.52205
H	-2.58034	0.39612	-1.82922
C	-4.62669	-0.27589	-1.60563
H	-2.75557	-1.34493	-1.85563
H	-2.93436	-1.58370	1.80041
C	-3.24221	-2.94035	0.16087
H	-4.45015	-1.29713	0.92821
C	-0.42880	-0.79162	2.01232
O	-0.17639	-2.63743	-0.18445
H	0.11822	-3.04741	0.63704
H	-2.17636	-3.12248	-0.07293
H	-3.84319	-3.03847	-0.75619
H	-3.59094	-3.70383	0.86859
H	-4.80781	-0.21749	-2.68943
H	-5.03495	0.64510	-1.16155
H	-5.20838	-1.12709	-1.22230
H	2.37599	-2.14707	-3.26386
H	1.27463	-0.75585	-3.11162
H	1.03384	-2.17538	-2.05570
H	3.86573	-2.82409	-1.55452
H	2.67531	-2.73449	-0.23591
H	4.23239	-1.84666	-0.12066
H	4.32954	-0.75890	-2.97077
H	4.57883	0.28829	-1.56235
H	3.35837	0.70854	-2.78858
H	4.85268	0.20776	0.48993
H	4.69648	1.39306	1.79777
H	4.17387	1.82343	0.15832
H	3.52252	-1.52815	1.78067
H	1.96980	-1.08747	2.52084
H	3.47731	-0.36929	3.12537
H	2.57082	1.82424	2.93635
H	1.02509	1.32521	2.20880
H	2.04757	2.54327	1.40092
O	-0.46674	-0.98768	3.15824

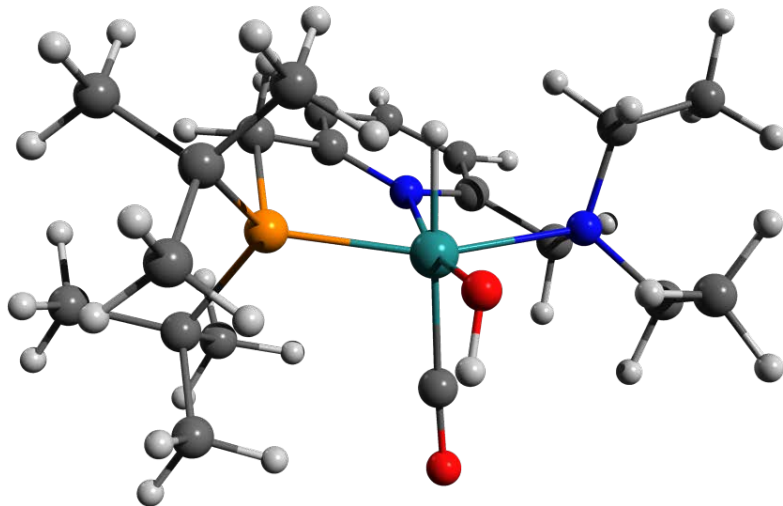
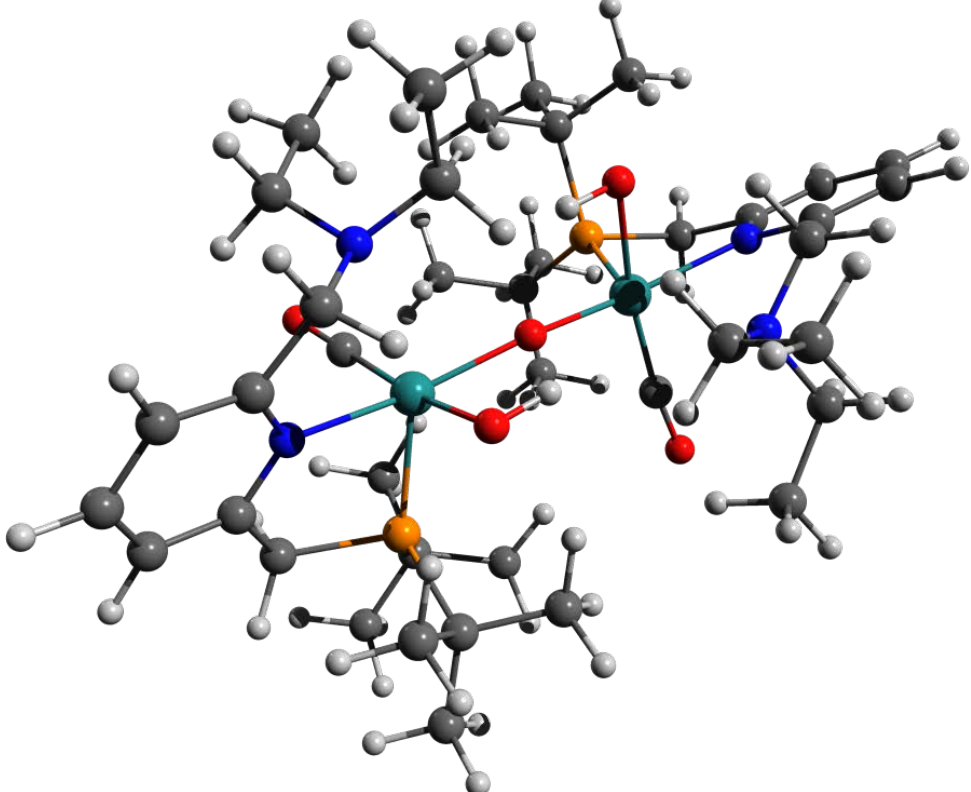


Figure 11.5-32 [Oxo Dimer] S_0 Structure and Coordinates

125

Energy: -1903622.5751306

Ru	1.95096	-0.14653	-0.32407
O	2.00832	-1.80029	0.92464
C	1.90893	1.05768	-1.69607
P	2.88599	1.33842	1.19148
N	4.01311	-0.56768	-0.70975
C	4.53000	1.60252	0.25451
H	4.32826	2.35352	-0.52810
H	5.31172	2.01152	0.91161
C	4.98001	0.33183	-0.38985
C	6.32650	0.06494	-0.62494
H	7.07516	0.80881	-0.35061
C	6.69055	-1.14695	-1.19781
H	7.73907	-1.37674	-1.39527
C	5.69184	-2.06110	-1.51010
H	5.92828	-3.02776	-1.95594
C	4.36117	-1.74588	-1.24971
C	3.26539	-2.73818	-1.48420
H	3.67502	-3.59036	-0.06069
H	2.93674	-3.07047	-0.48254
N	2.09801	-2.14698	-2.11742
C	2.29339	3.13737	1.30343
C	3.40572	4.10595	1.71752
H	4.20219	4.16830	0.96148
H	3.86246	3.86481	2.68306
H	2.96774	5.11464	1.80329
C	1.15082	3.17641	2.31683
H	0.65697	4.16110	2.27409
H	1.50238	3.02969	3.34710
H	0.39099	2.41354	2.10485
C	1.76662	3.60000	-0.05230
H	0.94948	2.96248	-0.40187
H	2.54516	3.60685	-0.82886
H	1.38789	4.63073	0.04669
C	3.33584	0.61429	2.80336
C	4.04527	1.59470	3.73568
H	3.39887	2.41977	4.06399
H	4.95979	2.01770	3.29136
H	4.35144	1.04365	4.64064
C	4.26228	-0.58364	2.56289
H	4.46589	-1.05356	3.54002
H	5.23222	-0.28524	2.13842
H	3.76716	-1.32593	1.92045
C	2.04916	0.09266	3.45054
H	2.30463	-0.40808	4.39646
H	1.57687	-0.62955	2.77817
H	1.33840	0.90239	3.68369
C	1.22294	-1.15312	-4.23495
H	0.48557	-1.25216	-4.49965
H	1.56895	-0.68709	-5.16917
H	0.71440	-2.13971	-3.63880
C	0.93641	-3.02622	-2.00061
H	0.06527	-2.47795	-2.38049
H	0.77323	-3.16167	-0.92130
C	1.03165	-4.37637	-2.69966
H	1.18407	-4.27465	-3.78584
H	0.09062	-4.92698	-2.55004
H	1.84534	-5.00091	-2.29982
C	2.40794	-1.72102	-3.48232
H	2.85340	-2.56024	-4.05949
H	3.10140	-0.95933	-3.0528
O	0.00019	-0.04384	0.00209
Ru	-1.95090	-0.44533	0.3007
C	-1.91025	1.06339	1.69316
O	-2.00709	-1.80036	-0.91908
P	-2.88590	1.33489	-1.10592
N	-2.09803	-2.13971	2.12450
N	-4.01323	-0.55597	0.71084
C	-3.26497	-2.73362	1.49287
H	-3.67443	-3.58398	2.07214
H	-2.93570	-3.06923	0.49252
C	-4.36107	-1.74256	1.25452
C	-5.69174	-2.05747	1.51527
H	-5.92807	-3.02278	1.96405
C	-6.69065	-1.14469	1.19955
H	-7.73918	-1.37425	1.39730
C	-6.32681	0.06549	0.62298
H	-7.07561	0.80824	0.34600
C	-4.98029	0.33212	0.38760
C	-4.53105	1.60091	-0.26057
H	-4.32960	2.35456	0.51970
H	-5.31194	2.00738	-0.91950
C	-3.33465	0.60529	-2.80560
C	-4.04399	1.58254	-3.74129
H	-4.34943	1.02859	-4.64473
H	-3.39782	2.40691	-4.07178
C	-4.95896	2.00646	-3.29877
C	-2.04740	0.09872	-3.45040
H	-2.30204	-0.42133	-4.39509
H	-1.57557	-0.63808	-2.77552
H	-1.33660	0.89131	-3.68528
C	-4.26076	-0.59225	-2.56192
H	-5.23202	-0.29293	-2.13882
H	-3.76567	-1.33238	-1.91697
H	-4.46372	-1.06522	-3.53771
C	-2.29407	3.13359	-1.31317
C	-3.40688	4.10043	-1.73009
H	-4.20333	4.16471	-0.97420
H	-3.86357	3.85624	-2.69489
H	-2.96935	5.10900	-1.81888
C	-1.76753	3.60044	0.04124
H	-1.38914	4.63095	-0.06073
H	-0.95022	2.96414	0.39276
H	-2.54614	3.60926	0.81771
C	-1.15158	3.17055	-2.32673
H	-0.65856	4.15578	-2.28685
H	-1.50303	3.02053	-3.35658
H	-0.39106	2.40898	-2.11267
C	-2.40857	-1.70893	3.48776
H	-2.85399	-2.54619	4.06781
H	-3.19324	-0.93918	3.40766
C	-1.22390	-1.13797	4.23864
H	-0.48672	-1.90899	4.50682
H	-1.57028	-0.66807	5.17077
H	-0.71499	-0.37267	3.63954
C	-0.93601	-3.01891	2.01126
H	-0.06533	-2.46892	2.38968
H	-0.77228	-3.15794	0.93250
C	-1.03102	-4.36670	2.1486
H	-1.18397	-4.26145	3.80063
H	-0.04966	-4.91737	2.56751
H	-1.84422	-4.99297	2.31671
O	-1.96237	1.73887	2.64636
O	1.96054	1.73006	-2.65157
H	1.03960	-1.82295	1.01395
H	-1.03823	-1.82607	-1.00680



12 References

1. J. Zhang, G. Leitus, Y. Ben-David, D. Milstein, Facile Conversion of Alcohols into Esters and Dihydrogen Catalyzed by New Ruthenium Complexes. *J. Am. Chem. Soc.* **127**, 10840–10841 (2005).
2. S. W. Kohl, L. Weiner, L. Schwartsburd, L. Konstantinovski, L. J. W. Shimon, Y. Ben-David, M. A. Iron, D. Milstein, Consecutive Thermal H₂ and Light-Induced O₂ Evolution from Water Promoted by a Metal Complex. *Science*. **324**, 74–77 (2009).
3. R. Dorta, H. Rozenberg, L. J. W. Shimon, D. Milstein, Dimethylsulfoxide as a Ligand for RhI and IrI Complexes—Isolation, Structure, and Reactivity Towards X-H Bonds (X=H, OH, OCH₃). *Chem. – Eur. J.* **9**, 5237–5249 (2003).
4. H. Weissman, PhD Thesis (2004), Weizmann Institute of Science.
5. J. Zhang, M. Gandelman, L. J. W. Shimon, D. Milstein, Electron-rich, bulky PNN-type ruthenium complexes: synthesis, characterization and catalysis of alcohol dehydrogenation. *Dalton Trans.* **0**, 107–113 (2006).
6. R. Barrios-Francisco, E. Balaraman, Y. Diskin-Posner, G. Leitus, L. J. W. Shimon, D. Milstein, PNN Ruthenium Pincer Complexes Based on Phosphinated 2,2'-Dipyridinemethane and 2,2'-Oxobispyridine. Metal–Ligand Cooperation in Cyclometalation and Catalysis. *Organometallics*. **32**, 2973–2982 (2013).
7. C. K. Ng, J. Wu, T. S. A. Hor, H.-K. Luo, A binary catalyst system of a cationic Ru–CNC pincer complex with an alkali metal salt for selective hydroboration of carbon dioxide. *Chem. Commun.* **52**, 11842–11845 (2016).
8. M. Hippler, Photochemical Kinetics: Reaction Orders and Analogies with Molecular Beam Scattering and Cavity Ring-Down Experiments. *J. Chem. Educ.* **80**, 1074 (2003).
9. S. L. Murov, *Handbook of Photochemistry*, Section 13, pp. 299-313 (Marcel Dekker, New York, ed. 2nd, 1993).
10. M. J. Frisch, G. W. Trucks, H. B. Schlegel, G. E. Scuseria, M. A. Robb, J. R. Cheeseman, G. Scalmani, V. Barone, G. A. Petersson, H. Nakatsuji, *Gaussian 16* (Gaussian, Inc. Wallingford, CT, 2016).
11. M. D. Hanwell, D. E. Curtis, D. C. Lonie, T. Vandermeersch, E. Zurek, G. R. Hutchison, Avogadro: an advanced semantic chemical editor, visualization, and analysis platform. *J. Cheminformatics*. **4**, 17 (2012).
12. A.-R. Allouche, Gabedit—A graphical user interface for computational chemistry softwares. *J. Comput. Chem.* **32**, 174–182 (2011).
13. W. L. DeLano, Pymol: An open-source molecular graphics tool. *CCP4 Newslett. Protein Crystallogr.* **40**, 82–92 (2002).
14. T. Plachetka, POV Ray: persistence of vision parallel raytracer, in *Proc. of Spring Conf. on Computer Graphics, Budmerice, Slovakia* (1998), vol. 123.
15. M. G. Delcey, T. B. Pedersen, F. Aquilante, R. Lindh, Analytical gradients of the state-average complete active space self-consistent field method with density fitting. *J. Chem. Phys.* **143**, 044110 (2015).

16. M. G. Delcey, L. Freitag, T. B. Pedersen, F. Aquilante, R. Lindh, L. González, Analytical gradients of complete active space self-consistent field energies using Cholesky decomposition: Geometry optimization and spin-state energetics of a ruthenium nitrosyl complex. *J. Chem. Phys.* **140**, 174103 (2014).
17. I. Fdez. Galván, M. G. Delcey, T. B. Pedersen, F. Aquilante, R. Lindh, Analytical State-Average Complete-Active-Space Self-Consistent Field Nonadiabatic Coupling Vectors: Implementation with Density-Fitted Two-Electron Integrals and Application to Conical Intersections. *J. Chem. Theory Comput.* **12**, 3636–3653 (2016).
18. F. Aquilante, J. Autschbach, A. Baiardi, S. Battaglia, V. A. Borin, L. F. Chibotaru, I. Conti, L. De Vico, M. Delcey, I. Fdez. Galván, N. Ferré, L. Freitag, M. Garavelli, X. Gong, S. Knecht, E. D. Larsson, R. Lindh, M. Lundberg, P. Å. Malmqvist, A. Nenov, J. Norell, M. Odelius, M. Olivucci, T. B. Pedersen, L. Pedraza-González, Q. M. Phung, K. Pierloot, M. Reiher, I. Schapiro, J. Segarra-Martí, F. Segatta, L. Seijo, S. Sen, D.-C. Sergentu, C. J. Stein, L. Ungur, M. Vacher, A. Valentini, V. Veryazov, Modern quantum chemistry with [Open]Molcas. *J. Chem. Phys.* **152**, 214117 (2020).
19. I. Fdez. Galván, M. Vacher, A. Alavi, C. Angeli, F. Aquilante, J. Autschbach, J. J. Bao, S. I. Bokarev, N. A. Bogdanov, R. K. Carlson, L. F. Chibotaru, J. Creutzberg, N. Dattani, M. G. Delcey, S. S. Dong, A. Dreuw, L. Freitag, L. M. Frutos, L. Gagliardi, F. Gendron, A. Giussani, L. González, G. Grell, M. Guo, C. E. Hoyer, M. Johansson, S. Keller, S. Knecht, G. Kovačević, E. Källman, G. Li Manni, M. Lundberg, Y. Ma, S. Mai, J. P. Malhado, P. Å. Malmqvist, P. Marquetand, S. A. Mewes, J. Norell, M. Olivucci, M. Oppel, Q. M. Phung, K. Pierloot, F. Plasser, M. Reiher, A. M. Sand, I. Schapiro, P. Sharma, C. J. Stein, L. K. Sørensen, D. G. Truhlar, M. Ugandi, L. Ungur, A. Valentini, S. Vancoillie, V. Veryazov, O. Weser, T. A. Wesołowski, P.-O. Widmark, S. Wouters, A. Zech, J. P. Zobel, R. Lindh, OpenMolcas: From Source Code to Insight. *J. Chem. Theory Comput.* **15**, 5925–5964 (2019).
20. A. D. Boese, Density Functional Theory and Hydrogen Bonds: Are We There Yet? *ChemPhysChem.* **16**, 978–985 (2015).
21. X. Yang, M. B. Hall, Mechanism of Water Splitting and Oxygen–Oxygen Bond Formation by a Mononuclear Ruthenium Complex. *J. Am. Chem. Soc.* **132**, 120–130 (2010).
22. Y. Chen, W.-H. Fang, Mechanism for the Light-Induced O₂ Evolution from H₂O Promoted by Ru(II) PNN Complex: A DFT Study. *J. Phys. Chem. A.* **114**, 10334–10338 (2010).